

GLOBE 11

## BOREHOLE GEOPHYSICAL TECHNIQUES FOR DEFINING PERMEABLE ZONES IN GEOTHERMAL SYSTEMS

Phillip M. Wright and Stanley H. Ward

Earth Science Laboratory  
University of Utah Research Institute  
391 Chipeta Way, Suite C  
Salt Lake City, Utah 84108

### ABSTRACT

Borehole electrical geophysical methods have considerable potential for helping to define hot and permeable zones in geothermal systems. Borehole geophysics differs from geophysical well logging and has a much greater area of search around a borehole. Very little developmental work has taken place in borehole electrical methods to date. At UURI, we have been developing computer methods to model various electrical arrays for borehole configurations. We plan to compare the several possible survey methods and then design a field system based on the method that appears from the computer studies to be optimum.

From our studies to date we tentatively conclude that the cross-borehole method produces larger anomalies than does the single-borehole method; cross-borehole anomalies using a pole-pole array are smaller than those for a dipole-dipole array; the cross-borehole *mise-à-la-masse* method produces larger anomalies than does other cross-borehole methods; and, the anomalies due to a thin structure are generally much smaller than those for a sphere, as is to be expected.

### INTRODUCTION

The key problem worldwide in development of hydrothermal resources appears to be more in locating permeable zones than in locating high temperatures. Grindly and Browne (1976) note that of 11 hydrothermal fields investigated in New Zealand, all of which have high temperatures (230°C to 300°C), five are non-productive chiefly because of low permeability. Three of the eleven fields are in production (Wairakei, Kawerau and Broadlands) and in each of these fields permeability limits production more than temperature does. Hot but unproductive holes have been drilled at many of the major geothermal areas in the world, including The Geysers, Roosevelt Hot Springs, Coso, and Meager Creek, to name a few.

Permeability can be primary or secondary. Primary permeability in clastic rocks originates from intergranular porosity and it generally decreases with depth due to compaction and cementation. In volcanic sequences, primary intergranular porosity and permeability exist, but greater permeability exists in open spaces at flow contacts and within the flows themselves. Primary permeability in crystalline igneous rocks is generally very low. Secondary permeability occurs in all rock types in open fault zones, fractures

and fracture intersections, along dikes and in breccia zones (Brace, 1968; Moore et al., 1985). Changes in permeability come about through mineral deposition in open spaces or by leaching by the thermal fluids.

Although none of the geophysical methods maps permeability directly, any geological, geochemical, or hydrological understanding of the factors that control the permeability in a geothermal reservoir can be used to help determine geophysical methods potentially useful for detecting the boundaries and more permeable parts of a hydrothermal system. At UURI, we have been developing electrical borehole techniques to detect and map permeable zones in the subsurface, especially fractures.

### BACKGROUND--BOREHOLE GEOPHYSICS

It is important to understand the differences between geophysical well logging and borehole geophysics. In geophysical well logging, the instruments are deployed in a single well in a tool or sonde, and the depth of investigation is usually limited to the first few meters from the well-bore. Well-logging techniques have been developed by the petroleum industry over a period of half a century and have been applied with variable success by the geothermal industry. The major adaptations to the geothermal environment are the requirements of high temperature tools and the different interpretation required for hard rock (volcanic, igneous) lithologies. Other differences include a strong emphasis in geothermal exploration on fracture identification and the effects of hydrothermal alteration upon certain log responses. Much research remains to be done in order to understand fully the responses of various well logs in geothermal reservoirs and their typically fractured, altered, commonly igneous and metamorphic host rocks. In spite of the relative lack of knowledge of well-log response in geothermal reservoirs, several logs or log combinations have been used successfully to investigate such properties as lithology, alteration, fracturing, density, porosity, fluid flow and sulfide content, all of which may be critical in deciding how and in what intervals to complete, case, cement or stimulate a well (Glenn and Hulén, 1979; Keys and Sullivan, 1979; Sanyal et al., 1980; Glenn and Ross, 1982; Halfman et al., 1982).

By contrast, borehole geophysics refers to those geophysical techniques where energy sources and sensors are deployed (1) at wide spacing in a

single borehole, (2) partly in one borehole and partly on the surface, or (3) partly in one borehole and partly in a second borehole. Thus, we speak of borehole-to-surface, surface-to-borehole and borehole-to-borehole surveys. The depth of investigation is generally much greater in borehole geophysical surveys than it is in geophysical well logging.

Only one of the several borehole geophysical techniques, namely vertical seismic profiling (VSP), has been developed to any extent. The petroleum industry has funded relatively rapid development of VSP over the past several years.

VSP

Vertical seismic profiling (VSP) can be done using both P- and S-wave surface sources (usually mechanical vibrators) arranged circumferentially around a well. Direct and reflected seismic waves are detected by strings of down-hole geophones clamped to the wall of the well or by hydrophones. VSP has been used mainly to trace seismic events observed at the surface to their point of origin in the earth and to obtain better estimates for the acoustic properties of a stratigraphic sequence. Oristaglio (1985) presents a guide to the current uses of VSP.

Borehole Electrical Techniques

Borehole-to-borehole and borehole-to-surface electrical methods appear to have considerable potential for application to geothermal exploration. In a benchmark introductory paper, Daniels (1983) illustrated the utility of hole-to-surface resistivity measurements with a detailed study of an area of volcanic tuff near Yucca Mountain, Nevada. He obtained total-field resistivity data for a grid of points on the surface with current sources in three drill holes, completed a layered-earth reduction of the data, and interpreted the residual resistivity anomalies with a 3D ellipsoidal modeling technique.

The borehole electrical techniques, however, are in general poorly developed. One reason for this is that there are a large number of ways that borehole electrical surveys can be performed and it has been unclear which methods are best. At the same time, computer algorithms to model the several methods have not existed so that it has not been possible to select among methods prior to committing to the expense of building a field system and obtaining test data.

R&D PROGRAM AT UURI

The objective of our program is to develop and demonstrate the use of borehole electrical techniques in geothermal exploration, reservoir delineation and reservoir exploitation. Our approach is:

1. Develop computer techniques to model the possible borehole electrical survey systems;
2. Design and construct a field data acquisition system based on the results of (1);
3. Acquire field data at sites where the nature and extent of permeability are known; and,

4. Develop techniques to interpret field data.

To the present time, we have made considerable progress on item (1) above and we are now at such a point that item (2) could be started.

Our research staff has consisted of the following personnel: Stanley H. Ward, Project Manager; Luis Rijo, Professor of Geophysics, Universidade Federal Do Para, Brazil (on 2-year post-doctoral leave at U of U and UURI); F. W. Yang, Peoples Republic of China (visiting scholar); J. X. Zhao, Peoples Republic of China (visiting scholar); Craig W. Beasley (doctoral candidate U of U, awarded MS degree); Richard C. West (MS candidate at UU). Additional technical support has been provided by Philip E. Wannamaker, Howard P. Ross and Phillip M. Wright of UURI and by Gerald W. Hohmann of U of U. Project costs for Rijo, Yang and Zhao have been minimal because these scientists have been supported by their governments. Thus, a great deal has been accomplished at minimal cost while supporting the education of several students. The remainder of this paper will discuss the significance of our research to date.

COMPUTER MODELING OF BOREHOLE ELECTRICAL METHODS

Computer techniques for modeling borehole electrical geophysics have largely been lacking, especially for three-dimensional (3D) cases. Figure 1 indicates conventional usage of the terms 1D, 2D and 3D in geophysical interpretation. In the 1D case, also called the "layered earth" case, the physical property of interest (resistivity for this study), varies only in the vertical direction. In the 2D case, physical property variations in the vertical and one horizontal dimension are allowed, and the anomalous body illustrated has the same shape in and out of the paper for infinite distance. In the 3D case, physical property variations are specified in all three space dimensions. Obviously, the real earth is only occasionally 1D in nature in geothermal areas. The usual case is for physical properties to vary in all three dimensions in the earth, the 3D case. However, the mathematical formulations for electrical anomalies of bodies increase greatly in complexity from the 1D case to the 3D case. This accounts for the fact that in order to begin our task of applying borehole electrical techniques to delineation of permeability, we were required to develop original mathematical formulations of the problem.

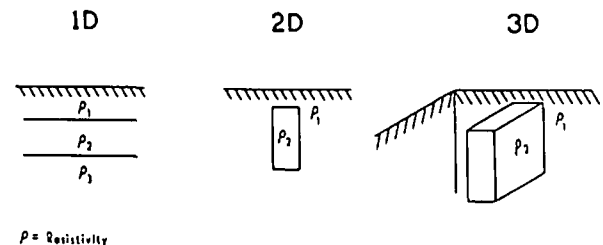


FIGURE 1  
Illustration of the meaning of the terms 1D, 2D and 3D in geophysical modeling.

### Thick-Body Studies

Prior to 1982, only three published papers considered computer modeling of downhole electrodes for three-dimensional bodies. Daniels (1977) studied six buried electrode configurations and plotted normalized apparent resistivity or apparent polarizability against such configuration parameters as 1) source and receiver depth, 2) depth/bipole length, 3) receiver distance from body, 4) depth of body, and 5) distance of source and receiver from body center. Snyder and Merke (1973), computed the IP and apparent resistivity responses resulting from a buried current pole in the presence of a buried sphere. Their plots are center-line profiles for normalized apparent resistivity and normalized IP response. Dobecki (1980) computed the effects of spheroidal bodies as measured in nearby single boreholes using the pole-pole electrode array. These three studies are obviously very limited in terms of the problems of defining permeability in geothermal systems.

In 1982, Newkirk (1982) from our group published a study of downhole electrical resistivity with 3D bodies. Using a numerical modeling technique described by Hohmann (1975), theoretical anomalies due to a three-dimensional body composed of simple prisms were computed. The results were presented in terms of 1) the potential, 2) the apparent resistivity calculated from the total horizontal electric field and 3) the apparent resistivity calculated from the potential. Two electrode configurations were considered for each model. Each configuration consisted of a pair of electrodes, where one of the electrodes was remote and the second electrode was located either in the body, for *mise-à-la-masse* or applied potential, or outside the body, simulating a near miss. Newkirk's computer program was used by Mackelprang (1985) of our group to compute a catalog of models due to bodies that might be of interest in detection of thick fracture zones.

Figures 2a and 2b show the conventions used by Newkirk (1982) and Mackelprang (1985) in calculations of the effects of 3D bodies. The bodies are buried in a homogeneous earth and two of many options for a downhole point electrode are illustrated. Figure 3a and 3b illustrate anomalies on a surface resistivity survey produced by a narrow conductive body buried at a depth of 7 units with the electrode in the body (Fig. 3a) and off the end of the body (Fig. 3b). The peanut shaped anomaly shown in Figure 3a is particularly characteristic on surface resistivity surveys with the borehole electrode in the body.

One basic shortcoming of Newkirk's (1982) algorithm is that it does not apply when the anomalous body becomes thin, i.e. to the case of delineation of fractures or thin fracture zones. To address this important problem, the thin-body studies described in the next section have been undertaken.

### Thin-Body Studies

These studies are aimed at targets simulating fracture zones which are thin relative to their

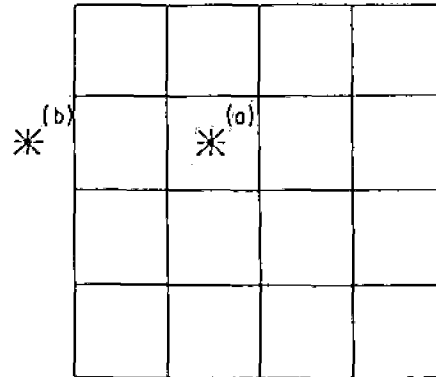


FIGURE 2a  
Plan view of standard model.

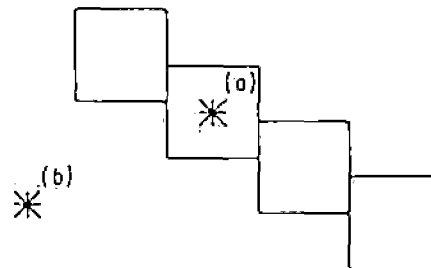


FIGURE 2b  
Cross-section view of standard model.

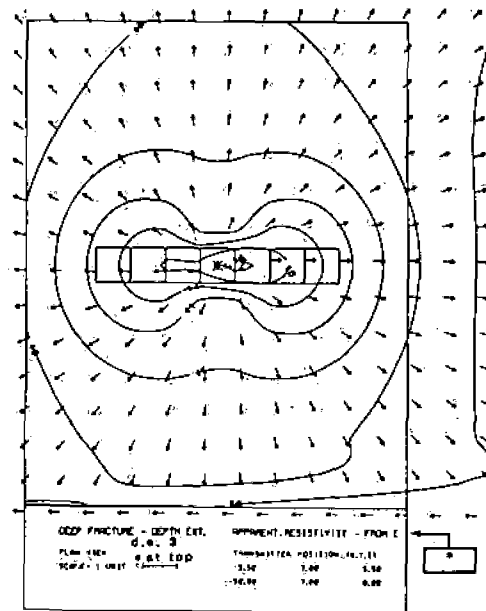


FIGURE 3a  
Surface resistivity anomaly due to deep fracture with downhole electrode in body.

other two dimensions. For the most part, we have standardized the aspect ratios of the target dimensions at 10:10:1. While the effect of varying the contrast in resistivity has been examined,

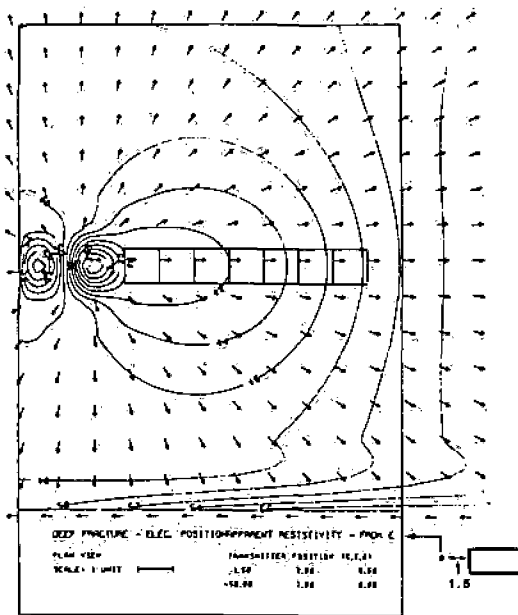


FIGURE 3b.

Surface resistivity anomaly due to deep fracture with downhole electrode at side of body.

most of the results are for the case of a fracture zone ten times more conductive than the host rocks.

Four numerical techniques have been utilized in the studies; three have been applied with the D.C. resistivity method. The techniques applied to the resistivity problem are (1) a 3D surface integral equation (Yang and Ward, 1985a,b), (2) a 3D volume integral equation (Beasley and Ward, 1986), and (3) a 2D finite element method (Zhao et al., 1985). A solution for the time domain EM method has also been obtained which uses a 3D volume integral equation formulation (West and Ward, 1985). Elaboration on these four approaches is given below.

Yang and Ward (1985a,b) present theoretical results relating to the detection of thin oblate spheroids and ellipsoids of arbitrary attitude. The effects of the surface of the earth are neglected and the body is assumed to be enclosed within an infinite homogeneous mass. The surface of the body is divided into a series of sub-surfaces, and a numerical solution of the Fredholm integral equation is applied. Once a solution for the surface charge distribution is determined, the potential can be specified anywhere by means of Coulomb's law. The theoretical model results indicate that cross-borehole resistivity measurements are a more effective technique than single-borehole measurements for delineating resistivity anomalies in the vicinity of a borehole.

Figure 4a shows cross-borehole resistivity responses of a vertical conductive fracture zone between two boreholes. The electrode configuration is the pole-pole array with electrode B fixed and electrode M moving in the second borehole. Several curves are plotted depending on the distance between the fracture and the second borehole. The larger anomalies occur when the second

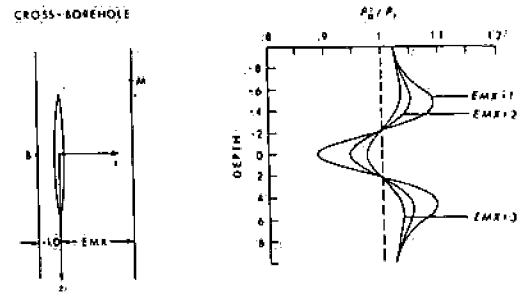


FIGURE 4a

Downhole cross-borehole resistivity anomalies for vertical fracture showing effect of varying distance from fracture to second borehole.

Electrode Configuration	Body Size	Angles	Resistivity Contrast
Fixed Source Moving Electrode SBX=1.0 SBY=SBZ=0 EMX=0	a=0.1e b=2 (u) c=0.2 (u)	$\alpha=0^\circ$ $\beta=90^\circ$ $\gamma=0^\circ$	$\frac{P_2}{P_1} = 0.10$

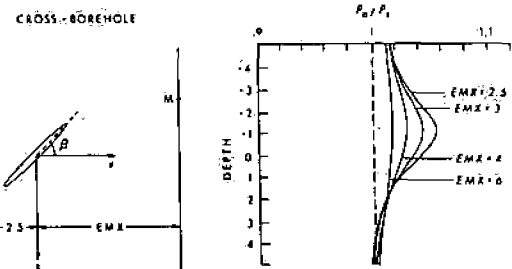


FIGURE 4b

Downhole cross-borehole resistivity anomalies for dipping fracture showing effect of varying distance from fracture to second borehole.

Electrode Configuration	Body Size	Angles	Resistivity Contrast
Fixed Source Moving Electrode SBX=7.5 SBY=SBZ=0 EMX=0	a=1 b=2 c=0.2	$\alpha=0^\circ$ $\beta=45^\circ$ $\gamma=0^\circ$	$\frac{P_2}{P_1} = 0.10$

borehole is nearer to the fracture zone. Figure 4b shows anomalies for the same situation as Figure 4a except that now the fracture dips toward the first borehole. Figure 4c shows the effect of varying the resistivity contrast between a dipping fracture and the host medium. As expected, the large contrast cases produce the largest anomalies. Figure 4d shows the change in anomaly shape for the dipping fracture when four electrodes are placed downhole instead of two (compare with Fig. 4b, EMX = 2.5). By study of a large suite of such graphs as these, the comparative capabilities of the various possible cross-borehole arrays can be determined.

The volume integral equation approach of Beasley and Ward (1986) incorporates a half-space formulation, i.e. the earth's surface is not neglected. As with the surface integral equation technique of Yang and Ward (1985a,b), the volume integral equation method requires that only inhomogeneities be discretized. Any number of inhomogeneities of differing sizes and physical properties can be accounted for by this algorithm. Inhomogeneities are discretized into rectangular cells whose size may vary in each of

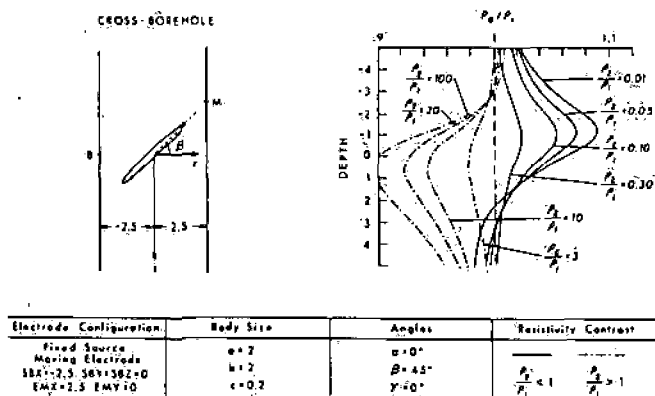


FIGURE 4c

Downhole cross-borehole resistivity anomalies for dipping fracture showing the effect of varying resistivity contrast between fracture and host medium.

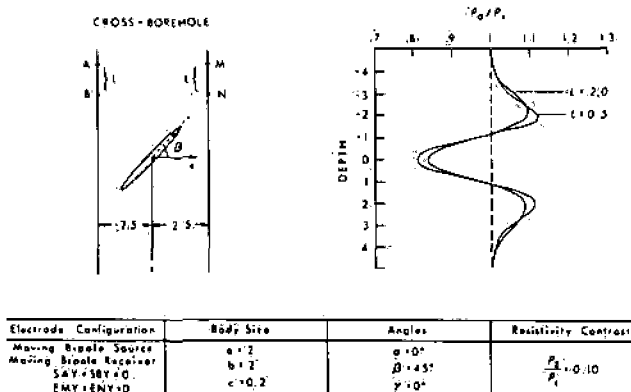


FIGURE 4d

Downhole cross-borehole resistivity anomalies for dipping fracture showing the effect of dipole length for downhole electrodes.

the three directions. The fact that targets must be comprised of rectangular or cubic cells means that dipping bodies must be simulated by cells arranged in a staircase fashion. Section and plan views of computed apparent resistivities are the end product of this algorithm. The algorithm is flexible in that it permits a buried electrode to be placed either inside (mise-à-la-masse) or outside (near-miss) the body. The dip of the body and the location of the energizing electrode within it were both varied. The maximum depth at which a body could be located and still produce a detectable anomaly on surface surveys was found to be dependent, as expected, upon the position of the buried electrode and upon the contrast in resistivity between the body and the host. It was found that locating the buried electrode just outside the body did not significantly alter the results from those when the electrode is embedded in the inhomogeneity.

Figures 5a, 5b and 5c show representative results from Beasley and Ward (1986). Each figure is a vertical section through the earth with contours of the resistivity anomaly. A borehole can be placed anywhere on this figure and the resistivity curve that would be observed in such a

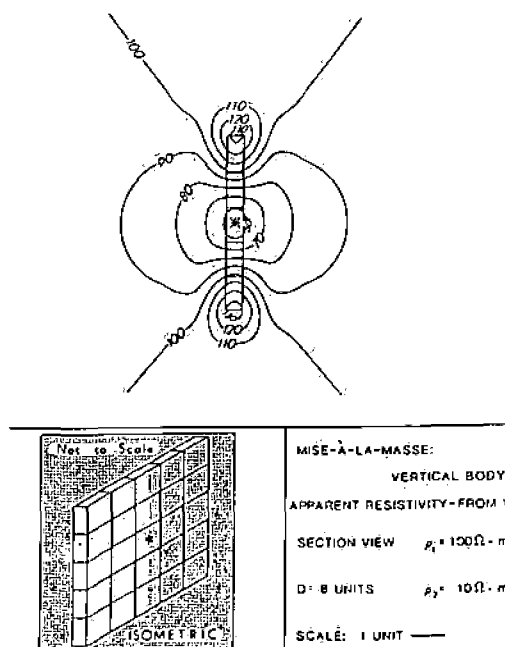


FIGURE 5a

Subsurface resistivity contours for a vertical permeable zone with an imbedded downhole current source.

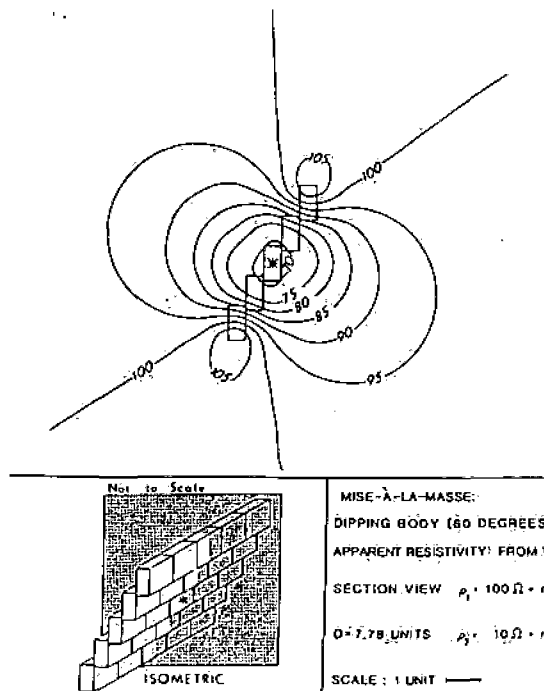


FIGURE 5b

Subsurface resistivity contours for a dipping permeable zone with an imbedded downhole current source.

borehole with a single downhole potential electrode would be given by the intersection of the borehole with the contours. The downhole current electrode source is shown by the star.

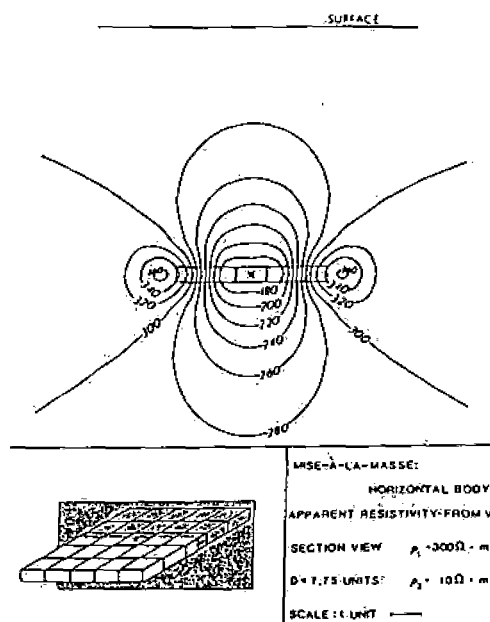


FIGURE 5c  
Subsurface resistivity contours for a horizontal permeable zone with an imbedded downhole current source.

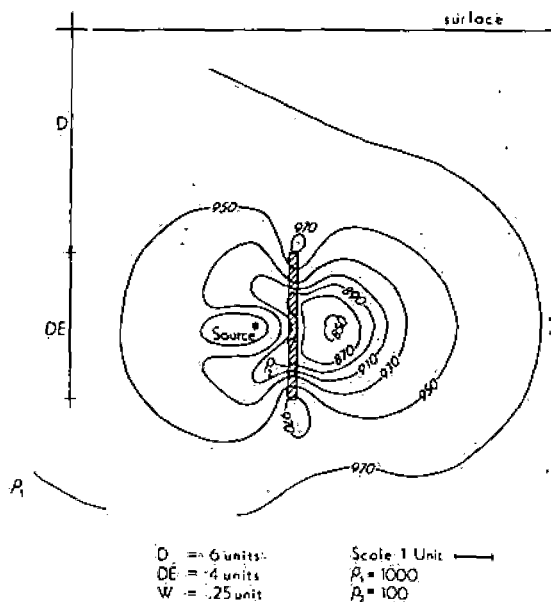


FIGURE 6a  
Subsurface resistivity contours for a vertical permeable zone with current source to the side.

Our most versatile algorithm for the borehole resistivity method is the 2-D finite element algorithm used by Zhao et al. (1985). The versatility of this algorithm arises from the fact that the entire subsurface is discretized. Since triangular elements are used for discretization, dipping bodies are readily handled. The algorithm also accommodates a layered-earth host environment. This algorithm was used to evaluate signal-to-noise ratio for various types of noise.

Figures 6a and 6b show typical results from

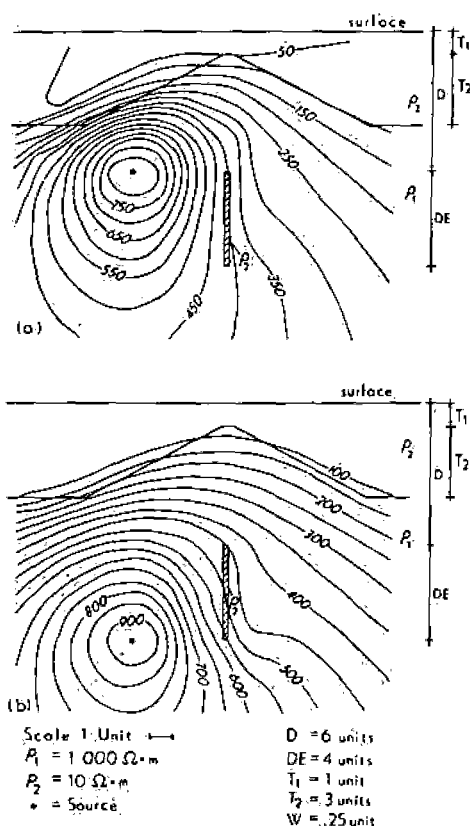


FIGURE 6b  
Subsurface resistivity contours for a vertical permeable zone beneath geologic structure with varying positions of the downhole current electrode.

Zhao et al. (1985). Figure 6a shows subsurface resistivity contours in section for a vertical fracture with a current source outside the body. This plot is similar to those given by Beasley and Ward (1986) in Figures 5a, 5b and 5c. Figure 6b illustrates how subsurface topography due to geologic structure affects results. Note that the anomaly due to the fracture is obscured to a great extent by the resistivity pattern created by the contact. This is due in part also to the relatively large distance of the fracture from the downhole current source, shown by the star. A current source in a borehole closer to the fracture would cause a much clearer anomaly.

All computations by Yang and Ward (1985a,b) and Zhao et al. (1985) were performed on an HP9826 desk top computer with 1.6 Mbytes of memory. The algorithm used by Zhao et al. (1985) is currently being extended to 3-D. It is probable that the HP9826 will accommodate the 3-D version. If so, these modeling programs could easily be used in the field with no need to return to a large computing facility.

From the above studies we tentatively conclude the following: the cross-borehole method produces larger anomalies than does a single-borehole method; the cross-borehole anomalies using a pole-pole array are smaller than those for a cross-borehole dipole-dipole array; the cross-borehole mise-à-la-masse method produces larger anomalies than for the other cross-borehole

methods; and, the anomalies due to a thin sheet were generally much smaller than those for a sphere, as is to be expected.

Using a 3-D integral equation algorithm developed by San Filippo and Hohmann (1985), West and Ward (1985) performed a model study to evaluate the time-domain electromagnetic (TDEM) response of a horizontal conductive body (fracture zone) imbedded in a half-space. Simplifying assumptions in the algorithm allow modeling only of bodies with two vertical symmetry planes with sources directly above or below. The source transmitter is a large square loop located on the surface of the earth. Receivers are located in boreholes at various locations in the vicinity of the body. Responses are computed at 60 time steps at intervals of 0.4 ms for a total data window of 24 ms. EM field decay curves and plots of decay versus depth are obtained for all three components of the primary, secondary, and total responses. The results are expressed in terms of percent difference plots, and are still under study at this time.

Surface-to-borehole EM in which a large transmitter is coaxial with the well and a down-hole detector is run in the well may provide useful information on the location of conductive fractures intersecting the wellbore. Whether this technique will work in cased wells and whether a "crack" anomaly can be distinguished from a stratigraphic conductor are topics under study.

The above discussion outlines our research to date. Other current research involves a model study using the VLF (very low-frequency) method as well as developing a borehole inversion scheme using the finite-element technique. Inversion of the 3D integral equation is also being investigated. An inversion scheme which can incorporate multi-array data is an ultimate goal. Interpretation of complex borehole field data from geothermal sites may then become a reality.

#### DISCUSSION

The problem of selecting an appropriate borehole electrical system is quite complex. Variables include where to place the electrodes, i.e. how many on the surface and how many down each borehole, and whether to use direct-current galvanic resistivity, which each of the above figures illustrate, or some alternating current, electromagnetic scheme. It is clear that the computer based study of these questions is cost effective in helping select and design an optimum field system.

Our current opinion is that the more data one can collect the better one should be able to characterize the subsurface. We have therefore been making a preliminary investigation of the design of a system for obtaining both borehole-to-borehole and borehole-to-surface data simultaneously. Such a scheme is conceptually illustrated in Figure 7. We believe we are nearing the stage when a field system can be designed with the very real hope of yielding much more subsurface information than can be realized by presently available systems.

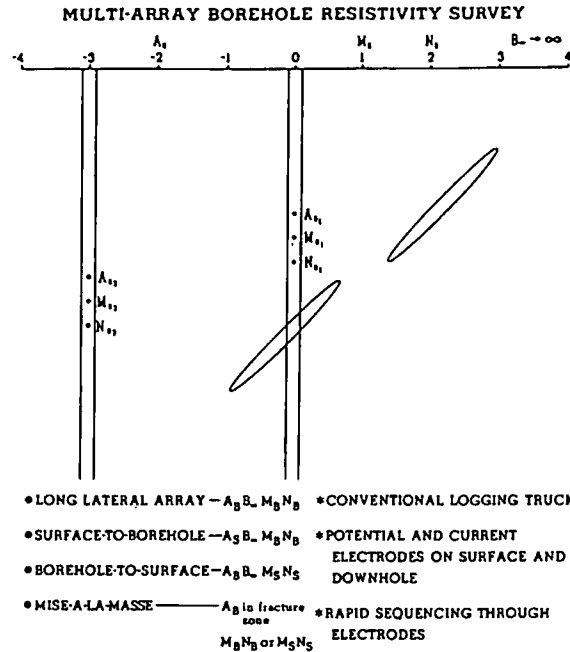


FIGURE 7  
Conceptual illustration of a multi-array borehole resistivity system.

#### REFERENCES

- Beasley, C. W., and Ward, S. H., 1986, Three-dimensional mise-à-la-masse modeling applied to mapping fracture zones: *Geophysics*, 51, January.
- Brace, W. F., 1968, The mechanical effects of pore pressure on the fracturing of rocks: *Geol. Survey Canada, Paper 68-52*.
- Daniels, J. J., 1977, Three-dimensional resistivity and induced-polarization modeling using buried electrodes: *Geophysics*, 42, 1006-1019.
- Daniels, J. J., 1983, Hole-to-surface resistivity measurements: *Geophysics*, 48, 897-97.
- Dobecki, T. L., 1980, Borehole resistivity curves near spheroidal masses: *Geophysics*, 45, 1513-1521.
- Glenn, W. E., and Hulen, J. B., 1979, A study of well logs from Roosevelt Hot Springs KGRA, Utah: in *SPWLA 20th Ann. Logging Sympos. Trans.*, II.
- Glenn, W. E., and Ross, H. P., 1982, A study of well logs from Cove Fort-Sulphurdale KGRA, Utah: *Univ. Res. Inst., Earth Sci. Lab.*, rep. 75.
- Grindly, G. W., and Browne, P. R. L., 1976, Structural and hydrological factors controlling the permeabilities of some hot-water geothermal fields: in *Proc. Second United Nations Sympos. on the Development and Use of Geoth. Res.*, San Francisco, 1, 377-386.

- Halfman, S. E., Lippmann, M. J., Zelwer, R., and Howard, J. H., 1984, Geologic interpretation of geothermal fluid movement in Cerro Prieto Field, Baja, California, Mexico: Bull. Am. Assn. Petr. Geol., 68, 18-30.
- Hohmann, G. W., 1975, Three-dimensional induced-polarization and electromagnetic modeling: Geophysics, 40, 309-324.
- Keys, W. S., and Sullivan, J. K., 1979, Role of borehole geophysics in defining the physical characteristics of the Raft River geothermal reservoir, Idaho: Geophysics, 44, 1116-1141.
- Mackelprang, C. E., 1985, A catalogue of total horizontal electric field resistivity models using three-dimensional conductive bodies and a downhole current electrode: Earth Sci. Lab., Univ. Utah Research Inst. Rept., in press.
- Moore, J. N., Adams, M. C., and Stauder, J. J., 1985, Geologic and geochemical investigations of the Meager Creek geothermal system, British Columbia, Canada: Proc. Tenth Workshop on Geoth. Res. Eng., Stanford Univ., Stanford, CA.
- Newkirk, D. J., 1982, Downhole electrode resistivity interpretation with three-dimensional models: Masters Thesis, Dept. of Geology and Geophys., Univ. of Utah.
- Oristaglio, M. L., 1985, A guide to the current uses of vertical seismic profiles: Geophysics, 50, in press.
- San Filippo, W. A., and Hohmann, G. W., 1985, Integral equation solution for the transient electromagnetic response of a three-dimensional body in a conductive half-space: Geophysics, 50, 798-809.
- Sanyal, S. K., Wells, L. E., and Bickham, R. E., 1980, Geothermal well log interpretation state of the art - Final report: Los Alamos Scientific Lab. Rep. LA-8211-MS.
- West, R. C., and Ward, S. H., 1985, The borehole transient EM response of a three-dimensional fracture zone in a conductive half-space: to be submitted to Geophysics.
- Yang, F. W., and Ward, S. H., 1985a, Single- and cross-borehole resistivity anomalies of thin ellipsoids and spheroids: Geophysics, 50, 637-655.
- Yang, F. W., and Ward, S. H., 1985b, On sensitivity of surface-to-borehole resistivity measurements to the attitude and the depth to the center of a 3-D oblate spheroid: Geophysics, 50, 1173-1178.
- Zhao, J. X., Rijo, L., and Ward, S. H., 1985, Evaluation of the ratio of signal-to-noise in cross-borehole electrical surveys: submitted to Geophysics.



## BOREHOLE GEOPHYSICAL TECHNIQUES FOR DEFINING PERMEABLE ZONES IN GEOTHERMAL SYSTEMS

Phillip M. Wright and Stanley H. Ward

Earth Science Laboratory  
University of Utah Research Institute  
391 Chipeta Way, Suite C  
Salt Lake City, Utah 84108

### ABSTRACT

Borehole electrical geophysical methods have considerable potential for helping to define hot and permeable zones in geothermal systems. Borehole geophysics differs from geophysical well logging and has a much greater area of search around a borehole. Very little developmental work has taken place in borehole electrical methods to date. At UURI, we have been developing computer methods to model various electrical arrays for borehole configurations. We plan to compare the several possible survey methods and then design a field system based on the method that appears from the computer studies to be optimum.

From our studies to date we tentatively conclude that the cross-borehole method produces larger anomalies than does the single-borehole method; cross-borehole anomalies using a pole-pole array are smaller than those for a dipole-dipole array; the cross-borehole *mise-à-la-masse* method produces larger anomalies than does other cross-borehole methods; and, the anomalies due to a thin structure are generally much smaller than those for a sphere, as is to be expected.

### INTRODUCTION

The key problem worldwide in development of hydrothermal resources appears to be more in locating permeable zones than in locating high temperatures. Grindly and Browne (1976) note that of 11 hydrothermal fields investigated in New Zealand, all of which have high temperatures (230°C to 300°C), five are non-productive chiefly because of low permeability. Three of the eleven fields are in production (Wairakei, Kawerau and Broadlands) and in each of these fields permeability limits production more than temperature does. Hot but unproductive holes have been drilled at many of the major geothermal areas in the world, including The Geysers, Roosevelt Hot Springs, Coso, and Meager Creek, to name a few.

Permeability can be primary or secondary. Primary permeability in clastic rocks originates from intergranular porosity and it generally decreases with depth due to compaction and cementation. In volcanic sequences, primary intergranular porosity and permeability exist, but greater permeability exists in open spaces at flow contacts and within the flows themselves. Primary permeability in crystalline igneous rocks is generally very low. Secondary permeability occurs in all rock types in open fault zones, fractures

and fracture intersections, along dikes and in breccia zones (Brace, 1968; Moore et al., 1985). Changes in permeability come about through mineral deposition in open spaces or by leaching by the thermal fluids.

Although none of the geophysical methods maps permeability directly, any geological, geochemical, or hydrological understanding of the factors that control the permeability in a geothermal reservoir can be used to help determine geophysical methods potentially useful for detecting the boundaries and more permeable parts of a hydrothermal system. At UURI, we have been developing electrical borehole techniques to detect and map permeable zones in the subsurface, especially fractures.

### BACKGROUND--BOREHOLE GEOPHYSICS

It is important to understand the differences between geophysical well logging and borehole geophysics. In geophysical well logging, the instruments are deployed in a single well in a tool or sonde, and the depth of investigation is usually limited to the first few meters from the well-bore. Well-logging techniques have been developed by the petroleum industry over a period of half a century and have been applied with variable success by the geothermal industry. The major adaptations to the geothermal environment are the requirements of high temperature tools and the different interpretation required for hard rock (volcanic, igneous) lithologies. Other differences include a strong emphasis in geothermal exploration on fracture identification and the effects of hydrothermal alteration upon certain log responses. Much research remains to be done in order to understand fully the responses of various well logs in geothermal reservoirs and their typically fractured, altered, commonly igneous and metamorphic host rocks. In spite of the relative lack of knowledge of well-log response in geothermal reservoirs, several logs or log combinations have been used successfully to investigate such properties as lithology, alteration, fracturing, density, porosity, fluid flow and sulfide content, all of which may be critical in deciding how and in what intervals to complete, case, cement or stimulate a well (Glenn and Hulen, 1979; Keys and Sullivan, 1979; Sanyal et al., 1980; Glenn and Ross, 1982; Halfman et al., 1982).

By contrast, borehole geophysics refers to those geophysical techniques where energy sources and sensors are deployed (1) at wide spacing in a

single borehole, (2) partly in one borehole and partly on the surface, or (3) partly in one borehole and partly in a second borehole. Thus, we speak of borehole-to-surface, surface-to-borehole and borehole-to-borehole surveys. The depth of investigation is generally much greater in borehole geophysical surveys than it is in geophysical well logging.

Only one of the several borehole geophysical techniques, namely vertical seismic profiling (VSP), has been developed to any extent. The petroleum industry has funded relatively rapid development of VSP over the past several years.

VSP

Vertical seismic profiling (VSP) can be done using both P- and S-wave surface sources (usually mechanical vibrators) arranged circumferentially around a well. Direct and reflected seismic waves are detected by strings of down-hole geophones clamped to the wall of the well or by hydrophones. VSP has been used mainly to trace seismic events observed at the surface to their point of origin in the earth and to obtain better estimates for the acoustic properties of a stratigraphic sequence. Oristaglio (1985) presents a guide to the current uses of VSP.

Borehole Electrical Techniques

Borehole-to-borehole and borehole-to-surface electrical methods appear to have considerable potential for application to geothermal exploration. In a benchmark introductory paper, Daniels (1983) illustrated the utility of hole-to-surface resistivity measurements with a detailed study of an area of volcanic tuff near Yucca Mountain, Nevada. He obtained total-field resistivity data for a grid of points on the surface with current sources in three drill holes, completed a layered-earth reduction of the data, and interpreted the residual resistivity anomalies with a 3D ellipsoidal modeling technique.

The borehole electrical techniques, however, are in general poorly developed. One reason for this is that there are a large number of ways that borehole electrical surveys can be performed and it has been unclear which methods are best. At the same time, computer algorithms to model the several methods have not existed so that it has not been possible to select among methods prior to committing to the expense of building a field system and obtaining test data.

R&D PROGRAM AT UURI

The objective of our program is to develop and demonstrate the use of borehole electrical techniques in geothermal exploration, reservoir delineation and reservoir exploitation. Our approach is:

1. Develop computer techniques to model the possible borehole electrical survey systems;
2. Design and construct a field data acquisition system based on the results of (1);
3. Acquire field data at sites where the nature and extent of permeability are known; and,

4. Develop techniques to interpret field data.

To the present time, we have made considerable progress on item (1) above and we are now at such a point that item (2) could be started.

Our research staff has consisted of the following personnel: Stanley H. Ward, Project Manager; Luis Rijo, Professor of Geophysics, Universidade Federal Do Para, Brazil (on 2-year post-doctoral leave at U of U and UURI); F. W. Yang, Peoples Republic of China (visiting scholar); J. X. Zhao, Peoples Republic of China (visiting scholar); Craig W. Beasley (doctoral candidate U of U, awarded MS degree); Richard C. West (MS candidate at UU). Additional technical support has been provided by Phillip E. Wannamaker, Howard P. Ross and Phillip M. Wright of UURI and by Gerald W. Hohmann of U of U. Project costs for Rijo, Yang and Zhao have been minimal because these scientists have been supported by their governments. Thus, a great deal has been accomplished at minimal cost while supporting the education of several students. The remainder of this paper will discuss the significance of our research to date.

COMPUTER MODELING OF BOREHOLE ELECTRICAL METHODS

Computer techniques for modeling borehole electrical geophysics have largely been lacking, especially for three-dimensional (3D) cases. Figure 1 indicates conventional usage of the terms 1D, 2D and 3D in geophysical interpretation. In the 1D case, also called the "layered earth" case, the physical property of interest (resistivity for this study), varies only in the vertical direction. In the 2D case, physical property variations in the vertical and one horizontal dimension are allowed, and the anomalous body illustrated has the same shape in and out of the paper for infinite distance. In the 3D case, physical property variations are specified in all three space dimensions. Obviously, the real earth is only occasionally 1D in nature in geothermal areas. The usual case is for physical properties to vary in all three dimensions in the earth, the 3D case. However, the mathematical formulations for electrical anomalies of bodies increase greatly in complexity from the 1D case to the 3D case. This accounts for the fact that in order to begin our task of applying borehole electrical techniques to delineation of permeability, we were required to develop original mathematical formulations of the problem.

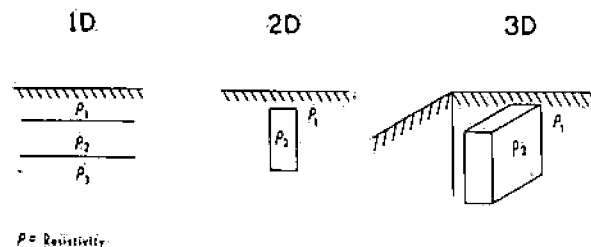


FIGURE 1  
Illustration of the meaning of the terms 1D, 2D and 3D in geophysical modeling.

Thick-Body Studies

Prior to 1982, only three published papers considered computer modeling of downhole electrodes for three-dimensional bodies. Daniels (1977) studied six buried electrode configurations and plotted normalized apparent resistivity or apparent polarizability against such configuration parameters as 1) source and receiver depth, 2) depth/bipole length, 3) receiver distance from body, 4) depth of body, and 5) distance of source and receiver from body center. Snyder and Merkel (1973), computed the IP and apparent resistivity responses resulting from a buried current pole in the presence of a buried sphere. Their plots are center-line profiles for normalized apparent resistivity and normalized IP response. Dobecki (1980) computed the effects of spheroidal bodies as measured in nearby single boreholes using the pole-pole electrode array. These three studies are obviously very limited in terms of the problems of defining permeability in geothermal systems.

In 1982, Newkirk (1982) from our group published a study of downhole electrical resistivity with 3D bodies. Using a numerical modeling technique described by Hohmann (1975), theoretical anomalies due to a three-dimensional body composed of simple prisms were computed. The results were presented in terms of 1) the potential, 2) the apparent resistivity calculated from the total horizontal electric field and 3) the apparent resistivity calculated from the potential. Two electrode configurations were considered for each model. Each configuration consisted of a pair of electrodes, where one of the electrodes was remote and the second electrode was located either in the body, for *mise-à-la-masse* or applied potential, or outside the body, simulating a near miss. Newkirk's computer program was used by Mackelprang (1985) of our group to compute a catalog of models due to bodies that might be of interest in detection of thick fracture zones.

Figures 2a and 2b show the conventions used by Newkirk (1982) and Mackelprang (1985) in calculations of the effects of 3D bodies. The bodies are buried in a homogeneous earth and two of many options for a downhole point electrode are illustrated. Figure 3a and 3b illustrate anomalies on a surface resistivity survey produced by a narrow conductive body buried at a depth of 7 units with the electrode in the body (Fig. 3a) and off the end of the body (Fig. 3b). The peanut shaped anomaly shown in Figure 3a is particularly characteristic on surface resistivity surveys with the borehole electrode in the body.

One basic shortcoming of Newkirk's (1982) algorithm is that it does not apply when the anomalous body becomes thin, i.e. to the case of delineation of fractures or thin fracture zones. To address this important problem, the thin-body studies described in the next section have been undertaken.

Thin-Body Studies

These studies are aimed at targets simulating fracture zones which are thin relative to their

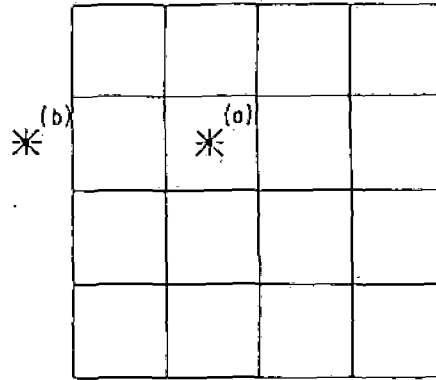


FIGURE 2a  
Plan view of standard model.

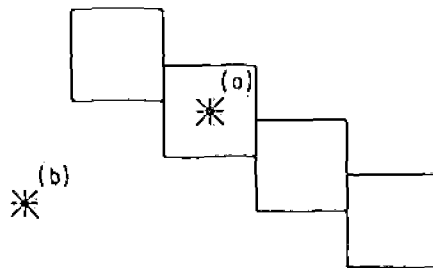


FIGURE 2b  
Cross-section view of standard model.

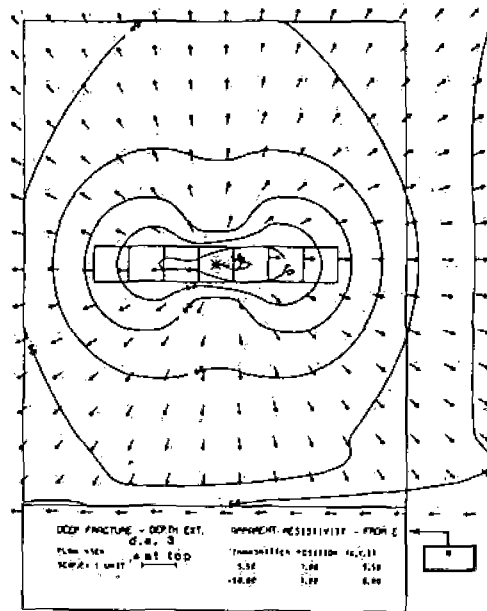


FIGURE 3a  
Surface resistivity anomaly due to deep fracture with downhole electrode in body.

other two dimensions. For the most part, we have standardized the aspect ratios of the target dimensions at 10:10:1. While the effect of varying the contrast in resistivity has been examined,

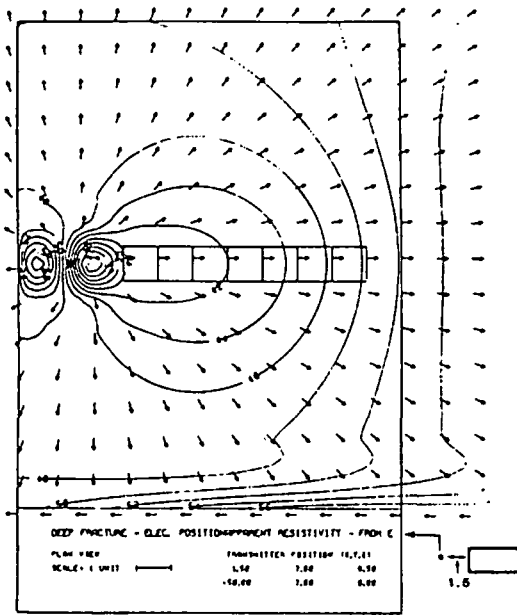


FIGURE 3b

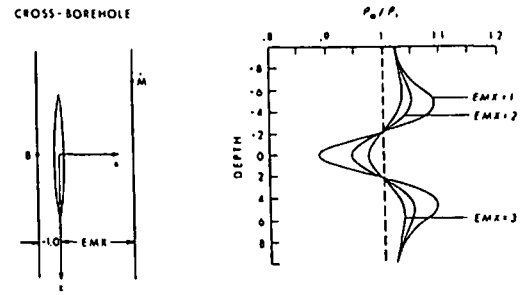
Surface resistivity anomaly due to deep fracture with downhole electrode at side of body.

most of the results are for the case of a fracture zone ten times more conductive than the host rocks.

Four numerical techniques have been utilized in the studies; three have been applied with the D.C. resistivity method. The techniques applied to the resistivity problem are (1) a 3D surface integral equation (Yang and Ward, 1985a,b), (2) a 3D volume integral equation (Beasley and Ward, 1986), and (3) a 2D finite element method (Zhao et al., 1985). A solution for the time domain EM method has also been obtained which uses a 3D volume integral equation formulation (West and Ward, 1985). Elaboration on these four approaches is given below.

Yang and Ward (1985a,b) present theoretical results relating to the detection of thin oblate spheroids and ellipsoids of arbitrary attitude. The effects of the surface of the earth are neglected and the body is assumed to be enclosed within an infinite homogeneous mass. The surface of the body is divided into a series of sub-surfaces, and a numerical solution of the Fredholm integral equation is applied. Once a solution for the surface charge distribution is determined, the potential can be specified anywhere by means of Coulomb's law. The theoretical model results indicate that cross-borehole resistivity measurements are a more effective technique than single-borehole measurements for delineating resistivity anomalies in the vicinity of a borehole.

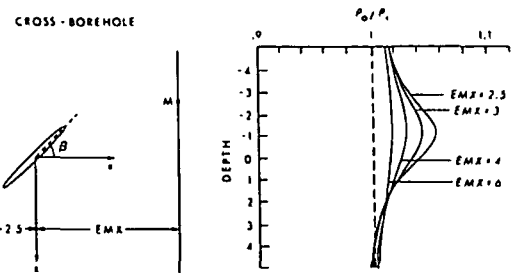
Figure 4a shows cross-borehole resistivity responses of a vertical conductive fracture zone between two boreholes. The electrode configuration is the pole-pole array with electrode B fixed and electrode M moving in the second borehole. Several curves are plotted depending on the distance between the fracture and the second borehole. The larger anomalies occur when the second



Electrode Configuration	Body Size	Angles	Resistivity Contrast
Fixed Source Moving Electrode SBX = -10 SBY = SBZ = 0 EMY = 0	a = 0 (z) b = 2 (y) c = 0.2 (x)	alpha = 0° beta = 90° gamma = 0°	$\frac{\rho_2}{\rho_1} = 0.10$

FIGURE 4a

Downhole cross-borehole resistivity anomalies for vertical fracture showing effect of varying distance from fracture to second borehole.



Electrode Configuration	Body Size	Angles	Resistivity Contrast
Fixed Source Moving Electrode SBX = -2.5 SBY = SBZ = 0 EMY = 0	a = 2 b = 7 c = 0.2	alpha = 0° beta = 45° gamma = 0°	$\frac{\rho_2}{\rho_1} = 0.10$

FIGURE 4b

Downhole cross-borehole resistivity anomalies for dipping fracture showing effect of varying distance from fracture to second borehole.

borehole is nearer to the fracture zone. Figure 4b shows anomalies for the same situation as Figure 4a except that now the fracture dips toward the first borehole. Figure 4c shows the effect of varying the resistivity contrast between a dipping fracture and the host medium. As expected, the large contrast cases produce the largest anomalies. Figure 4d shows the change in anomaly shape for the dipping fracture when four electrodes are placed downhole instead of two (compare with Fig. 4b, EMX = 2.5). By study of a large suite of such graphs as these, the comparative capabilities of the various possible cross-borehole arrays can be determined.

The volume integral equation approach of Beasley and Ward (1986) incorporates a half-space formulation, i.e. the earth's surface is not neglected. As with the surface integral equation technique of Yang and Ward (1985a,b), the volume integral equation method requires that only inhomogeneities be discretized. Any number of inhomogeneities of differing sizes and physical properties can be accounted for by this algorithm. Inhomogeneities are discretized into rectangular cells whose size may vary in each of

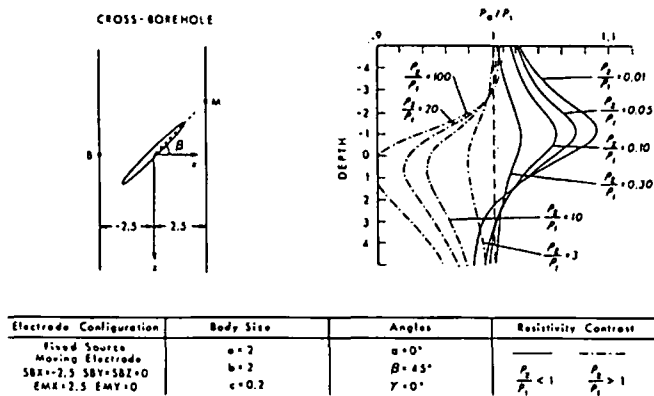


FIGURE 4c

Downhole cross-borehole resistivity anomalies for dipping fracture showing the effect of varying resistivity contrast between fracture and host medium.

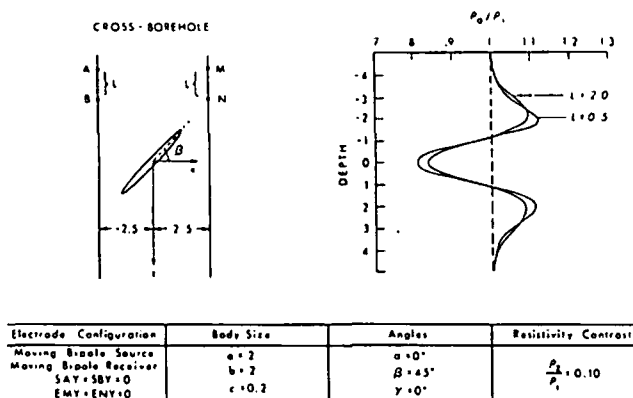


FIGURE 4d

Downhole cross-borehole resistivity anomalies for dipping fracture showing the effect of dipole length for downhole electrodes.

the three directions. The fact that targets must be comprised of rectangular or cubic cells means that dipping bodies must be simulated by cells arranged in a staircase fashion. Section and plan views of computed apparent resistivities are the end product of this algorithm. The algorithm is flexible in that it permits a buried electrode to be placed either inside (mise-à-la-masse) or outside (near-miss) the body. The dip of the body and the location of the energizing electrode within it were both varied. The maximum depth at which a body could be located and still produce a detectable anomaly on surface surveys was found to be dependent, as expected, upon the position of the buried electrode and upon the contrast in resistivity between the body and the host. It was found that locating the buried electrode just outside the body did not significantly alter the results from those when the electrode is embedded in the inhomogeneity.

Figures 5a, 5b and 5c show representative results from Beasley and Ward (1986). Each figure is a vertical section through the earth with contours of the resistivity anomaly. A borehole can be placed anywhere on this figure and the resistivity curve that would be observed in such a

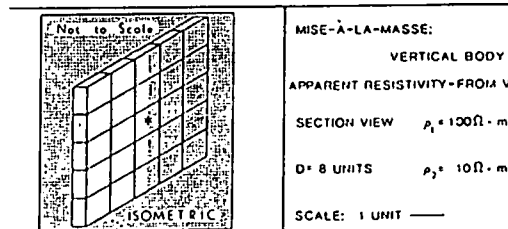
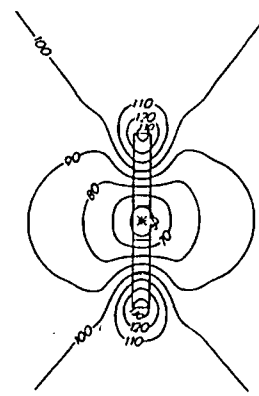


FIGURE 5a

Subsurface resistivity contours for a vertical permeable zone with an imbedded downhole current source.

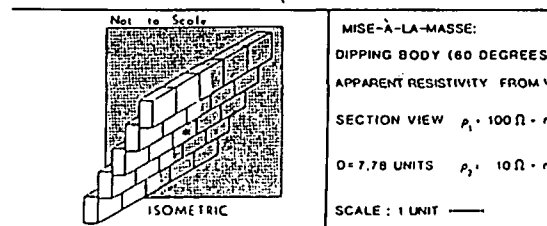
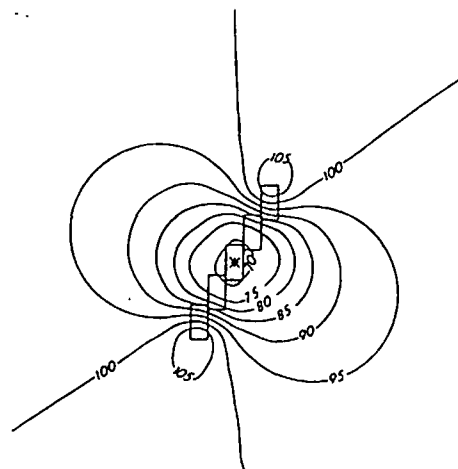


FIGURE 5b

Subsurface resistivity contours for a dipping permeable zone with an imbedded downhole current source.

borehole with a single downhole potential electrode would be given by the intersection of the borehole with the contours. The downhole current electrode source is shown by the star.

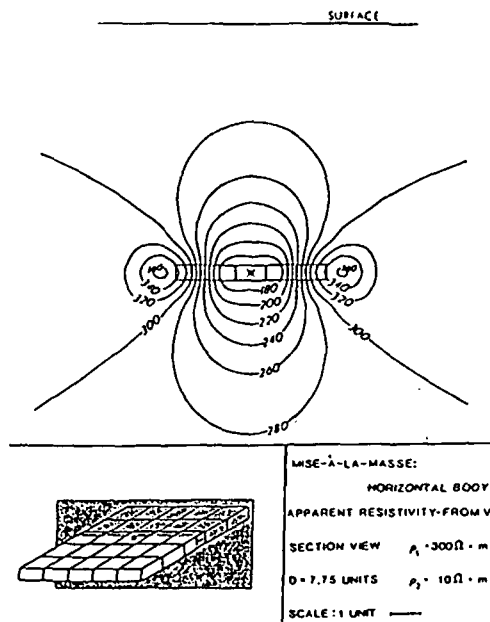


FIGURE 5c  
Subsurface resistivity contours for a horizontal permeable zone with an imbedded downhole current source.

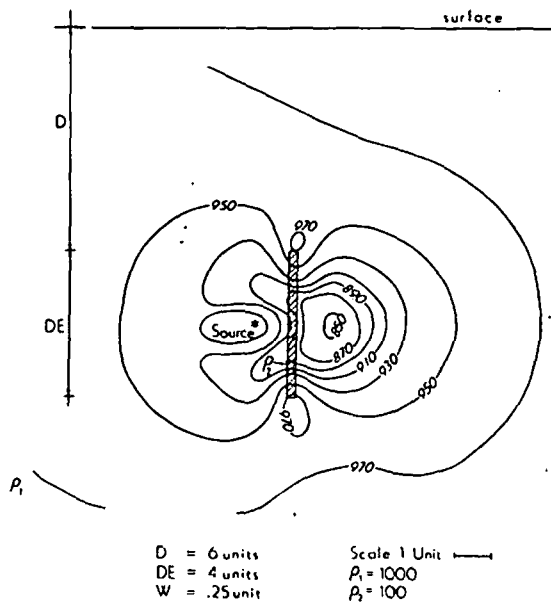


FIGURE 6a  
Subsurface resistivity contours for a vertical permeable zone with current source to the side.

Our most versatile algorithm for the borehole resistivity method is the 2-D finite element algorithm used by Zhao et al. (1985). The versatility of this algorithm arises from the fact that the entire subsurface is discretized. Since triangular elements are used for discretization, dipping bodies are readily handled. The algorithm also accommodates a layered-earth host environment. This algorithm was used to evaluate signal-to-noise ratio for various types of noise.

Figures 6a and 6b show typical results from

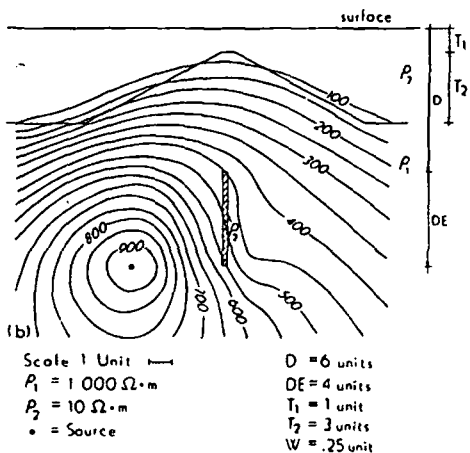
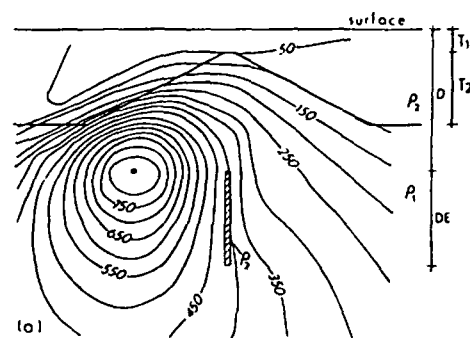


FIGURE 6b

Subsurface resistivity contours for a vertical permeable zone beneath geologic structure with varying positions of the downhole current electrode.

Zhao et al. (1985). Figure 6a shows subsurface resistivity contours in section for a vertical fracture with a current source outside the body. This plot is similar to those given by Beasley and Ward (1986) in Figures 5a, 5b and 5c. Figure 6b illustrates how subsurface topography due to geologic structure affects results. Note that the anomaly due to the fracture is obscured to a great extent by the resistivity pattern created by the contact. This is due in part also to the relatively large distance of the fracture from the downhole current source, shown by the star. A current source in a borehole closer to the fracture would cause a much clearer anomaly.

All computations by Yang and Ward (1985a,b) and Zhao et al. (1985) were performed on an HP9826 desk top computer with 1.6 Mbytes of memory. The algorithm used by Zhao et al. (1985) is currently being extended to 3-D. It is probable that the HP9826 will accommodate the 3-D version. If so, these modeling programs could easily be used in the field with no need to return to a large computing facility.

From the above studies we tentatively conclude the following: the cross-borehole method produces larger anomalies than does a single-borehole method; the cross-borehole anomalies using a pole-pole array are smaller than those for a cross-borehole dipole-dipole array; the cross-borehole mise-à-la-masse method produces larger anomalies than for the other cross-borehole

methods; and, the anomalies due to a thin sheet were generally much smaller than those for a sphere, as is to be expected.

Using a 3-D integral equation algorithm developed by San Filippo and Hohmann (1985), West and Ward (1985) performed a model study to evaluate the time-domain electromagnetic (TDEM) response of a horizontal conductive body (fracture zone) imbedded in a half-space. Simplifying assumptions in the algorithm allow modeling only of bodies with two vertical symmetry planes with sources directly above or below. The source transmitter is a large square loop located on the surface of the earth. Receivers are located in boreholes at various locations in the vicinity of the body. Responses are computed at 60 time steps at intervals of 0.4 ms for a total data window of 24 ms. EM field decay curves and plots of decay versus depth are obtained for all three components of the primary, secondary, and total responses. The results are expressed in terms of percent difference plots, and are still under study at this time.

Surface-to-borehole EM in which a large transmitter is coaxial with the well and a down-hole detector is run in the well may provide useful information on the location of conductive fractures intersecting the wellbore. Whether this technique will work in cased wells and whether a "crack" anomaly can be distinguished from a stratigraphic conductor are topics under study.

The above discussion outlines our research to date. Other current research involves a model study using the VLF (very low-frequency) method as well as developing a borehole inversion scheme using the finite-element technique. Inversion of the 3D integral equation is also being investigated. An inversion scheme which can incorporate multi-array data is an ultimate goal. Interpretation of complex borehole field data from geothermal sites may then become a reality.

#### DISCUSSION

The problem of selecting an appropriate borehole electrical system is quite complex. Variables include where to place the electrodes, i.e. how many on the surface and how many down each borehole, and whether to use direct-current galvanic resistivity, which each of the above figures illustrate, or some alternating current, electromagnetic scheme. It is clear that the computer based study of these questions is cost effective in helping select and design an optimum field system.

Our current opinion is that the more data one can collect the better one should be able to characterize the subsurface. We have therefore been making a preliminary investigation of the design of a system for obtaining both borehole-to-borehole and borehole-to-surface data simultaneously. Such a scheme is conceptually illustrated in Figure 7. We believe we are nearing the stage when a field system can be designed with the very real hope of yielding much more subsurface information than can be realized by presently available systems.

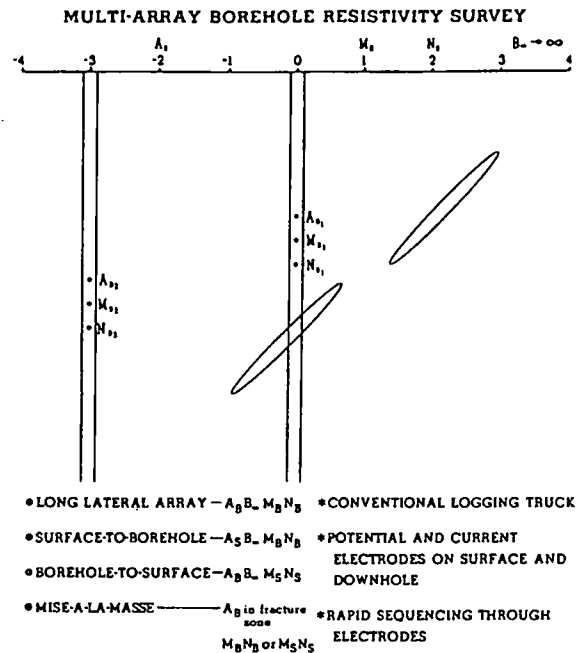


FIGURE 7  
Conceptual illustration of a multi-array borehole resistivity system.

#### REFERENCES

- Beasley, C. W., and Ward, S. H., 1986, Three-dimensional mise-à-la-masse modeling applied to mapping fracture zones: *Geophysics*, 51, January.
- Brace, W. F., 1968, The mechanical effects of pore pressure on the fracturing of rocks: *Geol. Survey Canada, Paper 68-52*.
- Daniels, J. J., 1977, Three-dimensional resistivity and induced-polarization modeling using buried electrodes: *Geophysics*, 42, 1006-1019.
- Daniels, J. J., 1983, Hole-to-surface resistivity measurements: *Geophysics*, 48, 897-97.
- Dobecki, T. L., 1980, Borehole resistivity curves near spheroidal masses: *Geophysics*, 45, 1513-1521.
- Glenn, W. E., and Hulen, J. B., 1979, A study of well logs from Roosevelt Hot Springs KGRA, Utah: in *SPWLA 20th Ann. Logging Sympos. Trans.*, II.
- Glenn, W. E., and Ross, H. P., 1982, A study of well logs from Cove Fort-Sulphurdale KGRA, Utah: *Univ. Res. Inst., Earth Sci. Lab.*, rep. 75.
- Grindly, G. W., and Browne, P. R. L., 1976, Structural and hydrological factors controlling the permeabilities of some hot-water geothermal fields: in *Proc. Second United Nations Sympos. on the Development and Use of Geoth. Res.*, San Francisco, 1, 377-386.

- Halfman, S. E., Lippmann, M. J., Zelwer, R., and Howard, J. H., 1984, Geologic interpretation of geothermal fluid movement in Cerro Prieto Field, Baja, California, Mexico: Bull. Am. Assn. Petr. Geol., 68, 18-30.
- Hohmann, G. W., 1975, Three-dimensional induced-polarization and electromagnetic modeling: Geophysics, 40, 309-324.
- Keys, W. S., and Sullivan, J. K., 1979, Role of borehole geophysics in defining the physical characteristics of the Raft River geothermal reservoir, Idaho: Geophysics, 44, 1116-1141.
- Mackelprang, C. E., 1985, A catalogue of total horizontal electric field resistivity models using three-dimensional conductive bodies and a downhole current electrode: Earth Sci. Lab., Univ. Utah Research Inst. Rept., in press.
- Moore, J. N., Adams, M. C., and Stauder, J. J., 1985, Geologic and geochemical investigations of the Meager Creek geothermal system, British Columbia, Canada: Proc. Tenth Workshop on Geoth. Res. Eng., Stanford Univ., Stanford, CA.
- Newkirk, D. J., 1982, Downhole electrode resistivity interpretation with three-dimensional models: Masters Thesis, Dept. of Geology and Geophys., Univ. of Utah.
- Oristaglio, M. L., 1985, A guide to the current uses of vertical seismic profiles: Geophysics, 50, in press.
- San Filippo, W. A., and Hohmann, G. W., 1985, Integral equation solution for the transient electromagnetic response of a three-dimensional body in a conductive half-space: Geophysics, 50, 798-809.
- Sanyal, S. K., Wells, L. E., and Bickham, R. E., 1980, Geothermal well log interpretation state of the art - Final report: Los Alamos Scientific Lab. Rep. LA-8211-MS.
- West, R. C., and Ward, S. H., 1985, The borehole transient EM response of a three-dimensional fracture zone in a conductive half-space: to be submitted to Geophysics.
- Yang, F. W., and Ward, S. H., 1985a, Single- and cross-borehole resistivity anomalies of thin ellipsoids and spheroids: Geophysics, 50, 637-655.
- Yang, F. W., and Ward, S. H., 1985b, On sensitivity of surface-to-borehole resistivity measurements to the attitude and the depth to the center of a 3-D oblate spheroid: Geophysics, 50, 1173-1178.
- Zhao, J. X., Rijo, L., and Ward, S. H., 1985, Evaluation of the ratio of signal-to-noise in cross-borehole electrical surveys: submitted to Geophysics.



## BOREHOLE GEOPHYSICAL TECHNIQUES FOR DEFINING PERMEABLE ZONES IN GEOTHERMAL SYSTEMS

Phillip M. Wright and Stanley H. Ward

Earth Science Laboratory  
University of Utah Research Institute  
391 Chipeta Way, Suite C  
Salt Lake City, Utah 84108

### ABSTRACT

Borehole electrical geophysical methods have considerable potential for helping to define hot and permeable zones in geothermal systems. Borehole geophysics differs from geophysical well logging and has a much greater area of search around a borehole. Very little developmental work has taken place in borehole electrical methods to date. At UURI, we have been developing computer methods to model various electrical arrays for borehole configurations. We plan to compare the several possible survey methods and then design a field system based on the method that appears from the computer studies to be optimum.

From our studies to date we tentatively conclude that the cross-borehole method produces larger anomalies than does the single-borehole method; cross-borehole anomalies using a pole-pole array are smaller than those for a dipole-dipole array; the cross-borehole *mise-à-la-masse* method produces larger anomalies than does other cross-borehole methods; and, the anomalies due to a thin structure are generally much smaller than those for a sphere, as is to be expected.

### INTRODUCTION

The key problem worldwide in development of hydrothermal resources appears to be more in locating permeable zones than in locating high temperatures. Grindly and Browne (1976) note that of 11 hydrothermal fields investigated in New Zealand, all of which have high temperatures (230°C to 300°C), five are non-productive chiefly because of low permeability. Three of the eleven fields are in production (Wairakei, Kawerau and Broadlands) and in each of these fields permeability limits production more than temperature does. Hot but unproductive holes have been drilled at many of the major geothermal areas in the world, including The Geysers, Roosevelt Hot Springs, Coso, and Meager Creek, to name a few.

Permeability can be primary or secondary. Primary permeability in clastic rocks originates from intergranular porosity and it generally decreases with depth due to compaction and cementation. In volcanic sequences, primary intergranular porosity and permeability exist, but greater permeability exists in open spaces at flow contacts and within the flows themselves. Primary permeability in crystalline igneous rocks is generally very low. Secondary permeability occurs in all rock types in open fault zones, fractures

and fracture intersections, along dikes and in breccia zones (Brace, 1968; Moore et al., 1985). Changes in permeability come about through mineral deposition in open spaces or by leaching by the thermal fluids.

Although none of the geophysical methods maps permeability directly, any geological, geochemical, or hydrological understanding of the factors that control the permeability in a geothermal reservoir can be used to help determine geophysical methods potentially useful for detecting the boundaries and more permeable parts of a hydrothermal system. At UURI, we have been developing electrical borehole techniques to detect and map permeable zones in the subsurface, especially fractures.

### BACKGROUND--BOREHOLE GEOPHYSICS

It is important to understand the differences between geophysical well logging and borehole geophysics. In geophysical well logging, the instruments are deployed in a single well in a tool or sonde, and the depth of investigation is usually limited to the first few meters from the wellbore. Well-logging techniques have been developed by the petroleum industry over a period of half a century and have been applied with variable success by the geothermal industry. The major adaptations to the geothermal environment are the requirements of high temperature tools and the different interpretation required for hard rock (volcanic, igneous) lithologies. Other differences include a strong emphasis in geothermal exploration on fracture identification and the effects of hydrothermal alteration upon certain log responses. Much research remains to be done in order to understand fully the responses of various well logs in geothermal reservoirs and their typically fractured, altered, commonly igneous and metamorphic host rocks. In spite of the relative lack of knowledge of well-log response in geothermal reservoirs, several logs or log combinations have been used successfully to investigate such properties as lithology, alteration, fracturing, density, porosity, fluid flow and sulfide content, all of which may be critical in deciding how and in what intervals to complete, case, cement or stimulate a well (Glenn and Hulen, 1979; Keys and Sullivan, 1979; Sanyal et al., 1980; Glenn and Ross, 1982; Halfman et al., 1982).

By contrast, borehole geophysics refers to those geophysical techniques where energy sources and sensors are deployed (1) at wide spacing in a

single borehole, (2) partly in one borehole and partly on the surface, or (3) partly in one borehole and partly in a second borehole. Thus, we speak of borehole-to-surface, surface-to-borehole and borehole-to-borehole surveys. The depth of investigation is generally much greater in borehole geophysical surveys than it is in geophysical well logging.

Only one of the several borehole geophysical techniques, namely vertical seismic profiling (VSP), has been developed to any extent. The petroleum industry has funded relatively rapid development of VSP over the past several years.

VSP

Vertical seismic profiling (VSP) can be done using both P- and S-wave surface sources (usually mechanical vibrators) arranged circumferentially around a well. Direct and reflected seismic waves are detected by strings of down-hole geophones clamped to the wall of the well or by hydrophones. VSP has been used mainly to trace seismic events observed at the surface to their point of origin in the earth and to obtain better estimates for the acoustic properties of a stratigraphic sequence. Oristaglio (1985) presents a guide to the current uses of VSP.

Borehole Electrical Techniques

Borehole-to-borehole and borehole-to-surface electrical methods appear to have considerable potential for application to geothermal exploration. In a benchmark introductory paper, Daniels (1983) illustrated the utility of hole-to-surface resistivity measurements with a detailed study of an area of volcanic tuff near Yucca Mountain, Nevada. He obtained total-field resistivity data for a grid of points on the surface with current sources in three drill holes, completed a layered-earth reduction of the data, and interpreted the residual resistivity anomalies with a 3D ellipsoidal modeling technique.

The borehole electrical techniques, however, are in general poorly developed. One reason for this is that there are a large number of ways that borehole electrical surveys can be performed and it has been unclear which methods are best. At the same time, computer algorithms to model the several methods have not existed so that it has not been possible to select among methods prior to committing to the expense of building a field system and obtaining test data.

R&D PROGRAM AT UURI

The objective of our program is to develop and demonstrate the use of borehole electrical techniques in geothermal exploration, reservoir delineation and reservoir exploitation. Our approach is:

1. Develop computer techniques to model the possible borehole electrical survey systems;
2. Design and construct a field data acquisition system based on the results of (1);
3. Acquire field data at sites where the nature and extent of permeability are known; and,

4. Develop techniques to interpret field data.

To the present time, we have made considerable progress on item (1) above and we are now at such a point that item (2) could be started.

Our research staff has consisted of the following personnel: Stanley H. Ward, Project Manager; Luis Rijo, Professor of Geophysics, Universidade Federal Do Para, Brazil (on 2-year post-doctoral leave at U of U and UURI); F. W. Yang, Peoples Republic of China (visiting scholar); J. X. Zhao, Peoples Republic of China (visiting scholar); Craig W. Beasley (doctoral candidate U of U, awarded MS degree); Richard C. West (MS candidate at UU). Additional technical support has been provided by Phillip E. Wannamaker, Howard P. Ross and Phillip M. Wright of UURI and by Gerald W. Hohmann of U of U. Project costs for Rijo, Yang and Zhao have been minimal because these scientists have been supported by their governments. Thus, a great deal has been accomplished at minimal cost while supporting the education of several students. The remainder of this paper will discuss the significance of our research to date.

COMPUTER MODELING OF BOREHOLE ELECTRICAL METHODS

Computer techniques for modeling borehole electrical geophysics have largely been lacking, especially for three-dimensional (3D) cases. Figure 1 indicates conventional usage of the terms 1D, 2D and 3D in geophysical interpretation. In the 1D case, also called the "layered earth" case, the physical property of interest (resistivity for this study), varies only in the vertical direction. In the 2D case, physical property variations in the vertical and one horizontal dimension are allowed, and the anomalous body illustrated has the same shape in and out of the paper for infinite distance. In the 3D case, physical property variations are specified in all three space dimensions. Obviously, the real earth is only occasionally 1D in nature in geothermal areas. The usual case is for physical properties to vary in all three dimensions in the earth, the 3D case. However, the mathematical formulations for electrical anomalies of bodies increase greatly in complexity from the 1D case to the 3D case. This accounts for the fact that in order to begin our task of applying borehole electrical techniques to delineation of permeability, we were required to develop original mathematical formulations of the problem.

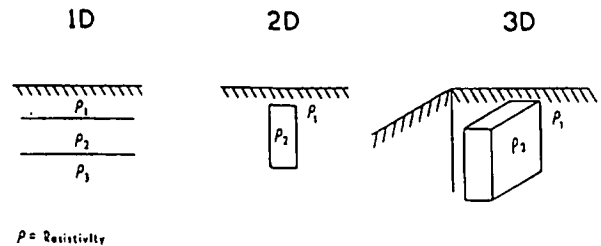


FIGURE 1  
Illustration of the meaning of the terms 1D, 2D and 3D in geophysical modeling.



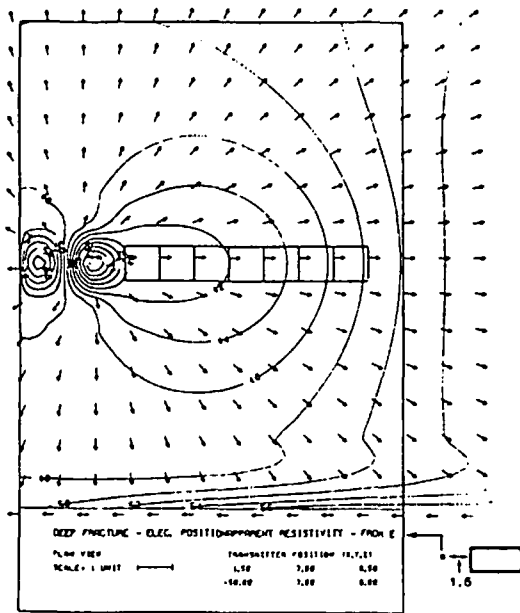


FIGURE 3b

Surface resistivity anomaly due to deep fracture with downhole electrode at side of body.

most of the results are for the case of a fracture zone ten times more conductive than the host rocks.

Four numerical techniques have been utilized in the studies; three have been applied with the D.C. resistivity method. The techniques applied to the resistivity problem are (1) a 3D surface integral equation (Yang and Ward, 1985a,b), (2) a 3D volume integral equation (Beasley and Ward, 1986), and (3) a 2D finite element method (Zhao et al., 1985). A solution for the time domain EM method has also been obtained which uses a 3D volume integral equation formulation (West and Ward, 1985). Elaboration on these four approaches is given below.

Yang and Ward (1985a,b) present theoretical results relating to the detection of thin oblate spheroids and ellipsoids of arbitrary attitude. The effects of the surface of the earth are neglected and the body is assumed to be enclosed within an infinite homogeneous mass. The surface of the body is divided into a series of subsurfaces, and a numerical solution of the Fredholm integral equation is applied. Once a solution for the surface charge distribution is determined, the potential can be specified anywhere by means of Coulomb's law. The theoretical model results indicate that cross-borehole resistivity measurements are a more effective technique than single-borehole measurements for delineating resistivity anomalies in the vicinity of a borehole.

Figure 4a shows cross-borehole resistivity responses of a vertical conductive fracture zone between two boreholes. The electrode configuration is the pole-pole array with electrode B fixed and electrode M moving in the second borehole. Several curves are plotted depending on the distance between the fracture and the second borehole. The larger anomalies occur when the second

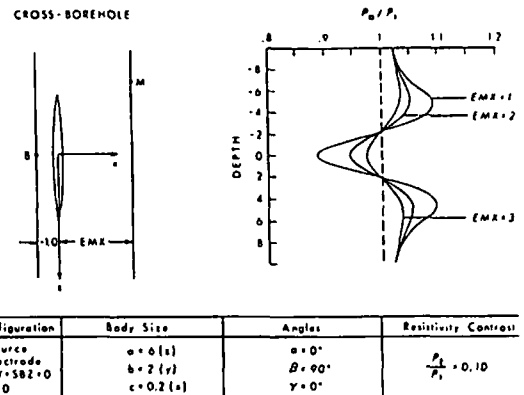


FIGURE 4a

Downhole cross-borehole resistivity anomalies for vertical fracture showing effect of varying distance from fracture to second borehole.

Electrode Configuration	Body Size	Angles	Resistivity Contrast
Fixed Source Moving Electrode SBX=1.0 SBY=SBZ=0 EMY=0	a = 0 (x) b = 2 (y) c = 0.2 (z)	$\alpha = 0^\circ$ $\beta = 90^\circ$ $\gamma = 0^\circ$	$\frac{\rho_2}{\rho_1} = 0.10$

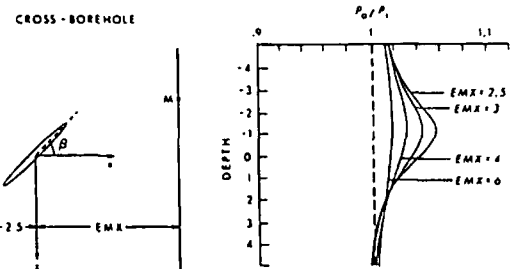


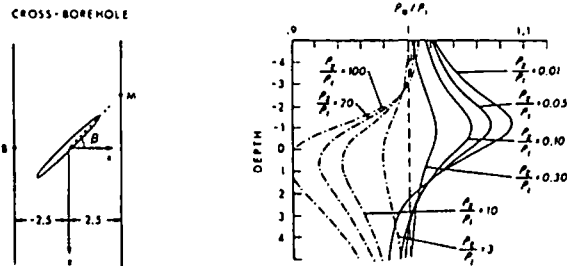
FIGURE 4b

Downhole cross-borehole resistivity anomalies for dipping fracture showing effect of varying distance from fracture to second borehole.

Electrode Configuration	Body Size	Angles	Resistivity Contrast
Fixed Source Moving Electrode SBX=2.5 SBY=SBZ=0 EMY=0	a = 2 b = 7 c = 0.2	$\alpha = 0^\circ$ $\beta = 45^\circ$ $\gamma = 0^\circ$	$\frac{\rho_2}{\rho_1} = 0.10$

borehole is nearer to the fracture zone. Figure 4b shows anomalies for the same situation as Figure 4a except that now the fracture dips toward the first borehole. Figure 4c shows the effect of varying the resistivity contrast between a dipping fracture and the host medium. As expected, the large contrast cases produce the largest anomalies. Figure 4d shows the change in anomaly shape for the dipping fracture when four electrodes are placed downhole instead of two (compare with Fig. 4b, EMX = 2.5). By study of a large suite of such graphs as these, the comparative capabilities of the various possible cross-borehole arrays can be determined.

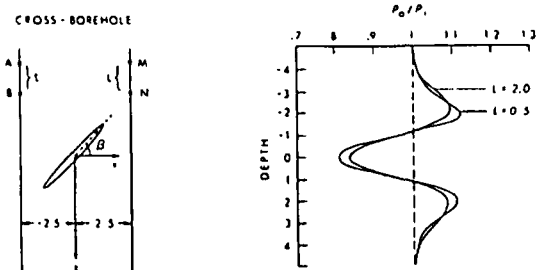
The volume integral equation approach of Beasley and Ward (1986) incorporates a half-space formulation, i.e. the earth's surface is not neglected. As with the surface integral equation technique of Yang and Ward (1985a,b), the volume integral equation method requires that only inhomogeneities be discretized. Any number of inhomogeneities of differing sizes and physical properties can be accounted for by this algorithm. Inhomogeneities are discretized into rectangular cells whose size may vary in each of



Electrode Configuration	Body Size	Angles	Resistivity Contrast
Fixed Source Moving Electrode	a = 2 b = 2 c = 0.2	alpha = 0° beta = 45° gamma = 0°	$\frac{\rho_2}{\rho_1} < 1$ $\frac{\rho_2}{\rho_1} > 1$

FIGURE 4c

Downhole cross-borehole resistivity anomalies for dipping fracture showing the effect of varying resistivity contrast between fracture and host medium.



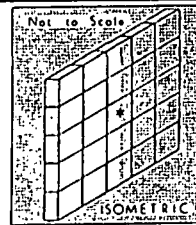
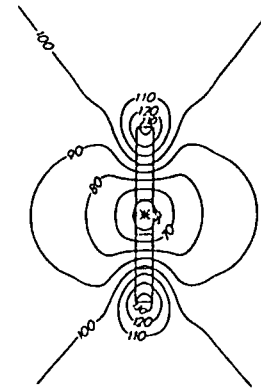
Electrode Configuration	Body Size	Angles	Resistivity Contrast
Moving Bipole Source Moving Bipole Receiver	a = 2 b = 2 c = 0.2	alpha = 0° beta = 45° gamma = 0°	$\frac{\rho_2}{\rho_1} = 0.10$

FIGURE 4d

Downhole cross-borehole resistivity anomalies for dipping fracture showing the effect of dipole length for downhole electrodes.

the three directions. The fact that targets must be comprised of rectangular or cubic cells means that dipping bodies must be simulated by cells arranged in a staircase fashion. Section and plan views of computed apparent resistivities are the end product of this algorithm. The algorithm is flexible in that it permits a buried electrode to be placed either inside (mise-à-la-masse) or outside (near-miss) the body. The dip of the body and the location of the energizing electrode within it were both varied. The maximum depth at which a body could be located and still produce a detectable anomaly on surface surveys was found to be dependent, as expected, upon the position of the buried electrode and upon the contrast in resistivity between the body and the host. It was found that locating the buried electrode just outside the body did not significantly alter the results from those when the electrode is embedded in the inhomogeneity.

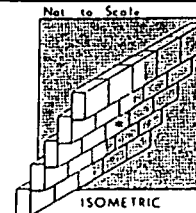
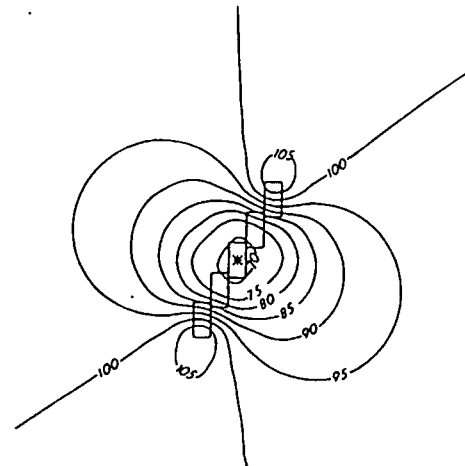
Figures 5a, 5b and 5c show representative results from Beasley and Ward (1986). Each figure is a vertical section through the earth with contours of the resistivity anomaly. A borehole can be placed anywhere on this figure and the resistivity curve that would be observed in such a



MISE-À-LA-MASSE:  
VERTICAL BODY  
APPARENT RESISTIVITY - FROM V  
SECTION VIEW  $\rho_1 = 100 \Omega \cdot m$   
D = 8 UNITS  $\rho_2 = 10 \Omega \cdot m$   
SCALE: 1 UNIT

FIGURE 5a

Subsurface resistivity contours for a vertical permeable zone with an imbedded downhole current source.



MISE-À-LA-MASSE:  
DIPPING BODY (60 DEGREES)  
APPARENT RESISTIVITY FROM V  
SECTION VIEW  $\rho_1 = 100 \Omega \cdot m$   
D = 7.78 UNITS  $\rho_2 = 10 \Omega \cdot m$   
SCALE: 1 UNIT

FIGURE 5b

Subsurface resistivity contours for a dipping permeable zone with an imbedded downhole current source.

borehole with a single downhole potential electrode would be given by the intersection of the borehole with the contours. The downhole current electrode source is shown by the star.

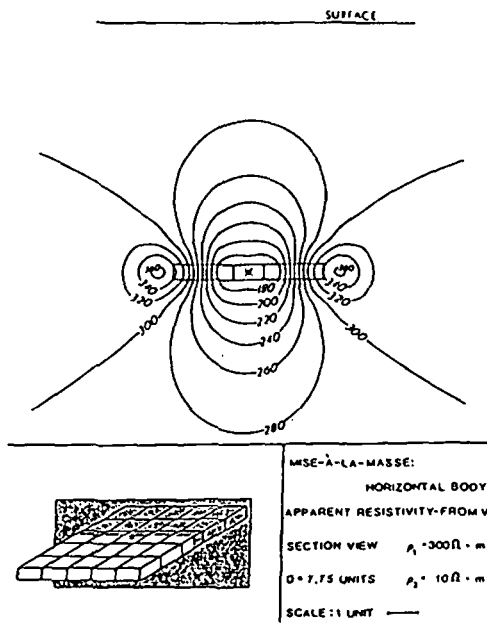


FIGURE 5c  
Subsurface resistivity contours for a horizontal permeable zone with an imbedded downhole current source.

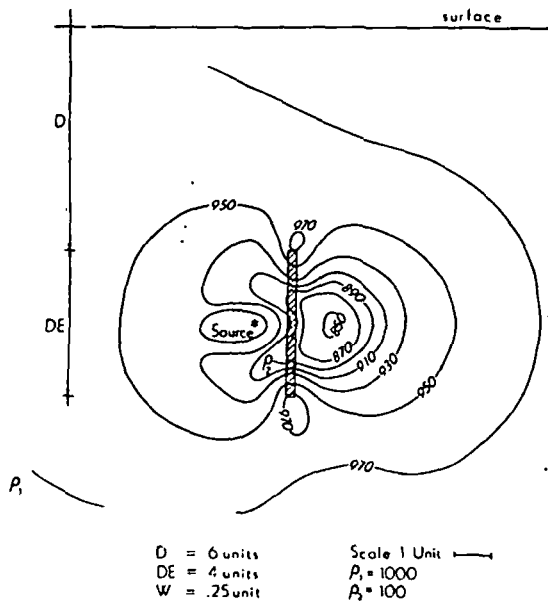


FIGURE 6a  
Subsurface resistivity contours for a vertical permeable zone with current source to the side.

Our most versatile algorithm for the borehole resistivity method is the 2-D finite element algorithm used by Zhao et al. (1985). The versatility of this algorithm arises from the fact that the entire subsurface is discretized. Since triangular elements are used for discretization, dipping bodies are readily handled. The algorithm also accommodates a layered-earth host environment. This algorithm was used to evaluate signal-to-noise ratio for various types of noise.

Figures 6a and 6b show typical results from

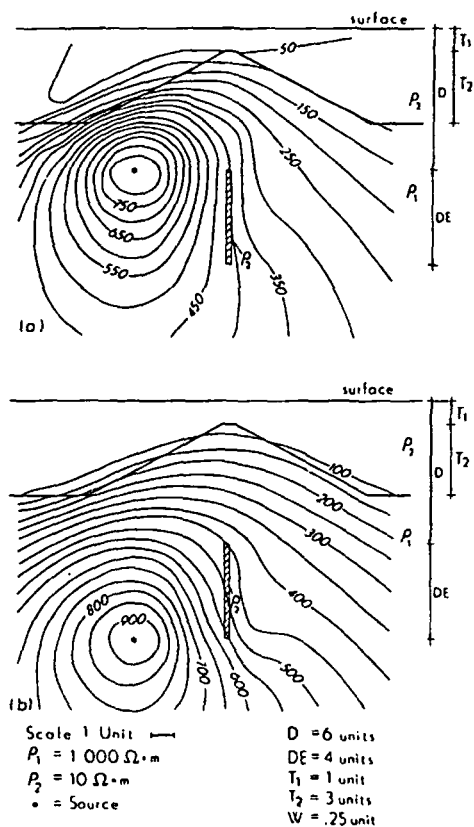


FIGURE 6b  
Subsurface resistivity contours for a vertical permeable zone beneath geologic structure with varying positions of the downhole current electrode.

Zhao et al. (1985). Figure 6a shows subsurface resistivity contours in section for a vertical fracture with a current source outside the body. This plot is similar to those given by Beasley and Ward (1986) in Figures 5a, 5b and 5c. Figure 6b illustrates how subsurface topography due to geologic structure affects results. Note that the anomaly due to the fracture is obscured to a great extent by the resistivity pattern created by the contact. This is due in part also to the relatively large distance of the fracture from the downhole current source, shown by the star. A current source in a borehole closer to the fracture would cause a much clearer anomaly.

All computations by Yang and Ward (1985a,b) and Zhao et al. (1985) were performed on an HP9826 desk top computer with 1.6 Mbytes of memory. The algorithm used by Zhao et al. (1985) is currently being extended to 3-D. It is probable that the HP9826 will accommodate the 3-D version. If so, these modeling programs could easily be used in the field with no need to return to a large computing facility.

From the above studies we tentatively conclude the following: the cross-borehole method produces larger anomalies than does a single-borehole method; the cross-borehole anomalies using a pole-pole array are smaller than those for a cross-borehole dipole-dipole array; the cross-borehole mise-à-la-masse method produces larger anomalies than for the other cross-borehole

methods; and, the anomalies due to a thin sheet were generally much smaller than those for a sphere, as is to be expected.

Using a 3-D integral equation algorithm developed by San Filippo and Hohmann (1985), West and Ward (1985) performed a model study to evaluate the time-domain electromagnetic (TDEM) response of a horizontal conductive body (fracture zone) imbedded in a half-space. Simplifying assumptions in the algorithm allow modeling only of bodies with two vertical symmetry planes with sources directly above or below. The source transmitter is a large square loop located on the surface of the earth. Receivers are located in boreholes at various locations in the vicinity of the body. Responses are computed at 60 time steps at intervals of 0.4 ms for a total data window of 24 ms. EM field decay curves and plots of decay versus depth are obtained for all three components of the primary, secondary, and total responses. The results are expressed in terms of percent difference plots, and are still under study at this time.

Surface-to-borehole EM in which a large transmitter is coaxial with the well and a down-hole detector is run in the well may provide useful information on the location of conductive fractures intersecting the wellbore. Whether this technique will work in cased wells and whether a "crack" anomaly can be distinguished from a stratigraphic conductor are topics under study.

The above discussion outlines our research to date. Other current research involves a model study using the VLF (very low-frequency) method as well as developing a borehole inversion scheme using the finite-element technique. Inversion of the 3D integral equation is also being investigated. An inversion scheme which can incorporate multi-array data is an ultimate goal. Interpretation of complex borehole field data from geothermal sites may then become a reality.

#### DISCUSSION

The problem of selecting an appropriate borehole electrical system is quite complex. Variables include where to place the electrodes, i.e. how many on the surface and how many down each borehole, and whether to use direct-current galvanic resistivity, which each of the above figures illustrate, or some alternating current, electromagnetic scheme. It is clear that the computer based study of these questions is cost effective in helping select and design an optimum field system.

Our current opinion is that the more data one can collect the better one should be able to characterize the subsurface. We have therefore been making a preliminary investigation of the design of a system for obtaining both borehole-to-borehole and borehole-to-surface data simultaneously. Such a scheme is conceptually illustrated in Figure 7. We believe we are nearing the stage when a field system can be designed with the very real hope of yielding much more subsurface information than can be realized by presently available systems.

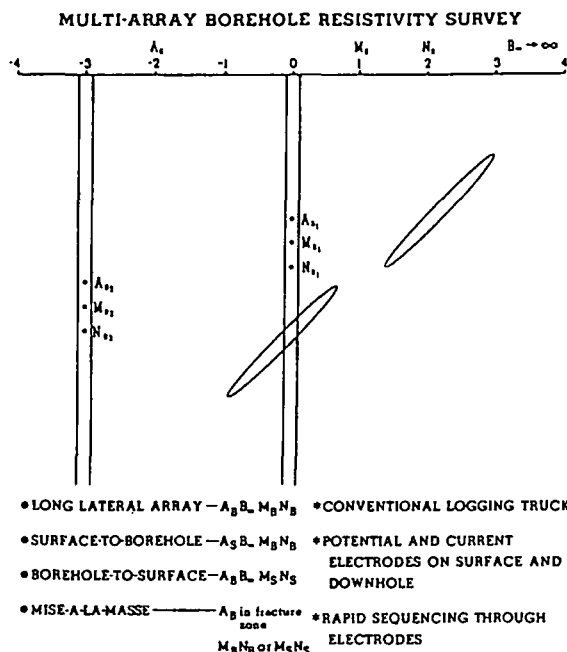


FIGURE 7  
Conceptual illustration of a multi-array borehole resistivity system.

#### REFERENCES

- Beasley, C. W., and Ward, S. H., 1986, Three-dimensional mise-à-la-masse modeling applied to mapping fracture zones: *Geophysics*, 51, January.
- Brace, W. F., 1968, The mechanical effects of pore pressure on the fracturing of rocks: *Geol. Survey Canada, Paper 68-52*.
- Daniels, J. J., 1977, Three-dimensional resistivity and induced-polarization modeling using buried electrodes: *Geophysics*, 42, 1006-1019.
- Daniels, J. J., 1983, Hole-to-surface resistivity measurements: *Geophysics*, 48, 897-97.
- Dobecki, T. L., 1980, Borehole resistivity curves near spheroidal masses: *Geophysics*, 45, 1513-1521.
- Glenn, W. E., and Hulen, J. B., 1979, A study of well logs from Roosevelt Hot Springs KGRA, Utah: in *SPWLA 20th Ann. Logging Sympos. Trans.*, II.
- Glenn, W. E., and Ross, H. P., 1982, A study of well logs from Cove Fort-Sulphurdale KGRA, Utah: *Univ. Res. Inst., Earth Sci. Lab.*, rep. 75.
- Grindly, G. W., and Browne, P. R. L., 1976, Structural and hydrological factors controlling the permeabilities of some hot-water geothermal fields: in *Proc. Second United Nations Sympos. on the Development and Use of Geoth. Res.*, San Francisco, 1, 377-386.

- Halfman, S. E., Lippmann, M. J., Zelwer, R., and Howard, J. H., 1984, Geologic interpretation of geothermal fluid movement in Cerro Prieto Field, Baja, California, Mexico: Bull. Am. Assn. Petr. Geol., 68, 18-30.
- Hohmann, G. W., 1975, Three-dimensional induced-polarization and electromagnetic modeling: Geophysics, 40, 309-324.
- Keys, W. S., and Sullivan, J. K., 1979, Role of borehole geophysics in defining the physical characteristics of the Raft River geothermal reservoir, Idaho: Geophysics, 44, 1116-1141.
- Mackelprang, C. E., 1985, A catalogue of total horizontal electric field resistivity models using three-dimensional conductive bodies and a downhole current electrode: Earth Sci. Lab., Univ. Utah Research Inst. Rept., in press.
- Moore, J. N., Adams, M. C., and Stauder, J. J., 1985, Geologic and geochemical investigations of the Meager Creek geothermal system, British Columbia, Canada: Proc. Tenth Workshop on Geoth. Res. Eng., Stanford Univ., Stanford, CA.
- Newkirk, D. J., 1982, Downhole electrode resistivity interpretation with three-dimensional models: Masters Thesis, Dept. of Geology and Geophys., Univ. of Utah.
- Oristaglio, M. L., 1985, A guide to the current uses of vertical seismic profiles: Geophysics, 50, in press.
- San Filippo, W. A., and Hohmann, G. W., 1985, Integral equation solution for the transient electromagnetic response of a three-dimensional body in a conductive half-space: Geophysics, 50, 798-809.
- Sanyal, S. K., Wells, L. E., and Bickham, R. E., 1980, Geothermal well log interpretation state of the art - Final report: Los Alamos Scientific Lab. Rep. LA-8211-MS.
- West, R. C., and Ward, S. H., 1985, The borehole transient EM response of a three-dimensional fracture zone in a conductive half-space: to be submitted to Geophysics.
- Yang, F. W., and Ward, S. H., 1985a, Single- and cross-borehole resistivity anomalies of thin ellipsoids and spheroids: Geophysics, 50, 637-655.
- Yang, F. W., and Ward, S. H., 1985b, On sensitivity of surface-to-borehole resistivity measurements to the attitude and the depth to the center of a 3-D oblate spheroid: Geophysics, 50, 1173-1178.
- Zhao, J. X., Rijo, L., and Ward, S. H., 1985, Evaluation of the ratio of signal-to-noise in cross-borehole electrical surveys: submitted to Geophysics.



Sent 8-29-85  


**BOREHOLE GEOPHYSICAL TECHNIQUES FOR DEFINING PERMEABLE ZONES  
IN GEOTHERMAL SYSTEMS**

Phillip M. Wright and Stanley H. Ward

Earth Science Laboratory  
University of Utah Research Institute  
391 Chipeta Way, Suite C  
Salt Lake City, Utah 84108

**ABSTRACT**

Borehole electrical geophysical methods have considerable potential for helping to define hot and permeable zones in geothermal systems. Borehole geophysics differs from geophysical well logging and has a much greater area of search around a borehole. Very little developmental work has taken place in borehole electrical methods to date. At UURI, we have been developing computer methods to model various electrical arrays for borehole configurations. We plan to compare the several possible survey methods and then design a field system based on the method that appears from the computer studies to be optimum.

From our studies to date we tentatively conclude that the cross-borehole method produces larger anomalies than does the single-borehole method; cross-borehole anomalies using a pole-pole array are smaller than those for a dipole-dipole array; the cross-borehole mise-à-la-masse method produces larger anomalies than does other cross-borehole methods; and, the anomalies due to a thin structure are generally much smaller than those for a sphere, as is to be expected.

**INTRODUCTION**

The key problem worldwide in development of hydrothermal resources appears to be more in locating permeable zones than in locating high temperatures. Grindly and Browne (1976) note that of 11 hydrothermal fields investigated in New Zealand, all of which have high temperatures (230°C to 300°C), five are non-productive chiefly because of low permeability. Three of the eleven fields are in production (Wairakei, Kawerau and Broadlands) and in each of these fields permeability limits production more than temperature does. Hot but unproductive holes have been drilled at many of the major geothermal areas in the world, including The Geysers, Roosevelt Hot Springs, Coso, and Meager Creek, to name a few.

Permeability can be primary or secondary. Primary permeability in clastic rocks originates from intergranular porosity and it generally decreases with depth due to compaction and cementation. In volcanic sequences, primary intergranular porosity and permeability exist, but greater permeability exists in open spaces at flow contacts and within the flows themselves. Primary permeability in crystalline igneous rocks is generally very low. Secondary permeability occurs in all rock types in open fault zones, fractures

and fracture intersections, along dikes and in breccia zones (Brace, 1968; Moore et al., 1985). Changes in permeability come about through mineral deposition in open spaces or by leaching by the thermal fluids.

Although none of the geophysical methods maps permeability directly, any geological, geochemical, or hydrological understanding of the factors that control the permeability in a geothermal reservoir can be used to help determine geophysical methods potentially useful for detecting the boundaries and more permeable parts of a hydrothermal system. At UURI, we have been developing electrical borehole techniques to detect and map permeable zones in the subsurface, especially fractures.

**BACKGROUND--BOREHOLE GEOPHYSICS**

It is important to understand the differences between geophysical well logging and borehole geophysics. In geophysical well logging, the instruments are deployed in a single well in a tool or sonde, and the depth of investigation is usually limited to the first few meters from the wellbore. Well-logging techniques have been developed by the petroleum industry over a period of half a century and have been applied with variable success by the geothermal industry. The major adaptations to the geothermal environment are the requirements of high temperature tools and the different interpretation required for hard rock (volcanic, igneous) lithologies. Other differences include a strong emphasis in geothermal exploration on fracture identification and the effects of hydrothermal alteration upon certain log responses. Much research remains to be done in order to understand fully the responses of various well logs in geothermal reservoirs and their typically fractured, altered, commonly igneous and metamorphic host rocks. In spite of the relative lack of knowledge of well-log response in geothermal reservoirs, several logs or log combinations have been used successfully to investigate such properties as lithology, alteration, fracturing, density, porosity, fluid flow and sulfide content, all of which may be critical in deciding how and in what intervals to complete, case, cement or stimulate a well (Glenn and Hulén, 1979; Keys and Sullivan, 1979; Sanyal et al., 1980; Glenn and Ross, 1982; Halfman et al., 1982).

By contrast, borehole geophysics refers to those geophysical techniques where energy sources and sensors are deployed (1) at wide spacing in a

single borehole, (2) partly in one borehole and partly on the surface, or (3) partly in one borehole and partly in a second borehole. Thus, we speak of borehole-to-surface, surface-to-borehole and borehole-to-borehole surveys. The depth of investigation is generally much greater in borehole geophysical surveys than it is in geophysical well logging.

Only one of the several borehole geophysical techniques, namely vertical seismic profiling (VSP), has been developed to any extent. The petroleum industry has funded relatively rapid development of VSP over the past several years.

#### VSP

Vertical seismic profiling (VSP) can be done using both P- and S-wave surface sources (usually mechanical vibrators) arranged circumferentially around a well. Direct and reflected seismic waves are detected by strings of down-hole geophones clamped to the wall of the well or by hydrophones. VSP has been used mainly to trace seismic events observed at the surface to their point of origin in the earth and to obtain better estimates for the acoustic properties of a stratigraphic sequence. Oristaglio (1985) presents a guide to the current uses of VSP.

#### Borehole Electrical Techniques

Borehole-to-borehole and borehole-to-surface electrical methods appear to have considerable potential for application to geothermal exploration. In a benchmark introductory paper, Daniels (1983) illustrated the utility of hole-to-surface resistivity measurements with a detailed study of an area of volcanic tuff near Yucca Mountain, Nevada. He obtained total-field resistivity data for a grid of points on the surface with current sources in three drill holes, completed a layered-earth reduction of the data, and interpreted the residual resistivity anomalies with a 3D ellipsoidal modeling technique.

The borehole electrical techniques, however, are in general poorly developed. One reason for this is that there are a large number of ways that borehole electrical surveys can be performed and it has been unclear which methods are best. At the same time, computer algorithms to model the several methods have not existed so that it has not been possible to select among methods prior to committing to the expense of building a field system and obtaining test data.

#### R&D PROGRAM AT UURI

The objective of our program is to develop and demonstrate the use of borehole electrical techniques in geothermal exploration, reservoir delineation and reservoir exploitation. Our approach is:

1. Develop computer techniques to model the possible borehole electrical survey systems;
2. Design and construct a field data acquisition system based on the results of (1);
3. Acquire field data at sites where the nature and extent of permeability are known; and,

#### 4. Develop techniques to interpret field data.

To the present time, we have made considerable progress on item (1) above and we are now at such a point that item (2) could be started.

Our research staff has consisted of the following personnel: Stanley H. Ward, Project Manager; Luis Rijo, Professor of Geophysics, Universidade Federal Do Para, Brazil (on 2-year post-doctoral leave at U of U and UURI); F. W. Yang, Peoples Republic of China (visiting scholar); J. X. Zhao, Peoples Republic of China (visiting scholar); Craig W. Beasley (doctoral candidate U of U, awarded MS degree); Richard C. West (MS candidate at UU). Additional technical support has been provided by Philip E. Wannamaker, Howard P. Ross and Phillip M. Wright of UURI and by Gerald W. Hohmann of U of U. Project costs for Rijo, Yang and Zhao have been minimal because these scientists have been supported by their governments. Thus, a great deal has been accomplished at minimal cost while supporting the education of several students. The remainder of this paper will discuss the significance of our research to date.

#### COMPUTER MODELING OF BOREHOLE ELECTRICAL METHODS

Computer techniques for modeling borehole electrical geophysics have largely been lacking, especially for three-dimensional (3D) cases. Figure 1 indicates conventional usage of the terms 1D, 2D and 3D in geophysical interpretation. In the 1D case, also called the "layered earth" case, the physical property of interest (resistivity for this study), varies only in the vertical direction. In the 2D case, physical property variations in the vertical and one horizontal dimension are allowed, and the anomalous body illustrated has the same shape in and out of the paper for infinite distance. In the 3D case, physical property variations are specified in all three space dimensions. Obviously, the real earth is only occasionally 1D in nature in geothermal areas. The usual case is for physical properties to vary in all three dimensions in the earth, the 3D case. However, the mathematical formulations for electrical anomalies of bodies increase greatly in complexity from the 1D case to the 3D case. This accounts for the fact that in order to begin our task of applying borehole electrical techniques to delineation of permeability, we were required to develop original mathematical formulations of the problem.

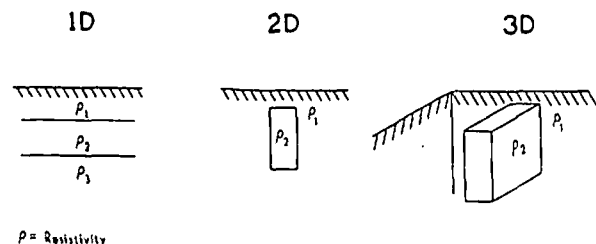


FIGURE 1  
Illustration of the meaning of the terms 1D, 2D and 3D in geophysical modeling.

Thick-Body Studies

Prior to 1982, only three published papers considered computer modeling of downhole electrodes for three-dimensional bodies. Daniels (1977) studied six buried electrode configurations and plotted normalized apparent resistivity or apparent polarizability against such configuration parameters as 1) source and receiver depth, 2) depth/bipole length, 3) receiver distance from body, 4) depth of body, and 5) distance of source and receiver from body center. Snyder and Merkel (1973), computed the IP and apparent resistivity responses resulting from a buried current pole in the presence of a buried sphere. Their plots are center-line profiles for normalized apparent resistivity and normalized IP response. Dobecki (1980) computed the effects of spheroidal bodies as measured in nearby single boreholes using the pole-pole electrode array. These three studies are obviously very limited in terms of the problems of defining permeability in geothermal systems.

In 1982, Newkirk (1982) from our group published a study of downhole electrical resistivity with 3D bodies. Using a numerical modeling technique described by Hohmann (1975), theoretical anomalies due to a three-dimensional body composed of simple prisms were computed. The results were presented in terms of 1) the potential, 2) the apparent resistivity calculated from the total horizontal electric field and 3) the apparent resistivity calculated from the potential. Two electrode configurations were considered for each model. Each configuration consisted of a pair of electrodes, where one of the electrodes was remote and the second electrode was located either in the body, for *mise-à-la-masse* or applied potential, or outside the body, simulating a near miss. Newkirk's computer program was used by Mackelprang (1985) of our group to compute a catalog of models due to bodies that might be of interest in detection of thick fracture zones.

Figures 2a and 2b show the conventions used by Newkirk (1982) and Mackelprang (1985) in calculations of the effects of 3D bodies. The bodies are buried in a homogeneous earth and two of many options for a downhole point electrode are illustrated. Figure 3a and 3b illustrate anomalies on a surface resistivity survey produced by a narrow conductive body buried at a depth of 7 units with the electrode in the body (Fig. 3a) and off the end of the body (Fig. 3b). The peanut shaped anomaly shown in Figure 3a is particularly characteristic on surface resistivity surveys with the borehole electrode in the body.

One basic shortcoming of Newkirk's (1982) algorithm is that it does not apply when the anomalous body becomes thin, i.e. to the case of delineation of fractures or thin fracture zones. To address this important problem, the thin-body studies described in the next section have been undertaken.

Thin-Body Studies

These studies are aimed at targets simulating fracture zones which are thin relative to their

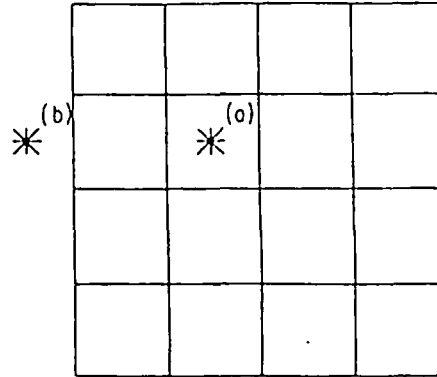


FIGURE 2a  
Plan view of standard model.

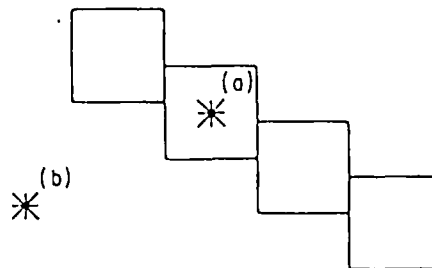


FIGURE 2b  
Cross-section view of standard model.

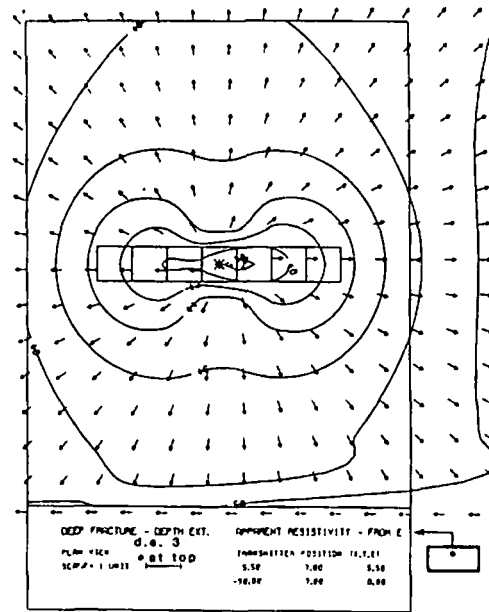


FIGURE 3a  
Surface resistivity anomaly due to deep fracture with downhole electrode in body.

other two dimensions. For the most part, we have standardized the aspect ratios of the target dimensions at 10:10:1. While the effect of varying the contrast in resistivity has been examined,

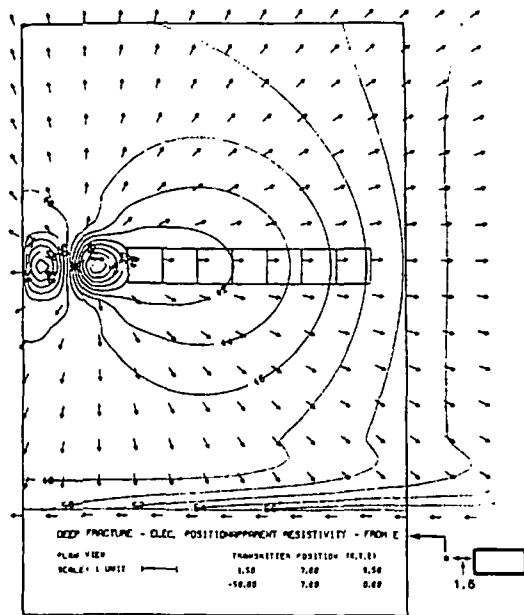


FIGURE 3b

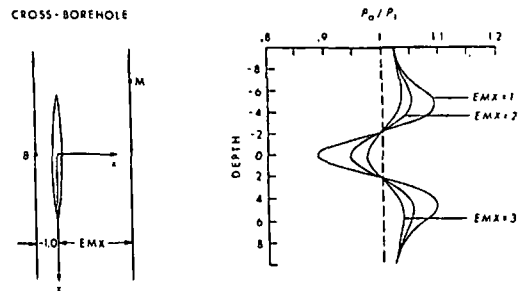
Surface resistivity anomaly due to deep fracture with downhole electrode at side of body.

most of the results are for the case of a fracture zone ten times more conductive than the host rocks.

Four numerical techniques have been utilized in the studies; three have been applied with the D.C. resistivity method. The techniques applied to the resistivity problem are (1) a 3D surface integral equation (Yang and Ward, 1985a,b), (2) a 3D volume integral equation (Beasley and Ward, 1986), and (3) a 2D finite element method (Zhao et al., 1985). A solution for the time domain EM method has also been obtained which uses a 3D volume integral equation formulation (West and Ward, 1985). Elaboration on these four approaches is given below.

Yang and Ward (1985a,b) present theoretical results relating to the detection of thin oblate spheroids and ellipsoids of arbitrary attitude. The effects of the surface of the earth are neglected and the body is assumed to be enclosed within an infinite homogeneous mass. The surface of the body is divided into a series of sub-surfaces, and a numerical solution of the Fredholm integral equation is applied. Once a solution for the surface charge distribution is determined, the potential can be specified anywhere by means of Coulomb's law. The theoretical model results indicate that cross-borehole resistivity measurements are a more effective technique than single-borehole measurements for delineating resistivity anomalies in the vicinity of a borehole.

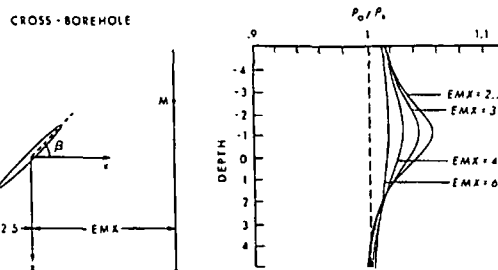
Figure 4a shows cross-borehole resistivity responses of a vertical conductive fracture zone between two boreholes. The electrode configuration is the pole-pole array with electrode B fixed and electrode M moving in the second borehole. Several curves are plotted depending on the distance between the fracture and the second borehole. The larger anomalies occur when the second



Electrode Configuration	Body Size	Angles	Resistivity Contrast
Fixed Source Moving Electrode SBX = -1.0 SBY = SBZ = 0 EMY = 0	a = 6 (x) b = 2 (y) c = 0.2 (z)	alpha = 0° beta = 90° gamma = 0°	$\frac{\rho_2}{\rho_1} = 0.10$

FIGURE 4a

Downhole cross-borehole resistivity anomalies for vertical fracture showing effect of varying distance from fracture to second borehole.



Electrode Configuration	Body Size	Angles	Resistivity Contrast
Fixed Source Moving Electrode SBX = -2.5 SBY = SBZ = 0 EMY = 0	a = 2 b = 2 c = 0.2	alpha = 0° beta = 45° gamma = 0°	$\frac{\rho_2}{\rho_1} = 0.10$

FIGURE 4b

Downhole cross-borehole resistivity anomalies for dipping fracture showing effect of varying distance from fracture to second borehole.

borehole is nearer to the fracture zone. Figure 4b shows anomalies for the same situation as Figure 4a except that now the fracture dips toward the first borehole. Figure 4c shows the effect of varying the resistivity contrast between a dipping fracture and the host medium. As expected, the large contrast cases produce the largest anomalies. Figure 4d shows the change in anomaly shape for the dipping fracture when four electrodes are placed downhole instead of two (compare with Fig. 4b, EMX = 2.5). By study of a large suite of such graphs as these, the comparative capabilities of the various possible cross-borehole arrays can be determined.

The volume integral equation approach of Beasley and Ward (1986) incorporates a half-space formulation, i.e. the earth's surface is not neglected. As with the surface integral equation technique of Yang and Ward (1985a,b), the volume integral equation method requires that only inhomogeneities be discretized. Any number of inhomogeneities of differing sizes and physical properties can be accounted for by this algorithm. Inhomogeneities are discretized into rectangular cells whose size may vary in each of

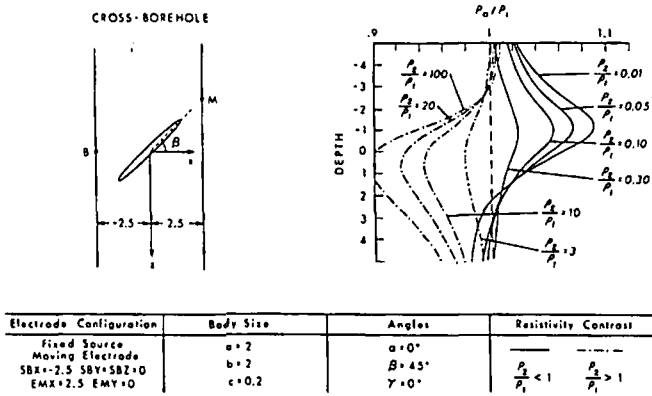


FIGURE 4c  
Downhole cross-borehole resistivity anomalies for dipping fracture showing the effect of varying resistivity contrast between fracture and host medium.

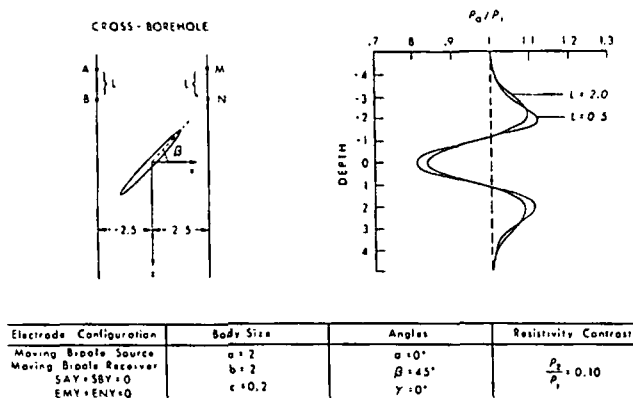


FIGURE 4d  
Downhole cross-borehole resistivity anomalies for dipping fracture showing the effect of dipole length for downhole electrodes.

the three directions. The fact that targets must be comprised of rectangular or cubic cells means that dipping bodies must be simulated by cells arranged in a staircase fashion. Section and plan views of computed apparent resistivities are the end product of this algorithm. The algorithm is flexible in that it permits a buried electrode to be placed either inside (mise-à-la-masse) or outside (near-miss) the body. The dip of the body and the location of the energizing electrode within it were both varied. The maximum depth at which a body could be located and still produce a detectable anomaly on surface surveys was found to be dependent, as expected, upon the position of the buried electrode and upon the contrast in resistivity between the body and the host. It was found that locating the buried electrode just outside the body did not significantly alter the results from those when the electrode is embedded in the inhomogeneity.

Figures 5a, 5b and 5c show representative results from Beasley and Ward (1986). Each figure is a vertical section through the earth with contours of the resistivity anomaly. A borehole can be placed anywhere on this figure and the resistivity curve that would be observed in such a

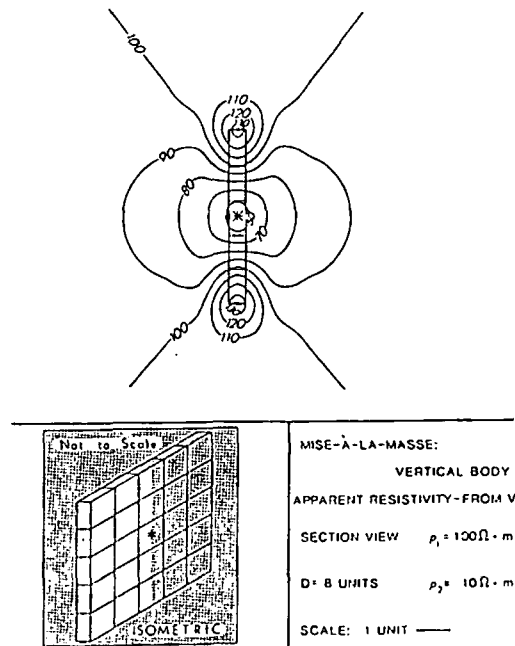


FIGURE 5a  
Subsurface resistivity contours for a vertical permeable zone with an imbedded downhole current source.

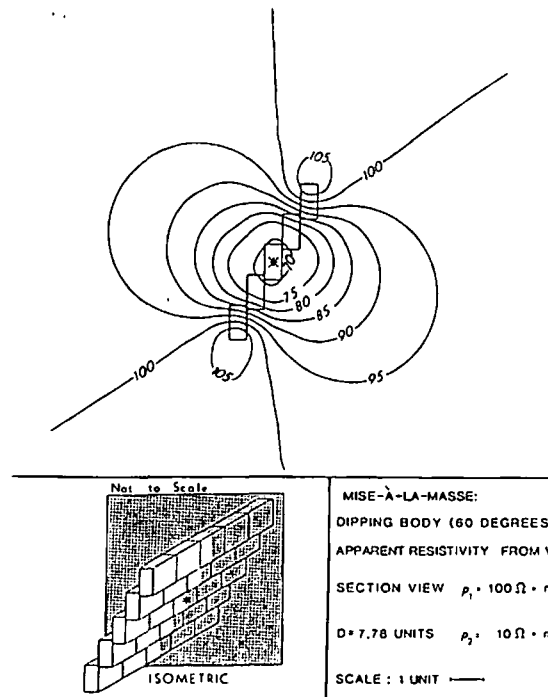


FIGURE 5b  
Subsurface resistivity contours for a dipping permeable zone with an imbedded downhole current source.

borehole with a single downhole potential electrode would be given by the intersection of the borehole with the contours. The downhole current electrode source is shown by the star.

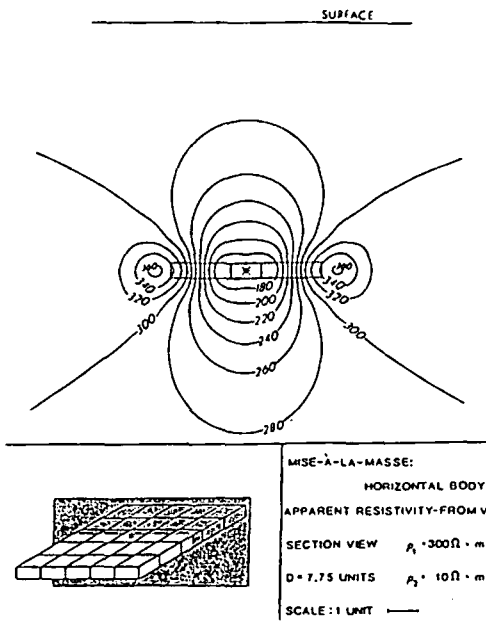


FIGURE 5c  
Subsurface resistivity contours for a horizontal permeable zone with an imbedded downhole current source.

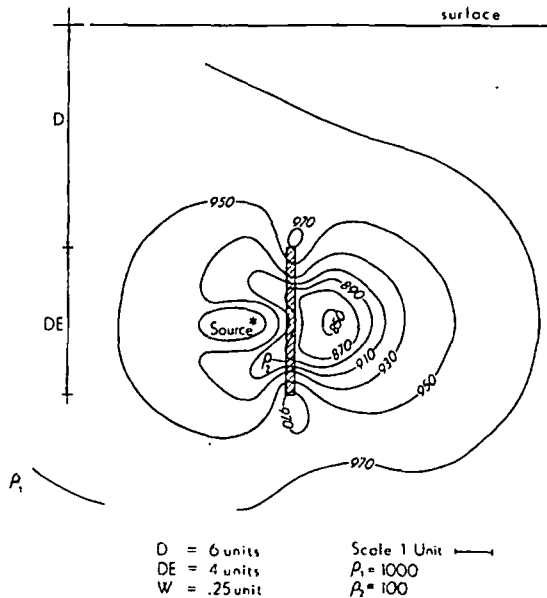


FIGURE 6a  
Subsurface resistivity contours for a vertical permeable zone with current source to the side.

Our most versatile algorithm for the borehole resistivity method is the 2-D finite element algorithm used by Zhao et al. (1985). The versatility of this algorithm arises from the fact that the entire subsurface is discretized. Since triangular elements are used for discretization, dipping bodies are readily handled. The algorithm also accommodates a layered-earth host environment. This algorithm was used to evaluate signal-to-noise ratio for various types of noise.

Figures 6a and 6b show typical results from

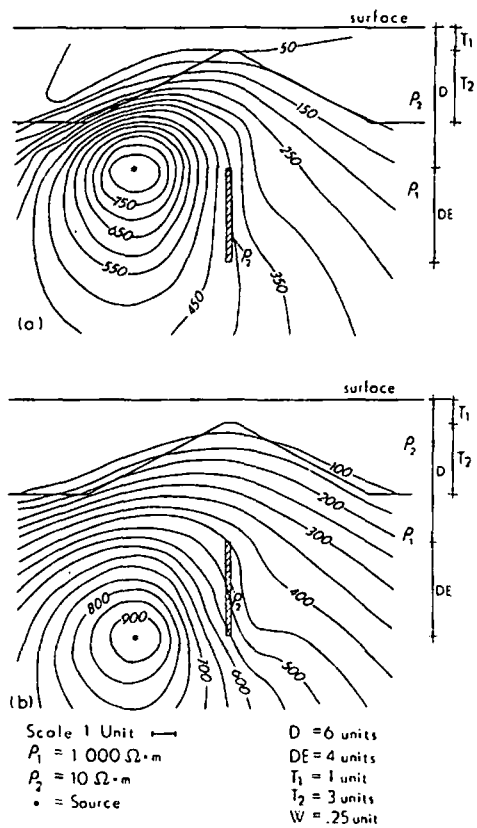


FIGURE 6b  
Subsurface resistivity contours for a vertical permeable zone beneath geologic structure with varying positions of the downhole current electrode.

Zhao et al. (1985). Figure 6a shows subsurface resistivity contours in section for a vertical fracture with a current source outside the body. This plot is similar to those given by Beasley and Ward (1986) in Figures 5a, 5b and 5c. Figure 6b illustrates how subsurface topography due to geologic structure affects results. Note that the anomaly due to the fracture is obscured to a great extent by the resistivity pattern created by the contact. This is due in part also to the relatively large distance of the fracture from the downhole current source, shown by the star. A current source in a borehole closer to the fracture would cause a much clearer anomaly.

All computations by Yang and Ward (1985a,b) and Zhao et al. (1985) were performed on an HP9826 desk top computer with 1.6 Mbytes of memory. The algorithm used by Zhao et al. (1985) is currently being extended to 3-D. It is probable that the HP9826 will accommodate the 3-D version. If so, these modeling programs could easily be used in the field with no need to return to a large computing facility.

From the above studies we tentatively conclude the following: the cross-borehole method produces larger anomalies than does a single-borehole method; the cross-borehole anomalies using a pole-pole array are smaller than those for a cross-borehole dipole-dipole array; the cross-borehole mise-à-la-masse method produces larger anomalies than for the other cross-borehole

methods; and, the anomalies due to a thin sheet were generally much smaller than those for a sphere, as is to be expected.

Using a 3-D integral equation algorithm developed by San Filippo and Hohmann (1985), West and Ward (1985) performed a model study to evaluate the time-domain electromagnetic (TDEM) response of a horizontal conductive body (fracture zone) imbedded in a half-space. Simplifying assumptions in the algorithm allow modeling only of bodies with two vertical symmetry planes with sources directly above or below. The source transmitter is a large square loop located on the surface of the earth. Receivers are located in boreholes at various locations in the vicinity of the body. Responses are computed at 60 time steps at intervals of 0.4 ms for a total data window of 24 ms. EM field decay curves and plots of decay versus depth are obtained for all three components of the primary, secondary, and total responses. The results are expressed in terms of percent difference plots, and are still under study at this time.

Surface-to-borehole EM in which a large transmitter is coaxial with the well and a down-hole detector is run in the well may provide useful information on the location of conductive fractures intersecting the wellbore. Whether this technique will work in cased wells and whether a "crack" anomaly can be distinguished from a stratigraphic conductor are topics under study.

The above discussion outlines our research to date. Other current research involves a model study using the VLF (very low-frequency) method as well as developing a borehole inversion scheme using the finite-element technique. Inversion of the 3D integral equation is also being investigated. An inversion scheme which can incorporate multi-array data is an ultimate goal. Interpretation of complex borehole field data from geothermal sites may then become a reality.

#### DISCUSSION

The problem of selecting an appropriate borehole electrical system is quite complex. Variables include where to place the electrodes, i.e. how many on the surface and how many down each borehole, and whether to use direct-current galvanic resistivity, which each of the above figures illustrate, or some alternating current, electromagnetic scheme. It is clear that the computer based study of these questions is cost effective in helping select and design an optimum field system.

Our current opinion is that the more data one can collect the better one should be able to characterize the subsurface. We have therefore been making a preliminary investigation of the design of a system for obtaining both borehole-to-borehole and borehole-to-surface data simultaneously. Such a scheme is conceptually illustrated in Figure 7. We believe we are nearing the stage when a field system can be designed with the very real hope of yielding much more subsurface information than can be realized by presently available systems.

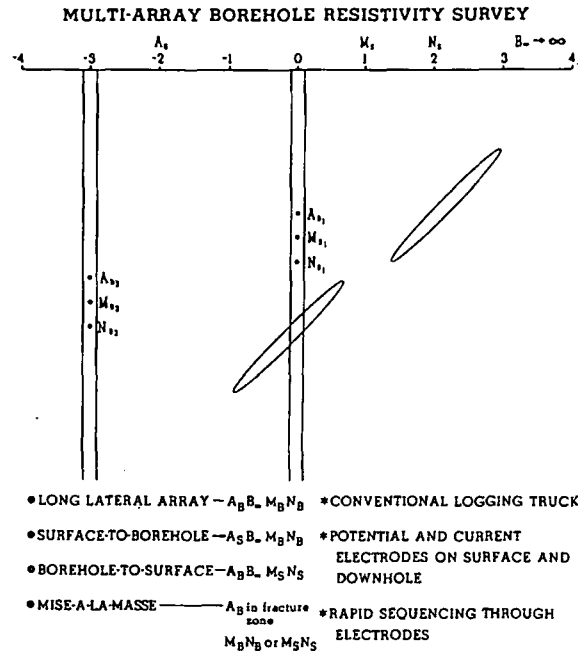


FIGURE 7  
Conceptual illustration of a multi-array borehole resistivity system.

#### REFERENCES

- Beasley, C. W., and Ward, S. H., 1986, Three-dimensional mise-à-la-masse modeling applied to mapping fracture zones: *Geophysics*, 51, January.
- Brace, W. F., 1968, The mechanical effects of pore pressure on the fracturing of rocks: *Geol. Survey Canada*, Paper 68-52.
- Daniels, J. J., 1977, Three-dimensional resistivity and induced-polarization modeling using buried electrodes: *Geophysics*, 42, 1006-1019.
- Daniels, J. J., 1983, Hole-to-surface resistivity measurements: *Geophysics*, 48, 897-97.
- Dobecki, T. L., 1980, Borehole resistivity curves near spheroidal masses: *Geophysics*, 45, 1513-1521.
- Glenn, W. E., and Hulen, J. B., 1979, A study of well logs from Roosevelt Hot Springs KGRA, Utah: in *SPWLA 20th Ann. Logging Sympos. Trans.*, II.
- Glenn, W. E., and Ross, H. P., 1982, A study of well logs from Cove Fort-Sulphurdale KGRA, Utah: *Univ. Res. Inst., Earth Sci. Lab.*, rep. 75.
- Grindly, G. W., and Browne, P. R. L., 1976, Structural and hydrological factors controlling the permeabilities of some hot-water geothermal fields: in *Proc. Second United Nations Sympos. on the Development and Use of Geoth. Res.*, San Francisco, 1, 377-386.

- Halfman, S. E., Lippmann, M. J., Zelwer, R., and Howard, J. H., 1984, Geologic interpretation of geothermal fluid movement in Cerro Prieto Field, Baja, California, Mexico: Bull. Am. Assn. Petr. Geol., 68, 18-30.
- Hohmann, G. W., 1975, Three-dimensional induced-polarization and electromagnetic modeling: Geophysics, 40, 309-324.
- Keys, W. S., and Sullivan, J. K., 1979, Role of borehole geophysics in defining the physical characteristics of the Raft River geothermal reservoir, Idaho: Geophysics, 44, 1116-1141.
- Mackelprang, C. E., 1985, A catalogue of total horizontal electric field resistivity models using three-dimensional conductive bodies and a downhole current electrode: Earth Sci. Lab., Univ. Utah Research Inst. Rept., in press.
- Moore, J. N., Adams, M. C., and Stauder, J. J., 1985, Geologic and geochemical investigations of the Meager Creek geothermal system, British Columbia, Canada: Proc. Tenth Workshop on Geoth. Res. Eng., Stanford Univ., Stanford, CA.
- Newkirk, D. J., 1982, Downhole electrode resistivity interpretation with three-dimensional models: Masters Thesis, Dept. of Geology and Geophys., Univ. of Utah.
- Oristaglio, M. L., 1985, A guide to the current uses of vertical seismic profiles: Geophysics, 50, in press.
- San Filippo, W. A., and Hohmann, G. W., 1985, Integral equation solution for the transient electromagnetic response of a three-dimensional body in a conductive half-space: Geophysics, 50, 798-809.
- Sanyal, S. K., Wells, L. E., and Bickham, R. E., 1980, Geothermal well log interpretation state of the art - Final report: Los Alamos Scientific Lab. Rep. LA-8211-MS.
- West, R. C., and Ward, S. H., 1985, The borehole transient EM response of a three-dimensional fracture zone in a conductive half-space: to be submitted to Geophysics.
- Yang, F. W., and Ward, S. H., 1985a, Single- and cross-borehole resistivity anomalies of thin ellipsoids and spheroids: Geophysics, 50, 637-655.
- Yang, F. W., and Ward, S. H., 1985b, On sensitivity of surface-to-borehole resistivity measurements to the attitude and the depth to the center of a 3-D oblate spheroid: Geophysics, 50, 1173-1178.
- Zhao, J. X., Rijo, L., and Ward, S. H., 1985, Evaluation of the ratio of signal-to-noise in cross-borehole electrical surveys: submitted to Geophysics.



# 0 1 6 0



Single- and Cross-Borehole Resistivity Anomalies  
of Thin Ellipsoids and Spheroids

by

Fang-wei Yang\*

Stanley H. Ward<sup>+</sup>

\*Ministry of Coal Industry, Peoples Republic of China, on leave at the Department of Geology and Geophysics, University of Utah.

<sup>+</sup>Department of Geology and Geophysics, University of Utah, and Earth Science Laboratory, University of Utah Research Institute.

## ABSTRACT

Hole-to-hole resistivity measurement is a useful method of detecting fractures and ore deposits in the subsurface. With drilling costs continually rising, there is a growing need for developing methods of borehole geophysics such as this. In this study, we present theoretical results relating to detection of thin oblate spheroids and ellipsoids with arbitrary attitude.

If we assume that individual fractures within a fracture zone are connected to each other and are of finite lateral and vertical extent, then we can model the fracture zone as a thin conductive oblate ellipsoid or spheroid with arbitrary orientation of the major axis. Detection of such fractures is the object of this study. In this study, the surface of the body is divided into a series of subsurfaces, and a numerical solution of the Fredholm integral equation is applied. Once a solution for the surface charge distribution is determined, the potential can be specified anywhere by means of Coulomb's law. The theoretical model results indicate that cross-borehole resistivity measurements are a more effective technique than single-borehole measurements for delineating resistivity anomalies in the vicinity of a borehole. In some cases, the depth to the center of the body and the dip and strike of the major axes of the body can be estimated.

## INTRODUCTION

The methods of single-borehole, cross-borehole and borehole-to-surface resistivity measurements for detecting anomalies in the vicinity of a borehole have been discussed by several authors. An analytical solution for a spherical body in a half-space, with a buried current source, was presented by Merkel (1971), Snyder and Merkel (1973), and Lee (1975). A solution for modeling the resistivity and induced electrical polarization response of two-dimensional (2-D) bodies in a half-space, using the method of moments (Harrington, 1968) was developed by Snyder (1976). A detailed discussion on the anomalies due to a spherical body in a half-space, for cross-borehole and borehole-to-surface configurations was given by Daniels (1977). Recently, theoretical solutions and discussions of the apparent resistivity anomalies of a sphere and a horizontal oblate or prolate spheroid in a whole space for cross-borehole and single-borehole methods, were presented by Dobecki (1980) and Lytle (1982). However, the computation of the potential about a thin ellipsoid with an arbitrary attitude is a practical problem which has not received sufficient attention. We can calculate this potential directly using the finite element method. However, in the following discussion it is demonstrated that there is an advantage in solving this problem by means of the surface-charge, integral equation technique.

The use of surface-charge integration to solve electric potential problems is a classical method in physics. Al'pin (1964) has shown the theoretical formula for the computation of a complicated horizontally layered model involving the drilling fluid and the invaded zone for resistivity logging with this technique. Harrington (1968) described its applications to electrostatic and electromagnetic fields. This approach was first applied to solve three-dimensional (3-D) problems in resistivity and induced electrical polarization by Dieter et al. (1969). Barnett (1972, 1976) and Daniels (1977) applied it to solve the potential problems for three-dimensional bodies of spherical and arbitrary

shape.

In conventional resistivity surveys, surface measurements are limited in their ability to locate deeply buried targets such as fracture zones or tabular orebodies, from which only small responses are measured using conventional surface electrode configurations. This paper investigates the possibility of detecting a thin anomalous body via borehole measurements. Several body attitudes and three different buried electrode configurations are considered. The theoretical modeling for a thin oblate body not only can be used to model fracture zones occurring in geothermal environments, but also can be used to model a thin resistive or thin conductive orebody in mining exploration. We shall use the term "spheroid" to describe a thin oblate ellipsoid possessing two axes of equal dimensions, and the term "ellipsoid" to describe a thin oblate triaxial ellipsoid. In all models studied, the dimensions of two axes are at least ten times that of the third, so that only thin oblate bodies are modeled.

*Etalics*

### THEORY

Consider the ellipsoidal model for single-borehole and cross-borehole techniques depicted in Figure 1, in which  $\rho_1$  is the resistivity of the whole space and  $\rho_2$  is the resistivity of the body. Assume that the depth to the anomalous body is much greater than its size so that the effects of the surface of the earth can be neglected. The current and measuring electrodes A and N are placed at infinity on the surface; the electrodes B and M are thus the only electrodes downhole. In this model the center of the ellipsoid is the zero of the coordinate system and the ellipsoid can take any attitude. If the effects of the borehole are neglected, then the potential  $U_M$  at point M is given by (Al'pin, 1964)

$$U_M = \frac{\rho_1 I}{4\pi} \frac{1}{R_{BM}} + \frac{1}{4\pi} \int_S \frac{\sigma(P)}{\epsilon R_{PM}} ds, \quad (1)$$

in which S is the series of sub-surfaces used to approximate the ellipsoid, P is a point on the surface of the ellipsoid,  $R_{BM}$  and  $R_{PM}$  are the distances from the current source B to the measuring electrode M and from point P to the measuring electrode M, respectively (Figure 1). The quantity  $\sigma(p)$  is the equivalent surface density of charge at the point P while  $\epsilon$  is the dielectric permittivity. From boundary conditions and using a simple transformation of  $S(P) = \frac{\sigma(P)}{\epsilon \rho_1 I}$ , the density of surface charge at any point Q on the body surface should satisfy the following integral equation (Al'pin, 1964)

$$S(Q) = \frac{K}{2\pi} \left[ \frac{\partial}{\partial n} \left( \frac{1}{R_{BQ}} \right) + \int_{S'} S(P) \frac{\partial}{\partial n} \left( \frac{1}{R_{PQ}} \right) ds \right], \quad (2)$$

where  $K = (\rho_2 - \rho_1) / (\rho_2 + \rho_1)$  is the reflection coefficient associated with the surface of the body,  $S'$  is all of the surface except that occupied by the point P.

We approximate S by an N-term expansion (Harrington, 1968),

$$S(P) \sim \sum_{j=1}^N f_j S_j, \quad (3)$$

where the expansion functions are given by

$$f_j = \begin{cases} 1 & \text{on the } j\text{th subsurface } S_j \\ 0 & \text{on all other subsurfaces.} \end{cases} \quad (4)$$

Substituting (3) into (2) gives

$$\sum_{j=i}^N S_j \int_{S_j} f_j \frac{\partial}{\partial n} \left( \frac{1}{R_{PQ}} \right) ds + \frac{2\pi}{K} S_i = \frac{\partial}{\partial n} \left( \frac{1}{R_{PQ}} \right); \quad j \neq i \quad (5)$$

Writing (5) for each of the  $N$  values of  $i$  results in the system of linear equations

$$\sum_{j=1}^N A_{ij} S_j = B_i \quad ; \quad (i=1, 2, \dots, N). \quad (6)$$

By solving this system of linear equations and utilizing the resulting values of  $S_j$ , we can calculate the potential and apparent resistivity at any point for different electrode configurations. Barnett (1972, 1976) discusses the singularity in the integral of equation (5) and also discusses the method of computation of the integral over a triangular facet. Hence, we will not discuss these matters here.

Now, the question is, "how to divide the body surface into a series of subsurfaces, suitable for any orientation of the ellipsoid, and satisfying the desired computational accuracy?" First, we divide the ellipsoid into 8 slices along the minor axis, by 7 contours (Figure 2(a)), and then create a series of triangles on the body surface. For the spheroid, we use a symmetric division of equal arc length and create 136 triangles on the body surface (Figure 2(b)). It is quite evident that most of the triangles are isosceles and the differences in their areas are small. For a thin ellipsoid, the surface of the body is

divided into 140 triangles as shown in Figure 2(c). Thus in this discretization, the 3-D body to be modeled is represented by a polyhedron bounded by a series of triangular facets.

In the computation procedure, a convenient method for specifying the size and dip of the body and assembling the subsurfaces of a polyhedron for an oblate spheroid in an arbitrary attitude is as follows: 1) first input the body size (semi-major axes  $a$ ,  $b$ , and  $c$ ), 2) assemble the coordinates of the apex for each triangle as a horizontal oblate spheroid, and 3) rotate the spheroid and transform the coordinates for each apex. We use  $x$ ,  $y$ ,  $z$  to represent the coordinates of the apex for each triangle in the original coordinate system  $X, Y, Z$  (Figure 3) for a horizontal oblate body. The new coordinates  $(x_{\text{new}}, y_{\text{new}}, z_{\text{new}})$  of each apex, after rotating successively about three semi-major axes by the angles  $\alpha$ ,  $\beta$ ,  $\gamma$ , are given by the following transformation

$$\begin{pmatrix} x_{\text{new}} \\ y_{\text{new}} \\ z_{\text{new}} \end{pmatrix} = \begin{pmatrix} (\cos \alpha \cdot \cos \beta) & (\cos \alpha \cdot \sin \beta \cdot \sin \gamma - \sin \alpha \cdot \cos \gamma) & (\cos \alpha \cdot \sin \beta \cdot \cos \gamma + \sin \alpha \cdot \sin \gamma) \\ (\sin \alpha \cdot \cos \beta) & (\sin \alpha \cdot \sin \beta \cdot \sin \gamma + \cos \alpha \cdot \cos \gamma) & (\sin \alpha \cdot \sin \beta \cdot \cos \gamma - \cos \alpha \cdot \sin \gamma) \\ (-\sin \beta) & (\cos \beta \cdot \sin \gamma) & (\cos \beta \cdot \cos \gamma) \end{pmatrix} \begin{pmatrix} x \\ y \\ z \end{pmatrix} \quad (7)$$

Of course we also can solve this potential problem by transforming the coordinates of the current and potential electrodes. A very important point to note is that by keeping the coordinates of the body in a horizontal attitude and transforming the coordinates of the positions of the current and potential electrodes we can save computation time, provided we do not change the body size but only the body attitude. It is obvious that the integration in equation (5) is not relative to the positions of the current and potential electrodes but only to the size and shape of the body. Thus if we

keep constant the size and shape of the body and only change its attitude, it is not necessary to recompute equation (5). Thus the integral equation method is more efficient than the finite element method in studying the responses of simple bodies.

In all of following figures,  $a, b, c$  represent the semi-major axes while,  $\alpha, \beta, \gamma$  represent the rotation angles shown in Figure 3, and  $(SBX, SBY, SBZ)$  and  $(EMX, EMY, EMZ)$  represent the coordinates of the current and potential electrodes, respectively. All computations were made on a Hewlett-Packard model 9826 desktop computer.

### Model Results

Throughout we use dimensionless units. The size of the body and all distances in the following model examples are expressed in terms of normalized distance units, the anomalous response is expressed by the normalized apparent resistivity ( $\rho_a / \rho_1$ ). For cross-borehole and single-borehole measurements, three different electrode configurations are considered. The simplest possible electrode configuration for cross-borehole measurements is the fixed single current electrode and moving single potential electrode. The other two arrays used are a widely spaced normal array (e.g., Figure 6) and a moving-bipole source with a moving-bipole receiver (e.g., Figure 22) for single- and cross-borehole measurements, respectively. Three typical cases, i.e., horizontal, dipping and vertical oblate spheroids, will be discussed separately. Finally, two representative results for an ellipsoid will be presented.

#### Horizontal oblate spheroid

The spatial variation of the normalized apparent resistivity ( $\rho_a / \rho_1$ ) for a conductive oblate spheroid with a resistivity contrast of  $\rho_2 / \rho_1 = 0.10$  in the plane defined by  $SBY = EMY = 0$  is shown in Figure 4. This result is very similar to the



apparent resistivity distribution from a spherical body (Lytle, 1982). As seen from Figure 4, the normalized apparent resistivity measured on the current-source side of the spheroid typically is less than one. However, on the side of the spheroid opposite the current source it typically is greater than one. This configuration of apparent resistivity indicates that charges of opposite sign are induced on opposite ends of the body. Thus a conductive body located between boreholes always produces  $\rho_a / \rho_1 > 1.00$  for the cross-borehole method. The resistivity anomaly in a vertical borehole containing the source is much smaller than in any borehole to the right of the source in Figure 4. This suggests that a larger anomaly can be detected using cross-borehole probing than using single-borehole probing.

Figure 5 illustrates borehole profiles of normalized apparent resistivity for different distances from the center of the body to the measuring borehole using the cross-borehole method. These curves indicate that the anomalous amplitude is highly dependent upon the location of the borehole in which the potential is measured. Model results for single-borehole measurement with a normal array of different L spacings are shown in Figure 6. Here the apparent resistivity has been calculated for a normal array whose M-B electrodes were reversed upon passing by the body, as shown in Figure 6; it is the same in other examples for single-borehole surveys presented later. This procedure has been used only to facilitate presentation of the profiles of apparent resistivity. The anomaly for single-borehole measurement in Figure 6 is quite small compared with the cross-borehole measurement in Figure 5.

#### Dipping oblate spheroid

If we rotate the oblate spheroid about the y axis, an asymmetrical spatial variation in normalized apparent resistivity will occur, along with an asymmetrical distribution of the induced surface charge on the boundary between the body and the surrounding

homogeneous medium. For a dipping conductive model of  $\beta = 45^\circ$  with the same size and resistivity contrast as in the horizontal case presented in Figure 4, the spatial distribution of the apparent resistivity in the x-z plane is depicted in Figure 7. It is quite evident that the anomaly is asymmetric about the body. The apparent resistivity perturbation is larger for cross-borehole than for single-borehole as before.

Figures 8 and 9 illustrate the anomalies caused by a conductive spheroid dipping at  $\beta = 45^\circ$  for resistivity contrasts of 0.01 and 0.10, respectively; the distances from the center of the body to the borehole in which the potential is measured are varied. The configuration used involves a fixed source and a moving potential electrode. As shown in these two figures, the asymmetry of the curves is related to the dip of the body. For both resistivity contrasts, the positions of peak amplitude of apparent resistivity not only are almost the same, but are very close to the upper edge of the body. Also note in these two figures, that the maxima of the anomalies decrease rapidly as the potential-measuring borehole is placed farther from the center of the body. When the distance EMX is three times greater than the semi-major axis ( $a = 2$ ) of the spheroid, the anomaly produced will be less than 2 percent\*. Of course, if the borehole containing the current source is located closer to the dipping oblate spheroid, the anomaly will be readily detected readily.

Next we rotate the thin oblate body about the y axis and observe the change in shape and amplitude of the profile of apparent resistivity. The plane of the body is perpendicular to the plane of the two boreholes used in a cross-borehole survey. The model results for various dips are given in Figures 10 and 11. The resistivity contrast is 0.10 for the data of both figures. Figure 10 illustrates the results for dips ( $\beta$ ) of  $0^\circ$ ,  $15^\circ$ , and  $30^\circ$ , while Figure 11 illustrates the results for dips ( $\beta$ ) of  $45^\circ$ ,  $60^\circ$ ,  $75^\circ$ , and  $90^\circ$ . As

\*The accuracy of the algorithm we believe to be better than 1% while field measurements are unlikely to have accuracies better than 1%.

would be expected, the anomalous amplitude decreases with the dip  $\beta$  from  $0^\circ$  to  $90^\circ$ . The positions of the peaks of the curves are always approximately opposite the upper edge of the body. It appears, therefore, that we can obtain a good idea of both the location and the dip of the body by using cross-borehole probing.

A comparison of the normalized apparent resistivity curves for various resistivity contrasts is shown in Figures 12 and 13. In these two figures, we keep the model parameters and electrode configuration constant, only the resistivity contrast is changed. The anomalous amplitude produced by a resistive body is slightly higher than that of a conductive body, under the condition that the magnitude of the resistivity contrast is the same. This result is identical with that obtained by Lytle (1982) for a spherical model. However, for a dipping thin conductive body (Figure 12), the position of the peak of the anomaly shifts to the depth of the upper edge of the body, as the resistivity contrast is increased. This does not happen for a dipping resistive thin body (Figure 13). While not shown here, these results pertain to dips of  $0 < \beta < 90^\circ$ .

The variation of  $\rho_a / \rho_1$  versus the size of the semi-minor axis  $c$ , for a thin conductive spheroid dipping at  $\beta = 45^\circ$ , with a resistivity contrast  $\rho_2 / \rho_1 = 0.10$ , is presented in Figure 14. The peak position of the curves gradually shifts to the depth of the edge of the body as the oblate spheroid becomes thinner, but the amplitude of the anomaly rapidly decreases (Figure 14).

Figure 15 shows the results of offsetting the borehole relative to the center of the dipping oblate body ( $\beta = 45^\circ$ ). The shapes of the anomalies vary slightly; the amplitude decreases very rapidly as the boreholes are offset. If the offsetting distance is greater than the semi-major axes of the thin spheroid, the anomaly virtually disappears. If the offset is in the negative direction of the  $y$ -axis by the same distances used for the data shown in Figure 15, the shape and the amplitude of the anomalies will appear the same as in Figure 15. Thus, it is impossible to determine on which side of the plane defined by

the two boreholes that the body lies.

For a dipping oblate body with the attitude of  $\gamma = 45^\circ$ , the results of offsetting the boreholes in the positive and negative y direction by the same distances applied in the example above are shown in Figure 16. The results are different from the last case; the anomalies in  $\rho_a / \rho_1$  are always greater than 1. If the offsetting distance (EMY) is zero, the anomaly appears as a symmetric curve. Comparing this curve with the curve ( $\beta = 0^\circ$ ) depicted by Figure 10, we see that the shape and amplitude of these two curves are almost the same; the maximum of the amplitude is exactly the same. Thus it is impossible to recognize the true dip of the oblate body from the curves, when the dip of the body is normal to the plane of the boreholes. For instance, as the oblate body takes the attitude of  $\gamma = 45^\circ$  or  $\gamma = -45^\circ$ , the anomalies from these two situations are exactly the same. Even if the boreholes are offset in the positive or negative y direction, as shown in Figure 16, it is still impossible to figure out the real dip of the oblate body, even though some small shifts occur in the peak position of the anomalies. We have found, for example, when the oblate body takes the attitude of  $\gamma = 45^\circ$  and the boreholes are offset by  $SBY = EMY = -1$ , or the body takes the symmetric attitude ( $\gamma = -45^\circ$ ) and boreholes are offset in the opposite direction by  $SBY = EMY = 1$ , the anomalies are identical.

#### Vertical oblate spheroid

For a thin vertical conductive spheroid, if the current source is placed on the axis of rotation of the body and close to the body, (Figure 17), a dramatic variation in the spatial distribution of normalized apparent resistivity occurs. As seen from Figure 17, the normalized apparent resistivity near the outer edges of the body is high. However, on the axis, and in the vicinity of the axis, on the side of the body opposite the current source, there is a low of normalized apparent resistivity. The reason for occurrence of

this "shielding effect" is the special distribution of the induced surface charge. The conditions causing this phenomenon include the eccentricity of the body, the resistivity contrast and the distance from the source to the center of the body. For the thin oblate model depicted in Figure 17, the induced negative charges are concentrated in the central area on the surface of the body facing the current source. However, most of the induced positive charges are repulsed and distributed on the outer edges of the body opposite the current source. The current flows out from the body in a "loudspeaker" shape. The current density near the axis of rotation probably is lower for the spheroid than for the sphere because of the surface charge distribution peculiar to the spheroid. Only at infinity does the current density recover to normal and the anomaly disappears. This is the reason why the two resistivity contours of  $\rho_a / \rho_1 = 1.00$  go to infinity along the rotation axis, on the side of the body opposite the current source. This conclusion is similar to the result described by Seigel (1952) for a special case in which the borehole just passes through the oblate body along its axis of rotation.

Figure 18 shows the normalized apparent resistivity responses versus the different positions of the borehole used for measurement of potential, with the configuration of a fixed current source and a moving potential electrode. Figure 18 illustrates that the three peaks of each anomaly, two positive and one negative, exactly indicate the positions of the center, the upper edge and the lower edge of the body. The amplitude of the anomaly decreases rapidly as the borehole used for potential measurements is located farther from the vertical oblate spheroid.

The model results with a widely spaced single-borehole normal array are given in Figure 19\*. Again, for convenience, the potential is reversed after passing the center of the body. It is seen that the anomalous shape and amplitude depend upon the array

\*The point of inscription of the measurement in Figure 19 is midway between the sources and the potential electrode M.

spacing. Referring back to Figure 7, assume that the borehole (dashed line) is parallel with the plane defined by the semimajor axes  $a$  and  $b$  and assume a normal array to move along the borehole. It is clear from Figure 7 that for the spacing  $L_1 = BM_1$ , which is less than  $a$  or  $b$ , then  $M_1$  is located in a region of  $\rho_a / \rho_1 = 1.00$ . On the other hand, for the spacing  $L_2 = BM_2$ , which is greater than  $a$  or  $b$ , then  $M_2$  is located in a region of  $\rho_a / \rho_1 > 1.00$ . These observations suggest, qualitatively, the reason for the reversal of the sign of the anomaly with array spacing shown in Figure 19. Therefore, it is necessary to exercise care in selecting the spacing of a normal array when attempting to detect a very thin oblate body from a single borehole.

#### Vertical ellipsoid

Here we present two typical model results of apparent resistivity profiles near a thin vertical ellipsoid using a fixed current source and moving potential electrode, to establish that the algorithm also can handle this geometry. The normalized apparent resistivity profile for a thin ellipsoid of  $a=6$ ,  $b=2$ ,  $c=0.2$ , for which  $\beta = 90^\circ$  is shown in Figure 20; the long axis of the body is vertical. The shape of the anomalies are almost the same as for the case of a thin vertical spheroid (Figure 18), but the amplitude is higher due to the larger size of the body. (Note the difference in scales between Figures 18 and 20). From these symmetric curves, the center of the body and the size of the major axis can be recognized easily from the locations of the negative and positive peaks. When the potential-measuring borehole is offset from opposite the center of the spheroid, i.e., moved into or out of the page in Figure 20, there is a change in amplitude of the anomaly, but there is no reversal of the sign of the anomaly. This result is not shown here in order to avoid clutter in Figure 20.

If the strike of the major axis of the body is parallel to the  $y$ -axis (Figure 21, note here  $b=6$ ) and the boreholes lie opposite the center of the body (zero offset distance), the

anomaly appears as  $\rho_a < \rho_1$  and the two minor peaks for  $\rho_a > \rho_1$  (as in Figure 20) disappear. However, if the boreholes are offset as depicted as EMY=3 and EMY=5 in Figure 21, the anomalies of  $\rho_a / \rho_1$  are positive, i.e.,  $\rho_a > \rho_1$ .

### Error analysis

There are three sources of error for calculating the potential by means of the surface charge integration described in this study. The first error arises in the integrations in equation (5). The second error is the accumulative error for solving the higher-order linear equations (6). Even though these two kinds of errors are hard to estimate, their effect is minor with computers of adequate precision. The third error is the major one and arises in the discretization of the surface of the body. For solving the integral equation, the body surface is divided into a series of triangular subareas over which the surface charge density is assumed to be constant. However, the surface charge distribution is highly dependent upon the attitude of the body and the location of the body relative to the current source, especially when the current source is very close to the body. Of course, we can always assemble a polyhedron using more facets, but it will cost more computer time and may cause the accuracy to decrease because linear equations of higher order must be solved.

We have checked the accuracy of the algorithm by two methods for each of the three typical attitudes of a spheroid and two attitudes of an ellipsoid. As shown in Table 1, when the current source is placed at "infinity" ( $SBX = -10^6$ ), the anomaly disappears and the apparent resistivity equals one, as it should be. As the potential electrode is far away from the center of the body along the z-axis ( $EMZ = 50$ ), the anomaly rapidly decreases and the apparent resistivity is very close to one. In addition, a comparison between the analytical solutions (Lytle, 1982; Seigel, 1952; and Dobecki, 1980) and the numerical solution applied in this study for a spherical body and a horizontal spheroid

indicates that the agreement is excellent on the condition that the current source is not on the surface of the body or approximately so (the errors are less than 1 or 2 percent).

In most cases, the main error appears as a shift of the baseline of the normalized apparent resistivity curves. The effects on the shape of the anomaly are less significant. So long as we appropriately adjust the discretization contour positions according to the variation of the surface charge distribution, a satisfactory result will be achieved.

We made a check in principal of the data of Figure 17, approximating the oblate spheroid by a thin polygon, using the volume integral equation algorithm of Hohmann (1975). The results, while not shown here, were gratifyingly similar to those of Figure 17.

Estimation of location of center, dip,  
and size of the semi-major axes of an oblate body

The cross-borehole and single-borehole modeling results illustrate that in some case it is possible to determine the depth of the center or the depth of the upper edge of the body and to estimate its dip and the size of its semi-major axes. For a vertically dipping oblate spheroid the depth of the center of the body and the size of semi-major axes can be figured out very easily from the data of Figure 18. However, for a horizontal oblate spheroid, estimation of the size of the semi-major axes is not obvious; the only hope is to seek help in curve matching via the modeling procedure (compare Figures 5 and 18 to perceive the problem).

For a dipping oblate body, which is the main target in this study, if two boreholes are located on opposite sides of the body and reasonably near it, an estimate of the depth of the center of the body, its size and its dip can be obtained with a moving-bipole source and moving-bipole receiver. Model results for a dipping oblate body of  $\beta = 45^\circ$  with the moving-bipole source and moving-bipole receiver are presented in Figure 22. As



mentioned by Daniels (1977) this is the "optimum" cross-borehole array configuration for eliminating singularities of the geometric factor. The negative peak accurately shows the depth of the center of the body and meanwhile an estimate of size of the body may be obtained from the positions of the positive peaks. Once this has been achieved, one may fix a current source at the depth of the center of the body in a borehole and make measurements of potential in another borehole with a moving electrode; then an estimate of dip may be achieved. Unfortunately, moving the source and receiver synchronously in two boreholes is difficult under typical field conditions.

A more simple and practical method applied in this study is to interchange the roles of two boreholes; first use one as a potential measuring location, and second use it as a source location. As seen from Figure 23, we first fix the current source at a depth below the center of the body in hole 1 and then measure the apparent resistivity with a moving electrode in hole 2. Then we use a current electrode located in hole 2, above the center of the body, and measure the potential in hole 1. The information about size, dip and the center of the body are given by the peak positions, the asymmetry of the curves and the crossover of the curves between the two peaks, respectively. All that is assumed is that the body is below  $B_2$  and above  $B_1$ . No formal interpretation procedure is suggested for this technique since it would require a catalogue of curves which is beyond the scope of the present study. The dip vector of this body is parallel to the plane of the boreholes.

If the dip vector of the body is normal to the plane of the boreholes (Figure 24), the midpoint of the dashed line between the two peaks indicates the depth of the center of the body. Unfortunately, in this case there is ambiguity in estimating dip as  $-45^\circ$  or  $+45^\circ$ . No information on the size of the body is evident in Figure 24.

Another special case is that in which the anomalous body is not located inside of the two boreholes (Figure 25). Then an estimate of the direction of the anomalous body also can be made. As seen from Figure 25, for a conductive oblate body which is placed

on the left-hand side of the two boreholes, the anomalies measured in both holes mainly appear as  $\rho_a < \rho_1$ . This point can be taken as evidence that an anomalous body does not exist between the boreholes. Meanwhile, the larger anomaly measured from hole 1 indicates that it is nearer to the body than is hole 2.

### Conclusion

The algorithm for surface charge integration is a powerful tool to solve potential problems arising in resistivity. In fact, the method applied in this study can be used to compute the profile of apparent resistivity for arbitrarily shaped 3-D bodies if they can be represented by a polyhedron bounded by triangular facets. The model results indicate that the amplitude of apparent resistivity is highly dependent upon the locations of the current source and the borehole in which potential measurements are made, relative to the body, especially for a measuring borehole offset in the strike direction. If a resistivity contrast of 10 or more exists and if the boreholes are located at reasonable distances, the measured  $\rho_a / \rho_1$  anomaly will be readily detectable above the noise, even though the ellipsoid is very thin.

As seen from the typical cases studied, for a vertical spheroid and a vertical ellipsoid the depth of the center of the body and the size of the major axis can be determined with the simple configuration of a fixed current electrode and a moving potential electrode. For a dipping spheroid or ellipsoid, in which the dip vector of the body lies in the plane defined by the two boreholes, the depth of the center of the body can be determined accurately and estimates of the dip and the size of the major axis can be made. However, if the dip vector is normal to the plane defined by the two boreholes, it is more difficult to figure out the true dip of the body. It is also difficult to estimate the size of the body when the spheroid is horizontal.

It has been shown that in comparison with single-borehole measurements, the cross-borehole measuring technique is a more effective procedure in providing detectability of the anomalous amplitude and the dip of a spheroid or ellipsoid in the vicinity of a borehole. In most cases, if the anomaly is detectable then the depth of the center of the body can be located accurately; meanwhile the size of the major axis of the body and the dip of the body can be approximately outlined.

The strike of thin ellipsoids relative to the azimuth between two boreholes critically affects the size and shape of the resistivity anomaly for the cross-borehole technique.

### Acknowledgements

One of us (F. W. Y.) was able to participate in this project via a two-year's leave granted by the People's Republic of China. Suzanne Zink typed the manuscript while Paul Onstott prepared the illustrations; we are indebted to them both. Funding for the typing and drafting came from the Geophysics Special Fund of the Department of Geology and Geophysics of the University of Utah. This fund arises in contributions from numerous industrial concerns to whom we are grateful.

W. R. Petrick initially advised us on the approach used for this study. G. W. Hohmann critically reviewed a draft of the manuscript and made many helpful suggestions. H. P. Ross was helpful in providing editorial comment. We thank each of them.

## References

- Alpin, L. M., 1964, On the solution of the fundamental problem of resistivity logging: Sci. Rep., Izv. Geophys., 236-238.
- Barnett, C. T., 1972, Theoretical modeling of induced polarization effects due to arbitrarily shaped bodies: Colorado School of Mines, Ph.D. thesis T-1453.
- Barnett, C. T., 1976, Theoretical modeling of the magnetic and gravitational fields of an arbitrarily shaped three-dimensional body: Geophysics, 41, 1353-1364.
- Daniels, J. J., 1977, Three-dimensional resistivity and induced polarization modeling using buried electrodes: Geophysics, 42, 1006-1009.
- Dieter, K., Paterson, N. R., and Grant, F. S., 1969, IP and resistivity type curves for three-dimensional bodies: Geophysics, 34, 615-632.
- Dobecki, T. L., 1980, Borehole resistivity curves near spheroidal masses: Geophysics, 45, 1513-1522.
- Harrington, R. F., 1968, Field computation by moment methods: The Macmillan Company.
- Hohmann, G. W., 1975, Three-dimensional induced polarization and electromagnetic modeling: Geophysics, 40, 309-324.
- Lee, T., 1975, An integral equation and its solution for some two- and three-dimensional problems in resistivity and induced polarization: Geophys. J. R. Astro. Soc., 42, 81-95.
- Lytle, R. J., 1982, Resistivity and induced-polarization probing in the vicinity of a spherical anomaly: Inst. of Elect. and Electron. Eng., Trans. on Geoscience and Remote Sensing, GE-20, 493-499.

Merkel, R. H., and Alexander, S. S., 1971, Resistivity analysis for models of a sphere in a half-space with buried current source: *Geophys. Prosp.*, **19**, 640-651.

Seigel, H. O., 1952, Ore body size determination in electrical prospecting: *Geophysics*, **17**, 907-914.

Snyder, D. D., 1976, A method for modeling the resistivity and IP response of two-dimensional bodies: *Geophysics*, **41**, 997-1015.

Snyder, D. D., and Merkel, R. M., 1973, Analytic models for the interpretation of electrical surveys using buried current electrodes: *Geophysics*, **38**, 513-529.

## Figure Captions

- Fig. 1. The configuration of electrodes and a thin ellipsoid for (a) single-borehole, and (b) cross-borehole measurements. The center of the ellipsoid is the origin of the coordinate system. The resistivity of the body is  $\rho_2$  while that of the host is  $\rho_1$ . P and Q are specific and arbitrary points of surface charge density.
- Fig. 2. The discretization of the surface of the oblate body: (a) division of contours normal to z-axis, (b) division of triangles for a spheroid and (c) division of triangles for an ellipsoid. The semi-axes are a, b, and c in the x, y, and z or x', y', z' directions, respectively.
- Fig. 3. The coordinate rotation and the positive direction of each rotation angle. The x', y', z'; x'', y'', z'' and x''', y''', z''' represent the new coordinate system after successive rotations about each of the Z, Y, and X axis, respectively. X, Y, Z is the original coordinate system.
- Fig. 4. The variation of normalized apparent resistivity ( $\rho_a / \rho_1$ ) for a horizontal spheroid in the x-z plane, with a resistivity contrast of  $\rho_2 / \rho_1 = 0.10$ , the body size is a = b = 2, c = 0.2. The coordinates of the current source are SBX = -3.0, SBY = SBZ = 0.
- Fig. 5. Cross-borehole resistivity profiles for a thin *horizontal* spheroid as functions of the position of the borehole in which potential measurements are made. The source electrode is fixed at B in the first borehole while the measuring electrode M is moved down the second borehole. All parameters are indicated in the figure.
- Fig. 6. Single-borehole resistivity profiles for a thin *horizontal* spheroid as functions of the electrode spacing L of a normal array. All parameters are indicated in the figure. These profiles should be compared with those of Figure 5.

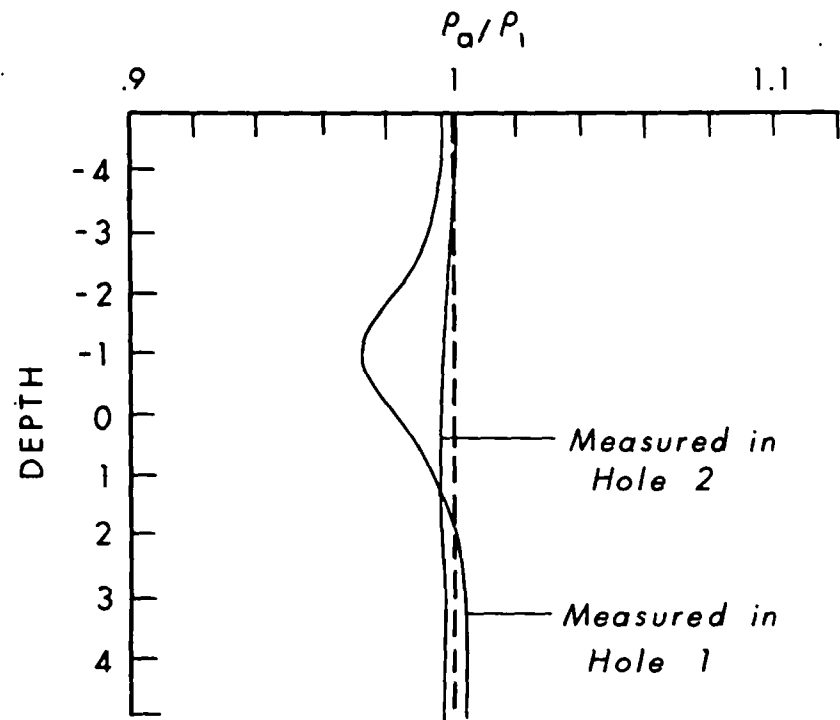
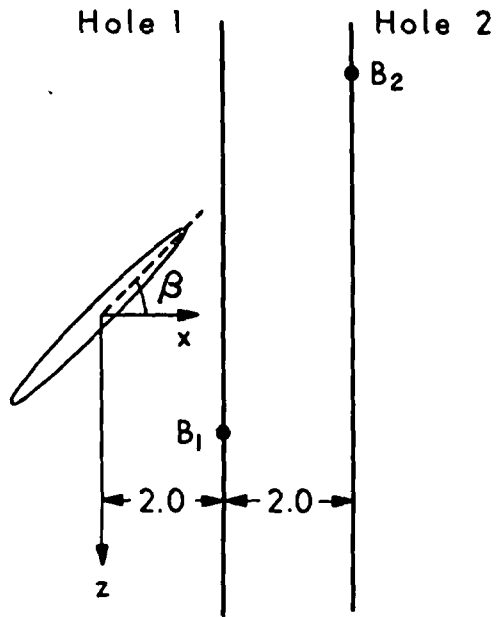


- Fig. 7. The spatial distribution of the normalized apparent resistivity caused by a dipping spheroid ( $\beta = 45^\circ$ ,  $a = 2$ ,  $b = 2$ ,  $c = 0.2$ ) in the  $x$ - $z$  plane. The current source is located at  $SBX = -2.5$ ,  $SBY = SBZ = 0$ . The resistivity contrast  $\rho_2/\rho_1$  is 0.10. A hypothetical borehole, containing the source, is shown in order to facilitate discussion of potentials measured at  $M_1$  and  $M_2$ .
- Fig. 8. Cross-borehole apparent resistivity profiles, for a conductive spheroid dipping at  $\beta = 45^\circ$ , versus the position of the borehole in which the potential measurements are made. The source electrode is fixed at B in the first borehole while the measuring electrode M is moved down the second borehole. All parameters are indicated in the figure. The resistivity contrast  $\rho_2/\rho_1$  is 0.01. These profiles should be compared with those of Figure 5.
- Fig. 9. Cross-borehole apparent resistivity profiles, for a conductive spheroid dipping at  $\beta = 45^\circ$ , versus the position of the borehole in which potential measurements are made. The only change from Figure 8 is that the resistivity contrast  $\rho_2/\rho_1$  is now 0.10. These profiles should be compared with those of Figure 8 and Figure 5.
- Fig. 10. Effect of dip on cross-borehole measurements for a *gently* dipping conductive spheroid. All parameters are indicated in the figure for this fixed-source, moving-potential configuration of electrodes.
- Fig. 11. Effect of dip on cross-borehole measurements, for a *steeply* dipping conductive spheroid. All parameters are indicated in the figure for this fixed-source, moving-potential, configuration of electrodes.
- Fig. 12. Effect of resistivity contrast on cross-borehole measurements, for a dipping *conductive* spheroid. All parameters are indicated in the figure for this fixed-source, moving-potential configuration of electrodes.
- Fig. 13. Effect of resistivity contrast on cross-borehole measurements, for a dipping *resistive* spheroid. All parameters are indicated in the figure for this fixed-source, moving-potential, configuration of electrodes.

- Fig. 14. Effect of aspect ratio  $c/a$  on cross-borehole measurements, for a dipping conductive spheroid. All parameters are indicated in the figure for this fixed-source, moving-potential, configuration of electrodes.
- Fig. 15. Effect of offset-distance for a spheroid whose dip vector is *parallel* to the plane of the two boreholes used in cross-borehole measurements. All parameters are indicated in the figure for this fixed-source, moving-potential, configuration of electrodes.
- Fig. 16. Effect of offset-distance for a spheroid whose dip vector is *perpendicular* to the plane of the two boreholes used in cross-borehole measurements. All parameters are indicated in the figure for this fixed-source, moving-potential, configuration of electrodes.
- Fig. 17. The variation of normalized apparent resistivity ( $\rho_a/\rho_1$ ) for a vertical spheroid in the x-z plane, with a resistivity contrast  $\rho_2/\rho_1 = 0.10$ : the body size is  $a = b = 2$ ,  $c = 0.2$ . The coordinates of the current source are  $SBX = -1.0$ ,  $SBY = SBZ = 0$ . Compare with Figure 4.
- Fig. 18. Cross-borehole resistivity profiles for a thin *vertical* spheroid as functions of the position of the borehole in which potential measurements are made. The source electrode is fixed at B in the first borehole while the measuring electrode M is moved down the second borehole. All parameters are indicated in the figure. Compare with Figure 5.
- Fig. 19. Effect of L-spacing for a vertical spheroid in single-borehole, widely spaced, reversed, *normal array* measurements All parameters are indicated in the figure.
- Fig. 20. Cross-borehole apparent resistivity profiles, for a vertical conductive *ellipsoid*, versus the position of the borehole in which the potential measurements are made. All parameters are shown in the figure. Compare with Figure 18 but note change of scales. The long axis of the ellipsoid is *parallel vertical*.

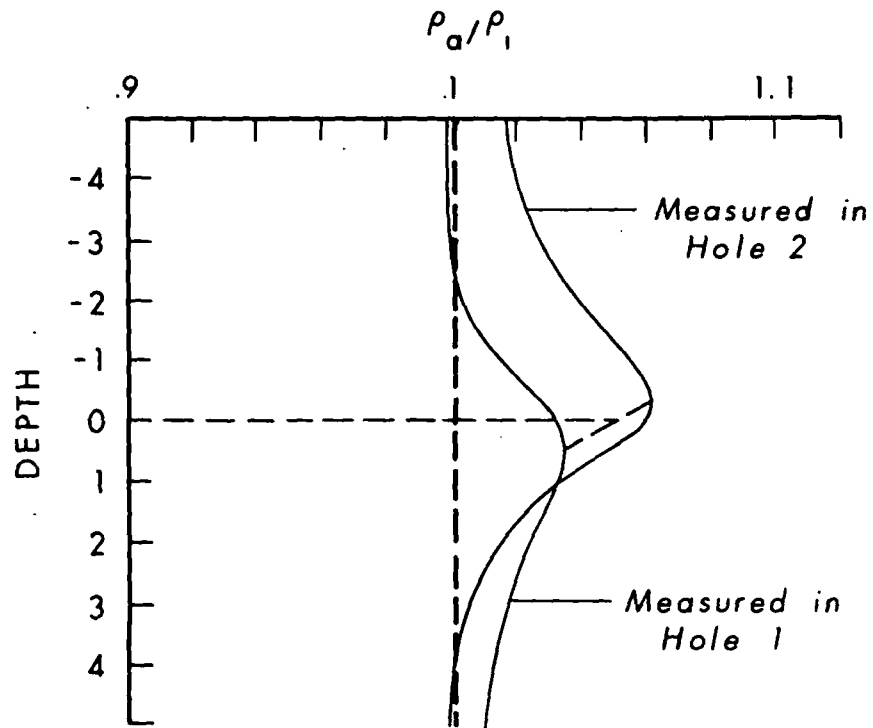
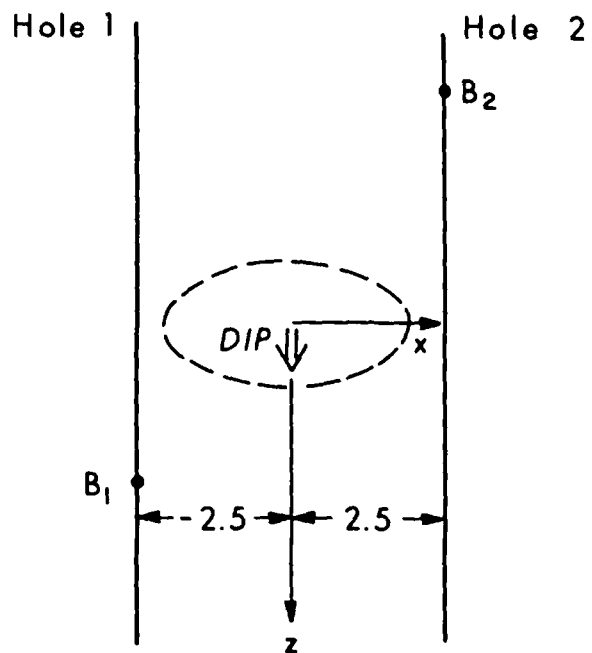
- Fig. 21. Cross-borehole apparent resistivity profiles, for a vertical conductive *ellipsoid* , versus offset of the position of the borehole in which potential measurements are made. The long axis of the ellipsoid is *horizontal* . All parameters are shown in the figure.
- Fig. 22. Cross-borehole apparent resistivity profiles, for a spheroid dipping at  $\beta = 45^\circ$ , versus the L-spacing used in a configuration consisting of a moving-bipole source, and a moving-bipole receiver. The midpoint of MN is the measuring point. All parameters are shown in the figure.
- Fig. 23. Estimation of size, dip, and center of a spheroid obtained with an interchange measurement procedure using two boreholes. All parameters are shown in the figure.
- Fig. 24. Estimation of the depth of the center of the body for a body whose dip vector is not parallel to the plane of the two boreholes used in cross-borehole measurements. All parameters are shown in the figure.
- Fig. 25. An illustration of the procedure to determine the direction to a thin spheroid from cross-borehole interchange measurements. All parameters are shown in the figure.
- Table 1. Accuracy of algorithms for five different body configurations.

### CROSS-BOREHOLE



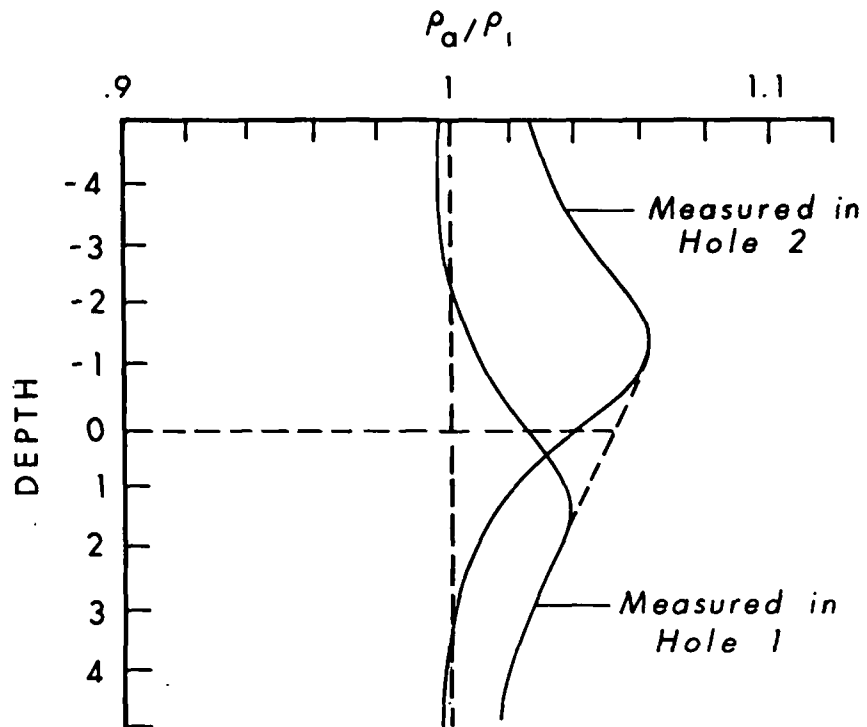
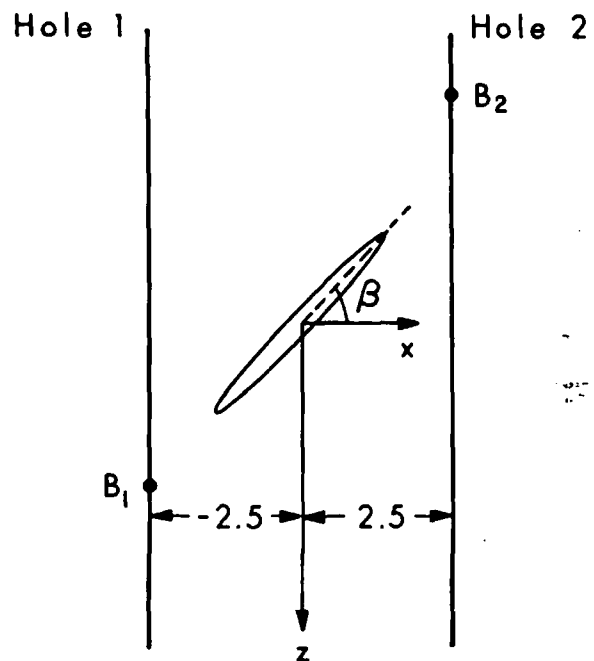
Electrode Configuration	Body Size	Angles	Resistivity Contrast
Exchanging Measurement $SB_1 Y = 0$ $SB_1 Z = 2.0$ $SB_2 Y = 0$ $SB_2 Z = -4.0$	$a = 2$ $b = 2$ $c = 0.2$	$\alpha = 0^\circ$ $\beta = 45^\circ$ $\gamma = 0^\circ$	$\frac{\rho_2}{\rho_1} = 0.10$

CROSS-BOREHOLE



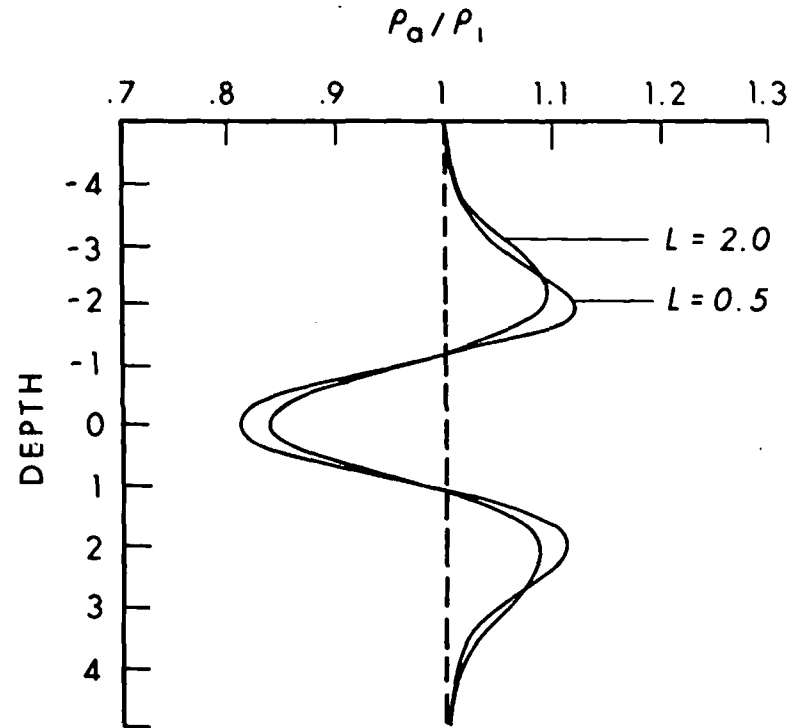
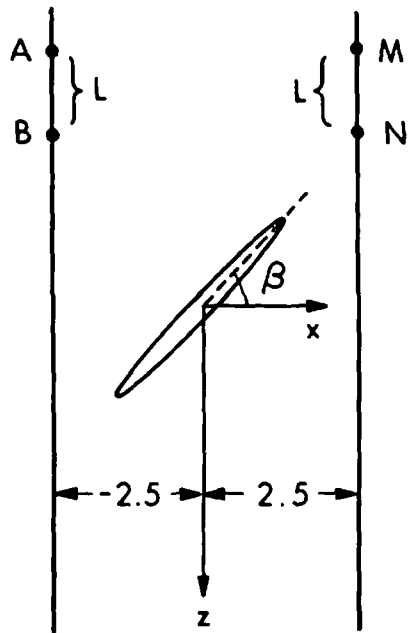
Electrode Configuration	Body Size	Angles	Resistivity Contrast
Exchanging Measurement $SB_1 Y=0 \quad SB_1 Z=2.5$ $SB_2 Y=0 \quad SB_2 Z=-4.0$	$a=2$ $b=2$ $c=0.2$	$\alpha=0^\circ$ $\beta=0^\circ$ $\gamma=45^\circ$	$\frac{\rho_2}{\rho_1} = 0.10$

CROSS - BOREHOLE



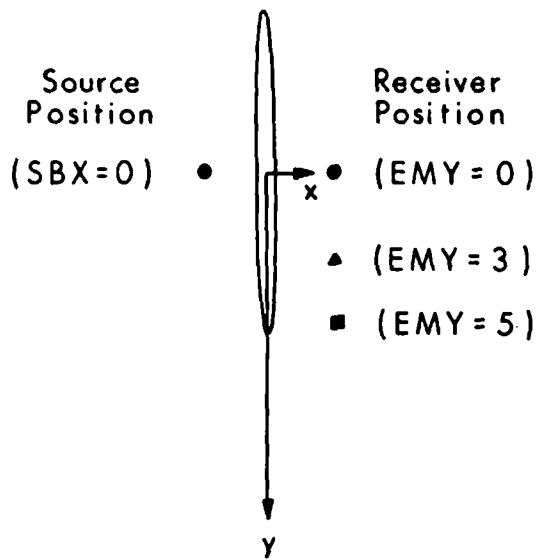
Electrode Configuration	Body Size	Angles	Resistivity Contrast
Exchanging Measurement $SB_1 Y=0$ $SB_1 Z=2.5$ $SB_2 Y=0$ $SB_2 Z=-4.0$	$a=2$ $b=2$ $c=0.2$	$\alpha=0^\circ$ $\beta=45^\circ$ $\gamma=0^\circ$	$\frac{\rho_2}{\rho_1} = 0.10$

CROSS - BOREHOLE

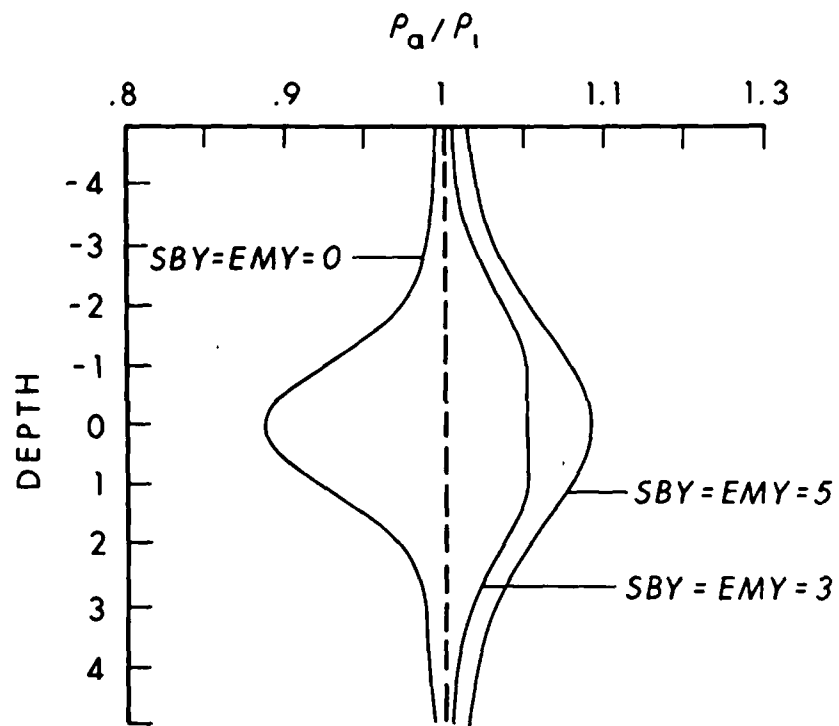


Electrode Configuration	Body Size	Angles	Resistivity Contrast
Moving Bipole Source Moving Bipole Receiver SAY = SBY = 0 EMY = ENY = 0	a = 2 b = 2 c = 0.2	$\alpha = 0^\circ$ $\beta = 45^\circ$ $\gamma = 0^\circ$	$\frac{\rho_2}{\rho_1} = 0.10$

CROSS - BOREHOLE



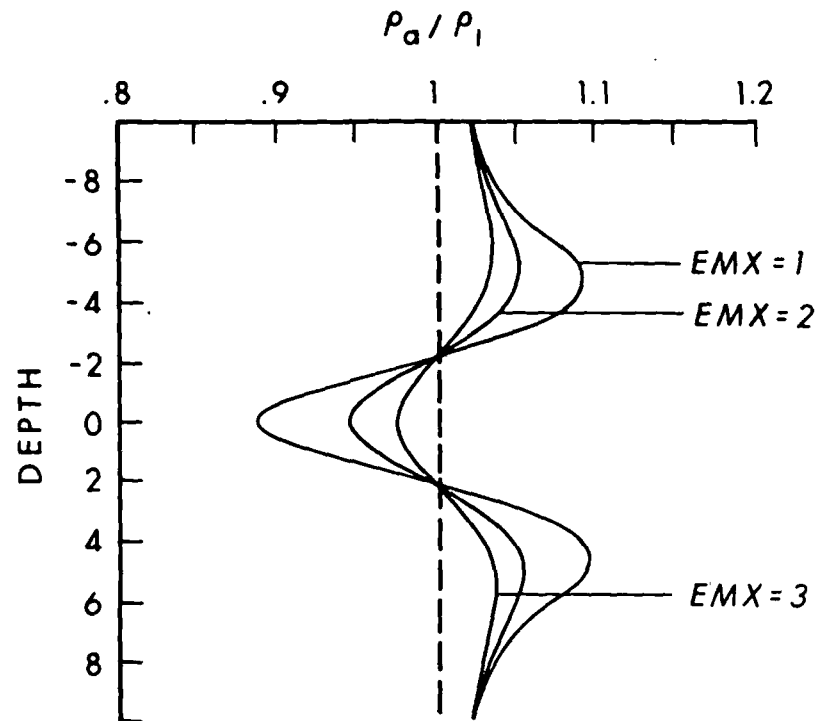
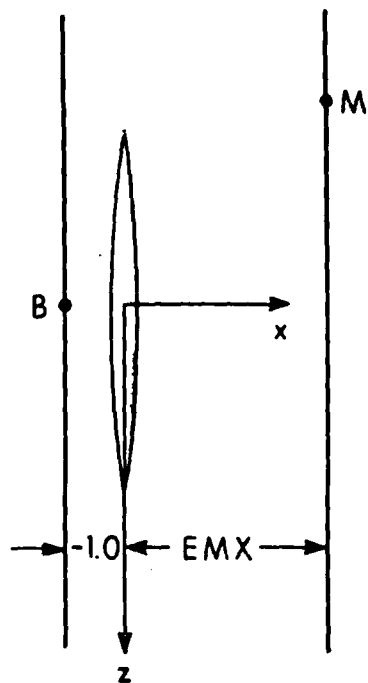
PLAN VIEW



Electrode Configuration	Body Size	Angles	Resistivity Contrast
Fixed Source Moving Electrode SBX=-1.0 SBZ=0 EMX = 1.0	a = 2 (z) b = 6 (y) c = 0.2 (x)	$\alpha = 0^\circ$ $\beta = 90^\circ$ $\gamma = 0^\circ$	$\frac{\rho_2}{\rho_1} = 0.10$

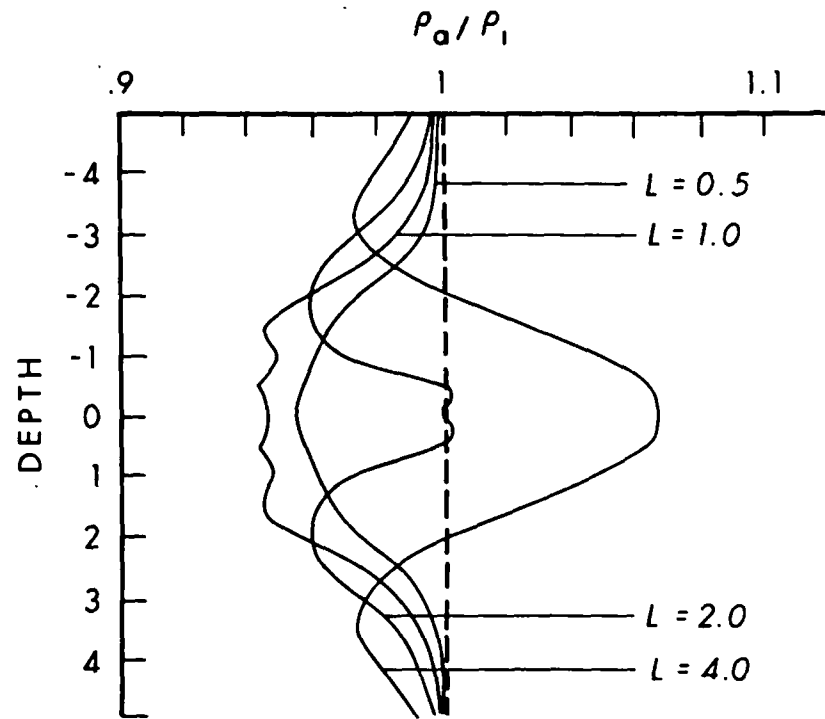
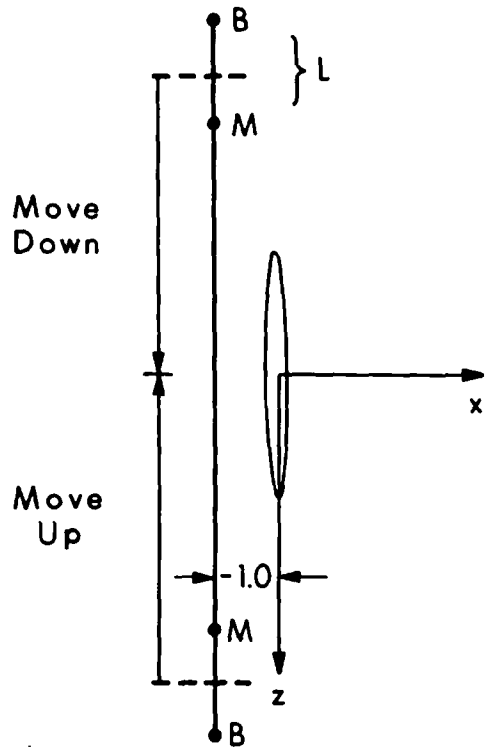


CROSS-BOREHOLE



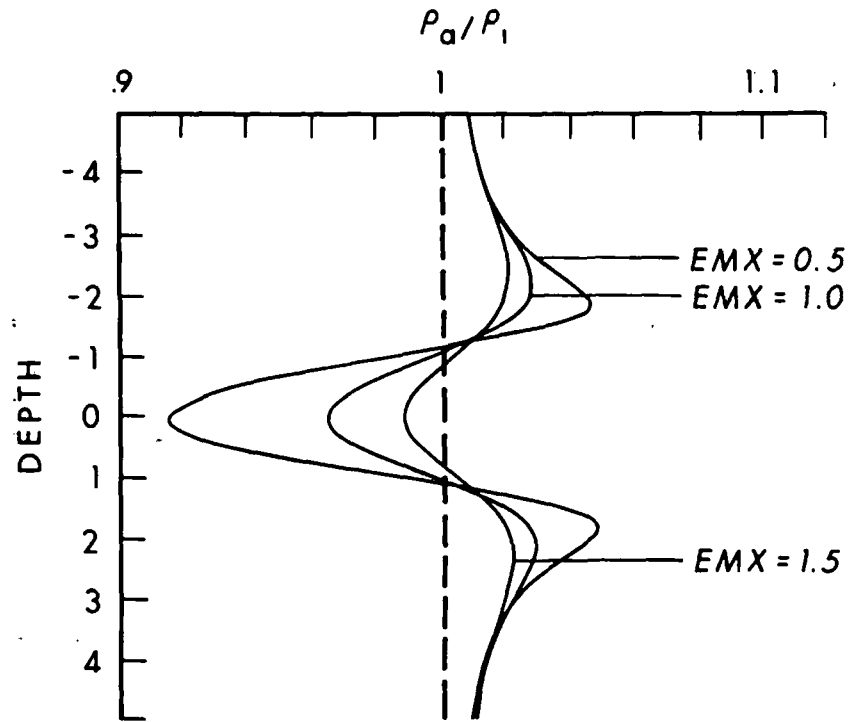
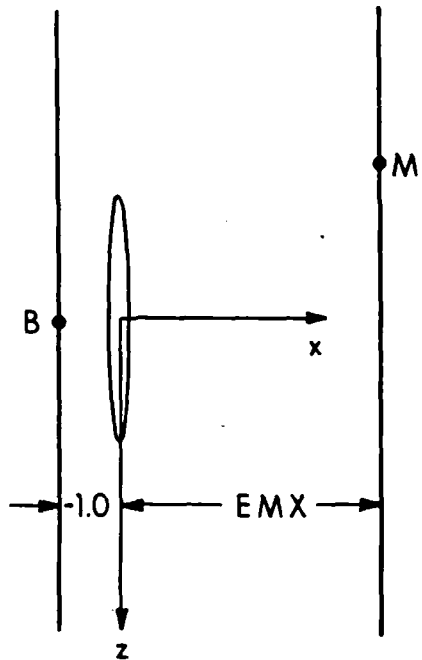
Electrode Configuration	Body Size	Angles	Resistivity Contrast
Fixed Source Moving Electrode $SBX = -1.0$ $SBY = SBZ = 0$ $EMY = 0$	$a = 6 (z)$ $b = 2 (y)$ $c = 0.2 (x)$	$\alpha = 0^\circ$ $\beta = 90^\circ$ $\gamma = 0^\circ$	$\frac{\rho_2}{\rho_1} = 0.10$

SINGLE - BOREHOLE

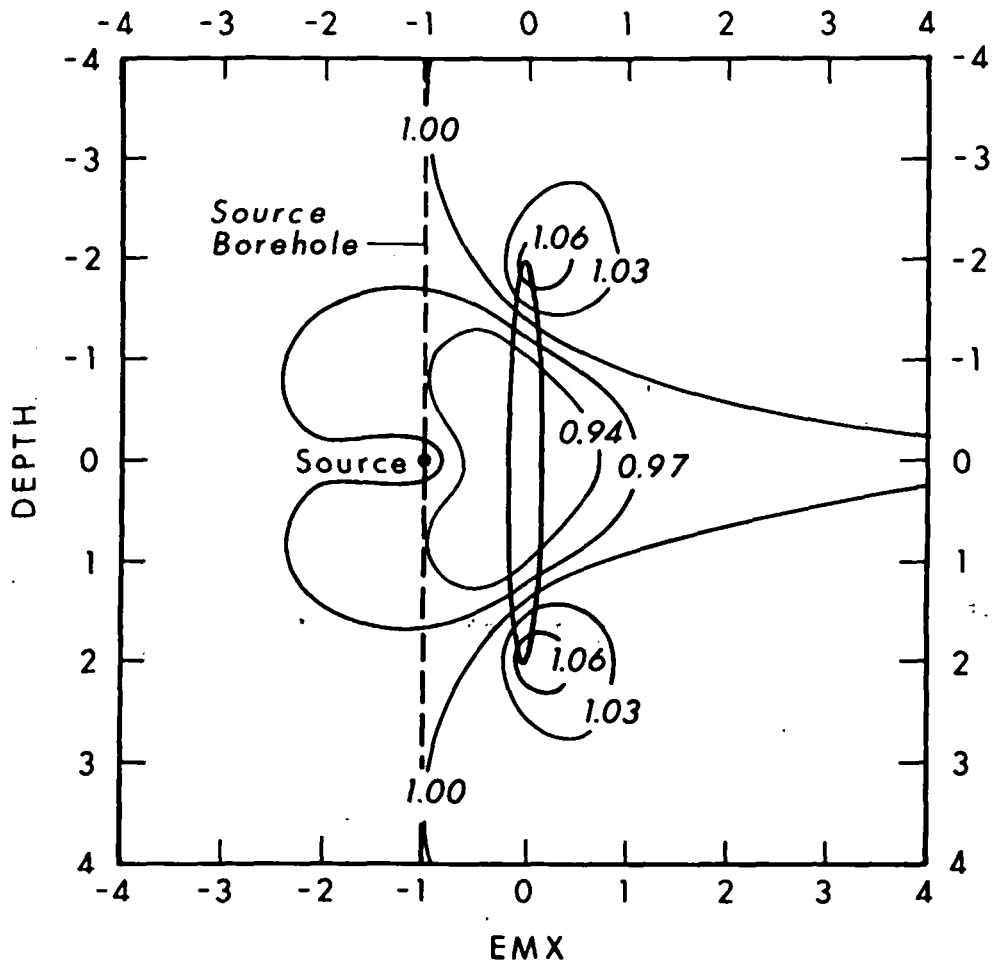


Electrode Configuration	Body Size	Angles	Resistivity Contrast
Normal Array SBY=0	$a = 2 (z)$ $b = 2 (y)$ $c = 0.2 (x)$	$\alpha = 0^\circ$ $\beta = 90^\circ$ $\gamma = 0^\circ$	$\frac{\rho_2}{\rho_1} = 0.10$

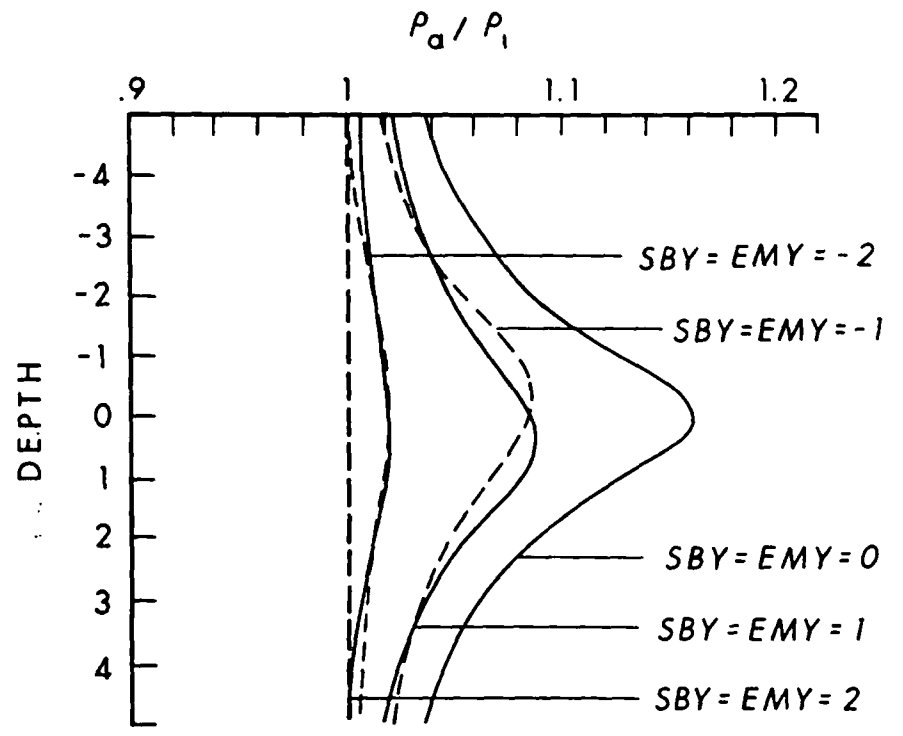
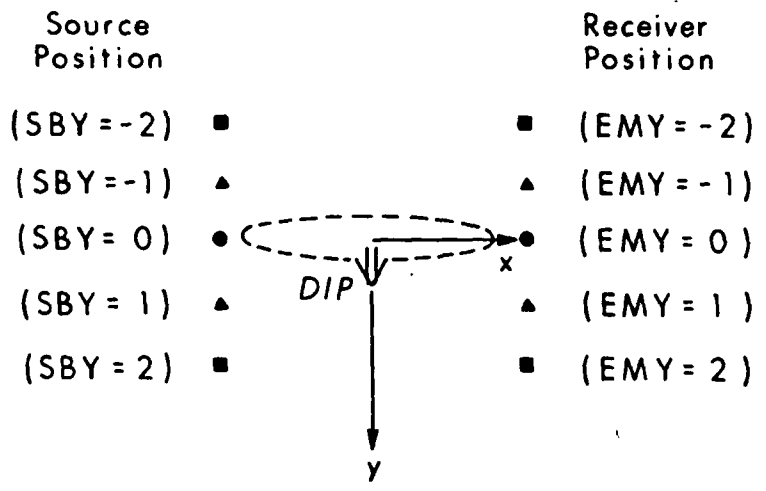
CROSS - BOREHOLE



Electrode Configuration	Body Size	Angles	Resistivity Contrast
Fixed Source Moving Electrode $SBX = -1.0$ $SBY = SBZ = 0$ $EMY = 0$	$a = 2 (z)$ $b = 2 (y)$ $c = 0.2 (x)$	$\alpha = 0^\circ$ $\beta = 90^\circ$ $\gamma = 0^\circ$	$\frac{\rho_2}{\rho_1} = 0.10$



CROSS - BOREHOLE

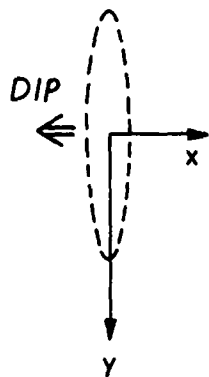


Electrode Configuration	Body Size	Angles	Resistivity Contrast
Fixed Source Moving Electrode SBX = -2.5 SBZ = 0 EMX = 2.5	a = 2 (x) b = 2 c = 0.2	$\alpha = 0^\circ$ $\beta = 0^\circ$ $\gamma = 45^\circ$	$\frac{\rho_2}{\rho_1} = 0.10$

CROSS - BOREHOLE

Source Position

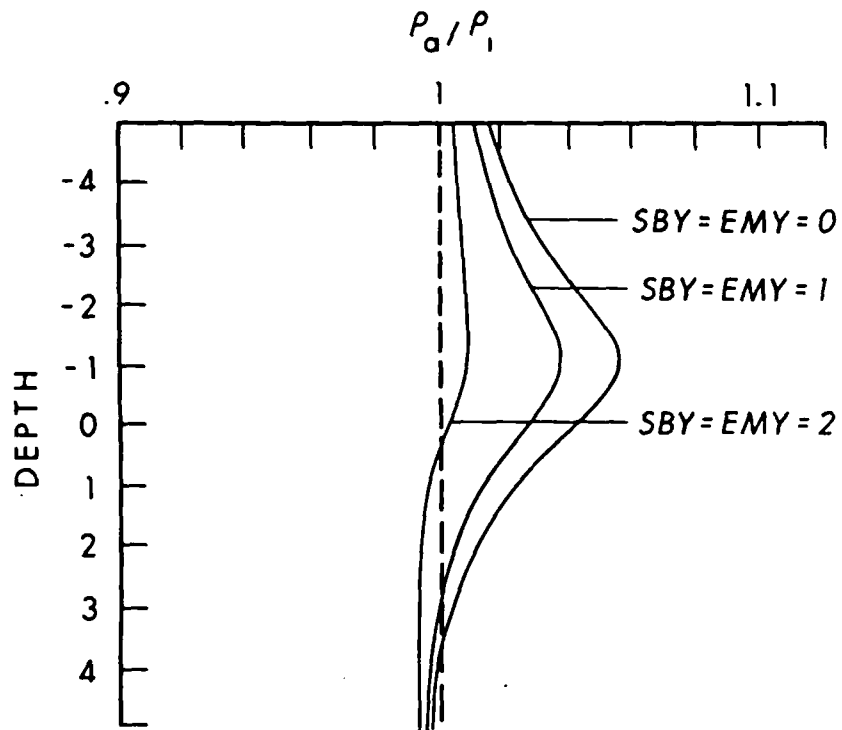
- (SBY = 0) ●
- (SBY = 1) ▲
- (SBY = 2) ■



Receiver Position

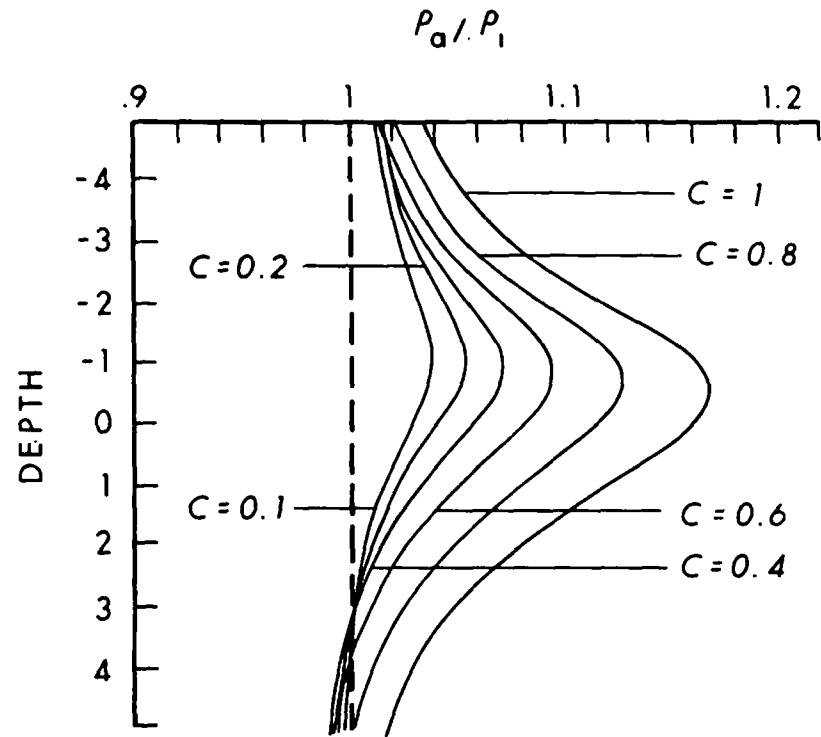
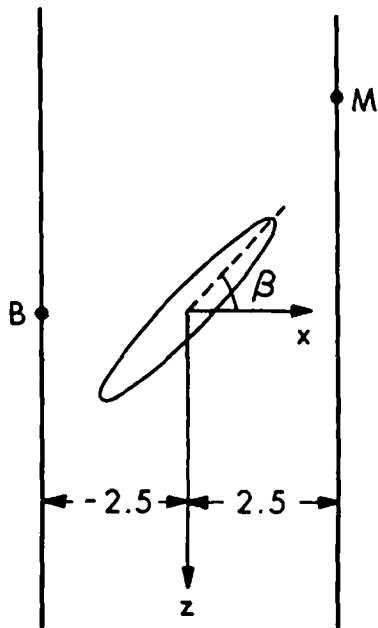
- (EMY = 0)
- ▲ (EMY = 1)
- (EMY = 2)

PLAN VIEW



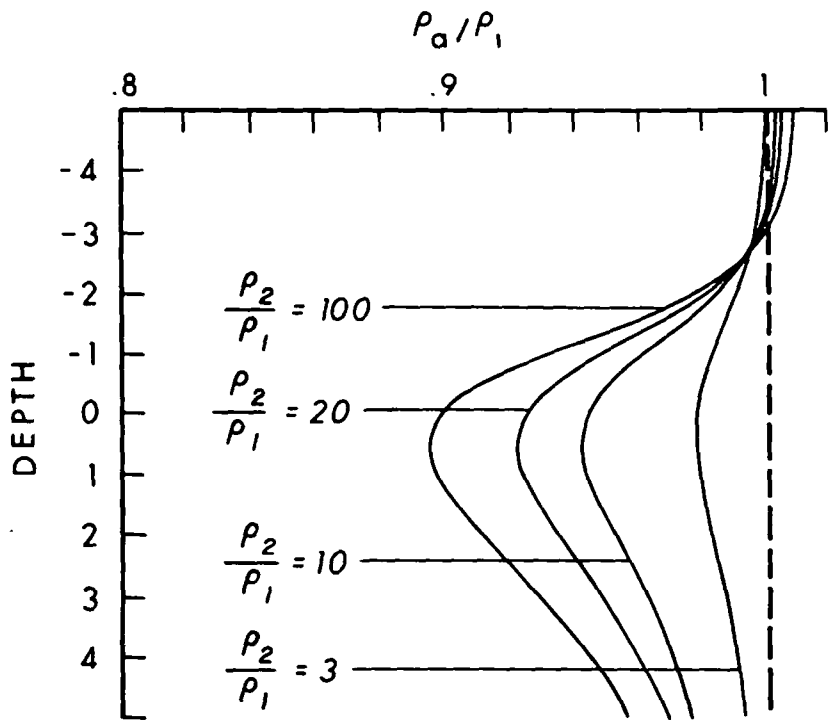
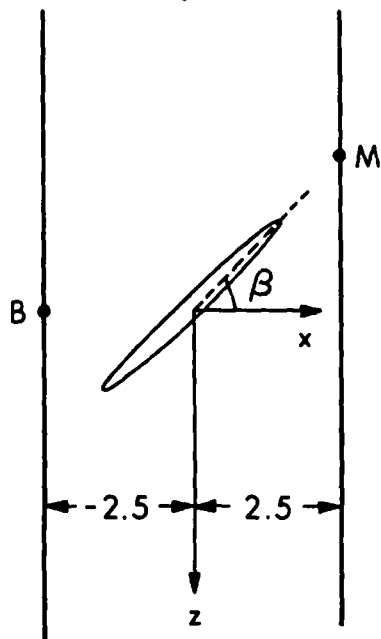
Electrode Configuration	Body Size	Angles	Resistivity Contrast
Fixed Source Moving Electrode SBX = -2.5 SBZ = 0 EMX = 2.5	a = 2 b = 2 (y) c = 0.2	$\alpha = 0^\circ$ $\beta = 45^\circ$ $\gamma = 0^\circ$	$\frac{\rho_2}{\rho_1} = 0.10$

CROSS-BOREHOLE



Electrode Configuration	Body Size	Angles	Resistivity Contrast
Fixed Source Moving Electrode SBX=-2.5 SBY=SBZ=0 EMX=2.5 EMY=0	$a = 2$ $b = 2$ $c = 0.1, 0.2, 0.4, 0.6, 0.8, 1$	$\alpha = 0^\circ$ $\beta = 45^\circ$ $\gamma = 0^\circ$	$\frac{\rho_2}{\rho_1} = 0.10$

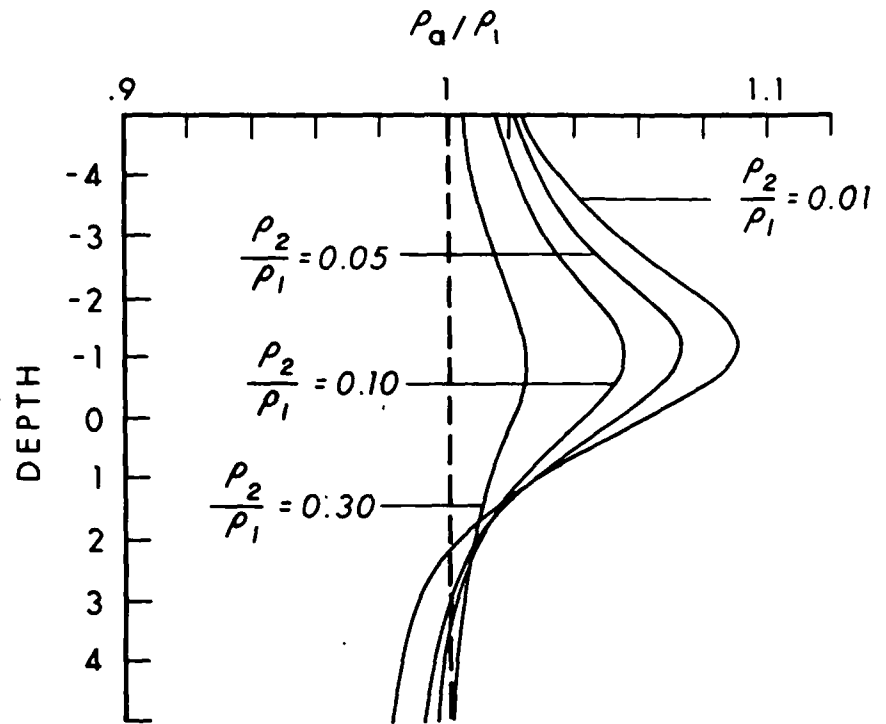
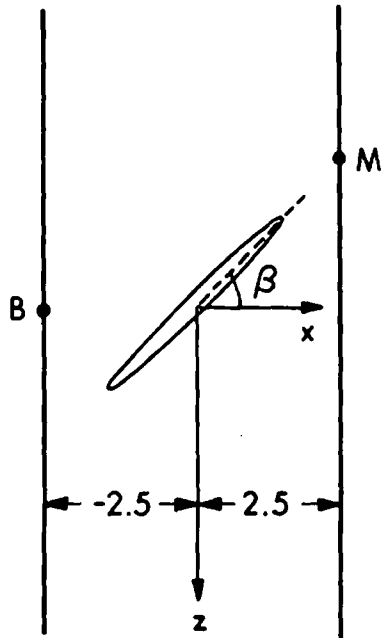
CROSS-BOREHOLE



Electrode Configuration	Body Size	Angles	Resistivity Contrast
Fixed Source Moving Electrode $SBX = -2.5$ $SBY = SBZ = 0$ $EMX = 2.5$ $EMY = 0$	$a = 2$ $b = 2$ $c = 0.2$	$\alpha = 0^\circ$ $\beta = 45^\circ$ $\gamma = 0^\circ$	$\frac{\rho_2}{\rho_1} > 1$

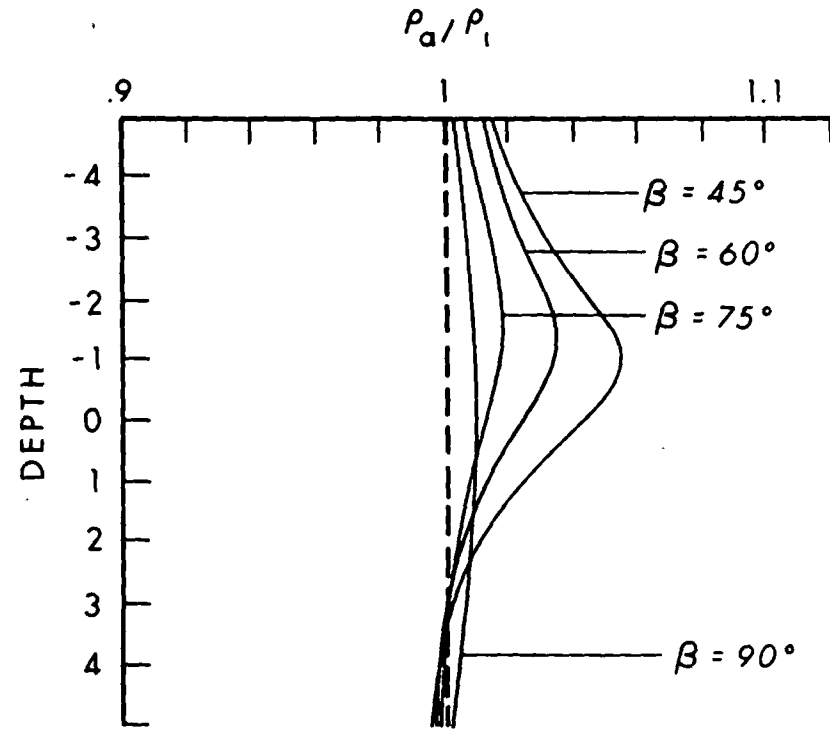
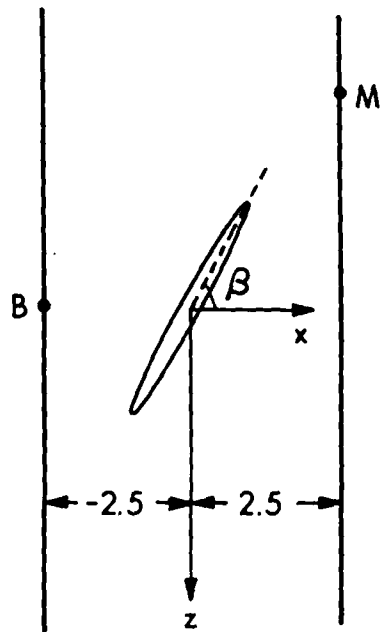


CROSS-BOREHOLE



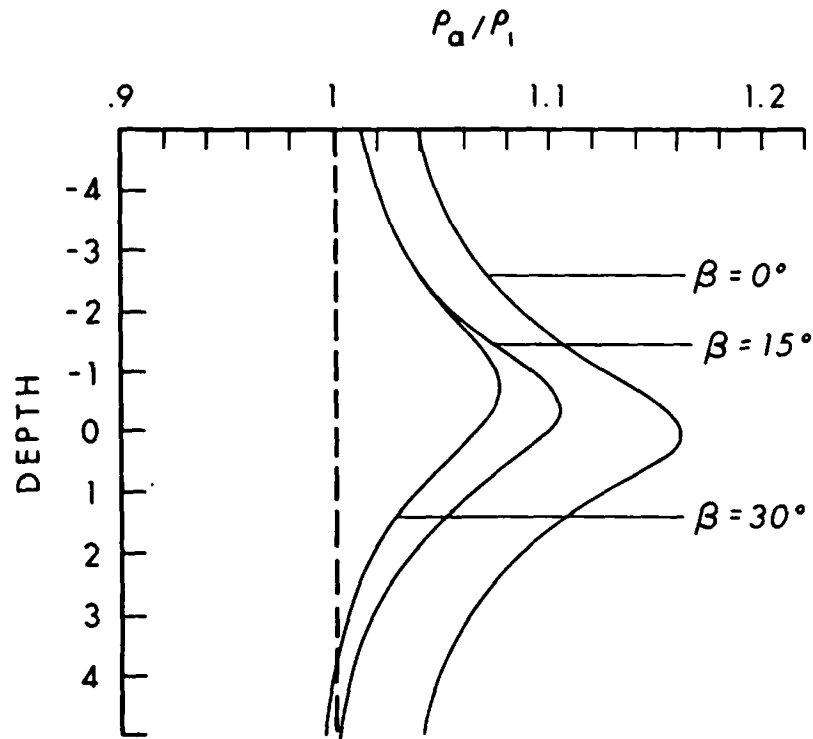
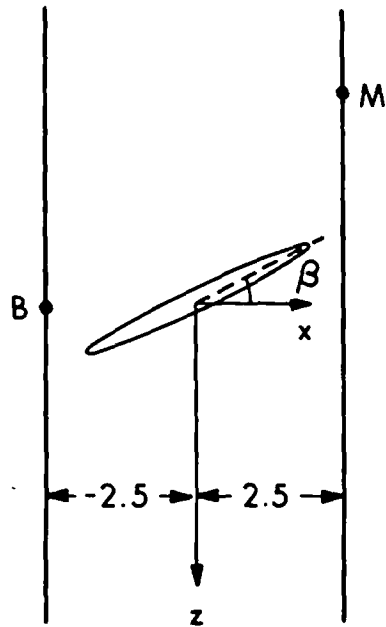
Electrode Configuration	Body Size	Angles	Resistivity Contrast
Fixed Source Moving Electrode $SBX = -2.5$ $SBY = SBZ = 0$ $EMX = 2.5$ $EMY = 0$	$a = 2$ $b = 2$ $c = 0.2$	$\alpha = 0^\circ$ $\beta = 45^\circ$ $\gamma = 0^\circ$	$\frac{\rho_2}{\rho_1} < 1$

CROSS-BOREHOLE



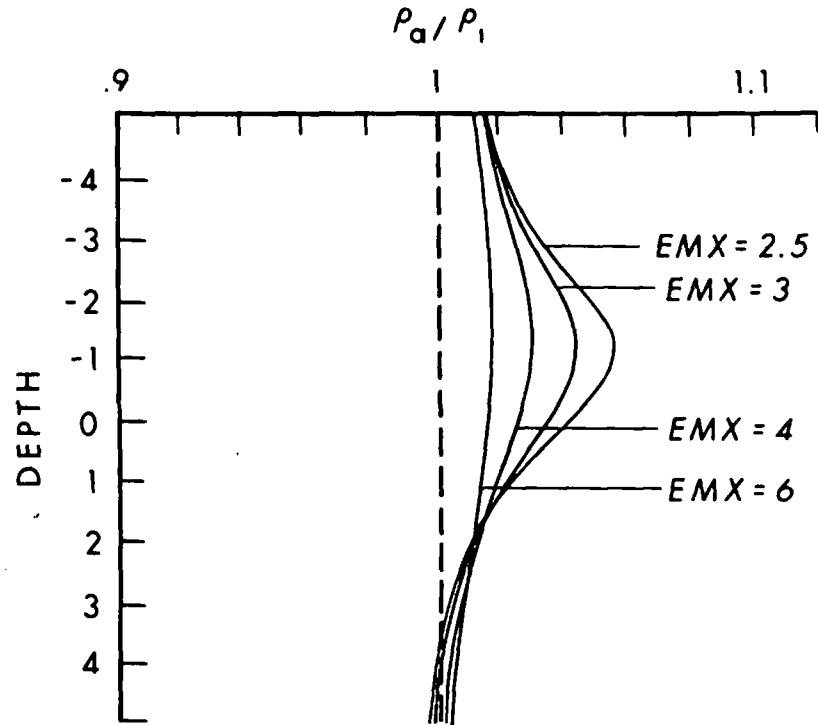
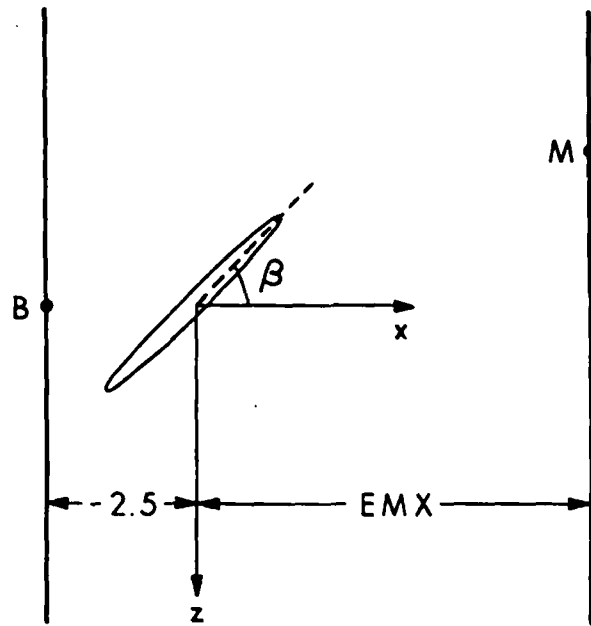
Electrode Configuration	Body Size	Angles	Resistivity Contrast
Fixed Source Moving Electrode $SBX = -2.5$ $SBY = SBZ = 0$ $EMX = 2.5$ $EMY = 0$	$a = 2$ $b = 2$ $c = 0.2$	$\alpha = 0^\circ$ $\beta = 45^\circ, 60^\circ, 75^\circ, 90^\circ$ $\gamma = 0^\circ$	$\frac{\rho_2}{\rho_1} = 0.10$

CROSS-BOREHOLE



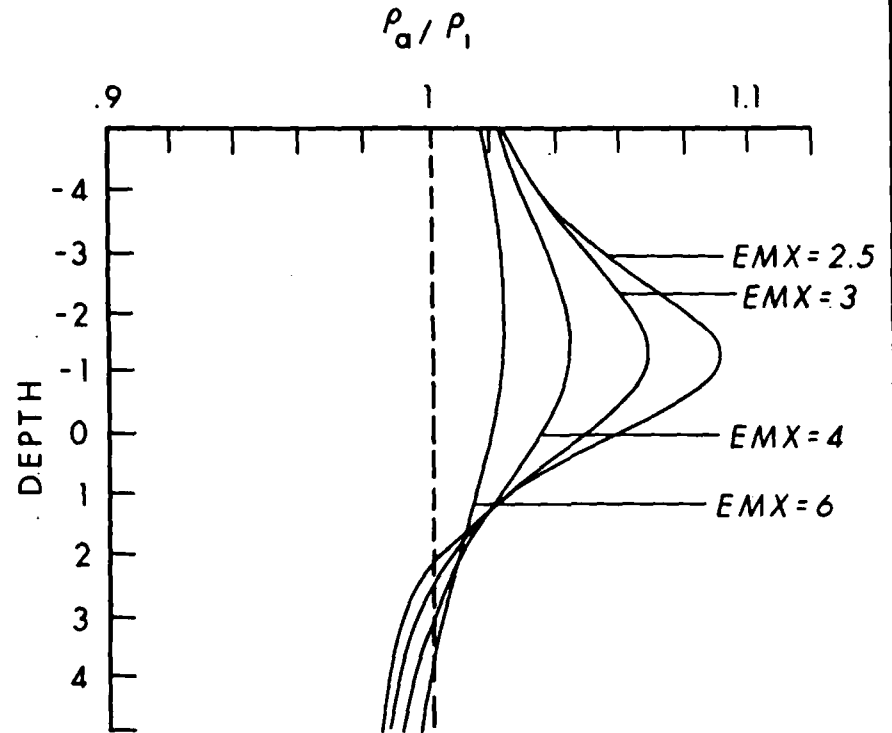
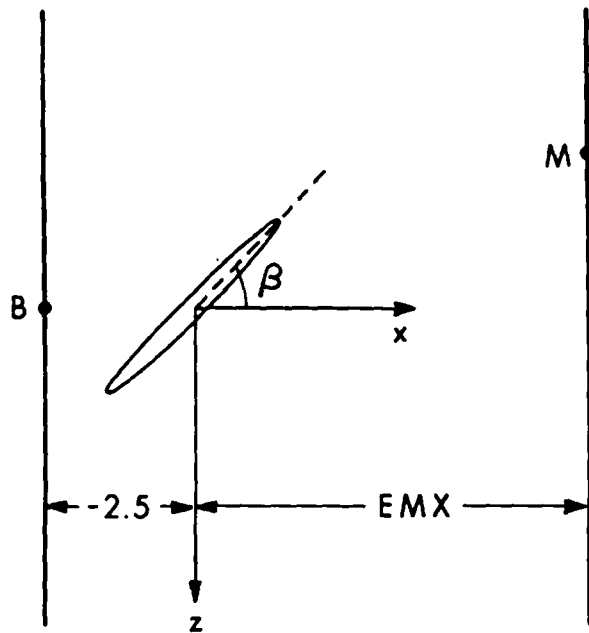
Electrode Configuration	Body Size	Angles	Resistivity Contrast
Fixed Source Moving Electrode $SBX = -2.5$ $SBY = SBZ = 0$ $EMX = 2.5$ $EMY = 0$	$a = 2$ $b = 2$ $c = 0.2$	$\alpha = 0^\circ$ $\beta = 0^\circ, 15^\circ, 30^\circ$ $\gamma = 0^\circ$	$\frac{\rho_2}{\rho_1} = 0.10$

CROSS - BOREHOLE

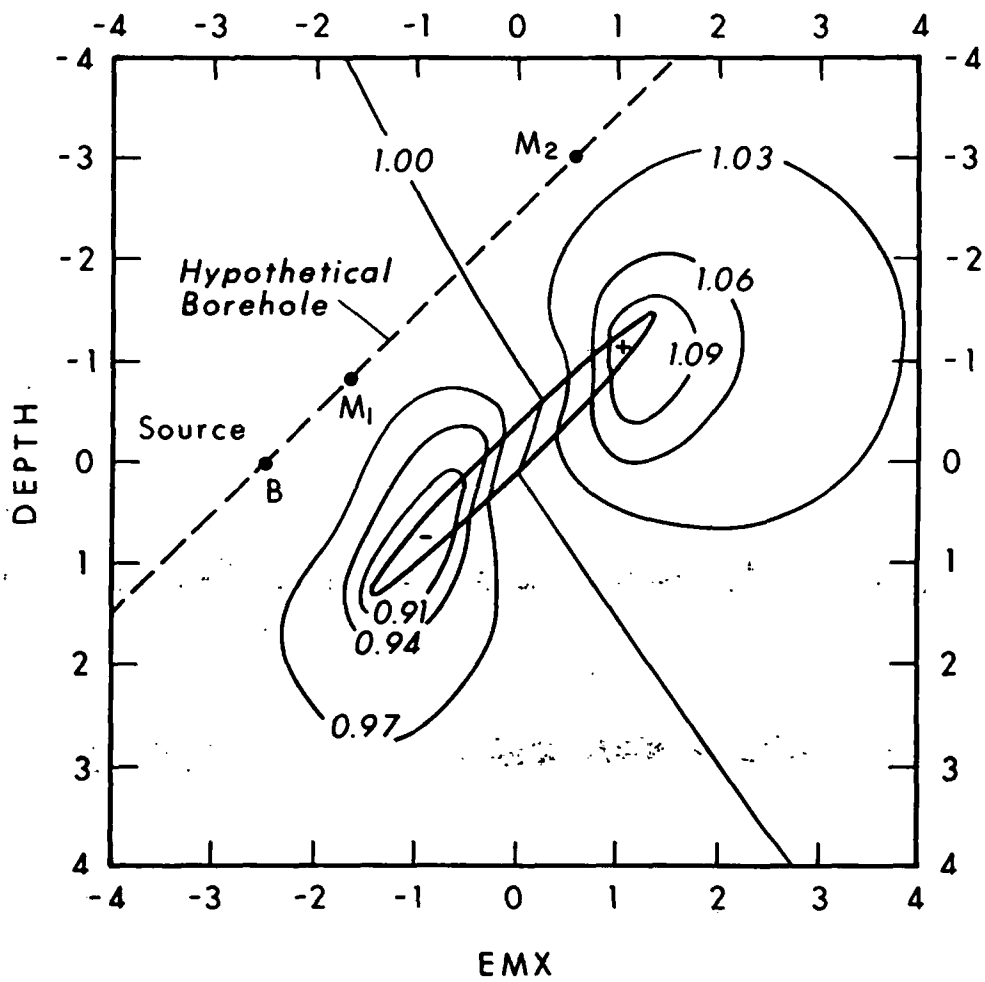


Electrode Configuration	Body Size	Angles	Resistivity Contrast
Fixed Source Moving Electrode $SBX = -2.5$ $SBY = SBZ = 0$ $EMY = 0$	$a = 2$ $b = 2$ $c = 0.2$	$\alpha = 0^\circ$ $\beta = 45^\circ$ $\gamma = 0^\circ$	$\frac{\rho_2}{\rho_1} = 0.10$

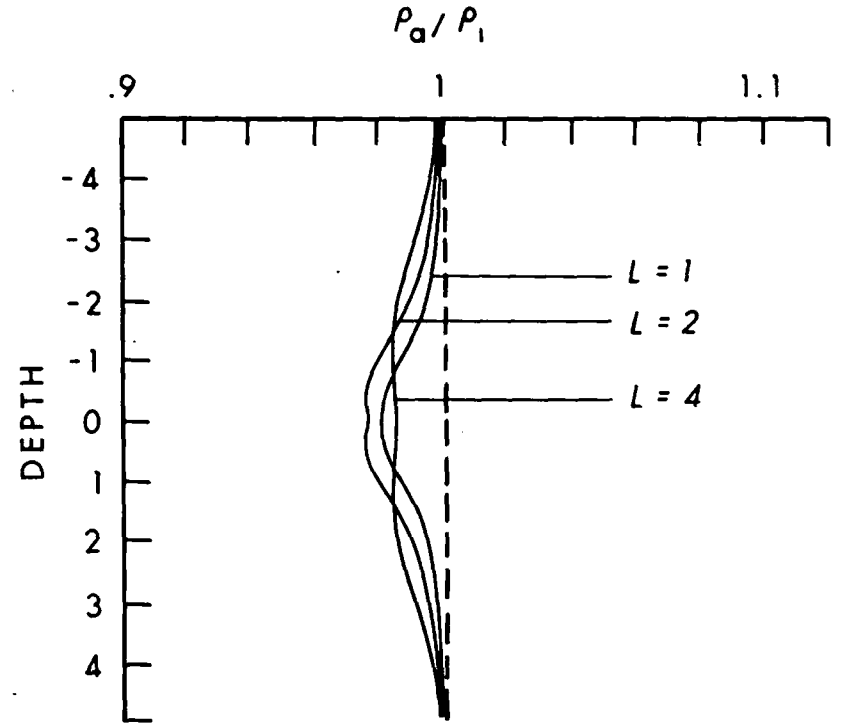
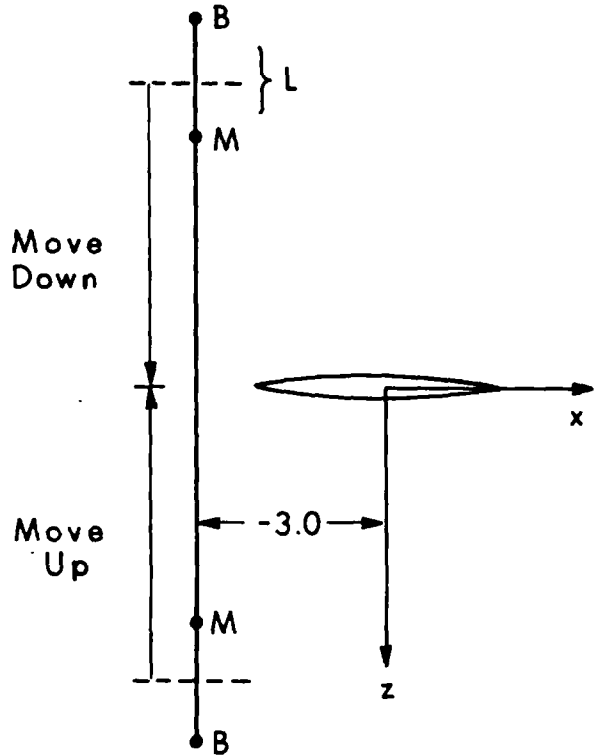
CROSS - BOREHOLE



Electrode Configuration	Body Size	Angles	Resistivity Contrast
Fixed Source Moving Electrode $SBX = -2.5$ $SBY = SBZ = 0$ $EMY = 0$	$a = 2$ $b = 2$ $c = 0.2$	$\alpha = 0^\circ$ $\beta = 45^\circ$ $\gamma = 0^\circ$	$\frac{\rho_2}{\rho_1} = 0.01$

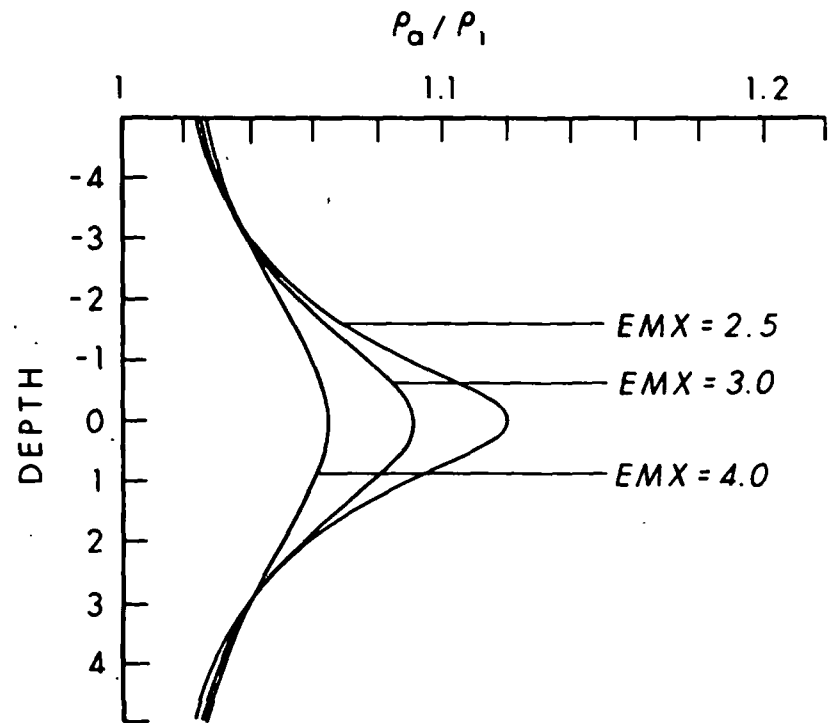
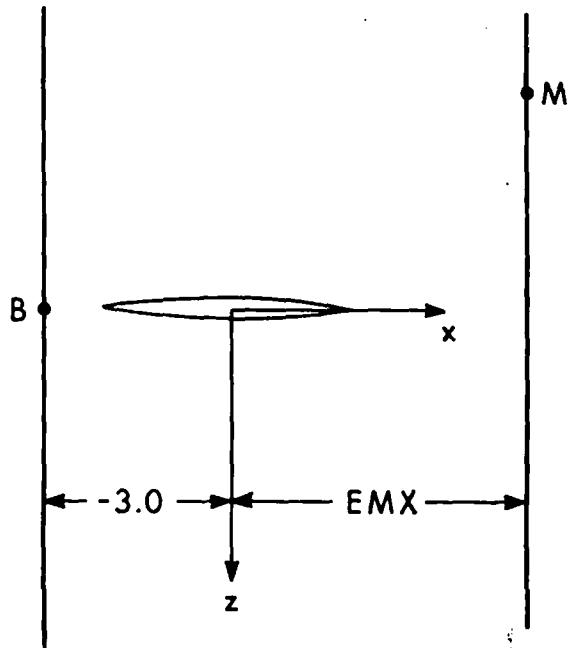


SINGLE-BOREHOLE



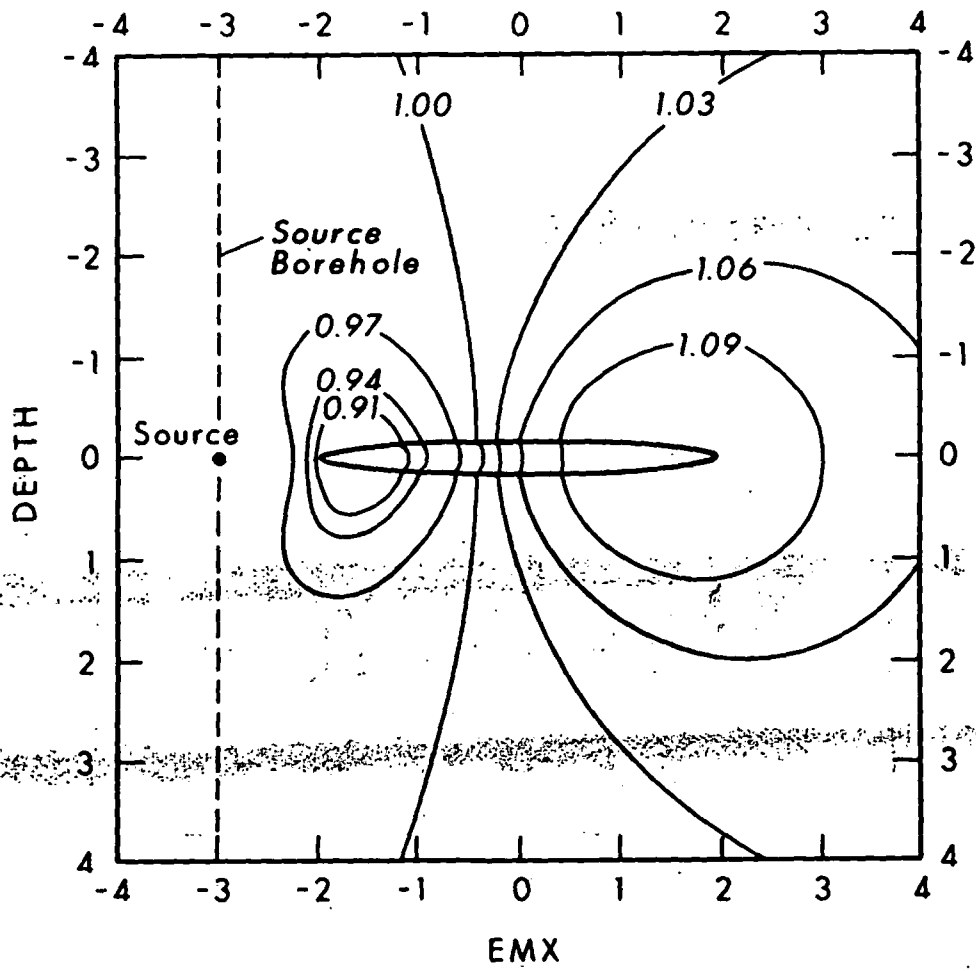
Electrode Configuration	Body Size	Angles	Resistivity Contrast
Normal Array SBY=0	$a = 2 (x)$ $b = 2 (y)$ $c = 0.2 (z)$	$\alpha = 0^\circ$ $\beta = 0^\circ$ $\gamma = 0^\circ$	$\frac{\rho_2}{\rho_1} = 0.10$

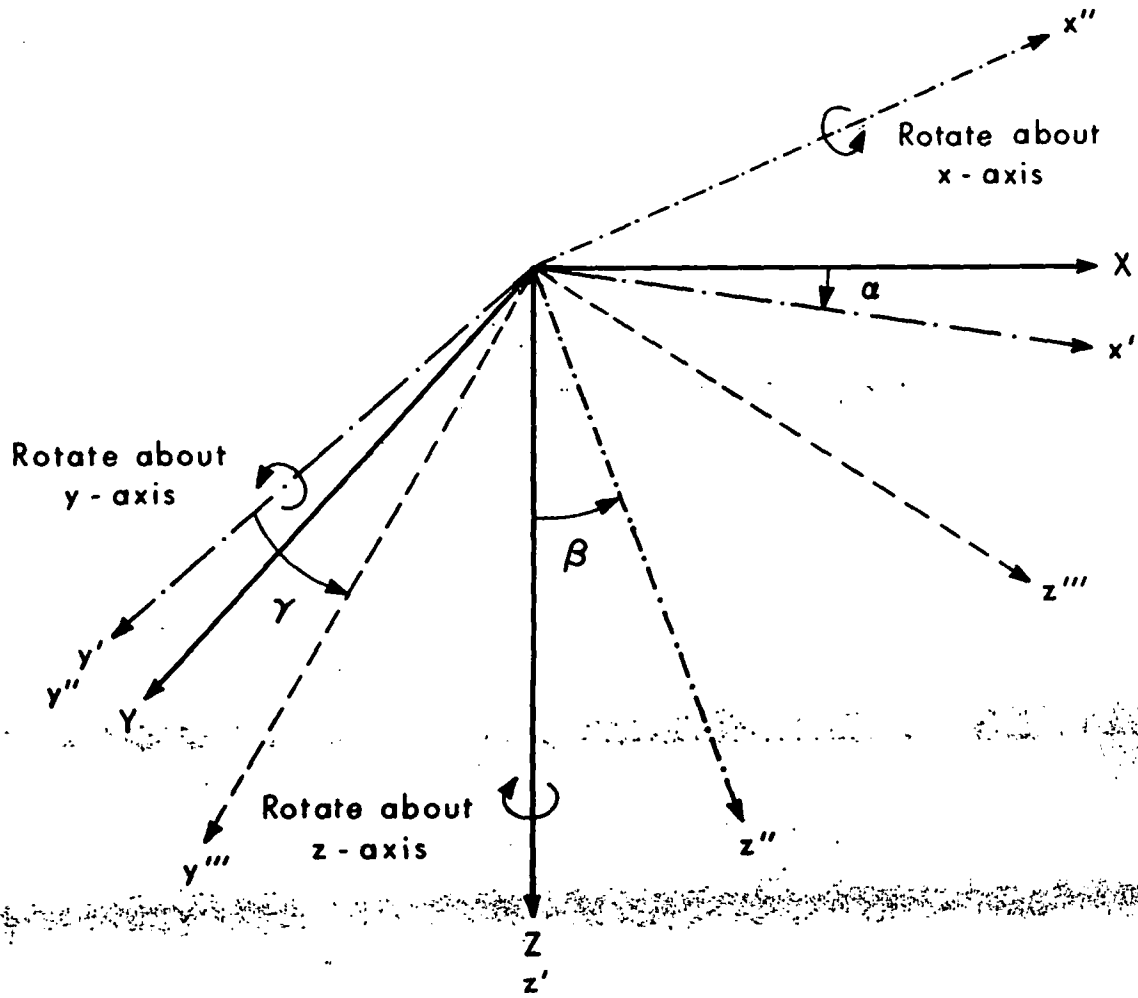
CROSS-BOREHOLE

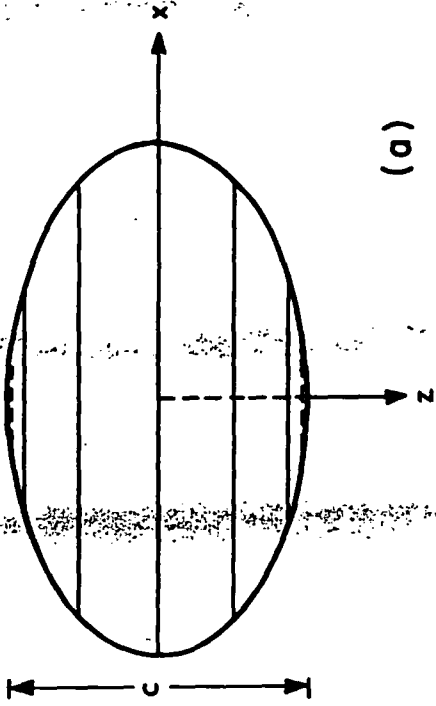


Electrode Configuration	Body Size	Angles	Resistivity Contrast
Fixed Source Moving Electrode $SBX = -3.0$ $SBY = SBZ = 0$ $EMY = 0$	$a = 2 (x)$ $b = 2 (y)$ $c = 0.2 (z)$	$\alpha = 0^\circ$ $\beta = 0^\circ$ $\gamma = 0^\circ$	$\frac{\rho_2}{\rho_1} = 0.10$

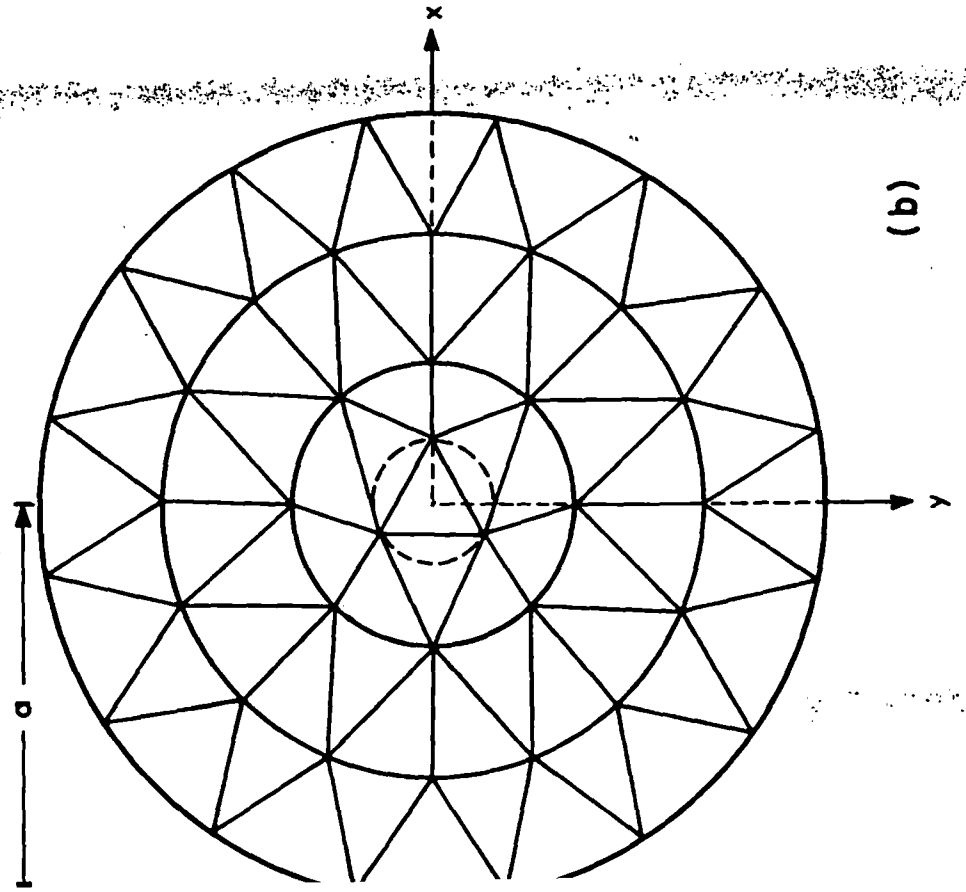




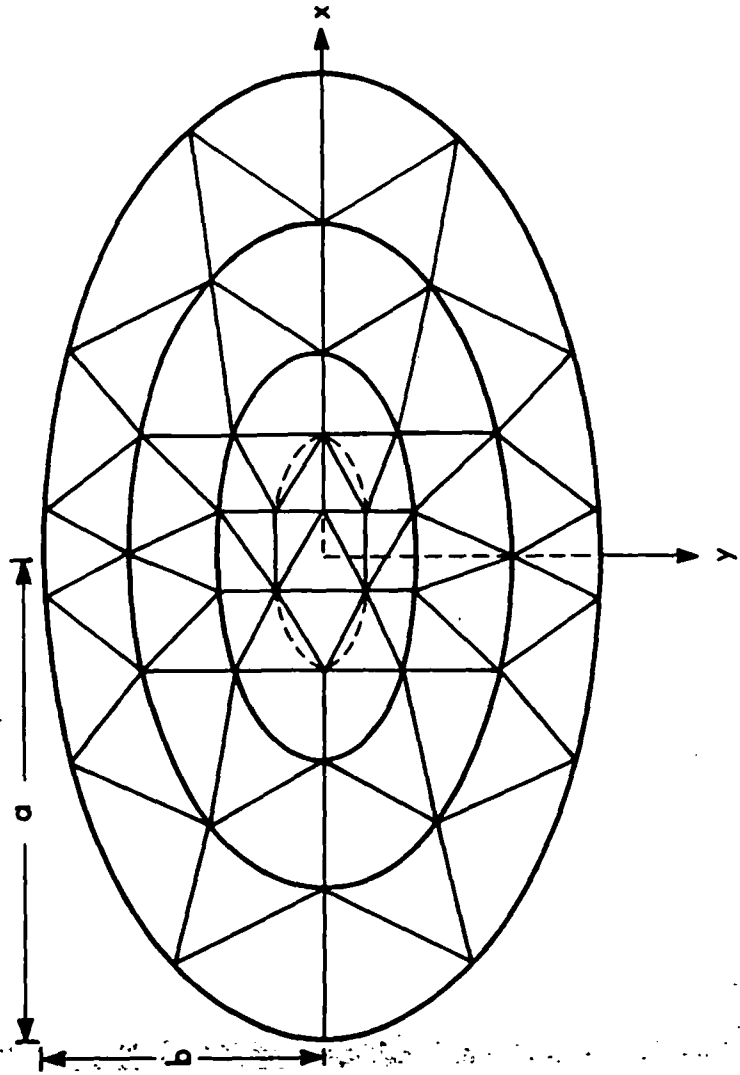




(a)

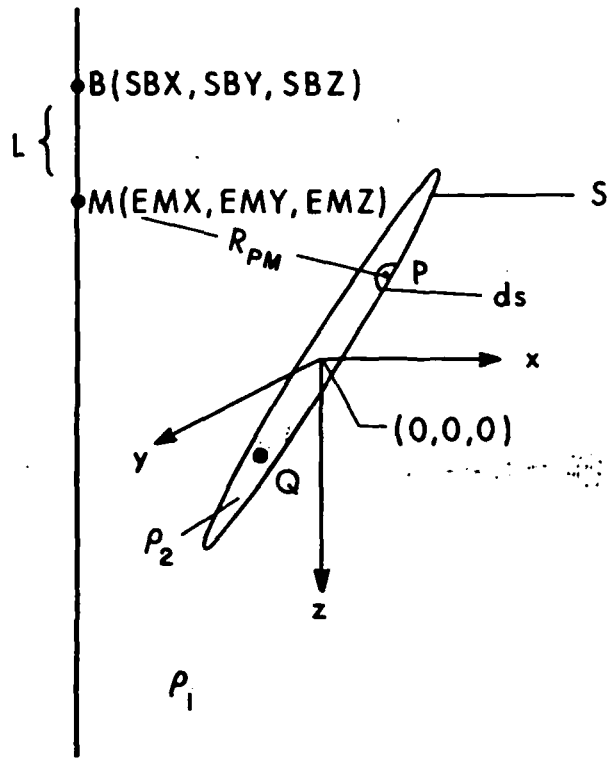


(b)



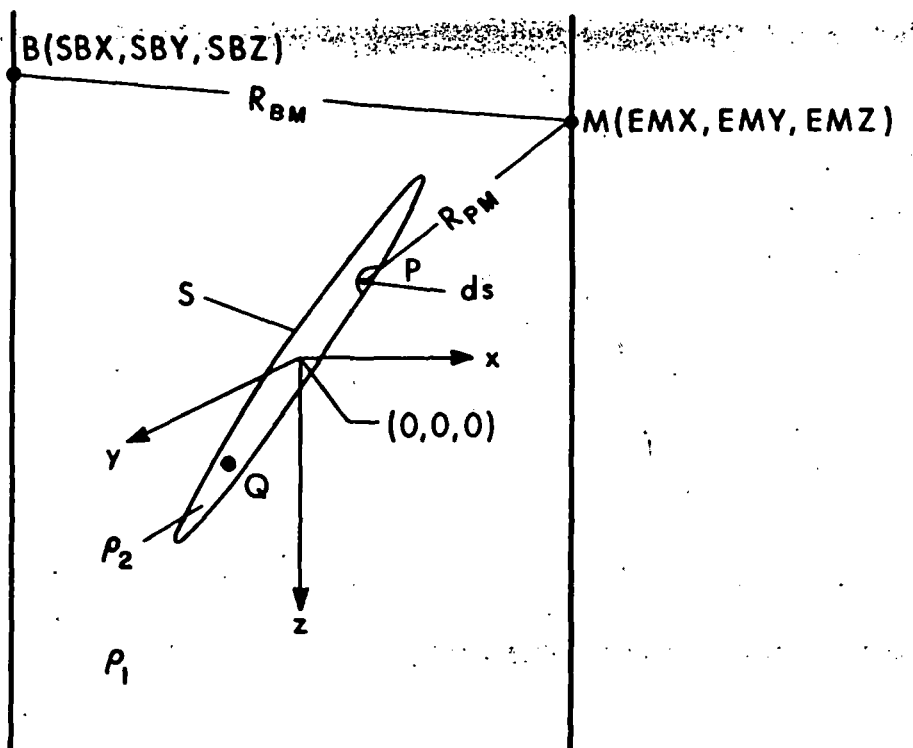
(c)

### SINGLE - BOREHOLE



(a)

### CROSS - BOREHOLE



(b)

	Current Source Position	Potential Electrode Position	Apparent Resistivity
<i>Horizontal Spheroid</i>	SBX = $-10^6$ SBY = 0 SBZ = 0	EMX = 3.0 EMY = 0 EMZ = 0	1.00000
	SBX = -3.0 SBY = 0 SBZ = 0	EMX = 0 EMY = 0 EMZ = 50.0	1.00686
<i>Dipping Spheroid</i> ( $\beta = 45^\circ$ )	SBX = $-10^6$ SBY = 0 SBZ = 0	EMX = 2.5 EMY = 0 EMZ = 0	1.00000
	SBX = -2.5 SBY = 0 SBZ = 0	EMX = 0 EMY = 0 EMZ = 50.0	0.99765
<i>Vertical Spheroid</i> ( $\beta = 90^\circ$ )	SBX = $-10^6$ SBY = 0 SBZ = 0	EMX = 1.0 EMY = 0 EMZ = 0	1.00000
	SBX = -1.0 SBY = 0 SBZ = 0	EMX = 0 EMY = 0 EMZ = 50.0	1.00102
<i>Vertical Ellipsoid</i> ( $a = 6$ $b = 2$ $c = 0.2$ $\beta = 90^\circ$ )	SBX = $-10^6$ SBY = 0 SBZ = 0	EMX = 1.0 EMY = 0 EMZ = 0	1.00000
	SBX = -1.0 SBY = 0 SBZ = 0	EMX = 0 EMY = 0 EMZ = 50.0	1.00621
<i>Vertical Ellipsoid</i> ( $a = 2$ $b = 6$ $c = 0.2$ $\beta = 90^\circ$ )	SBX = $-10^6$ SBY = 0 SBZ = 0	EMX = 1.0 EMY = 0 EMZ = 0	1.00000
	SBX = -1.0 SBY = 0 SBZ = 0	EMX = 0 EMY = 0 EMZ = 50.0	1.00549

Berkeley Geographers meeting

1. Frank Singer at 5:30 - proposed to us Army  
re EM methods - inverse methods
2. Lew Bartell - Santha - can we use group?  
3. Art Dyck wants to join us for 2 years.  
- propose to DGE?  
- need \$ to help get him here -  
- Utah atmospheric
- A. Zhou - DC FE modeling & topo, etc. Thin bodies -  
- laid out some models
- B. Bessing - will work on inversion -
- C. Call Phil Allan - tell him what you're up  
to -- does he have data we could get?  
D. West - and stuff of VLF using 30 mV  
f = 20k 100:1 cast -  
freq of no topo & case of irregularities occur -

W/ Stang & Phil

1. money for 1 yr for Dyche  
- assoc. ed bachelor

⇒ \$50K for him

December 9, 1984

Jeff Daniels  
U.S. Geological Survey, ms 964  
Box 25046, Federal Center  
Denver, Colorado 80225



Dr. Stanley H. Ward  
University of Utah Research Institute  
Earth Science Laboratory  
391 Chipeta Way, suite C  
Salt Lake City, Utah 84108

Dear Stan:

I have enclosed a proposed outline for a symposium/workshop on geotechnical borehole geophysics. I suggest that we now need to establish four things: (1) funding, (2) interest level, (3) papers to be invited, (4) a firm time and agenda. I assume that item-1 is my job? First, I suggest that we canvas the geophysics/geotechnical community to determine if we can get the 20-plus speakers that are needed for this meeting. I could send out a letter-of-inquiry to persons on my mailing list, if you feel that it is appropriate at this time. I also think that plans should be made to pay travel expenses for a few (4-6) invited speakers (for invited speakers that have non-government related jobs).

The idea for this meeting is yours, but I will continue to help you when my input is requested. However, I would like to propose the following outline for the meeting. The outline is very preliminary (written at midnight on sat. night).

I. Hydrology

- A. Determination of porosity & permeability
- B. Logging in unsaturated zones
- C. Determination of water quality
- D. Determination of fluid migration
- E. Use of fractures

II. Toxic and nuclear waste

- A. Detecting chemical contaminants
- B. Determination of nuclear contaminants
- C. Delineation of contaminant zones
- D. Long-term borehole monitoring of waste sites
- E. Identification of adsorbant species
- F. water/rock interaction

III. Determination of in-situ strength parameters

- A. Geomechanical measurements
- B. Acoustic and density measurements
- C. Determination and delineation of fractures
- D. Liquefaction potential
- E. Relating laboratory measurements to in-situ measurements

Please let me know if you are still interested in pursuing the idea of holding this meeting in (or near) Salt Lake. I must get started on obtaining the funding for it.



Another topic: High temperature/high pressure logging workshop

Approximate date: 1-day workshop in March, or April, 1985

Purpose: To discuss high temperature and high pressure borehole geophysics with investigators and managers in the geothermal and the Continental Drilling Program. It is my opinion that a major R&D effort is necessary. This will require the cooperation of many groups. However, first the managers controlling funding must be convinced of the necessity and feasibility of this effort.

Size of meeting: Approximately 20-30 invited scientists and scientific managers.

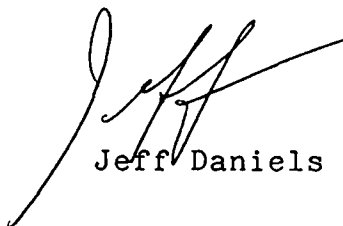
Some Topics for discussion:

- I. Current technology review
- II. Purpose of in-situ physical property measurements
- III. Measurements needed in various programs
- IV. Equipment R & D needed (dewars, cables, electronics, etc.)
- V. Possible timetable and an outline of organizations needed to accomplish the task

I would appreciate your suggestions concerning the workshop. I particularly need suggestions concerning specialists that should be invited to give short (informal) presentations. However, I do not think that this workshop should be too technical.

Thanks for you help, and have a nice Holiday Season.

Best Regards,



Jeff Daniels

## Workshop

### CONTINENTAL SCIENTIFIC DRILLING PROGRAM

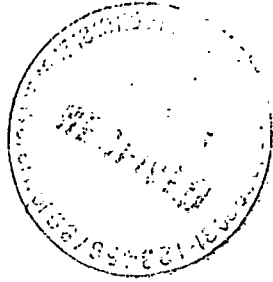
A workshop will be held on April 29 - May 1, 1985 (location to be announced at later date) to develop a plan for drilling and research to pursue basic studies of the continental lithosphere. The National Science Foundation has indicated its intention to accept a proposal by DOSECC, Inc., a non-profit corporation representing eighteen major universities, to plan and subsequently manage NSF's activities in the area of continental scientific drilling. These activities would be carried out under the interagency accord on continental scientific drilling signed in April 1984 by NSF, USGS, and DOE, and in accordance with a recent congressional resolution supporting such activities (Section 323 of Public Law 98-473). Although there is as of now no assurance that funding for major drilling projects will be obtained, it is necessary to begin the planning process as early as possible. DOSECC, Inc. expects to convene this workshop. The workshop will provide an opportunity to those who have an interest in continental scientific drilling, are contemplating plans for experiments or are actively developing scientific drilling projects, to present their plans and ideas for possible inclusion in a scientific program plan to be considered for funding under the NSF activity in CSD. (see EOS, 65 No. 43, pg. 771, 10/23/84) The ongoing and planned programs will also be presented. To provide the scientifically strongest plan possible, it is important that it represents a cross-section of the interests of the involved scientific community and takes into account efforts of other agencies under the Interagency Accord.

The workshop will provide a forum for full and open discussion to all those who are interested. The workshop program is open to representatives of groups or consortia who are developing plans for research requiring continental drilling in order to help answer basic questions on the structure and evolution of the continental crust. Groups of scientists who convene to prepare the arguments for a given experiment should select a spokesman who will present the scientific rationale for the experiment, including the reasons why drilling is essential to the solution of the problem presented. The more supporting geological and geophysical data that can be used to identify the drilling target the better. It will also be important to present a plan which includes pre-drilling site surveying, an approximate design for the hole or holes to be drilled and the logging and post-drilling analysis of core and other data. The emphasis must be on the expected scientific results, however. Researchers with plans to make use of existing or planned drill holes available from industry, government, or other sources are also invited to present the case for their scientific objectives.

Following the Workshop, the Scientific Advisory Committee of DOSECC will draw up a Science Plan for presentation to the National Science Foundation and may make recommendations to the other agencies if requested to do so. The experiments should, in general, be conducted by a group of principal investigators who will take responsibility for site surveys, scientific oversight of the drilling, analysis of core and logs and publication of the results. As funds become available, it is expected that formal proposals for experiments included in the initial years of the program plan will be requested.

Those wishing to attend the Workshop on Continental Scientific Drilling should write to Dr. Frank Stehli, Chairman of the Scientific Advisory Committee, School of Geology and Geophysics, University of Oklahoma, Norman, Oklahoma 73019. An abstract of approximately two pages should be submitted by March 30, 1985 to ensure participation in the program.

# 04676



April 21, 1985

Jeff Daniels  
ms 964  
U.S. Geological Survey  
Box 25046, Federal Center  
Denver, CO 80225

Stanley H. Ward  
UURI  
Earth Sciences Laboratory  
391 Chipeta Way, Suite C  
Salt Lake City, Utah 84108

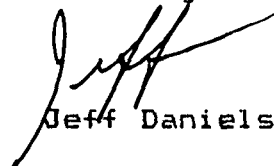
Dear Stan:

I have enclosed my comments on Alf's paper. In general, I feel that it is a good paper for the Golden Anniversary Issue.

I am sorry for the delay in reviewing this paper. I have decided to leave the USGS, and I have accepted a teaching position at Ohio State. I have spent the past two weeks trying to re-schedule the time that I have remaining with the Survey. Unfortunately, I decided that there is not enough time to conduct the High Temperature Logging Workshop. However, there is a crying need for the workshop prior to upcoming decisions by DOSECC concerning logging in the CSDP. I think that UURI should give serious consideration to holding the workshop, and to submitting a proposal to DOSECC for coordinating the scientific logging in the CSDP. I would like to propose to you that we work together and write a proposal for the CSDP work. I feel that the proposal should include several key institutions, with a good geographic distribution and technical experts in contrasting disciplines. The group would function in a manner similar to the Lamont Doherty/Texas A&M consortium in the ODP, and would require hiring (or contracting) a few technicians. I will be attending the DOSECC meeting in Houston next week, and I should be able to get a better focus on the feasibility of such an effort.

I have appreciated our recent communications, and I am looking forward to the possibility of fruitful cooperation in the near future.

Best Regards,

  
Jeff Daniels

## APPLICATION OF BOREHOLE GEOPHYSICS AT AN EXPERIMENTAL WASTE STORAGE SITE\*

P.H. NELSON,\*\* K.A. MAGNUSSON\*\*\*  
and R. RACHIELE\*\*

### ABSTRACT

NELSON, P.H., MAGNUSSON, K.A. and RACHIELE, R. 1982, Application of Borehole Geophysics at an Experimental Waste Storage Site, *Geophysical Prospecting* 30, 910-934.

A suite of electrical, radiation, and mechanical borehole probes were run in a 76-mm-diameter borehole drilled to a slant depth of 380 m in leptite and granite. The hole is located in Precambrian bedrock in central Sweden where a site is dedicated to in-situ experiments pertaining to the disposal of radioactive wastes. The challenge to borehole logging methods for such site investigations is to resolve geological features and fluid flow parameters in geological sites which are initially chosen for their homogeneity, low porosity, and minimal fracturing. The Stripa borehole is characterized by high electrical resistivity values in the 20-100 k $\Omega$ m range, by acoustic velocities around 5800 m s<sup>-1</sup> (which is close to laboratory values on intact specimens), and by total porosity of around one volume percent. In this context, probe resolution was adequate to produce interpretable information on almost all of the logs.

Two principal rock types were encountered in the hole: granite, of quartz monzonitic composition, and leptite. The granite and leptite intercepts are subdivided into units characterized by mafic mineral content, sulfide mineral content, and electrical and radiation properties. Iron-rich zones in the leptite are highly anomalous on the gamma-gamma and neutron logs; thin mafic zones in the granite can also be distinguished. Occurrences of a few percent pyrite are detected by the electrical, gamma-gamma, and neutron logs. Although overall porosity is quite low throughout the hole, analysis of the resistivity and neutron logs indicates the porosity increases by a few volume percent at fracture zones. The differential resistance and caliper probes detect borehole diameter roughness of less than 1 mm, helping to confirm acoustic waveform anomalies which are indicative of fracture zones. Compressional wave transit time and shear-wave interference patterns usually occur coincident with open fractures observed in core, the correlation being especially good at major fracture zones.

\* Received August 1981, revision March 1982.

\*\* Lawrence Berkeley Laboratory, Earth Sciences Division, Berkeley, California 94720, USA.

\*\*\* Geological Survey of Sweden, Box 670, 75128 Uppsala, Sweden.

Immediate requirements for this application of borehole geophysics are the need to increase understanding and experience in fracture detection with the acoustic probe and to develop the quantitative evaluation of that fraction of porosity accessible to fluid flow.

## INTRODUCTION

A Swedish-American cooperative research program commenced in 1977 at the Siripa mine in central Sweden, in which cooperating investigators explore the geological, geophysical, geotechnical, geochemical, hydrological, and mechanical effects anticipated from the use of a large crystalline rock mass as a repository for nuclear waste (Witherspoon, Cook and Gale 1980).

The evaluation of potential sites for radioactive waste repositories places some new requirements on the tools and techniques for borehole measurements. The hydrological regime is of primary importance, requiring the measurement of permeability to unusually low levels, since in-situ permeabilities in crystalline rocks commonly range as low as  $10^{-18}$  m<sup>2</sup> (Brace 1980). In crystalline rock, fluid flows along interconnected fractures; hence the detection and characterization of fractures, even very fine fractures of less than 0.1 mm aperture, are important goals for detection by borehole logging. The storage of fluid afforded by pore space is also an important parameter for site characterization; hence the measurement of porosity at levels of 1% is desired. Most logging experience is based on the evaluation of lithologic units for the recovery of oil and gas, and to a lesser extent, for minerals. There the objective is usually to locate significant anomalies of fluid or mineral content. In the repository case, however, we seek a geological environment free of any significant perturbations which might in some way be injurious to the long-term integrity of the repository. Therefore, another goal of borehole logging is to aid the geologist in defining the geological and mineralogical character of a potential site.

This study in a crystalline rock site is directed towards evaluating different slim-hole logs for the following purposes:

- recognizing and characterizing different rock units specified by bulk physical properties,
- detecting mineralization and mineralogical variations,
- monitoring variations of porosity or water content in rock,
- detecting fractures.

To support this study, geophysical logs from a cored borehole (SBH-1) of 76 mm diameter are used. Two systems of geophysical borehole logs have been applied: one system was applied by the Lawrence Berkeley Laboratory (LBL) and the other by the Geological Survey of Sweden (SGU). LBL used the following suite of logs: neutron, gamma-gamma, gamma ray, sonic, caliper, and temperature, while SGU used point resistance, differential resistance, resistivity, spontaneous potential (SP), induced polarization (IP), radiowave propagation (VLF), and gamma ray. It is therefore possible to evaluate the performance of a wide variety of logs in crystalline rock. Specifications of the borehole probes are described in the Appendix.

PHYSICS

E

\*\*\*

Borehole Geophysics  
-934.

run in a 76-mm-  
hole is located  
in experiments  
le logging methods  
flow parameters in  
osity, and minimal  
ivity values in the  
close to laboratory  
ne percent. In this  
on on almost all of

quartz monzonitic  
divided into units  
rical and radiation  
amma-gamma and  
urrences of a few  
on logs. Although  
and neutron logs  
s. The differential  
an 1 mm, helping  
zones. Compre-  
ir coincident with  
for fracture zones.

California 94720,

© 1982 EAEG

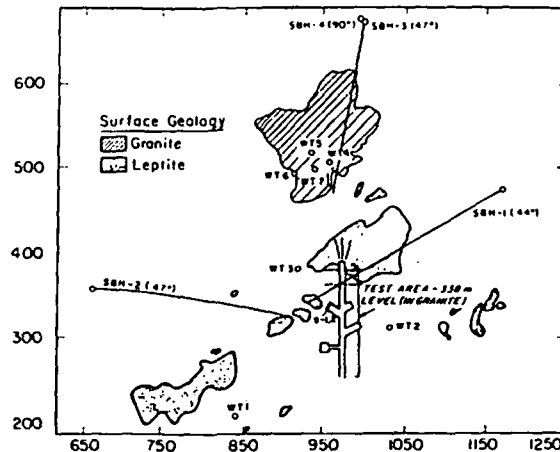


Fig. 1. Plan map of the Stripa site in central Sweden showing rock outcrop, inclined surface boreholes and underground experimental drifts. Mine coordinates given in meters.

The 380 m length borehole designated SBH-1 (fig. 1) is drilled at a  $44^\circ$  inclination from the surface towards the test drift of the mine. The borehole alternately penetrates granite and leptite, terminating in granite at an elevation above the underground test site. The Stripa granite is a relatively uniform, massive and medium grained rock, generally of quartz monzonite composition. The matrix mineralogy is composed of the primary minerals quartz, plagioclase, and microcline, with some muscovite and biotite altered to chlorite. Opaque minerals, garnet, and zircon occur as accessories. The rock is highly fractured, but the majority of the fractures are tightly healed. Common fracture-filling minerals are chlorite, sericite, quartz, epidote, and carbonate minerals, with fluorite and opaques (often pyrite or hematite) less common (Wollenberg, Flexser and Andersson 1980).

The leptite consists of strongly metamorphosed rhyolite lavas and tuffs. Almost all of the iron ore deposits occur in the leptite. The leptite composition is similar to that of granite, except the mafic mineral content is generally higher, especially in the iron-rich horizons where the leptite assumes a distinct banded character. Like the granite, the leptite is highly fractured. Fracture mineralogy is similar to that of the Stripa granite, but with epidote being more common in the leptite.

#### CHARACTERIZATION OF THE ROCK UNITS

A combination of geophysical measurements is an important aid for the recognition and characterization of the physical properties of different rock units along the borehole. The penetrated rock types can therefore be divided into sub-units characterized by different bulk physical properties.

Core drilling gives an almost continuous record of the penetrated rocks and therefore its compositional variations, structures, fractures, and fracture coatings can be determined. The core is mainly investigated by visual inspection, where more

detail  
which  
serve  
micro-  
varia-  
gatic  
com-  
can  
alog  
sub-  
ing,  
first

is m

—g  
—n

F  
g  
(l

detailed studies are carried out on a few samples. The sub-units of the rock types which are characterized by different bulk physical properties are not always observed by visual inspection of the core. This might be due to variations in the microscopic scale; for example, texture, and microfracturing. Also, mineralogical variations might only be detectable by chemical analysis or microscopic investigations of thin sections. Thus geophysical borehole investigations will give valuable complementary information about the physical properties of the rocks, which also can be used for direct sampling of the core for geomechanical, chemical and mineralogical investigations. Re-examination of the core in order to check the different sub-units established by borehole geophysics often shows slight differences in coloring, texture, and mineral distribution between units which were overlooked in the first ocular inspection.

The physical contrast between leptite and granite is visible in several logs, but it is most clearly seen in the following ones (fig. 2a):

- gamma-gamma: the leptite is a denser rock than the granite;
- natural gamma ray: the leptite has a lower count rate than the adjacent granite;

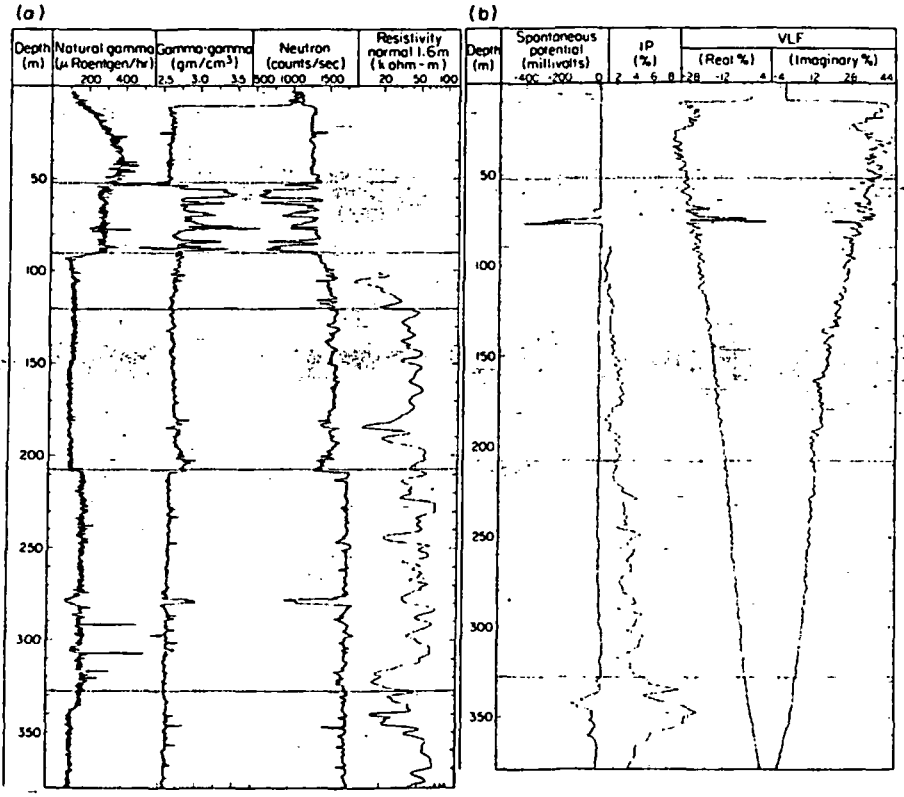


Fig. 2. (a) Geophysical logs in borehole SBH-1. Water level is at 80-90 m. Much of the high gamma-ray response is due to radon daughter products within the borehole (see text). (b) Geophysical logs in SBH-1, as in (a).

—*neutron*: the leptite has a higher content of mafic minerals (see section on specific minerals) and a slightly higher porosity than the granite.

Sonic waveform records of the leptite (not shown) are generally more disturbed, reflecting more fracturing, though at greater depth one cannot distinguish the granite from the leptite using just the waveform log. Also, the Stripa leptite unit has a lower maximum resistivity of 60 000  $\Omega\text{m}$  compared to a maximum resistivity of 80 000  $\Omega\text{m}$  in the granite.

The water level in the hole was at 80 m during LBL's measurements and at 90 m during SGU's measurements. The electrical measurements (point resistance, differential resistance, resistivity, IP, and SP) need water-filled boreholes to permit electrical contact between the electrodes (in the tool) and the surrounding rock. However, inflowing water above the water table will flow along the lower borehole wall down to the water table. Due to the 45° inclination of the borehole there is enough water along the borehole to get reliable SP measurements (fig. 2b).

In a comprehensive study of all gamma-ray logs at Stripa, Nelson, Rachiele and Smith (1980) found that extremely high concentrations of radon in groundwater have contributed to the gamma-ray levels measured in boreholes wherever there is sufficient movement of water into a borehole. The uranium-238 concentration in Stripa granite is in the 30 to 40 p.p.m. range, considerably greater than in most silicic rock, and uranium is apparently distributed in the rock in such a way that emanation of radon into water-filled cracks and fractures is quite high. The radon is then transported by groundwater flow through fractures into the open borehole where gamma rays emitted by its daughter products, bismuth-214 and lead-214, are detected by the gamma probe. Gamma spectrometric measurements on core samples have determined that the uranium concentration is fairly uniform throughout the Stripa granite. Where the rock contributes all of the gamma emission, the probe measures 120  $\mu\text{rad h}^{-1}$  in granite. This level is reached only at the bottom of SBH-1 below 340 m (fig. 2). Throughout the rest of the hole excessive counts are provided by radon-charged water which infiltrates into the hole above the water level, trickles down the side of the hole to the top of the water column, then continues to move downward in steady flow to about 320 m where most of the water exits the hole at a major fracture zone. Superposed on this pattern are variations in count rate due to variations in radio-element concentration of the wallrock; the natural background of the leptite is obviously less than that of the granite.

Both the granite and the leptite are subdivided based upon physical property changes apparent in the geophysical logs. The depth stated is actually the slant depth along the borehole, not the true vertical depth, which can be approximated by multiplying the slant depth by 0.7. The characterization of the different rock units which follows is also summarized in fig. 3.

#### *Upper granite, 0–52 m*

The striking build-up in the gamma curve is attributed to the infiltration of radon-charged water into the borehole. The maximum at 40 m indicates that most of the



ee section on specific

rally more disturbed, distinguish the gran- pa leptite unit has a ximum resistivity of

ements and at 90 m resistance, differen- s to permit electrical ing rock. However, borehole wall down ere is enough water

elson, Rachiele and on in groundwater s wherever there is 8 concentration in ater than in most n such a way that hie. The radon is he. en borehole and lead-214, are ents on core sam- iform throughout mission, the probe bottom of SBH-1 units are provided ater level, trickles ontinues to move exits the hole at a count rate due to tural background

ophysical property ctually the slant approximated by ferent rock units

ration of radon- that most of the

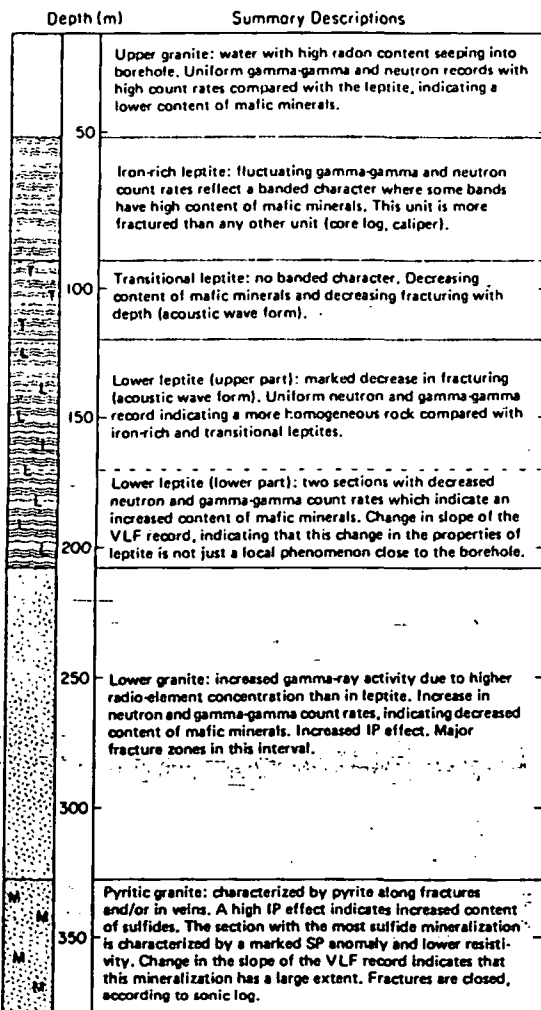


Fig. 3. Summary of geological inferences based on inspection of the geophysical logs.

infiltration occurs above this depth. Caliper openings (not shown) are most frequent above 25 m. The natural gamma activity is so high in the hole that the gamma-gamma response is affected in this zone and cannot be compared with that of the lower rock units. Because the hole is air-filled in this upper zone rather than water-filled, the neutron response is shifted in comparison with that of granite deeper down the hole; however, the response can be compared directly with that in the leptite down to the top of the water column.

*Banded leptite with iron-rich zones, 52-89.5 m*

The outstanding features in this zone are the gamma-gamma and neutron fluctuations shown in fig. 2(a). As discussed further in the section on mineralization, the

iron-rich intervals are clearly delineated by the reduced count rates recorded by the two logs. The caliper log (not shown) indicated that the borehole wall is rougher than any other interval in the hole, although the diameter increases only a few millimeters. The short portion of sonic record obtained in this interval confirms that it is more fractured than any other interval in the hole. The iron-rich intervals appear to be more broken than the iron-free intervals. The constancy of the gamma count rate reflects the fact that the granite rather than the leptite is the radon source, and that no significant dilution occurs within this interval. That is, there may be some entry of water within this interval, but it is either of insufficient volume or insufficient radon content to perturb the gamma record.

#### *Transitional leptite, 89.5–120 m*

This is a transitional zone between the fractured, banded leptite above and the competent leptite below. The neutron and gamma-gamma logs are more uniform, lacking the banded character of the iron-rich unit. There is an increase in the neutron count rate (1340 to 1600 ct s<sup>-1</sup>) from the contact at 90 to 115 m, and also a less pronounced density decrease in the gamma-gamma log attributed to a decrease in mafic mineral content. The sonic waveform, gamma-gamma, caliper, and core logs all indicate that fracturing decreases with depth in this interval. The low uniform IP effect of 1% indicates that sulfide and clay content is negligible.

#### *Lower leptite, 120–208 m*

The lower leptite is a more competent and less fractured rock than the transitional leptite unit. This change in competence is best revealed by the sonic waveform record (not reproduced here, refer to fig. 2.4 of Nelson, Paulsson, Rachiele, Andersson, Schrauf, Hustrulid, Duran, and Magnusson 1979) which is generally quite uniform throughout the 120–208 m interval. Those anomalous zones which are present reveal individual features of less than 1 m intercept. At a depth of about 148 m the gamma-ray activity decreases from 120 to 100  $\mu$ rad h<sup>-1</sup>. This step-like decrease is attributed to a decrease in the radio-element concentration in the leptite.

There are no indications in the neutron or gamma-gamma records when passing into the lower leptite unit. However, the lower part of this unit, 170 to 208 m, does have a more variable neutron and gamma-gamma count rate. Two sections in particular, from 177 to 188 m, and from 192 to 208 m, have low neutron and gamma-gamma count rates (fig. 2a), indicating higher mafic mineral content. Also, the rock appears visually somewhat darker in these intervals. Electrically these two intervals can be separated. The upper one, from 177 to 188 m, is of reduced resistivity and IP response, and the lower one from 192 to 208 m is of higher IP and resistivity.

The real VLF component shows a slight change in slope and the imaginary VLF component a marked change in slope at 170 m (fig. 2b). It seems probable that the resistivity decrease and its associated compositional change is not a local phenomenon close to the borehole but has a large lateral extent.

Low  
The g  
radio-  
due to  
higher  
Th  
above  
272.5-  
permi  
and to

#### *Pyrit*

The  
pyrite  
lower  
sulfid  
340 m  
comp  
grani  
borel  
A  
At 32  
in fa  
anon  
respe  
328 m  
rado.  
nota  
pyrit

The  
of th  
mafi  
by v  
nece  
fluid

#### *Iron*

Exa  
log  
dec.

is recorded by the  
e wall is rougher  
eases only a few  
rval confirms that  
ron-rich intervals  
cy of the gamma  
tite is the radon  
al. That is, there  
insufficient volume

above and the  
e more uniform,  
increase in the  
15 m, and also a  
ted to a decrease  
aliper, and core  
al the low uni-  
b.

the transitional  
sonic waveform  
achieve, Anders-  
generally quite  
ones which are  
depth of about  
l. This step-like  
n in the leptite.  
ls when passing  
to 208 m, does  
wo sections in  
v neutron and  
l content. Also,  
cally these two  
reduced resis-  
higher IP and

maginary VLF  
obable that the  
ocal phenome-

#### *Lower granite, 208–328 m*

The granite has a higher gamma count rate than the leptite due to the higher radio-element content, and a lower gamma-gamma and a higher neutron response due to the lower mafic mineral content. Its IP effect of 2.5 to 4.0% is somewhat higher and more variable than the leptite.

The logs show that the lower granite is more fractured than the lower leptite above and the pyritic granite below. Two 8 m fracture zone intercepts stand out at 272.5–280 m and at 316.5–324.5 m (figs 2 and 8). The latter is permeable enough to permit flow under steady-state open hole conditions, as shown by the gamma-ray and temperature logs.

#### *Pyritic granite, 328–380 m*

The pyritic granite unit is characterized by fractures containing sulfides, mainly pyrite, which are rare in the other units. A most pronounced difference between the lower and pyritic granites is the very marked SP and IP anomalies indicating the sulfide occurrences to be rather extensive. The peaks of the SP and IP anomalies at 340 m slant depth (fig. 2b) coincide with the section of highest pyrite content. Both components of the VLF record show a change in slope when passing into the pyritic granite. Thus the sulfide occurrences are not just isolated occurrences close to the borehole but must have considerable extent.

A second distinction between the two granite units is provided by the sonic log. At 328 m there is a noticeable decrease in the frequency of sonic waveform features; in fact, below 338 m the sonic waveform record (fig. 8) is remarkably free of any anomalous features. The core log is not consistent with the sonic record in this respect in that the frequency of observed fractures in core does not decrease below 328 m. At 337 m the gamma-ray log drops by 40%. The decline is due to loss of radon-charged groundwater from the borehole into a permeable fracture. With this notable exception, the logs give no evidence of significant fracturing within the pyritic granite.

### EFFECTS OF SPECIFIC MINERALS

The mineralogical variations seen in the core have characteristic responses on some of the geophysical logs. The occurrence of quartz veins, pegmatite dikes, sulfides, mafic minerals, and iron oxides can be identified in igneous and metamorphic rocks by using a combination of geophysical borehole logs. Such identification is in fact necessary so that their effects can be eliminated or avoided in analyzing the logs for fluid flow properties.

#### *Iron oxides and silicates*

Examination of the gamma-gamma and neutron logs in fig. 2 and in the expanded log section in fig. 4 shows a number of well-defined coincident deflections. Spike-like decreases in the gamma-gamma count rate caused by density increases are often

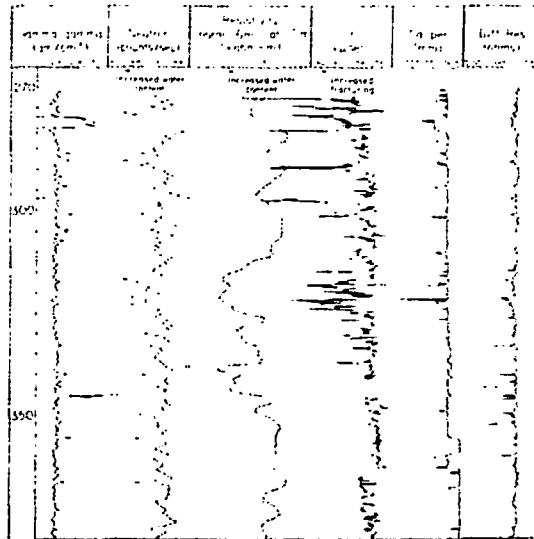


Fig. 4. Geophysical logs in SBH-1, section 270–380 m. The symbol “py” denotes presence of pyrite in the core.

associated with decreases in the neutron count rate, which would usually be attributed to increasing water content. However, porosity effects cannot produce such coincident responses, because a bulk density increase without a grain density increase implies a porosity decrease, not an increase. The effect of bound water is more difficult to assess here, since in some cases mineralogically bound water can completely dominate the neutron log (Nelson and Glenn 1975). It may well be a contributing factor to the neutron response in SBH-1, but it is not believed to be the controlling factor because some of the observed deflections are too large to be accounted for by bound water. Borehole roughness is also discounted because the caliper shows that diametral roughness is usually less than a few millimeters, not enough to affect the neutron log, and opposite in effect to the observed density increases. Having eliminated the above contributing factors, we attribute the density increases to the presence of high-density minerals, the chief heavy constituent being iron. Iron is also a good absorber of thermal neutrons, having an absorption cross-section about 15 times that of silicon.

The core record shows that iron is usually visibly present wherever the anomalous deflections occur. Pyrite and chlorite are present in the interval 337–345 m, where three such anomalous peaks are located. Two greenstone intercepts, at 245–246 m and 277–280 m, coincide with two similar neutron and gamma-gamma deflections. The effect is most dramatic in the banded leptite unit from 52 to 89 m, where the leptite consists of bands of very fine-grained, light-gray rock alternating with bands of mottled green coloration. The neutron and gamma-gamma deflections of fig. 2(a) match perfectly the green zones which are generally about 1 m thick. According to thin section inspection, the rock at 87.9 m is composed mostly (~80%) of an iron-rich amphibole, probably actinolite, intergrown with epidote

Fig.  
neut  
cont

whi  
rocl  
stiti  
cor-  
tion  
epi

fra  
fits  
wa  
sar  
the  
ab  
ap  
ex

at

w  
at  
e:  
tr  
F  
ii

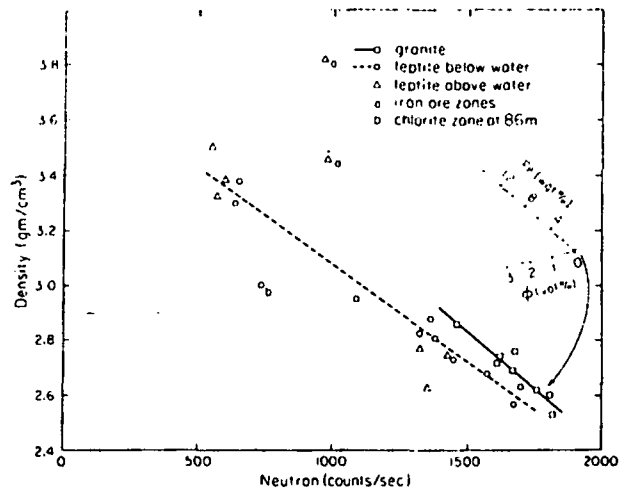


Fig. 5. Density anomalies from the gamma-gamma probe plotted against corresponding neutron responses. The overall trend is dominated by iron-rich minerals rather than the water contained in fractures and pores.

which comprises 10 to 15% of the sample. A thin section from 86.5 m shows the rock to be a breccia comprised mostly (~90%) of chlorite and epidote, with interstitial fine clay. In addition, the high density/high absorption records at 76-77 m correlate well with iron oxides, probably hematite, observed in core. Hence, observation has clearly documented the high percentages of iron-rich minerals hematite, epidote, chlorite, and actinolite within the 52 to 89 m depth interval.

A fraction of the coincident gamma-gamma and neutron peaks, selected to omit fractured intervals, is cross-plotted in fig. 5. Two trendlines represent least-squares fits through the points from the granite and leptite intervals which lie below the water level. The range of points from the leptite is much greater than the granite samples, since the iron content of the leptite varies much more widely. Despite this, the two straight-line fits are nearly parallel, indicating that the gamma and neutron absorption mechanisms are similar in the two rock types. Inserted into fig. 5 is an approximate scale reflecting the effect of porosity and iron variations, which are expressed as

$$N(\text{ct s}^{-1}) = 1800 - 85\phi - 24 \text{ Fe}$$

and

$$\rho_b(\text{g cm}^{-3}) = (1 - 0.01\phi)(2.62 + 0.02 \text{ Fe}) + 0.01\phi,$$

where  $N$  is the neutron count rate,  $\rho_b$  is bulk density,  $\phi$  is volume percent porosity and Fe is iron content in weight percent. The porosity scale, based on the above expressions for zero Fe content, explains the offset between granite and leptite trends as due to the leptite having a porosity about 1% higher than the granite. The Fe scale was established by computing the bulk density for increasing amounts of iron substituting for magnesium in chlorite (composition:  $(\text{Mg}, \text{Fe})_6\text{Si}_4\text{O}_{10}(\text{OH})_8$ ).

and adhering to the trendline established empirically for the granite. Hence it should be recognized that these scales are appropriate only for this particular neutron probe, and are probably valid only over small excursions of iron and porosity from the chosen base values.

### *Pyrite*

As mentioned before, the granite at the bottom of the borehole (328–380 m) contains sulfide minerals. Pyrite constitutes less than 1% of the minerals seen in the core, except in the interval 338–345 m, where it occurs more abundantly, filling fractures or in veins along with quartz and chlorite. These sulfide-mineralized sections of core typically contain 2–10% pyrite and are 6–30 cm wide.

In the interval 330–355 m (fig. 4), the pyritic zones are reflected in peaks on the gamma-gamma, neutron, resistivity, and resistance logs. The neutron and gamma-gamma peaks are believed to be controlled by the iron content, while the electrical logs respond to the enhanced conductivity.

Over this same interval, the IP log (fig. 2b) increases to over 8%. Because the IP log was run on a 5 m electrode spacing, it lacks the spatial resolution of the other logs mentioned; however, the broad peak convincingly demonstrates the existence of sulfides. At other depths in the hole, the IP response declines where the resistivity drops (compare 245 m and 317 m, for example); that is, above 330 m much of the IP response is controlled by porosity fluctuations. However, below 330 m the IP and resistivity logs no longer correlate, and the IP response is dominated by the sulfide content.

The spontaneous potential (SP) log, also shown in fig. 2, responds within the pyritic interval as does the IP log. Note that the SP log is featureless throughout the hole except at the iron sulfide and iron oxide mineralization occurrences. The series of pyrite occurrences is extensive enough to produce a clear change in the gradient of the VLF records.

## POROSITY AND WATER CONTENT

Four of the probes run in SBH-1 respond in some way to the volume fraction of water-filled pore space. Each of the gamma-gamma, neutron, electrical resistivity, and sonic probes has been used to a greater or lesser extent to estimate porosity in sedimentary reservoir rocks. In igneous rock of low porosity it is not at all obvious that a particular technique has adequate sensitivity to measure small porosity variations, or that other competing factors will not mask the porosity effect.

One of these four, the gamma-gamma probe, lacked the sensitivity required to measure porosity fluctuations at the 0.01 level. Calibration of this particular probe (see Appendix), along with count rate and averaging time considerations, shows that density variations less than  $0.06 \text{ g cm}^{-3}$  are not detectable. If the grain density  $\rho_g$  is held constant at  $2.65 \text{ g cm}^{-3}$ , an apparent change in bulk density  $\rho_b$  affects the porosity as

$$\Delta\phi = -\Delta\rho_b/(\rho_g - 1) = -0.6 \Delta\rho_b.$$

Fig.  
Con  
the  
Stra  
lepti  
give

Cor  
less  
gan  
frot  
rec  
can  
cre:  
by

net  
occ  
are  
eff  
fea  
sor  
res  
exc

bl

ite. Hence it should particular neutron and porosity from

(328-380 m) con- minerals seen in the abundantly, filling le-mineralized sec-

d in peaks on the neutron and gamma- while the electrical

%. Because the IP ation of the other ates the existence here the resistivity 10 m much of the ow 330 m the IP or ed by the

onds within the s throughout the ences. The series e in the gradient

lume fraction of trical resistivity, nate porosity in t at all obvious ll porosity vari- ect.

ity required to particular probe ons, shows that in density  $\rho_s$  is  $\rho_b$  affects the

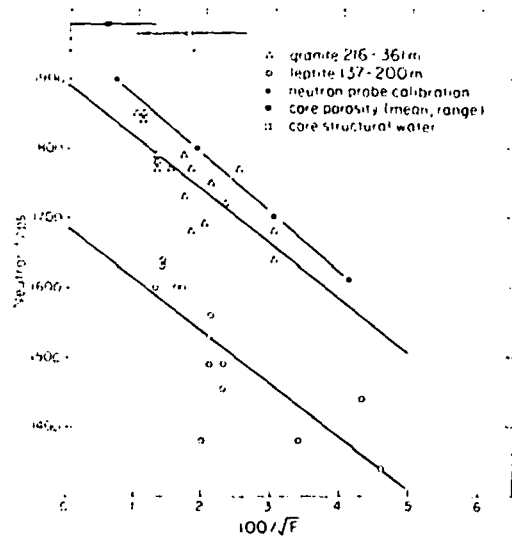


Fig. 6. Neutron porosity cross-plot. Bottom scale is equivalent to volume percent porosity. Conversion of resistivity data to formation factor  $F$  and to equivalent porosity is described in the text. Standard deviation of neutron count rate is equivalent to the size of the symbols. Straight lines represent least-squares fits to the probe calibration, the granite data, and the leptite data. Mean values and range of core porosity and structural water measurements are given at the top of the figure.

Consequently, the gamma-gamma probe is insensitive to fractional porosity changes less than 0.035. Visual inspection of the log in figs 1 and 4 shows that the gamma-gamma probe responds well to variations in mafic mineral content. However, aside from these variations caused by grain density fluctuations, the gamma-gamma record is uniform and shows no influence from fracture zones or any other significant density decreases which are porosity controlled. It appears that porosity increases of more than 0.035 are uncommon in SBH-1, an observation corroborated by the neutron and resistivity logs discussed in the following paragraphs.

On the other hand, inspection of the logs shows a number of fluctuations in the neutron, resistivity, and sonic records indicating porosity increases, most of which occur at fracture zones. Lacking core measurements of the actual porosity (which are not meaningful in fractured media), a standard method of examining physical effects on pairs of logs is the cross-plot utilized in figs 6 and 7. Values of correlated features are digitized and plotted, without any correction applied to the neutron and sonic logs, but with borehole and Archie's law considerations incorporated into the resistivity evaluation. Mafic zones identified by the gamma-gamma log are generally excluded from the cross-plots.

As discussed in the Appendix, the neutron probe was calibrated in a granitic block, giving the dependence of neutron count rate  $N$  upon porosity  $\phi$

$$N = C - D\phi,$$

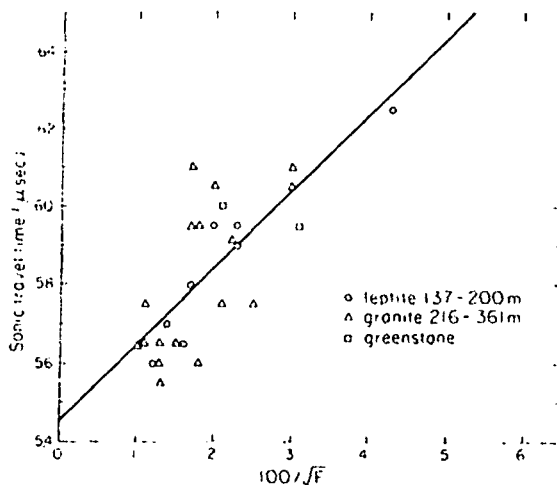


Fig. 7. Sonic porosity cross-plot. Bottom scale is equivalent to volume percent porosity, derived from resistivity as in fig. 6. Data from all three rock types are included in the least-squares fit. Sonic travel times are uncompensated for probe effects.

where  $C$  and  $D$  are constants for a given rock type. The value  $D = -85 \text{ ct s}^{-1}$  per one volume percent is assumed to hold approximately for the Stripa granite. The value of  $C$  is more subject to matrix effects; it is fixed somewhat arbitrarily in fig. 6 to give reasonable porosity values based on water content of the calibration block.

The electrical resistivity data are reduced to the formation factor  $F = R_i/R_w$ , where  $R_i$  is the true formation resistivity and  $R_w$  is the effective resistivity of the pore fluid. Due to the high resistivity contrast between the borehole fluid and surrounding rock, the current density is higher in the fluid and in the rock close to the borehole. To account for this loss of spherical symmetry, the formation factor  $F$  is determined from a borehole correction chart such as fig. 22 in Glenn and Nelson (1979) by entering the ratio of measured (apparent) resistivity  $R_a$  to fluid resistivity  $R_w$ , and the ratio of the 1.6 m electrode spacing to the 76 mm borehole diameter. For this particular data set, the nonlinear chart correction yields  $R_i$  values roughly equal to  $0.6 R_a$ . No bed correction was applied; that is, the effect of adjacent rock units of different resistivity was ignored.

The reciprocal square root of  $F$  is plotted in fig. 6 to give a porosity estimate according to Archie's law as

$$F = \phi^{-m},$$

where  $m$  appears to be about 2.0 for igneous rock (Brace and Orange 1968). The horizontal scale of fig. 6 is therefore equivalent to volume percent porosity; some laboratory measurements on granite core samples taken from an underground borehole near the bottom of SBH-1 are included in fig. 6 to show the water content of relatively unfractured rock.

The  
waters at  
50  $\Omega\text{m}$ .  
lower du  
A more  
the effect  
compens  
rock Bra  
duction  
correctic

Face  
for surfa  
successiv  
proxima  
permissi  
tively to  
low-por  
Waxma  
an equi  
independ  
contri

The  
9.0  $\Omega\text{m}$   
validity  
lation  
respons  
fractur  
the cor  
sidered

The  
leptite  
tinguis  
tron sh  
indicat  
of our  
leptite

Th  
fig. 7.  
directl  
been a  
travel  
data p  
lines r  
treatm  
Fi



The evaluation of  $R_w$  presents two problems. Measurements of underground waters at Stripa (see appendix of Fritz, Barker and Gale 1979) range between 38 and 50  $\Omega\text{m}$ . However, fluid resistivity in parts of the borehole could be either higher or lower due to infiltration during and after drilling, so the uncertainty is even greater. A more serious problem is that surface conduction effects can significantly reduce the effective pore water resistivity below that of the bulk sample. Such effects can be compensated in some sedimentary situations (Waxman and Smits 1968). In igneous rock Brace, Orange and Madden (1965) found that the correction for surface conduction can require as much as a factor of ten, but no means of computing such a correction directly from rock and fluid properties has yet been developed.

Faced with the dual problem of inadequate measurement and no compensation for surface conduction, we have chosen to let  $R_w$  vary as an independent parameter, successively iterating to remove borehole effects until the least-squares slope approximately matches the calibration slope for the neutron probe. This procedure is permissible because surface conduction and electrolyte conduction contribute additively to the overall conductivity, as demonstrated experimentally for a suite of low-porosity rock samples by Brace et al. (1965), and for clay-rich sandstones by Waxman and Smits (1968). Because of the two-element additive conductivity model, an equivalent water resistivity equal to  $R_w R_s / (R_w + R_s)$  can be allowed to vary independently to achieve the fit without knowledge of  $R_s$ , the surface resistivity contribution.

The resulting data values using  $R_w = 9.0 \Omega\text{m}$  are shown in fig. 6. The estimate of 9.0  $\Omega\text{m}$  is only as realistic as the other assumptions implicit in fig. 6, such as the validity of the neutron calibration, its applicability to Stripa granite, and the correlation of adjacent peaks on the neutron and resistivity logs. Also, the neutron response may be distorted because fracture zones are generally characterized by fractures coated with hydrated minerals such as chlorite. Despite these uncertainties, the construction of fig. 6 leaves little doubt that surface conduction must be considered in a porosity evaluation of the Stripa granite based on Archie's law.

The reduced counting rate of the neutron probe in the leptite separates the leptite data from the granite in fig. 6; hence the two rock types are easily distinguished on this cross-plot. Using  $R_w = 9.0 \Omega\text{m}$ , the leptite data also give a neutron slope of about  $-80 \text{ ct s}^{-1}$  per percent porosity similar to the granite, thereby indicating that the slope is not much affected by matrix effects and confirming one of our assumptions in the construction of fig. 6. The statistics in both granite and leptite are only fair; both linear regression fits have correlation coefficients of  $-0.8$ .

The compressional wave traveltimes are plotted against the resistivity values in fig. 7. The resistivity values are the same as in fig. 6. The traveltime values are taken directly from corresponding anomalous points on the sonic log; no correction has been applied for fluid traveltime or for any other effects occurring over the one-foot travel path between transmitter and receiver. The least-squares line is a fit to all data points irrespective of rock type. There is a suggestion that two different trend lines might be fitted to the leptite and granite, but the data do not warrant separate treatment.

Figure 7 shows that transit times increase with decreasing resistivity, here ex-

me percent porosity,  
are included in the

$= -85 \text{ ct s}^{-1}$  per  
St granite. The  
arbitrarily in fig. 6  
calibration block.  
factor  $F = R_s/R_w$ ,  
sistivity of the pore  
ole fluid and sur-  
e rock close to the  
mation factor  $F$  is  
Glenn and Nelson  
to fluid resistivity  
borehole diameter.  
 $R_s$  values roughly  
t of adjacent rock

porosity estimate

range 1968). The  
t porosity; some  
idground bore-  
water content of

pressed as an equivalent porosity. In sedimentary rock with intergranular porosity, a cross-plot of this type would be expected to produce a linear trend because of the tendency of sonic travelltime data to obey the time-average equation. No equivalent experience exists in igneous rock; in the following section we show that the compressional wave transit time is quite useful as a fracture indicator. The transit time delays must be controlled by such details of fracture surfaces as the point-to-point contact and any infilling mineralogy. It seems likely that the apparent correlation of fig. 7 will vary considerably from site to site, depending upon the details of porosity associated with fracture zones, development of alteration products and the magnitude and direction of tectonic stress.

Norton and Knapp (1977) propose that total porosity in fractured rock be considered as the sum of the effective flow porosity  $\phi_f$ , or that portion of the rock which constitutes permeability; the diffusion porosity  $\phi_d$ , representing pores which are interconnected but in which flow is unimportant and chemical transport occurs by diffusion; and the residual porosity  $\phi_r$ , which includes all pores independent of  $\phi_f$  or  $\phi_d$ . By considering permeability measurements and field estimates of fracture spacing and aperture, they conclude that flow porosity  $\phi_f$  is a very small fraction of total porosity in representative igneous rock. By conducting diffusional measurements on rock wafers in the laboratory they likewise show that the diffusional porosity  $\phi_d$  is but a small fraction of the total porosity. The resulting inference is that residual porosity  $\phi_r$  constitutes most (90%) of total rock porosity.

Because the different borehole probes respond to different physical properties, some inferences can be drawn from the log behavior regarding the nature of porosity structure. The neutron log is the only one of the three considered in figs 6 and 7 which can be considered a total porosity log; thermalization of neutrons by water occurs regardless of whether or not the pore space is interconnected. The electrical resistivity, on the other hand, must be governed by the flow porosity, and to a lesser extent, by the diffusional porosity. The residual porosity and that fraction of the diffusional porosity which is discontinuous cannot contribute to electrical conduction processes. For these reasons, the correlation between the resistivity and neutron logs shown in fig. 6 indicates that in the fractured zones the porosity increase occurs in the flow mode and the diffusional mode. Residual porosity is not increasing significantly, or the correlation would not hold. It also seems unlikely that much of the new pore space is created by interconnecting what was residual pore space before fracturing occurred, for if this were true the neutron response would be the same in fractured and unfractured zones. It seems most likely that porosity increases associated with fracturing are of the flow/diffusional type. Since the increases are of a few volume percent, we infer that fracturing induces flow/diffusional porosity which is greater than the residual porosity and thus comprises the greater fraction of total porosity.

#### FRACTURE DETECTION

The acoustic, caliper, and differential resistance logs have the best vertical resolution of the suite of logs applied at Stripa. These logs, useful in detecting thin structures such as individual fractures and thin fracture zones, are shown in fig. 8, together

tergranular porosity, trend because of the alteration. No equivalent show that the com- tor. The transit time is the point-to-point parent correlation of the details of porosity ducts and the mag-

fractured rock be portion of the rock sending pores which cal transport occurs ores independent of estimates of fracture ry small fraction of iffusional measure- hat the diffusional esulting inference is osity.

physical properties, he are of poros- ered in figs 6 and 7 neutrons by water cted. The electrical sity, and to a lesser hat fraction of the electrical conduc- stivity and neutron sity increase occurs is not increasing ikely that much of sidual pore space onse would be the porosity increases he increases are of iffusional porosity greater fraction of

vertical resolution ng thin structures in fig. 8, together

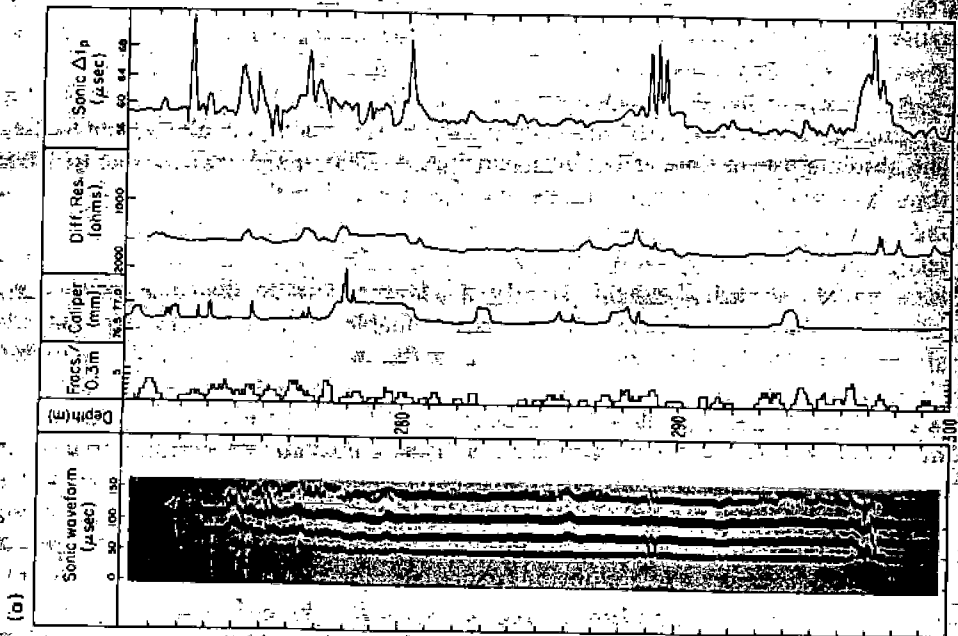
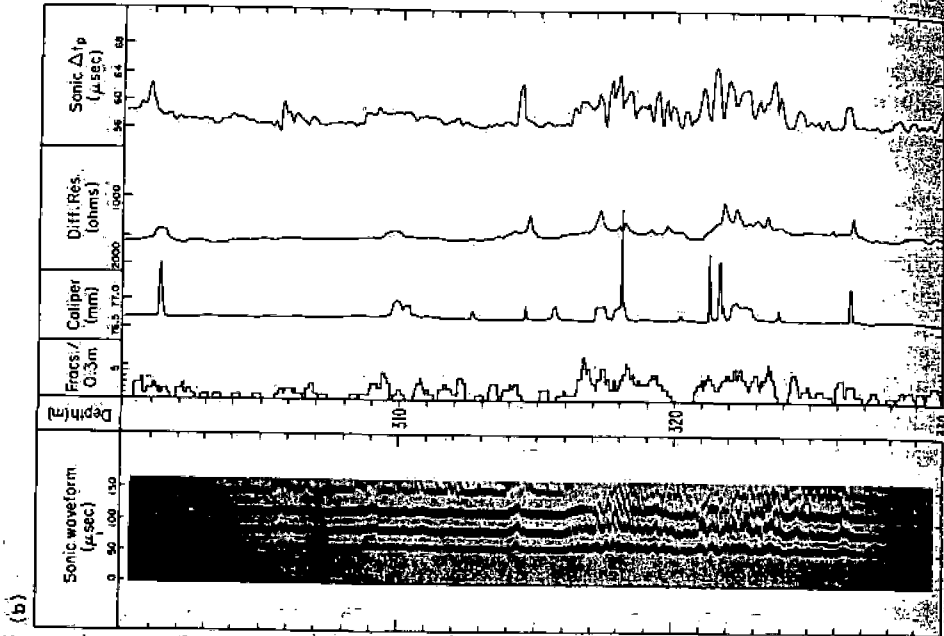
with core information. The open fractures observed in cores have been averaged over 0.3 m corresponding to the transmitter-receiver separation of the acoustic probe. Fractures judged to have been not open in situ, as indicated by the lack of alteration minerals on the fracture surface, have been omitted from the fracture column. To accommodate the acoustic waveform record, the depth scale in fig. 8(a) is expanded against previous figures.

The caliper and differential resistance respond to borehole roughness and are closely correlated (figs 4 and 8). Most of the caliper variations are close to the limit of resolution of 0.2 mm, as evidenced by the step-like nature of the log. Narrow spikes occur where the borehole has intercepted a fracture, causing loss of small chips from the borewall. Borehole roughness can be due to causes other than fractures, however. The broad increases in hole diameter at 360.1 m, 368.8 m, and 380 m coincide with the commencement of drilling after a core run, suggesting that renewed drilling sometimes enlarges the hole slightly. Operation of a mechanical caliper at this sensitivity level is unusual, but proved relatively straightforward and worthwhile in providing correlative information with the other logs.

The differential resistance is also quite sensitive to changes in borehole diameter, being at least comparable to the caliper. Laboratory tests showed that the probe is able to detect fractures of 1 mm aperture and 1 mm change of diameter. Its sensitivity to fracture openings which do not produce borehole roughness is not known. However, conductive veins do produce peaks in the differential resistance log, as shown in the interval between 330 and 355 m, where pyrite is observed in the core. Such mineralization shunts the current flow between the two closely spaced electrodes. Using other logs such as caliper and acoustic, which do not respond to the pyrite veins, and SP and IP, which do respond, the effect of conductive minerals can be separated from the response of open fractures.

As shown in fig. 8, the acoustic log recordings in SBH-1 were limited to the compressional wave transit time and the waveform record on photographic film. The absolute transit time values give velocities of  $5800 \text{ m s}^{-1}$ , comparable to those observed elsewhere on Stripa granite, both in situ and in the laboratory (Paulsson and King 1980). The waveform record gives a visual presentation of zero-crossing delays and interference patterns of several wave modes. No amplitude measurements were made, although it would have been advantageous to do so. Despite these limitations, the acoustic records are the most valuable for fracture detection.

The most outstanding features in fig. 8 are the two 8 m zones at 272-280 m and 316-325 m, where the acoustic records, caliper, and differential resistance all indicate that the borehole wall is disturbed and that the intervals are fractured. Open fractures in cores are also more numerous in these intervals, especially in the lower of the two intervals. In addition, the gamma-ray log already mentioned and a temperature log (not shown) showed that the lower zone at 316-325 m was taking fluid even under static open hole conditions, thereby confirming the fracture logs of fig. 8. Zones such as these are obvious candidates for extensive hydrological testing in a site characterization program for a waste repository. The acoustic log also pinpoints a few other narrower zones, such as the ones at 289 m, 297 m, and 337 m, where fracturing is apparent.



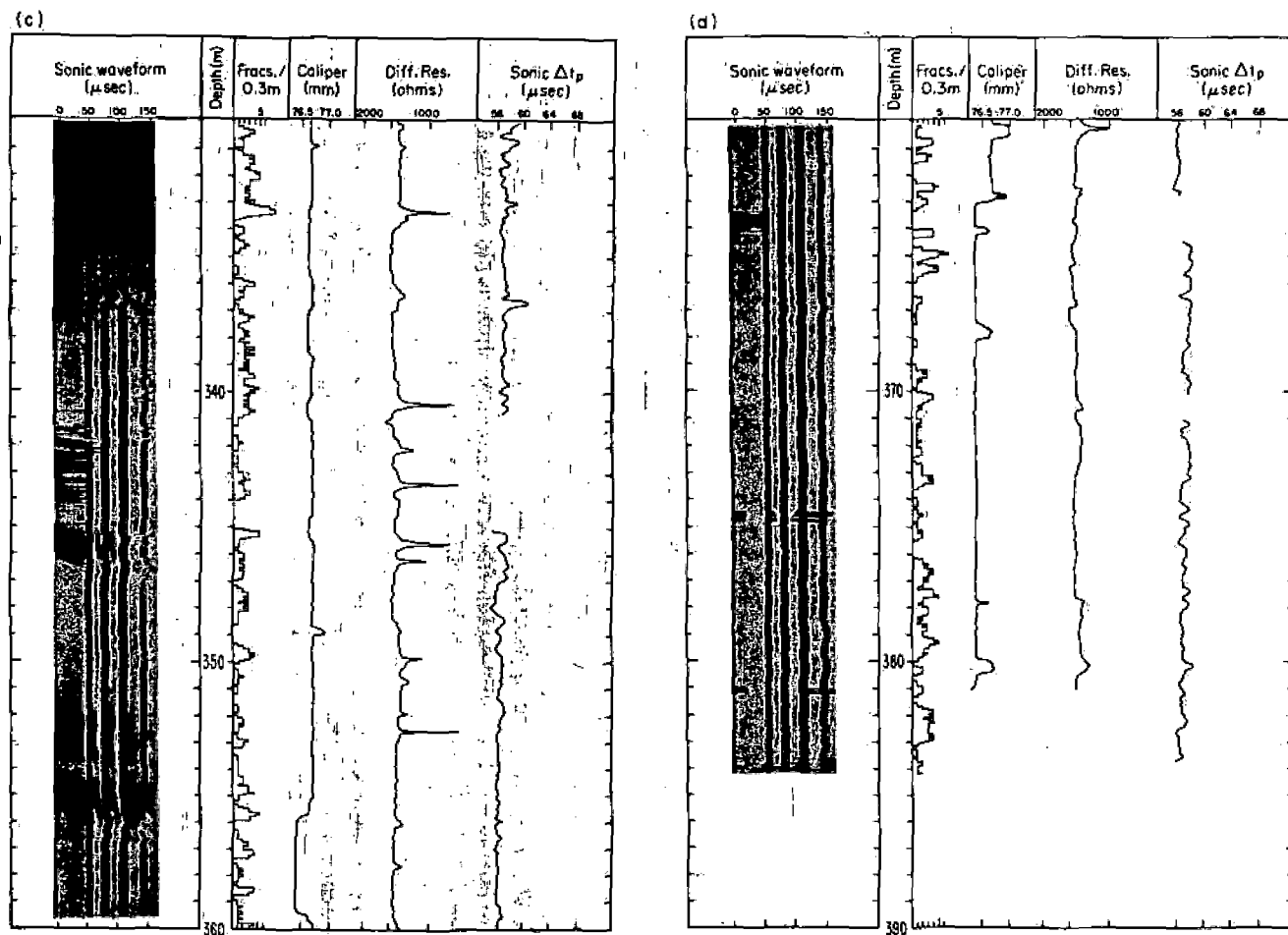


Fig. 8. (a-d) Geophysical logs most sensitive to fracturing in granite on SBH-1. Depth scale has been expanded to accommodate the sonic waveform log. Core data are averaged over 0.3 m length to match the transmitter-receiver separation of the sonic probe.

Below 330 m slant depth the acoustic log in particular indicates remarkably few fracture zones. The core record, however, continues unabated with about the same density of open fractures to the bottom of the hole. Stress conditions and fracture character may be such that acoustic transmission properties change considerably below 330 m. As stated earlier, the Stripa granite and the leptite contain numerous fractures, the majority of which are healed. Open fractures in cores are most commonly coated with chlorite, sericite, calcite, or a combination of the above. These minerals are mechanically weak, so there is a good probability that fractures seen in cores were opened by the drilling and core recovery process. Analysis of the core data from the underground experiment at Stripa by Paulsson, Nelson and Kurfurst (1981) suggests that drilling opened a large number of the open fractures seen in the core. A comparison of TV logging with core retrieved from two 12 m holes in the underground experiment area revealed that less than 10% of the fractures which were open in cores also appeared to be open in situ. In any case, the sonic probe as well as the caliper and differential resistance probes appear to provide information on fracturing in situ that the core-log does not.

The compressional wave transit time has been examined by others as a measure of fracture frequency. King, Stauffer and Pandit (1978) found in borehole measurements carried out under low lithostatic stress conditions that the ratio  $(V_f/V_i)^2$ , where  $V_f$  and  $V_i$  are, respectively, the in-situ velocity and the intact rock velocity, decreases linearly with increasing fracture frequency. A comprehensive set of refraction measurements on igneous and metamorphic outcrop were compared with fracture frequency intercepted by shallow slant boreholes in a paper by Sjögren, Ofsthus and Sandberg (1979). The results, averaged from 15 sites, appear to obey a dependence similar to that observed by King et al. (1978). These findings are not at all unreasonable for near-surface measurements, where a fracture observed in the core is also likely to be sufficiently open in the rock mass to delay the acoustic wave. However, at depth the connection between fracture frequency observed in cores and the propagation of acoustic energy is less straightforward. Higher stress may close, partially or totally, otherwise open fractures. As noted above, many open fractures seen in the cores at Stripa may be drilling induced.

The compressional wave transit time is the easiest measurement to extract from an acoustic probe, but it is not as sensitive to the presence of fractures as is the amplitude of the other modes of wave propagation. For example, Dzeban (1970) simulated fractures with cuts in aluminum blocks which were then pressured to simulate lithostatic pressure. Fractures at a simulated depth of 1000 m had a significant impact on shear-wave attenuation, whereas compressional waves reacted weakly to them. A recent study of acoustic borehole records by Paillet (1980) convincingly demonstrates the utility of shear- and tube-wave amplitude measurements for fracture detection through the correlation of gated amplitudes with fractures recorded in cores and by the acoustic televiewer. In addition, Paillet's computed borehole acoustic waveforms provide additional insight into the patterns produced by interfering modes.

The or  
may b  
illustra  
menta  
specifi  
Ge  
pass u  
of figs  
three  
which  
transi  
leptit  
inter  
decre  
of th  
A  
gamy  
The  
The  
and  
sub  
por  
figs  
ces  
cle  
fro  
car  
ob  
ga  
se  
ro  
su  
st  
cc  
pr  
n  
d  
n  
t  
f

## SUMMARY AND CONCLUSIONS

The organization of this paper underscores the four purposes to which borehole logs may be applied in site characterization for radioactive waste repositories. We have illustrated these applications by discussing logs from a single borehole at an experimental site at Stripa, Sweden. The following paragraphs highlight some of our specific findings on log behavior in an igneous/metamorphic rock mass.

Geophysical logs can be used to characterize rock units which otherwise would pass unnoticed from visual inspection of the core, as demonstrated in the discussion of figs. 2 and 3. As summarized in fig. 3, the leptite intercept can be categorized into three units: an iron-rich unit revealed by gamma-gamma and neutron responses, which is also more fractured and broken than other intervals in the borehole; a transitional unit in which fracturing decreases with depth; and a lower, competent leptite unit. Within the granite, several extensive fracture zones occur within the interval 208–328 m, designated the "lower granite"; below this depth fracturing decreases markedly and sulfide occurrences are the most outstanding characteristic of the pyritic granite.

Mafic minerals produce well-defined coincident deflections on the gamma-gamma and neutron logs, due to density increases and thermal neutron absorption. These deflections are particularly outstanding at the iron-rich zones in the leptite. The overall trend is summarized in fig. 5. Pyrite similarly affects the gamma-gamma and neutron logs, as well as the electrical resistivity, resistance, and IP logs.

Quantification of porosity fluctuations at the 1% level in igneous rock offers a substantial challenge for borehole measurements, especially since the nature of the pore space and its interconnectivity is not well understood. Our efforts, shown in figs 5 and 6, indicate that the current standard methods used in sedimentary sequences may be applicable in igneous rock with proper modifications. For example, it is clear that surface conduction effects must be considered in the estimate of porosity from formation factor. The neutron probe appears to be sufficiently sensitive, but care must be taken to remove the effects of mafic minerals. The reasonable results obtained with the acoustic probe are encouraging but may be fortuitous. The gamma-gamma probe used in this study requires an order-of-magnitude increase in sensitivity to respond to 1% porosity variations.

The acoustic log is the most promising for the detection of fractures in igneous rock, but should be augmented by probes responsive to borehole wall roughness, such as the differential resistance, sensitive caliper, or televiwer (not used in this study). Compressional wave transit times respond to the major fracture zones encountered at 200 m true vertical depth, and interference patterns in the shear-wave portion of the waveform respond at other zones where the compressional arrival is not disturbed. Recent progress by others shows that amplitude data are even more definitive in fracture delineation and characterization.

In general, the logs appear as one might expect in a competent granitic rock: resistivities are high, acoustic velocity is quite comparable to laboratory values, and the borehole well is exceptionally smooth for the most part. One rather surprising finding was observed at the fractured zones, however. The porosity estimates, admit-

tedly crude, indicate that the porosity increases are of the order of a few volume percent, far greater than would occur if the fracture zones consisted of a limited number of parallel planar features. It is likely that such zones are, in fact, highly complex on a local scale, permitting enhanced porosity and permeability values above what would be expected from a simple parallel-plate fracture model.

For waste repository investigations, it will be desirable to extract as much information as possible from exploratory boreholes, and therefore at this stage it is desirable to run a full suite of logs. This is particularly so in igneous and metamorphic rocks where the experience base is less than in sediments. A critical feature such as a fracture or dike is more readily diagnosed if more than one log responds to that feature. Similarly, an anomalous response on one log due to an unusual or unexpected cause can very easily be misinterpreted unless contradictory or confirmatory evidence is available to check the interpretation. Also, surprises do occur, as evidenced by the extraordinary gamma-ray response mentioned earlier in this paper, which is caused by radon migration in groundwater. Since repository usage will continue for some time, it is important to carefully establish the true baseline conditions.

#### ACKNOWLEDGMENTS

We wish to thank Hal Wollenberg for his encouragement and review of this work, and Steve Flexser for contributing the petrological descriptions. The sonic waveform data were acquired through the cooperation of H. Harrell and D. Scott of the Tennessee Valley Authority.

This work was supported by the Assistant Secretary for Nuclear Energy, Office of Waste Isolation of the US Department of Energy under contract W-7405-ENG-48. Funding for this project is administered by the Office of Nuclear Waste Isolation at Battelle Memorial Institute.

#### APPENDIX: DESCRIPTION OF BOREHOLE PROBES

The measurement technology for borehole investigations is now well described in various engineering journals and symposia proceedings. A monograph by Keys and MacCary (1971) describes at length the principles of the measurement methods which we have used in our investigations. The following paragraphs summarize the specifications of the probes used in our investigations at Stripa. More detailed descriptions are given in reports by Nelson et al. (1979) and Magnusson and Duran (1978).

These specifications in no way imply that any of the probes is optimized for repository site characterization work. For the most part, the probes used were either readily available commercially or else were a prototype developmental version. Each could be improved in some way to improve sensitivity, spatial resolution, or information content.

*Gamma ray*  
Both the  
discrimina  
radioisoto  
normally f

*Neutron-*  
The neut  
source at  
calibrated  
holes per  
calibratio  
in low p  
per one v

*Gamma*  
The gar  
source  
sequenc  
such th  
against  
appears  
respons

*Sonic*  
The sc  
strictiv  
first co  
racy o  
film in  
The w  
severa

*Calip*  
The c  
borel  
linea



order of a few volume  
consisted of a limited  
nes are, in fact, highly  
nd permeability values  
acture model.

extract as much infor-  
fore at this stage it is  
igneous and metamor-  
. A critical feature such  
ne log responds to that  
o an unusual or unex-  
lictory or confirmatory  
rises do occur, as evi-  
d earlier in this paper,  
e repository usage will  
lish the true baseline

nd review of this work,  
is. ( sonic waveform  
and D. Scott of the

Nuclear Energy, Office  
ontract W-7405-ENG-  
uclear Waste Isolation

## PROBES

now well described in  
nograph by Keys and  
neasurement methods  
graphs summarize the  
Stripa. More detailed  
fagnusson and Duran

obes is optimized for  
obes used were either  
velopmental version.  
spatial resolution, or

### *Gamma ray*

Both the LBL and SGU gamma-ray probes use NaI(Tl) detectors. No spectral discrimination was employed, so the total count is sensitive to the gamma-emitting radioisotopes of potassium and the decay series of uranium and thorium which are normally found in crystalline rock.

### *Neutron-thermal neutron*

The neutron probe (outer diameter 32 mm, length 1.5 m) uses a 1.4 Ci Am-Be source and a He-3 detector spaced approximately 20 cm apart. The probe was calibrated in a cubic block of granite 1 m on a side perforated with small diameter holes permitting amounts of water up to 3% of the rock volume to be added. The calibrations established an effective radius of investigation of approximately 0.4 m in low porosity rock. The sensitivity to water changes was found to be  $-85 \text{ ct s}^{-1}$  per one volume percent increase in water content.

### *Gamma-gamma (density)*

The gamma-gamma probe (outer diameter 31 mm, length 2.5 m) uses a 16 mCi source of Am-241. The probe was designed to detect thin beds in sedimentary sequences using a single gamma-ray detector located immediately above the source such that the effective spacing is about 57 mm. In operation the probe is held against the borehole wall with a motorized decentralizer arm. Spatial resolution appears to be about 40 mm. Based on measured core density  $\rho$  ( $\text{g cm}^{-3}$ ) and log response  $I$  ( $\text{ct s}^{-1}$ ), the response equation is  $\log I = -0.344\rho + 3.305$ .

### *Sonic velocity and waveform*

The sonic velocity probe (outer diameter 60 mm, length 1.4 m) uses a magnetostrictive source and piezoelectric receiver spaced 0.3 m apart. The transit time of the first compressional wave arrival was recorded in analog form at an absolute accuracy of about  $3 \mu\text{s}$  and a relative accuracy of  $1 \mu\text{s}$ . A waveform log was recorded on film in variable density format using a scale of  $20 \mu\text{s}$  per cm on the oscilloscope face. The waveforms are a record of zero-crossing delays and interference patterns of several wave modes.

### *Caliper*

The caliper probe (outer diameter 51 mm, length 1.2 m) measured fluctuations in the borehole diameter by sensing the displacement of three mechanical arms linked to a linear potentiometer. A special set of short arms was acquired for use in the 76 mm

boreholes, affording a great improvement in sensitivity. The resolution of the caliper, determined from a machined calibrator, was about 0.2 mm change of diameter, a limitation imposed by the potentiometer. Sensitivity to vertical aperture has not been established but is limited by the radius of curvature of the arm tips. Hysteresis, or the ability to track the diameter as the arms are closing or opening, is about 0.3 mm.

#### *Differential resistance*

The differential resistance probe measures the changes in resistance between a pair of electrodes spaced 12 mm apart. Since the borehole fluid furnishes the conductive path, the probe behaves qualitatively as a caliper, with small borehole enlargements decreasing the resistance between the electrodes. The probe sensitivity is enhanced if the annulus between the insulating guard and the borehole wall is as small as possible, preferably a fraction of a millimeter. Fractures simulated in a non-conducting plastic tube show that the tool can detect fractures of 1 mm aperture and 1 mm depth.

#### *Resistivity*

Electrical resistivity is measured with a set of three electrode arrays; a normal array with 1.6 m spacing, and two lateral arrays with 1.65 m and 1.05 m spacing, respectively. To avoid induction effects, a switching frequency of 0.25 Hz is used.

#### *Self-potential*

Self-potential is measured between a borehole electrode and a surface electrode. Both electrodes are nonpolarizing copper/copper-sulphate electrodes.

#### *Induced polarization*

A time-domain system measures the ratio of the integrated voltage to the applied voltage in the 0.24–0.48 s window. The excitation pulse length is 1.96 s. The probe consists of two potential electrodes below the current electrode. Electrode spacing is 5 m. A remote current electrode is placed on the surface about 50 m from the borehole. The potential electrodes are nonpolarizing copper/copper-sulphate.

#### *VLF*

The VLF receiver is tuned to station GBR in England which broadcasts at 16 kHz. The ferrite core antenna measures the vector component of the magnetic field aligned along the borehole axis. A second antenna on the surface provides a reference signal for resolving real and imaginary components.

BRACE  
R.  
BRACE  
re  
BRACE  
el  
71  
DZEM  
A  
FRITZ  
w  
L  
GLEN  
c  
e  
KEYS  
I  
I  
KINC  
MAG  
NELS  
NEL  
NEL  
NO  
PAI  
PA  
PA  
SP  
W

## REFERENCES

- BRACE, W.F. 1980, Permeability of crystalline and argillaceous rocks, *International Journal of Rock Mechanics, Mineral Science and Geomechanics* 17, 241-251.
- BRACE, W.F. and ORANGE, A.F. 1968, Further studies of the effects of pressure on electrical resistivity of rocks, *Journal of Geophysical Research* 73, 5407-5420.
- BRACE, W.F., ORANGE, A.S. and MADDEN, T.R. 1965, The effect of pressure on the electrical resistivity of water saturated crystalline rocks, *Journal of Geophysical Research*, 70, 5669-5678.
- DZEBAN, I.P. 1970, Elastic wave propagation in fractured and vuggy media, *Bulletin of the Academy of Sciences of the USSR, Earth Physics*, 10, 31-38.
- FRITZ, P., BARKER, J.F. and GALE, J.E. 1979, Geochemistry and isotope hydrology of groundwaters in the Stripa granite: results and preliminary interpretation, Lawrence Berkeley Laboratory Report LBL-8285, SAC-12, University of California, Berkeley.
- GLENN, W.E. and NELSON, P.H. 1979, Borehole logging techniques applied to base metal ore deposits, pp. 273-294 in *Geophysics and Geochemistry in the Search for Metallic Ores*, ed. P.J. Hood, Geological Survey of Canada, Economic Geology Report 31, Ottawa.
- KEYS, W.S. and MACCARY, L.M. 1971, Applications of borehole geophysics to water-resources investigations, Chap. E1 in *Techniques of Water-Resource Investigations of the United States Geological Survey*, US Geological Survey, Washington, DC.
- KING, M.S., STAUFFER, M.R. and PANDIT, B.I. 1978, Quality of rock masses by acoustic borehole logging, *Proceedings of the III International Congress, IAEG*, 156-164.
- MAGNUSSON, K. and DURAN, O. 1978, Permeabilitetsbestämningar och geofysik borholmsmatning, KBS (Karnbransle-Sakerhet) Teknisk rapport 61, Stockholm.
- NELSON, P.H. and GLENN, W.E. 1975, Influence of bound water on the neutron log in mineralized igneous rocks, *Society of Professional Well Log Analysts, 16th Annual Logging Symposium*, M1-M9.
- NELSON, P.H., RACHIELE, R. and SMITH, A. 1980, The effect of radon transport in groundwater upon gamma ray borehole logs, Lawrence Berkeley Laboratory Report LBL-11180, SAC-30, University of California, Berkeley.
- NELSON, P.H., PAULSSON, B., RACHIELE, R., ANDERSSON, L., SCHRAUF, T., HUSTRULID, W., DURAN, O. and MAGNUSSON, K. 1979, Preliminary report on geophysical and mechanical borehole measurements at Stripa, Lawrence Berkeley Laboratory Report LBL-8280, SAC-16, University of California, Berkeley.
- NORTON, D. and KNAPP, R. 1977, Transport phenomena in hydrothermal systems: The nature of porosity, *American Journal of Science* 277, 913-936.
- PAILLET, F.L. 1980, Acoustic propagation in the vicinity of fractures which intersect a fluid-filled borehole, *Society of Professional Well Log Analysts, 21st Annual Logging Symposium*, Houston, Texas, DDI-33.
- PAULSSON, B.N.P. and KING, M.S. 1980, A cross-hole investigation of a rock mass subjected to heating, in *Ultrasonic and Acoustic Emission Results from the Stripa Heater Experiments*, Lawrence Berkeley Laboratory Report LBL-10975, SAC-32, University of California, Berkeley.
- PAULSSON, B.N.P., NELSON, P.H. and KURFURST, P. 1981, Characterization of discontinuities in the Stripa granite—Full scale heater experiments, Lawrence Berkeley Laboratory Report LBL-9063, University of California, Berkeley.
- SJÖGREN, B., OFSTHUS, A. and SANDBERG, J. 1979, Seismic classification of rock mass qualities, *Geophysical Prospecting* 27, 409-442.
- WAXMAN, M.H. and SMITS, L.J.M. 1968, Electrical conductivities in oil-bearing shaly sands, *Society of Petroleum Engineers' Journal, Transactions AIME* 243, 107-122.

- WITHERSPOON, P.A., COOK, N.G.W. and GALE, J.E. 1980, Progress with field investigations at Stripa, Lawrence Berkeley Laboratory Report LBL-10559, SAC-27, University of California, Berkeley.
- WOLLENBERG, H.A., FLEXSER, S. and ANDERSSON, L. 1980, Petrology and radiology of the Stripa pluton, Lawrence Berkeley Laboratory Report LBL-11654, University of California, Berkeley.

Geophys

COM

In this  
reactio  
with t  
appre  
eratic  
the ar  
T.  
resen  
defin

$X_r =$   
 $X_b =$   
 $F_a =$

 $F_t$  $F_b$  $M_r$  $M_b$  $K_a$  $D_a$  $M_t$  $K_t$  $D_t$ 

•

••

α

## 8.0 REFERENCES

- Alfano, L., 1962, Geoelectrical prospecting with underground electrodes: *Geophys. Prosp.*, **10**, 290-303.
- Barnett, C. T., 1972, Theoretical modeling of induced polarization effects due to arbitrarily shaped bodies: Colorado School of Mines, Ph.D. thesis T-1453.
- Beasley, C. W., and Ward, S. H., 1985, Theoretical borehole-to-borehole and borehole-to-surface resistivity anomalies of geothermal fracture zones: submitted to *Geophysics*.
- Daniels, J. J., 1977, Three-dimensional resistivity and induced polarization modeling using buried electrodes: *Geophysics*, **42**, 1006-1019.
- \_\_\_\_\_, 1978, Interpretation of buried electrode resistivity data using the layered earth model: *Geophysics*, **43**, 988-1001.
- \_\_\_\_\_, 1983, Hole-to-surface resistivity measurements: *Geophysics*, **48**, 87-97.
- Daniels, J. J., and Dyck, A. V., 1984, Borehole resistivity and electromagnetic methods applied to mineral exploration: *Trans. Geosc. and Remote Sensing, Inst. Elect. and Electron. Eng.*, GE-22, 80-87.
- Dyck, A. V., ed., 1975, Borehole geophysics applied to metallic mineral prospecting: a review: *Energy, Mines and Resources of Canada, Geol. Surv. Paper* 75-31.
- Dynes, K. A., and Lytle, R. J., 1981, Analysis of electrical conductivity imaging: *Geophysics*, **46**, 1025-1036.
- Fox, R. C., Hohmann, G. W., Killpack, T. J., and Rijo, L., 1980, Topographic effects in resistivity and induced polarization surveys: *Geophysics*, **45**, 75-93.
- Holcombe, H. T., and Jiracek, G. R., 1984, Three-dimensional terrain corrections in resistivity surveys: *Geophysics*, **49**, 439-452.
- Holladay, J. S., and West, G. F., 1984, Effect of well casing on surface electrical surveys: *Geophysics*, **49**, 177-188.
- Luth, W. C., and Hardee, H. C., 1980, Comparative assessment of five potential sites for hydrothermal-magma systems: summary: U. S. Department of Energy, DOE/TIC-11303, 51 p.
- Merkel, R. H., 1971, Resistivity analysis for plane-layer half-space models with buried current source: *Geophys. Prosp.*, **19**, 626-639.
- Merkel, R. H., and Alexander, S. S., 1971, Resistivity analysis for models of a sphere in a half-space with buried current source: *Geophys. Prosp.*, **19**, 640-651.

Morrison, B. C., 1971, Electrical potential method used at a single hole to indicate direction to better mineralization: Soc. of Min. Eng., 250.

Newman, G. A., and Hohmann, G. W., 1984, Time-domain response of a 3-D body in a layered earth: Expanded Abstracts, The 54th Ann. Internat. Mtg. and Expos., Soc. Explor. Geophys., Atlanta, 67-69.

Newman, G. A., Wannamaker, P. E., and Hohmann, G. W., 1985, On the detection of crustal magma chambers using the magnetotelluric method: Geophysics, 50, July.

Oppliger, G. L., 1984, Three-dimensional terrain corrections for mise-a-la-masse and magnetometric resistivity surveys: Geophysics, 49, 1718-1729.

Pridmore, D. F., Hohmann, G. W., Ward, S. H., and Sill, W. R., 1981, An investigation of finite-element modeling for electrical and electromagnetic data in three dimensions: Geophysics, 46, 1009-1024.

[ Ross, H. P., and Ward, S. H., 1984, Borehole electrical geophysical methods: A review of the state-of-the-art and preliminary evaluation of the application of fracture mapping in geothermal systems: Univ. of Utah Res. Inst., Earth Sci. Lab. Rep. DOE/SAN/12196-2.

Snyder, D. D., 1976, A method for modeling the resistivity and IP responses of two-dimensional bodies: Geophysics, 41, 997-1015.

Snyder, D. D., and Merkel, R. H., 1973, Analytic models for the interpretation of electrical surveys using buried current electrodes: Geophysics, 38, 513-529.

Wannamaker, P. E., Hohmann, G. W., and Ward, S. H., 1984, Magnetotelluric responses of three-dimensional bodies in layered earths: Geophysics, 49, 1517-1533.

Ward, S. H., 1983, Geophysical studies of active geothermal systems in the northern Basin and Range province: Proc. Geoth. Res. Council. Sympos. on "The role of heat in development of energy and mineral resources in the northern Basin and Range province, G.R.C. Rep. 13, 121-158.

Ward, S. H., Glenn, W. E., Hohmann, G. W., Dey, A., and Smith, R. B., 1974, Electromagnetic methods in conductive terranes: Geoexploration, 12, 121-183.

[ West, R. C., and Ward, S. H., 1985, The borehole transient EM response of a 3-D fracture zone in a conductive half-space: to be submitted to Geophysics.

[ Yang, F. W., and Ward, S. H., 1985a, Single- and cross-borehole resistivity anomalies of thin ellipsoids and spheroids: Geophysics, 50, 637-655.

[ Yang, F. W., and Ward, S. H., 1985b, On sensitivity of surface-to-borehole resistivity measurements to the attitude and the depth to the center of a 3-D oblate spheroid: Geophysics, 50, July.

Zhao, J. X., Rijo, L., and Ward, S. H., 1985, Signal-to-noise considerations for borehole resistivity and induced polarization methods: manuscript in preparation.

BOREHOLE ELECTRICAL GEOPHYSICAL METHODS

A Review of the State-of-the-Art and  
Evaluation of the Application to Fracture  
Mapping in Geothermal Systems

by

Howard P. Ross

June 1984



## CONTENTS

Introduction

Mise-A-La-Masse Methods

Hole-to-Surface Resistivity/IP

Magnetometric Resistivity (MMR)

Borehole Electromagnetic (EM)

Borehole Radar

Summary

Conclusions

Annotated Bibliography

## MISE-A'-LA-MASSE METHODS

### Historical Development

The mise-a'-la-masse method was first developed and used by Schlumberger (1920). The method utilizes a buried current electrode within a conductive body of interest (massive sulfide, low resistivity fracture zone, etc.) and the other current electrode a large distance away from the anomalous mass and at the surface. If the conductivity of the anomalous body is very low, there will be relatively little potential drop across the body itself, and the buried body (presumably) can be mapped at the earth's surface as a zone of low potential gradient.

McMurry and Hoagland (1956) report a detailed field study at Austinville, Virginia, where a current electrode was placed in pencil shaped ore bodies of disseminated sphalerite, pyrite, and galena which occur in a high resistivity dolomite host rock. The resistivity of the country rock was 10x to 100x the resistivity of the ore bodies. Potential measurements were made on the surface and in a large number (~ 30) of drill holes and the potential values contoured in cross section. The mapped potentials aided in the delineation of the ore bodies, and indicated the continuity or lack of continuity of ore zones. The observed potential distribution was compared to the computed potential distribution about an isolated source embedded below the surface of an anisotropic medium of horizontal bedding.

Clark (1965) described the electrical potential distribution near a spheroidal ore body for cases where the current source is in or near the surface of the ore.

Parasnis (1966) describes the mise-a'-la-masse method and presents a detailed field study of a lead-zinc-copper deposit in Central Sweden (Parasnis, 1967) where electric potentials were measured on the ground surface

and in some 25 drill holes. He thus developed a three-dimensional map of electric potentials about the deposit. The survey indicated the dip and pitch of the ore body, the continuity of different ore widths and the general shape of the mass. Numerical calculations were made to evaluate the importance of host rock anisotropy as compared to the effect of the somewhat resistive ore zones. Ketola (1972) also presented a case history including borehole and surface potential measurements.

More recently Bartel et al. (1976) reported the use of mapping potential gradients as an aid in mapping and characterizing massive hydraulic fracturing. Bartel (1977) also described the mapping of the reaction zone of an in-situ coal gasification experiment using a variation on the *mise-a'-la-masse* method in which one current electrode was the production well casing and the other electrode was an outlying well. Potentials measured with a fixed surface array mapped the reaction zone at 300 feet depth, over a period exceeding 140 days. No quantitative interpretation was presented.

Mansinha and Mwenifumbo (1983) report a *mise-a'-la-masse* study with surface potential measurements at the well documented Cavendish Geophysical Test Site in Ontario, Canada. No new numerical treatment was presented. Kauahikaua et al. (1980) describe a *mise-a-la-masse* type survey using the well casing of the high temperature geothermal well HGP-A as one electrode and a return electrode grounded 6 km away in the ocean. Electric potentials were measured at the surface and apparent resistivities calculated. A more detailed resistivity structure of the reservoir resulted.

### Present Assessment

The *mise-a'-la-masse* method can often be expected to provide more definition of a buried conductive body than can be achieved by surface-only resistivity or equipotential surveys. However a substantial resistivity

contrast (10x-100x) with background, a substantial volume of conductive body, and limited depth are required for significant enhancement above survey noise levels. Delineation of fractures associated with a geothermal reservoir would probably require an extensive zone (50 m or more) or wall rock alteration and low resistivity fluids in fractures (0.1-3 ohm-m) for detection at depths exceeding 500 m. More quantitative borehole resistivity methods offer greater promise for fracture detection.

#### REFERENCES (Chronological)

- Schlumberger, 1920
- Clark, 1956
- McMurry and Hoagland, 1956
- Parasnis, 1966
- Parasnis, 1967
- Ketola, 1972
- Bartel et al., 1976
- Bartel, 1977
- Kauahikaua, J., Mattice, M., and Jackson, D., 1980
- Mansinha and Mwenifumbo, 1983

## HOLE-TO-SURFACE RESISTIVITY/IP

### Historical Development

The hole-to-surface and hole-to-hole resistivity methods have gradually evolved from the corresponding surface resistivity arrays. Thus several early papers contributed to the mathematical and technique development of hole-to-surface and hole-to-hole resistivity methods. Some of these more pertinent contributions are cited here. The mise-a-la-masse method, probably the first hole-to-surface resistivity technique, is reviewed in another section.

Webb (1931a) provided detailed solutions of Laplace's equation,  $\nabla^2 \phi = 0$ , for the electric potential due to a buried sphere using surface electrodes. Webb (1931b) then extended the solution to the potential due to a buried spheroid using an expression in spheroidal harmonics for the inverse distance ( $r^{-1}$ ) formula. In 1952 Seigel described a technique for determining the size of a spheroidal ore zone when a single current and two potential probes are located in a boring which penetrates the body. The mathematics were developed for current and potential probes located along the axis of rotation of an oblate spheroid. Van Nostrand (1953) discussed the limitations of resistivity methods by considering the buried sphere problem and surface electrodes.

Alfano (1962) and Merkel and Alexander (1971) developed expressions for the theoretical apparent resistivity for the three-layered model with a buried current electrode. Alfano calculated theoretical curves for the pole-dipole array and Merkel and Alexander computed resistivities for the modified dipole-dipole array with one buried current electrode. Snyder and Merkel (1973) calculated the induced polarization (IP) and apparent resistivity responses from a buried current pole in the presence of a three-layered half-space and from a buried sphere in a half-space model. Wagg and Seigel (1963) described the application of surface-to-borehole arrays to the search for massive and

disseminated mineralization which may have been missed by a drill hole. They described drill hole arrays for 'detection logging' ( $C_1P_1$  downhole,  $C_2P_2$  on surface), and directional logging ( $P_2$  downhole,  $C_1, C_2, P_1$  on surface). Alpin (1964) presents an integral equation solution for the potential and electric field due to a current electrode in a borehole in the presence of a conductive fluid, for different cross sections.

Dieter et al. (1969) published a solution for the boundary value problem for a point source of current near a body of arbitrary shape. The solution took the form of an inhomogeneous integral equation which was solved numerically by the method of least squares. The solution is then used to calculate apparent resistivity and apparent chargeability functions for three- and four-electrode (surface) arrays.

Merkel (1971) described a numerical solution for the boundary-value problem in steady-state current flow for 1 and 2 layers over a half-space, with one current source below the surface, the second at a finite distance from the drill hole. The analysis found that the optimum placement of the buried electrode, within the conductive region, led to better resolution of the lateral extent of the body. In a companion study, Merkel and Alexander (1971) reported a numerical solution in bispherical coordinates for the boundary value problem of steady state current flow about a sphere of arbitrary conductivity in a half-space. The authors examined and compared the cases of current sources on the surface; on the surface and above the sphere; and on the surface and inside the conducting sphere. They noted the results were similar to the layered case, and that the use of the buried source improved the determination of depth to the conductor.

Barnett (1972, 1976) recognized that the electrical potential integral expresses the potential in terms of an equivalent surface layer of charge. He

then developed a method for representing the surface of an arbitrary 3-D body as a group of connected triangular facets and solved the surface integrals over the triangular domains. The solutions to the integrals are analytic and in closed form. Barnett (1972, 1976) further contributed a convenient method for inputting the apices and assembling the facets of the polyhedron, and applied these advances to 3-D IP and resistivity modeling for surface measurements.

Increasing interest in borehole geophysics resulted in the publication of review papers. Dyck (1975) edited a review of all borehole geophysical methods applied to metalliferous mineral deposits, including seismic, electrical, gravimetric, magnetic, nuclear, temperature and directional surveying techniques. Dyck provides an extensive bibliography for borehole geophysics to 1975. Scott et al. (1975) described research in hole-to-hole geophysical measurements as also applied to mineral exploration.

Hohmann (1975) presented a new numerical solution for calculating the induced polarization and electromagnetic responses of 3-D bodies buried in the earth. The integral equation for the response is reduced to a matrix equation which is solved numerically for the scattering current in the body. The electric and magnetic fields at any point outside the body are found by integrating the appropriate half-space dyadic Green's function over the volume of scattering current. Hohmann (1975) compares his results for the IP response of a buried sphere with a buried current electrode with the theoretical results of Snyder and Merkel (1973) and finds excellent agreement. Hohmann also computes the IP response and the direction of the quadrature electric field for a short receiver dipole down the borehole and surface current electrodes.

An integral equation solution for resistivity and induced polarization

responses of two- and three-dimensional bodies is also given by Lee (1975). The buried electrode case is not specifically addressed. Snyder (1976) uses yet another technique for the solution of resistivity and IP modeling of two-dimensional inhomogeneities. The boundary value problem reduces to a Fredholm integral equation of the second kind which is parametrically a function of the spatial wavenumber. Using the method of moments the integral equation is solved for a number of values of the wavenumber. An inverse Fourier transform is performed to obtain the electric potential at any point of interest. The method is computationally more efficient than the network or finite element techniques. The examples considered were restricted to surface arrays.

Daniels (1977a, 1977b) adapted Barnett's (1972) 3-D IP modeling scheme to compute model responses for six different buried electrode configurations: (1) hole-to-hole (fixed source), (2) hole-to-hole (moving bipole source), (3) hole-to-hole (moving pole source), (4) single-hole (bipole-bipole), (5) hole-to-surface (buried source pole), and (6) surface-to-hole (surface source pole). Daniels presented the variations in the geometric factor as a function of depth and presented the responses for spherical and lens shaped bodies.

Daniels (1978) extended earlier theoretical solutions for the apparent resistivity due to a buried electrode in a one- or two-layered medium (Dakhnov, 1959; Van Nostrand and Cook, 1966) to an arbitrary number of layers. The modeling theory is developed for the general case of buried current electrodes and potential receiver electrodes contained anywhere within a horizontally stratified medium.

Dey and Morrison (1979) developed the mathematics for numerical modeling of the potential distribution about a point source of current located in or on the surface of a half-space containing an arbitrary two-dimensional conduc-



tivity distribution. The finite difference equations are obtained for Poisson's equations using point- as well as area-discretization of the subsurface. Accurate computational results were obtained at less time and cost than with finite-element or network solution techniques. Only the surface electrode case was presented as an example. Merrick et al. (1979) developed an algorithm for the numerical solution of the apparent resistivity observed in a borehole for a multi-layer medium with a buried current source.

Dobecki (1980) provides solutions of the Laplace equation in oblate and prolate spheroidal coordinate systems to model the electrical potential distribution for current and potential electrodes in a borehole which is near an anomalous body of oblate or prolate shape. Model results are presented as vertical profiling and electric sounding profiles.

Lytle (1981,1982) compared model results for single borehole and cross-borehole resistivity measurements in the vicinity of a spherical anomaly. The anomalous body was embedded in an infinite homogeneous medium. In a subsequent paper Lytle and Hanson (1983) examine the influence of electrode configuration on detectability of anomalous bodies and demonstrate the superiority of three- and four-electrode systems over two-electrode arrays.

Newkirk (1982) published a catalog of apparent resistivity responses for a buried current electrode and surface or borehole potential electrodes for a large number of three-dimensional bodies. The responses were calculated by a computer program which effects the integral equation numerical solution of Hohmann (1975).

Wait (1982) discusses electromagnetic fields due to vertically oriented electric dipole sources, including current sources in a borehole.

Daniels (1983) described in detail a hole-to-surface resistivity study in which apparent resistivity was calculated from total electric field measure-

ments made at the surface, using four different boreholes for buried electrode emplacement. The response of three-dimensional bodies was enhanced by subtracting a layered earth model response from the field data.

A recent presentation by Koulikov and Rocroi (1983) describes the use of steel drill casings as vertical line-source electrodes to achieve a higher current density at depth than could be obtained by surface current electrodes. They note that anomalies due to resistive hydrocarbon deposits have been mapped using drill casing as a line current source. Kauahikaua et al. (1980) describe a similar survey where one current electrode was the drill casing of the high temperature geothermal well HGP-A on Hawaii.

Mackelprang (1984) computed a catalog of apparent resistivity responses for thin and dipping three-dimensional bodies which simulate the buried electrode case in the geothermal environment. These models extend the catalog developed by Newkirk (1982) using the finite element integral equation solution of Hohmann (1975).

Yang and Ward (in prep) have modeled the electrical resistivity anomaly arising from thin spheroids and ellipsoids using downhole electrodes. These algorithms may provide the best approximation to the thin conductive zones of interest in geothermal reservoir delineation studies.

### Present Assessment

Theoretical and numerical modeling techniques are well developed for hole-to-surface resistivity methods as applied to mineral exploration. The geothermal reservoir however is most often a group of thin near vertical fractures and can be envisioned as a thin conductive zone in a background of finite (and varying) conductivity, and will generally be a more difficult target to model and interpret than a mineral deposit.

Detailed and precise total field resistivity surveys using deeply buried

electrodes in one or more holes have been reported by Daniels and others, with major improvements in detectability over surface electrical surveys. A dense surface grid of total field measurements may define the elongation of conductive zones associated with the geothermal reservoir which have been penetrated by a borehole. It may be expedient to use the well casing as the downhole electrode, but the current distribution due to this line source must be modeled and applied to the apparent resistivity calculation.

## REFERENCES (Chronological)

- Webb, J. H., 1931a  
Webb, J. H., 1931b  
Seigel, H. O., 1952  
Van Nostrand, R. G., 1953  
Alfano, L., 1959  
Dakhnov, V. N., 1959  
Alfano, L., 1962  
Wagg, D. M., and Seigel, H. O., 1963  
Al'pin, L. M., 1964  
Van Nostrand, R. G., and Cook, K. L., 1966  
Mathisrud, G. C., and Sumner, J. S., 1967  
Dieter, K., Paterson, N. R., and Grant, F. S., 1969  
Merkel, R. H., 1971  
Merkel, R. H., and Alexander, S. S., 1971  
Barnett, C. T., 1972  
Snyder, D. D., and Merkel, R. M., 1973  
Scott, J. H., Daniels, J. J., Hasbrouck, W. P., and Guu, J. Y., 1975  
Dyck, A. V., ed, 1975  
Hohmann, G. W., 1975  
Lee, T., 1975  
Snyder, D. D., 1976  
Barnett, C. T., 1976  
Daniels, J. J., 1977a  
Daniels, J. J., 1977b  
Tikhonov, A. N., Dmitriyev, V. I., and Zakharov, Ye. V., 1977  
Daniels, J. J., 1978  
Dey, A., and Morrison, H. F., 1979  
Merrik, B. R., Checkin, G. H., and Popov, V. V., 1979  
Dobecki, T. L., 1980  
Witherly, K. E., 1980  
Kauahikaua, J., Mattice, M., and Jackson, D., 1980  
Daniels, J. J., and Scott, J. H., 1981  
Lytle, R. J., 1981  
Lytle, R. J., 1982  
Newkirk, D. J., 1982  
Wait, J. R., 1982  
Daniels, J. J., 1982  
Lytle, R. J., and Hanson, J. M., 1983  
Daniels, J. J., 1983  
Koulikov, A. V., and Rocroi, J. P., 1983  
Bassian, A. E., 1983  
Holcombe, H. T., and Jiracek, G. R., 1984  
Mackelprang, C. E., 1984  
Yang, F., and Ward, S. H., 1984

## MAGNETOMETRIC RESISTIVITY (MMR)

### Historical Development

The MMR method was first patented by Jakosky (1933) and is briefly described in his text on exploration geophysics (Jakosky, 1940). The method is based on the measurement of low level (about 100 milligamma), low frequency (1-5 Hz) magnetic fields associated with noninductive current flow in the ground. The MMR method differs from conventional resistivity techniques in that potential measuring electrodes are replaced by a sensitive coil or magnetometer, and a component of the magnetic field due to the current flow is recorded (Edwards and Howell, 1976). Edwards (1974) recorded the first successful field survey using the gradient array (surface only), and developed the methodology and the procedures for normalizing and interpreting the data which are obtained in this work. He clearly demonstrated that the MMR method was effective in a region of severe topography where the overburden was quite thick, and other electrical methods were less effective.

Edwards and Howell (1976) present the formulations for the MMR response: a) over a uniform earth; b) for a vertical contact; and c) for a thick outcropping dike based on earlier work by Stefanescu and Nabighian (1962) and Edwards (1975). Edwards and Howell (1976) describe alpha center modeling, utilizing earlier mathematical developments by Stefanescu (1950, 1970) and Tang Muoi (1972). Edwards et al. (1978) presented an integrated mathematical theory for the MMR method drawing upon earlier theoretical papers by Stefanescu and others which are difficult to obtain. They also present several new theoretical solutions. They noted the correspondence of the magnetic induced polarization (MIP) method described by Seigel (1974).

Acosta (1981) applied the MMR method to the borehole geophysics problem. Utilizing the theory presented in Dey and Morrison (1979) and in

Acosta (1981), a finite-difference program was developed which produces a numerical representation of the Fourier transform for the three-dimensional potential distribution about point sources of current located in a half-space. The half-space contains an arbitrary two-dimensional conductivity distribution. The transform values are used to evaluate a modified expression of the Biot-Savart law for the magnetic field in terms of the electrical potential and conductivity gradients.

Acosta and Worthington (1983) report a detailed field experiment where the electric current was constrained to flow through surface electrode pairs in a quarry where only one borehole intersected a low resistivity zone of fissuring. A vertical magnetic field detector recorded the magnetic response at intervals of 2.5 m in the centrally located borehole, for each of 8 current electrode arrays. A finite difference modeling program was used in interpretation of the data. They conclude that the borehole MMR method is very sensitive to electrical current channeling within an otherwise resistive medium, and that the method is well suited to exploration for ground waters in fractured media.

Nabighian et al. (1984) describe model and field results which further demonstrate a substantial improvement in anomaly amplitudes when the recording magnetometer is lowered within the borehole. The lowering of current electrodes beneath the surface may not significantly improve the surface NMR response, however. Massive sulfide mineralization was detected at 250 m depth.

#### Present Assessment

As noted by Acosta and Worthington (1983), the MMR method has some extremely advantageous characteristics for application to fracture mapping. These include: a) the reservoir need not be in electrical contact with the

ground; b) the method can be used in dry or plastic-cased boreholes; c) the magnetic field variations are very sensitive to electric current channeling (as expected in fracture zones). Using appropriate array geometries, the method is relatively insensitive to near surface resistivity variations and topography, as compared to the deeper fractured bedrock response which is sought. These characteristics, coupled with recent developments in high sensitivity magnetometers and electronics, suggest that the borehole MMR method may have some potential for the detection of fracture zones carrying geothermal fields at depth. There is a need to evaluate the magnitude of anticipated MMR responses, and other anomaly characteristics for appropriate geometries and resistivities. This need is best addressed by numerical modeling, such as presently underway at the University of Utah and the Earth Science Laboratory, UURI.

#### REFERENCES (Chronological)

- Jakosky, J. J., 1933  
Jakosky, J. J., 1940  
Stefanescu, S. S., 1950  
Stefanescu, S. S., and Nabighian, M. N., 1962  
Stefanescu, S. S., 1970  
Stefanescu, S. S., and Stefanescu, D., 1974  
Tang, Muoi, 1972  
Edwards, R. N., 1974  
Seigel, H. O., 1974  
Edwards, R. N., and Howell, E. C., 1976  
Edwards, R. N., Lee, H., and Nabighian, M. N., 1978  
Acosta, J. E., 1981  
Acosta, J. E., and Worthington, M. H., 1983  
Nabighian, M. N., Oppliger, G. L., Edwards, R. N., Lo, B. B. H., and Chessman, S. J., 1984

## BOREHOLE EM

### Historical Development

Doll (1949) and Roy and Dhar (1970) have investigated the radius of investigation of a two-coil induction logging system (single borehole) and show that the region of ground that affects the received signal increases in proportion to the transmitter-receiver coil spacing (Worthington et al., 1981). Doll (1949) and Roy and Dhar (1970) further show that for a homogeneous earth, the signal received is principally affected by an annulus of ground twice the transmitter-receiver separation in thickness and 0.1 the transmitter-receiver separation in radius.

Moran and Kunz (1962) presented a rigorous mathematical development from Maxwell's equations, for the response of a two-coil induction sonde in homogeneous and nonhomogeneous media. Their results allow for an evaluation of the skin effect in induction logging.

Gabillard et al. (1971) and Bassiouni et al. (1972) describe the telelog method which is reportedly capable of detecting resistive zones at considerable distances. A low frequency (12.5 Hz or 3125 Hz) alternating field is generated by a transmitter and conductively coupled to the earth via surface current electrodes. The vertical component of the electric field is detected at various depths in the hole. The method has been successfully applied in locating the edge of a gas field from a development well (Dyck, 1975).

Oristaglio and Worthington (1980) derived a finite element solution of the forward problem for electromagnetic fields induced by a line source for a buried conductive body in a conductive media. They demonstrated the poor resolving power for bodies buried deeper than 0.2 skin depths for surface data alone and incorporated borehole electromagnetic field values in the inversion study. Oristaglio and Worthington (1980) used a combination of the finite



element and the damped least squares methods to invert the electromagnetic fields scattered from multiple two-dimensional bodies.

Worthington et al. (1981) describe a two-coil induction logging system in which an alternating magnetic field is established by transmitting current through a horizontal loop of wire symmetrically positioned about the borehole on the surface of the earth. The amplitude and phase of the resulting field are measured downhole using a phase sensitive detector. Theoretical modeling using a finite-element program developed by Oristaglio (1978) and Oristaglio and Worthington (1980) verified the interpretation of a field experiment for a buried massive sulfide conductor intersected by one of two boreholes. The technique substantially increases the detection range of conductive zones peripheral to the borehole.

The problem of detecting vertical structures near a borehole in the presence of a high borehole fluid conductivity was discussed by Howard (1981) who develops the expressions for electric and magnetic field responses for single borehole logging in the presence of vertical fractures. Analytic expressions were presented which predict the effect of the cavity, misalignment of coils in the cavity, and an upper bound on the effect of the borehole fluid. The attenuation of the electromagnetic energy as a function of conductivity, and the depth of many geothermal resources (1000 m or more), and the presence of drill casing are limitations to the mapping potential of the electromagnetic hole-to-surface methods.

In 1975 Woods completed a model study of the Crone borehole pulse electromagnetic (PEM) system. The Newmont organization also developed a borehole electromagnetic pulse system (EMP) which has been widely used in mineral exploration throughout the world. The earth is energized with a large fixed transmitter loop by a pulse of 50 A and 20 ms duration on half second

intervals (Boyd and Wiles, 1984). A single component of the secondary field is measured downhole. Small vertical, conductive ore zones have been mapped to depths of 250 m with this method.

Eaton and Hohmann (1984) computed transient borehole electromagnetic (EM) responses of thin horizontal conductor in a conductive half space. They note that current channeling is strongly influenced by the conductivity of the host and may be an important contribution to the transient electromagnetic response. Borehole profiles of vertical system response ( $dH/dt$ ) for the PEM, EM 37, Sirotem and UTEM systems are compared for a 0.1 ohm-m body in a 100 ohm-m half-space.

#### Present Assessment

The single borehole electromagnetic methods are essentially well logging techniques where the radius of investigation is expanded by focusing the transmitted electromagnetic energy, or by increasing the transmitter-receiver separation within the borehole. The detection range for vertical fractures filled with conductive fluids is still small when compared to typical spacings between geothermal exploration or development wells.

Hole-to-surface electromagnetic methods which may substantially increase the range of fracture detection utilize a large transmitting coil on the surface and a sensitive magnetic field detector downhole. The use of such methods is increasing rapidly, especially the pulsed electromagnetic methods. The direction of fracture trends may be more readily determined using multiple transmitting loops at the surface. Data interpretation is developing rapidly and can be quite accurate for a single conductive body in a resistive half-space environment. The application to narrow, vertical conductive (fracture) zones in a complex resistivity environment, as required for geothermal development, will be more challenging and complex.

## REFERENCES (Chronological)

- Doll, H. G., 1949  
Moran, J. H., and Kunz, K. S., 1962  
Roy, A., and Dhar, R. L., 1970  
Gabillard et al., 1971  
Bassiouni et al., 1972  
Woods, D. V., 1975  
Landt, J. A., 1978  
Oristaglio, M. L., 1978  
Oristaglio, M. L., and Worthington, M. H., 1980  
Witherly, K. E., 1980  
Howard, A. Q., Jr., 1981  
Worthington, M. H., Kuckes, A., and Oristaglio, M., 1981  
Goldman, M. M., and Stoyer, C. H., 1983  
Pascal, H., 1983  
Eaton, P. A., and Hohmann, G. W., 1984  
Dyck, A. D., 1984  
Boyd and Wiles, 1984

## BOREHOLE RADAR

### Historical Development

The first well documented use of subsurface radar equipment for mapping geologic features appears to be a patent issued to Holser et al. (1966) for mapping a salt dome from a borehole. Fredriksson et al. (1969) later patented a helical antenna designed specifically for borehole irradiation. Holser et al. (1972) describe their 230 MHz pulse-radar well-logging system and the interpretation of data taken from an 8208 feet deep drill hole in the Pine Prairie salt dome in Louisiana. The authors noted that signals were received out to 2000 or 4000 feet of range, and noted the desirability of increased range possible with a 15 MHz tool. Holser et al. (1972) present the basic equations for reflected signal power, signal-to-noise ratio, attenuation, etc. for helical and dipole antennas.

Dolphin et al. (1974) describe detecting reflections from chambers within a dolomite mine at distances of 100-130 feet, using frequencies of 17.5 - 35 MHz for transmitters and receivers on the surface. The dolomite was described as faulted and jointed, and well above the water table. Cook (1975) reported on laboratory measurements of RF complex permittivity for a variety of rocks with "natural" moisture contents at frequencies of 1, 5, 25 and 100 MHz. He concluded that VHF mining radar equipment should be capable of exploring to distances of up to hundreds of feet in several low-loss rocks such as granites, limestones and coals. Useful but shorter probing distances were predicted for other coals, gypsums, oil shales, dry sandstones, high grade tar sands, and schists. Radar probing distances of less than 10 feet are to be expected for most shales and clays. Cook (1977) later reported borehole radar exploration in coal seams, where probing distances of 60 to 90 feet were achieved using 31 MHz energy.

Daily et al. (1982) used cross-borehole electromagnetic sounding with frequencies between 1 and 40 MHz and tomographic image reconstruction (geotomography) to map the in situ electromagnetic attenuation of oil shale. The study was designed to evaluate the technique as a means for remote monitoring of in situ retorting. The tomography mapped a plane 27 m wide by 12 m high. They concluded that commercial-sized retorts, requiring transmission paths of 50-100 m, may require probing at about 1 MHz, but that the combustion zone (well over 400°C) could probably be mapped because of its much higher electrical conductivity. Somerstein et al. (1984) also report attenuation studies for 25 and 1.5 MHz for in situ oil shale retorts.

Nickel et al. (1983) describe single borehole (reflection) and cross borehole (em HF absorption) techniques to map structures in the interior of salt domes. They used frequencies of 20 and 40 MHz for the reflection measurements and a broad range of frequencies between 4 and 25.6 MHz for the absorption study. Antenna lengths were 1.5 to 4 m long. The authors report that the 40 MHz system was effective for distances up to 300 m, but that the 20 MHz proved to be more favorable for greater distances. Nickel et al. (1983) note a disadvantage of the reflection method is the lack of azimuthal resolution, but that the absorption method presents nearly ideal input data for computerized geophysical tomography. In a paper presented at the 1983 EAEG annual meeting, Sender et al. (1983) described a new borehole antenna system designed to overcome some limitations in antenna array directive properties which result from the fact that the borehole diameter is rather small compared to the wavelength.

### Present Assessment

The methodology for borehole radar measurements is already well developed and improved borehole antenna systems are being developed. Researchers at

Lawrence Livermore National Laboratory have reported on field and interpretation techniques for cross-borehole measurements and tomographic mapping. Unfortunately the successful use of radar methods requires probing distance typical of development drill hole distances, or greater. This restricts the use of the method to relatively low loss (high resistivity) rocks such as salt, oil shale, and possibly some massive carbonate units. Most productive geothermal systems, in contrast, are typified by low resistivity fluids and fracture zones. Radar probing distances would typically be less than 200 feet (excepting possibly the hot dry rock case) hence the method should not receive a high priority for geothermal fracture delineation research.

#### REFERENCES (Chronological)

- Holser, W. T., Unterberger, R. R., and Jones, S. B., 1966  
Fredriksson, O. A., Fossati, F. N., and Robert, F. A., 1969  
Hosler, W. T., Brown, R. J. S., Roberts, F. A., Fredriksson, O. A., and Unterberger, R. R., 1972  
Dolphin, L. T., Jr., Bollen, R. L., and Oetzel, G. N., 1974  
Cook, J. C., 1975  
Cook, J. C., 1977  
Daily, W. D., Lytle, R. J., Laine, E. F., Okada, J. T., and Deadrick, F. J., 1982  
Nickel, H., Sender, F., Thierbach, R., and Weichart, H., 1983  
Sender, F., Thierbach, R., and Weichart, H., 1983  
Sommerstein, S. F., Berg, M., Chang, D., Chung, H., Johnson, H., Richardson, B., Pizzicara, J., and Salisbury, W. W., 1984.

## SUMMARY

The delineation of fracture zones in a geothermal reservoir is an important problem but the solution, in the general case, is not easily achieved. Surface geophysical methods generally lack sufficient depth penetration and resolution, and deep exploration or production drill holes are costly, generally more than one million dollars. The presence of one or more boreholes within, or near to, the geothermal reservoir offers an opportunity to increase the signal or current density in the target zone or alternatively to measure the anomalous response induced in this area by surface sources with minimal degradation.

The design of a successful borehole geophysical method must consider the details of the borehole itself and the geologic setting. The borehole will generally exceed 1000 m in depth, and will probably be cased for most or all of this length. Geothermal reservoirs are typically in complex geologic settings and may include low or high resistivity surface layers, near vertical faulting, and irregular zones of low resistivity fluids or clay alteration associated with the geothermal reservoir.

Let us consider the suitability of the several borehole electrical methods in this environment.

Borehole radar. Borehole radar would generally be useless in a cased drill hole. In the absence of drill casing probing distances of much less than 100 feet can be expected for most geothermal rock environments (shales, clays and altered rocks, volcanic units, metamorphic rocks). Thus this method does not seem appropriate for geothermal reservoir delineation, in distinction with its use in rock salt, tar sands, oil shale, coal seams, and granite.

Mise-a-la-masse methods. The traditional mise-a-la-masse survey has largely been replaced by total field resistivity measurements in more detailed

and quantitative studies. The buried electrode energizing the low resistivity zone may be below or peripheral to the actual low resistivity target zone. Thus it is desirable to address the more general hole-to-surface (or hole-to-hole) resistivity/IP method.

Hole-to-surface resistivity/IP. The improvements in anomalous response for a buried conductive body using one or both buried current electrodes is well known from numerous model and field studies. The gain in response results from increased current density in the conductive target body. Surface measurements can be conducted over a large area and often to an arbitrary degree of detail (grid spacing) and precision. Field methods and interpretation techniques are well developed. Model studies by Newkirk (1982) and Mackelprang (1984) suggest elongate bodies which simulate geothermal reservoirs. Thin disc shaped bodies may be better modeled by thin ellipoids (Yang and Ward, 1984) and additional modeling is needed which more closely simulates a complex geothermal reservoir model. The probable presence of steel drill casing may complicate the current distribution and interpretation.

The probable presence of steel casing may provide an easy means for increasing the current density at depth but this line electrode is somewhat less effective and perhaps more difficult to interpret than the buried point source. Numerical modeling which addresses this array is needed.

Magnetometric Resistivity. (MMR) As noted earlier, the greatest improvement of anomaly amplitudes is achieved when the magnetometer is lowered down the borehole. Additional boreholes in a geothermal reservoir would offer an opportunity for enhanced current channeling by using a downhole current electrode or drill casing. Numerical modeling is needed to assess the probable anomaly amplitudes for borehole MMR anomalies. Although massive sulfide mineralization can be mapped in boreholes at depth of 250 m, the



response of a thin, conductive fracture zone at 1000 m may be too small to measure or interpret.

Borehole EM. Substantial depth probing has been achieved in mineral exploration by using a large transmitter loop near the borehole and a large current (50 amp) pulsed signal. The high resistivity environment and absence of drill casing makes the mineral exploration case well suited to a pulsed EM method. Drill casing may preclude the EM methods for geothermal fracture detection. In those selected hard rock cases where drill casing is not required the pulsed EM techniques may respond well to high conductivity fracture zones. Numerical modeling of thin conductive zones and drill casing above sensor depths is required to evaluate the applicability of the EM methods.

#### CONCLUSIONS

It would appear, for the general case of a deep (71000 m) geothermal reservoir and drill casing for most of the hole, that a hole-to-surface total field resistivity survey would be the borehole geophysical method most likely to succeed. If the borehole geophysical surveys could be conducted while only the near surface portions of the hole are cased (at some risk of losing the hole), then pulsed EM or MMR surveys, with a downhole magnetic field detector, may delineate the location and orientation of near borehole fractures. Additional numerical modeling is needed to establish realistic anomaly response levels, and to evaluate these amplitudes with probable instrumental and geologic noise levels.

## BIBLIOGRAPHY

### Borehole Geophysical Methods

Topics Include: electrical resistivity  
induced polarization  
magnetometric resistivity  
mise-a-la-masse  
time domain e.m.  
radar

Acosta, J. E., 1981, Investigation of borehole electrical and magnetometric resistivity methods: D. Phil. thesis, Oxford Univ.

This thesis describes the application of the  $\overset{M}{MMR}$  method to borehole geophysics. Computer modeling of the  $\overset{M}{MMR}$  response is accomplished via a finite-difference program based on the theory of Dey and Morrison (1979) and developed in this thesis.

Acosta, J. E., and Worthington, M. H., 1983, A borehole magnetometric resistivity experiment: Geophys. Prosp., 31, 800-809.

The authors describe in detail a borehole  $\overset{M}{MMR}$  experiment to determine the extent and orientation of zones of fissuring within massive limestones. A finite-difference modeling program was used in the interpretation of the data. The borehole  $\overset{M}{MMR}$  method was very sensitive to current channeling in the fissure zone.

Alfano, L., 1959, Introduction to the interpretation of resistivity measurements for complicated structural conditions: Geophys. Prosp., 7, 311-368.

This paper is a comprehensive work on the theory for modeling resistivity inhomogeneities using the method of integral equations.

Alfano, L., 1962, Geoelectrical prospecting with underground electrodes: Geophys. Prosp., 10, 290-303.

The author presents solutions to Laplace's equation for a single pole current source buried in a plane-layered half-space. Theoretical curves are presented for the pole-dipole array when the current pole is placed in the second layer.

Al'pin, L. M., 1964, On the solution of the fundamental problem of resistivity logging: Sci. Rep., Izv. Geophys., 236-238.

This paper presents an integral equation solution for the potential and electric field due to a current electrode in a borehole in the presence of a conductive borehole fluid, for different resistivity cross sections.

Barnett, C. T., 1972, Theoretical modeling of induced polarization effects due to arbitrarily shaped bodies: Ph.D. thesis, Colorado School of Mines.

This thesis presents a method for solving integrals over a triangular domain,  $\Delta S_i$ , arbitrarily oriented with respect to the  $xyz$  axes through coordinate rotation. The electric potential integral expresses the potential due to an equivalent surface layer of charge.

Barnett, C. T., 1976, Theoretical modeling of the magnetic and gravitational fields of an arbitrarily shaped three-dimensional body: Geophysics, 41, 1353-1364.

The author presents an analytical solution to the problem of magnetic and gravitational fields of an arbitrary shaped homogeneous three-dimensional body. The body is represented by a polyhedron and a convenient method of

inputing apices and assembling the facets of the polyhedron is developed. This facilitates the numerical method for performing the surface integration.

Bartel, L. C., 1977, Mapping of the reaction zone in an in-situ coal gasification experiment using an electrical technique: Presented at the 47th Ann. Int. SEG Meeting, Sept. 21, in Calgary.

This paper describes a dynamic mise-à-la-masse method where one current electrode is the production well casing and the other electrode is an outlying well. Potentials mapped at the surface appear to map the reaction zone, at 300 feet depth, of an in-situ coal gasification experiment.

Bartel, L. C., McCann, R. P., and Keck, L. J., 1976, Use of potential gradients in massive hydraulic fracture mapping and characterization: Presented at the 51st Technical Conf. of the SPE of the AIME, in New Orleans.

Bassiouni, A. A. F., Bagillard, R. L. A., Desbrandes, R., and deGelis, E. F., 1972, A new application of telelog--locating oil and gas field limits: Soc. Prof. Well Log Analysts Trans., 13th Annual Logging Symp., p. E1-E15.

This paper describes a field survey technique in which surface current electrodes and a downhole receiver dipole are used to detect conductive anomalies away from the borehole. A low frequency (12.5 Hz or 3125 Hz) alternating field is generated and the vertical component of the electric field is measured at various depths in the borehole.

Boyd, G. W., and Wiles, C. J., 1984, The Newmont drill hole EMP system - examples from Eastern Australia: Geophysics, **49**, in publ.

Results from drill hole Electromagnetic Pulse (EMP) surveys on three base metal deposits in New South Wales are presented and discussed. Computer modeling of the EMP data helped determine the location, depth, strike, dip and quality of the conductors. A small, near vertical conductor which occurs at a depth of 250 m is accurately mapped by the survey data and model interpretation.

Braekken, H., 1950, Deep ore prospecting by charged potential studies I: Det Kongelige Norske Videnskabers Selskabs Forhandling, **32**, 126-133.

The author describes a method in which the ore body is energized by direct current and the resulting potentials are mapped at the surface. A general discussion of the method, overburden and terrain effects, and preliminary model results is presented without field data or model results.

Bryant, H. L., 1960, Production well logging techniques: Geophysics, **25**, 905-927.

This paper presents an excellent summary of the state-of-the-art (to 1960)

of well log application to well evaluation, cement bond, casing, fracture detection, etc. Hole-to-surface studies are not discussed.

Bussian, A. E., 1983, Electrical conductance in a porous medium: *Geophysics*, **48**, 1258-1268.

The Hanai-Bruggeman equation is applied to develop a theoretical model of a conductive rock matrix immersed in water. A general two-component equation results which relates the electrical properties of the rock matrix and the water at any frequency. (Reservoir evaluation applications).

Chang, Hsi-Tien, and Suhler, S. A., 1984, Evaluation of borehole electromagnetic and seismic detection of fractures: Sandia Nat. Lab. contractor report SAND84-7109, 75 p.

The authors describe controlled experiments to determine the detectability of a 5-10 cm wide cut, filled with brine, in a granite quarry. Radar methods detect the artificial fracture at a distance of 12 m.

Chang, H. T., and Scott, L., 1984, Development of a borehole directional antenna at VHF: Sandia Nat. Lab. Tech. Rept. **84-0254**.

This report describes the feasibility of designing a directional antenna to operate to VHF (30 MHz to 300 MHz) which will physically fit into a 15 cm diameter borehole.

Clark, A. R., 1956, The determination of the long dimension of conducting ore bodies: *Geophysics*, **21**, 470-478.

Laplace's equation in prolate spheroidal coordinates is used to show that, with one current electrode in the conducting body, an estimate of the extent of the body along the long axis may be determined from the resistivity profile. Theoretical and experimental curves from a dipping conductor are compared.

Cook, J. C., 1975, Radar transparencies of mine and tunnel rocks: *Geophysics*, **40**, 865-885.

Laboratory measurements of RF complex permittivity were made on a variety of common rock types at frequencies of 1, 5, 25, and 100 MHz. Low loss propagation was noted for certain granites, limestones and coals, suggesting exploration distances up to hundreds of feet. Radar probing distances of less than 10 feet are predicted for most shales, clays, and fine-grained soils.

Cook, J. C., 1977, Borehole-radar exploration in a coal seam: short note, *Geophysics*, **42**, 1254-1257.

The author describes the results of borehole radar probing of coal seams. VHF radar pulses over 60 ft distance through coal was demonstrated. A coal-air interface was detected at an average distance of 90 feet.

Daily, W. D., Lytle, R. J., Laine, E. F., Okada, J. T., and Deadrick, F. J.,

1982, Geotomography in oil shale: J. Geophys. Res., **87**, B7, 5507-5515.

This paper describes mapping of in situ radio frequency attenuation of oil shale between 1 and 40 MHz using cross borehole measurements. The rubble zone was successfully mapped. Basic propagation theory is presented, and modeling results are described.

Dakhnov, V. N., 1959, Geophysical well logging: Quart. Colo. School of Mines, **57**, 443 p. (trans. by G. V. Keller).

Theoretical solutions are presented for buried electrodes in a one- and two-layered medium. Example curves are presented for the normal and lateral well logging arrays.

Daniels, J. J., 1977, Three-dimensional resistivity and induced polarization modeling using buried electrodes: Geophysics, **42**, 1006-1019.

A modified form of Barnett's surface integral technique, originally developed for surface electrode configurations, is used to calculate electric fields and potentials for a 3-D body in a homogeneous half-space, for six buried electrode configurations. Geometric factors are examined and computed responses are compared.

Daniels, J. J., 1977, Extending the range of investigation of borehole electrical measurements: SPWLA Eighteenth annual logging symposium, June 5-8, 1977.

This paper investigates the use of widely spaced buried electrodes in the presence of a three dimensional body and in a layered medium for six arrays including hole-to-hole and hole-to-surface geometries. Resolving capabilities and anomaly types of the various arrays are compared.

Daniels, J. J., 1978, Interpretation of buried electrode resistivity data using a layered earth model: Geophysics, **43**, 988-1001.

The author extends the theoretical solution for the apparent resistivity due to a buried electrode in a one- or two-layered medium to an arbitrary number of layers. Modeling theory is developed for the general case of buried current electrodes and potential receiver electrodes anywhere in a horizontally stratified earth. Well log and hole-to-hole data are integrated to form an interpretation.

Daniels, J. J., 1982, Hole-to-surface resistivity measurements at Gibson Dome (drill hole GD-1), Paradox Basin, Utah: U.S.G.S. Open file rept., **82-320**, 23 p.

A hole-to-surface resistivity survey at Gibson Dome is described and the resulting data are presented and described.

Daniels, J. J., 1983, Hole-to-surface resistivity measurements: Geophysics, **48**, 87-97.

The author describes in detail a hole-to-surface resistivity survey for four boreholes, drilled in a layered sequence of volcanic tuff. The field

data are reduced in terms of a layered earth model and residual anomalies are interpreted as 3-D ellipsoids.

Daniels, J. J., and Scott, J. H., 1981, Hole-to-surface resistivity measurements at Yucca Mountain, Nevada Test Site: U.S.G.S. Open file rept. 81-1336.

A field survey is described which used current electrodes in four different boreholes. Field data are presented and described.

Dey, A., and Morrison, H. F., 1979, Resistivity modeling for arbitrary shaped two-dimensional structures: Geophys. Prosp., 27, 106-136.

The authors develop the mathematics for numerical modeling of the potential distribution about a point source of current located in, or on the surface of, a half-space containing an arbitrary two-dimensional conductivity distribution. The finite difference equations are obtained for Poisson's equation using point-as well as area-discretization of the subsurface. (Surface arrays).

Dieter, K., Paterson, N. R., and Grant, F. S., 1969, IP and resistivity type curve for three-dimensional bodies: Geophysics, 34, 615-632.

The authors present a solution for the boundary value problem for a point source of current near a body of arbitrary shape in the form of an inhomogeneous integral equation which is solved numerically by the method of least squares. Apparent resistivity and IP are computed for surface arrays.

Dobecki, T. L., 1980, Borehole resistivity curves near spheroidal masses: Geophysics, 45, 1513-1522.

Laplace's equation is solved in oblate and prolate spheroidal coordinate systems to model the electrical potential distribution for current and potential electrodes in a borehole which is near an anomalous body of oblate or prolate shape.

Doll, H. G., 1949, Introduction to induction logging and application to logging of wells drilled with oil base mud: A.I.M.E. Pet. Trans., T.P. 2641, 148-162.

The author discusses the radius of investigation of a two-coil induction logging system (single borehole). The radius of ground affecting the received signal increases in proportion to the transmitter-receiver coil spacing.

Dolphin, L. T., Jr., Bollen, R. L., and Oetzel, G. N., 1974, An underground electromagnetic sounder experiment: Geophysics, 31, 49-55.

The authors describe detecting reflections from chambers within a dolomite mine at distances of 100-130 feet, using frequencies of 17.5-35 MHz for radar transmitters and receivers located on the surface.

Dyck, A. V., ed., 1975, Borehole geophysics applied to metallic mineral

prospecting: a review: Energy, Mines and Resources of Canada, Geological Survey Paper 75-31, 66 p.

This is an excellent review paper covering all methods of borehole geophysics as applied to metallic mineral exploration, including seismic and drill hole surveying. An extensive bibliography is provided.

Dyck, A. V., 1981, A method for quantitative interpretation of wideband, drill-hole EM surveys in mineral exploration: Ph.D. Thesis, Geophysics Laboratory, Dept. of Physics, University of Toronto, 170 p.

This thesis describes combined field and model studies of an EM prospecting method which uses a large, fixed transmitter loop with a downhole axial-component magnetic field sensor. An interpretation technique is described which is based on forward EM modeling of a thin conductive plate, and a conductive, two-layer sphere.

Dyck, A. D., 1984, The role of simple computer models in interpretations of wide-band, drill-hole electromagnetic surveys in mineral exploration: Geophysics, 49.

Eaton, P. A., and Hohmann, G. W., 1984, The influence of a conductive host on two-dimensional borehole transient electromagnetic responses: Geophysics, 49, (in publ.).

The authors computed the transient borehole electromagnetic (EM) responses of a horizontal two-dimensional model using a direct and explicit finite difference algorithm. Secondary responses for models with different host resistivities (10-1000 ohm-m) are approximately the same at late time. Computed borehole profiles of  $dH/dt$  are presented as a function of depth for boreholes near and within the conductive model.

Edwards, R. N., 1974, The magnetometric resistivity method and its application to the mapping of a fault: Canadian Journal of Earth Sciences, 11, 1136-1150.

This paper describes the first successful magnetometric resistivity (MMR) field survey using the gradient array (surface only). The methodology and procedures for normalizing and interpreting the field data are discussed.

Edwards, R. N., and Howell, E. C., 1976, A field test of the magnetometric resistivity (MMR) method: Geophysics, 41, 1170-1183.

The authors describe a field test of the MMR method using grounded current electrodes, and measuring the horizontal component of the magnetic field generated by the low frequency (1-5 Hz) electric current. The measured anomalies are interpreted with reference to theoretical anomalies due to an alpha center model.

Edwards, R. N., Lee, H., and Nabighian, M. N., 1978, On the theory of magnetometric resistivity (MMR) methods: Geophysics, 43, 1176-1203.

An integrated theory for the MMR method is presented which summarizes earlier theoretical papers by Stăfănescu and others. The characteristic



anomalies for an anisotropic earth, vertical and dipping contacts, thick and thin dikes, and other bodies are presented in detail.

Fredriksson, O. A., Fossati, F. N., and Robert, F. A., 1969, Helical antenna for irradiating an earth formation penetrated by a borehole and method of using same: U.S. Patent No. 3, 449,657.

The design of a helical antenna for borehole radar probing is described.

— Gabillard, R. L. A., Lovage, F. C. J., Bassiouni, Z. A. F., and Desbrandes, R., 1971, Telelog, electromagnetic method of directional exploration at great distances from boreholes: Soc. Prof. Well Log Analysts Trans., 12th Annual Logging Symposium, p. J1-J23.

The authors describe the Telelog survey method in which widely spaced electrodes at the surface and a downhole receiver dipole are employed to detect anomalies away from the borehole.

Gleeson, L. J., and Thio, Y. C., 1975, Downhole induced-polarization detection of ore bodies: conductive overburden effects: Aust. Jour. Phys., 28, 557-574.

The excitation and response of an IP source obtained by borehole electrodes is investigated for a uniform surface layer and a small spherical ore body. The mathematics is developed from Poisson's equation and Green's function. A signal improvement of 500x can be demonstrated for borehole (as opposed to surface) electrodes.

Gleeson, L. J., and Thio, Y. C., 1976, An application of downhole electrodes in induced polarization exploration: Austral. SEG Bull., 7, 60-65.

— Goldman, M. M., and Stoyer, C. H., 1983, Finite-difference calculations of the transient field of an axially symmetric earth for vertical magnetic dipole excitation: Geophysics, 48, 953-963.

The authors present a finite-difference formulation of the coaxial-loop or wire-loop transient electromagnetic prospecting system, which is used to model the fields from a buried cylindrical conductor. Axial symmetry of the conductor and source loop is required for this surface loop exploration method.

Hofmann, G. W., 1975, Three-dimensional induced-polarization and electromagnetic modeling: Geophysics, 40, 309-324.

This paper describes a numerical solution for calculating the induced polarization and electromagnetic responses of 3-D bodies buried in the earth. The integral equation is reduced to a matrix equation which is

solved numerically for the scattering current in the body. The electric and magnetic fields outside the body are found by integrating the appropriate half-space dyadic Green's function.

Holcombe, H. T., and Jiracek, G. R., 1984, Three-dimensional terrain corrections in resistivity surveys: *Geophysics*, **49**, 439-452.

The authors describe a three-dimensional finite-element computer algorithm which can accommodate arbitrarily complex topography and subsurface structure to model the resistivity response of the earth. A favorable comparison is achieved with a buried current electrode analytic solution of Snyder and Markel.

Holser, W. T., Unterberger, R. R., and Jones, S. B., 1966, Method for mapping a salt dome at depth by measuring the traveltime of electromagnetic energy emitted from a borehole drilled within the salt dome: U.S. Patent No. 3,286,163.

This patent describes a method of mapping geologic features in a salt dome using radar transmitting and receiving antennas in a borehole.

Hosler, W. T., Brown, R. J. S., Roberts, F. A., Fredriksson, O. A., and Unterberger, R. R., 1972, Radar logging of a salt dome: *Geophysics*, **37**, 889-906.

The authors describe a 230 MHz pulse-radar well-logging system and the interpretation of data taken from a 8208 feet deep drill hole in the Pine Prairie salt dome in Louisiana. Signals were received out to 2000 or 4000 feet of range. The basic equations for reflected signal power, attenuation, and other parameters are presented.

Howard, A. Q., Jr., 1981, Induction logging for vertical structures in the presence of a borehole fluid: *Geophysics*, **46**, 68-75.

The author discusses the problem of detecting vertical structures near a borehole in the presence of a high borehole fluid conductivity, and develops the expressions for electric and magnetic field responses for single borehole logging in the presence of vertical fractures.

Jakosky, J. J., 1933, Method and apparatus for determining underground structure: U.S. Patent No. 1,906,271.

This patent describes the magnetometric method of conductive exploration, using a horizontal component magnetometer to determine the magnetic field generated by the subsurface current flow.

Jakosky, J. J., 1940, *Exploration geophysics*: Los Angeles, Times-Mirror.

The magnetometric method of conductive exploration is described.

Kauahikaua, J., Mattice, M., Jackson, D., 1980, Mise-a-la-masse mapping of the HGP-A geothermal reservoir, Hawaii: Geothermal Resources Council, *Trans.* **4**, 65-68.

The well casing of the high temperature geothermal well HGP-A was used as one electrode and a return electrode was grounded in the ocean 6 km away from HGP-A. Electrical potentials were measured at the surface along roads, and apparent resistivities were computed. A zone of 10-20 ohm-m resistivity, thought to be dike-impounded warm water, overlies the thermal reservoir and is surrounded by a 5 ohm-m zone of sea water saturated lavas.

Ketola, M., 1972, Some points of view concerning mise-à-la-masse measurements: *Geoexploration*, 10, 1-21.

The author describes mise-à-la-masse measurements using different electrode arrays in surface and borehole positions. Surface potentials, apparent resistivity and induced polarization data are presented for a survey in the Ahokkala area.

Koulikov, A. V., and Rocroi, J. P., 1983, Use of vertical line-source in electrical prospecting for oil: an example: abstract, EAEG 45th Annual Meeting, Oslo, 14-17 June: Tech. Prog. and Abstracts of Papers, p. 48.

This abstract describes the use of steel casings of drill holes as vertical line source electrodes to achieve a higher current density at depth for electrical surveys. A survey of this type in the USSR proves that a residual-resistivity anomaly roughly delineates the contours of a known hydrocarbon deposit.

Landt, J. A., 1978, A magnetic induction technique for mapping vertical conductive fractures: Theory of operation: Los Alamos Scientific Lab. informal rep. LA-7333-MS.

The author examines the response of a vertical fracture to a single hole induction log. The cavity region may dominate the response of the fracture and must be considered for proper experimental and interpretation procedures.

Lee, T., 1975, An integral equation and its solution for some two- and three-dimensional problems in resistivity and induced polarization: *Geophys. Jour. Roy. Astr. Soc.*, 42, 81-95.

The potential about a point electrode at the surface of a layered ground in which a heterogeneity is embedded is expressed as an integral equation of a Green's function. The integral equation is solved by using the Galerkin method, and the apparent resistivity and chargeability can be calculated for any electrode configuration.

Lytle, R. J., 1981, Electrode configuration influence on resistivity and induced polarization measurements about a spherical anomaly: Lawrence Livermore Laboratory rep. UCRL-85434.

Two-, three-, and four-electrode configurations are evaluated for cross-borehole resistivity and induced polarization probing. Various current source locations exterior to the sphere are considered.

Lytle, R. J., 1982, Resistivity and induced-polarization probing in the

vicinity of a spherical anomaly: Inst. of Elect. and Electron. Eng., Trans. on geoscience and remote sensing, **GE-20**, 493-499.

The mathematical formulae governing the interaction of a low frequency source of electric current with a spherical anomaly are given. The formulae are used to determine the apparent resistivity and induced-polarization response between electrodes located within boreholes in the medium.

Lytle, R. J., and Hanson, J. M., 1983, Electrode configuration influence on resistivity measurements about a spherical anomaly: *Geophysics*, **48**, 1113-1119.

The response of a spherical resistivity anomaly for various two-, three-, and four-electrode configurations are investigated. Cross-borehole probing will have significantly better results with three- and four-electrode configurations.

Mackelprang, C. E., 1984, Resistivity model catalogue for buried electrode in geothermal environments: Earth Science Lab. Univ. Utah Res. Inst. rept. (in prep.).

The total field electrical resistivity is computed and presented for a large number of thin and dipping three-dimensional bodies which simulate the hole-to-surface survey in the geothermal environment.

Mansinha, L., and Mwenifumbo, C. J., 1983, A mise-à-la-masse study of the Cavendish Geophysical test site: *Geophysics*, **48**, 1252-1257.

The authors describe a detailed mise-à-la-masse survey at the well documented Cavendish geophysical test site. Survey results are presented as profiles of potential versus distance without any new numerical treatment or interpretation techniques.

Mathisrud, G. C., and Sumner, J. S., 1967, Underground IP surveying at Homestake Mine: *Mining Congress Journal*, **53**, 66-69.

This paper describes an underground induced polarization survey using the gradient array where current electrodes were placed at either end of a drift and potentials were measured to distances of 500 feet in horizontal boreholes. The survey mapped sulfide distributions associated with the gold mineralization.

McMurry, H. V., and Hoagland, A. D., 1956, Three-dimensional applied potential studies at Austinville, Virginia: *Bull. Geol. Soc. America*, **67**, 683-696.

The authors report a detailed field study where current electrodes were placed in pencil shaped ore bodies of disseminated sulfides and potential measurements were made on the surface and in approximately 30 boreholes. The mapped potentials were presented in map and section form and aided in the delineation of ore bodies.

Merkel, R. H., 1971, Resistivity analysis for plane-layered half-space models with buried current electrodes: *Geophys. Prosp.*, **19**, 626-639.

A numerical solution is presented for the boundary value problem in steady-state current flow for one and two layers over a half space with a current source below the surface. The optimum placement of the electrode, in the conductive region, leads to a better resolution of the lateral extent of the body. Several references to related work by Russian authors are included.

- Merkel, R. H., and Alexander, S. S., 1971, Resistivity analysis for models of a sphere in a half-space with buried current source: *Geophys. Prosp.*, **19**, 640-651.

Boundary-value problems in steady-state current flow for a sphere of arbitrary conductivity in a half-space are solved numerically in bispherical coordinates. The current sources may be on the surface or one electrode on the surface and a buried electrode above or in the sphere.

- Merrik, B. R., Checkin, G. H., and Popov, V. V., 1979, Numerical solution of the forward problem of the apparent resistivity method for a thin layered medium in a borehole: *Izvestiya, Earth Physics*, **15**, 354-357.

The authors present an algorithm for numerical solution of the forward problem of computing the apparent resistivity for a multilayer medium penetrated by an orthogonal borehole. A system of integral equations is solved for the surface density charge on the interfaces.

- Moran, J. H., and Kunz, K. S., 1962, Basic theory of induction logging and application to study of two-coil sondes: *Geophysics*, **27**, 829-858.

The authors solve Maxwell's equations for the response of a two-coil induction sonde in homogeneous and nonhomogeneous media. The results allow evaluation of the skin effect in induction logging.

- Morrison, B. C., 1971, Electrical potential method used at a single hole to indicate direction of better mineralization: *American Institute of Mining Metallurgical and Petroleum Engineers, Trans.*, **250**, 337-340.

A field survey is reported in which downhole electrodes are used to help define flat lying lead-zinc ore bodies in Missouri. Current electrodes were placed in two peripheral boreholes and one potential electrode was located in a central mineralized borehole while several other holes were logged with a second potential electrode.

- Nabighian, M. N., Oppliger, G. L., Edwards, R. N., Lo, B. B. H., and Cheesman, S. J., 1984, Cross-hole magnetometric resistivity (MMR): *Geophysics*, in publ.

The authors describe theoretical (and modeling) and field results that demonstrate a substantial improvement in anomaly amplitudes when the recording magnetometer is lowered within the borehole. The lowering of current electrodes beneath the surface may not significantly improve the surface MMR response. Massive sulfide mineralization is mapped at a depth exceeding 500 m.

Newkirk, D. J., 1982, Downhole electrode resistivity interpretation with three-dimensional models: Dept. Geology and Geophysics, Univ. Utah Tech. Rept. DOE/ID/12079-47 for Dept. of Energy, 27 p.

A catalogue of three-dimensional model responses (potential and apparent resistivity) was computed using Hohmann's integral equation numerical solution for a buried current electrode and surface or subsurface potential electrodes.

Nickel, H., Sender, F., Thierbach, R., and Weichart, H., 1983, Exploring the interior of salt domes from boreholes: Geophys. Prosp., 31, 131-148.

The authors describe borehole-to-borehole attenuation and single borehole reflection probing using radar frequencies of 25 MHz and 50-100 MHz in the high resistivity interior of a salt dome. A probing range of some hundred meters was achieved.

Oristaglio, M. L., 1978, Geophysical investigations of earth structure within the vicinity of boreholes: Ph.D. thesis, Oxford Univ.

The magnetic field response resulting from a line induction source, at a borehole detector, is derived and estimated using a 2-D finite-element modeling program.

Oristaglio, M. L., and Worthington, M. H., 1980, Inversion of surface and borehole electromagnetic data for two-dimensional electrical conductivity models: Geophys. Prosp., 28, 633-657.

A method is developed for inverting electromagnetic fields induced by a line source in an earth of two-dimensional conductivity structure. A combination of finite element and damped least squares methods are used to effect an efficient and accurate calculation.

Parasnis, D. S., 1966, Mining geophysics: Elsevier, Amsterdam, 356 p.

The author describes the mise-a-la-masse survey method.

Parasnis, D. S., 1967, Three-dimensional mise-a-la-masse survey of an irregular lead-zinc-copper deposit in Central Sweden: Geophys. Prosp., 15, 407-437.

This paper describes a detailed field study in which potentials were measured on the surface and in 25 drill holes at a lead-zinc-copper deposit in central Sweden. The three dimensional potential distribution indicated continuity of ore zones, dip and pitch of the ore body, and the general shape of the ore zones.

Pascal, H., 1983, Further discussion on attenuation and dispersion of electromagnetic wave propagation in fluid-saturated porous rocks and applications to dielectric-constant well logging: Geophysics, 48, 1373-1380.

This paper presents a detailed quantitative analysis of some basic problems of electromagnetic wave propagation through a porous medium

saturated with fluid, as related to the quantitative interpretation of dielectric constant logging.

- Roy, A., and Dhar, R. L., 1970, Relative contribution to signal by ground elements in two-coil induction logging system: *Geophys. Prospecting*, **18**, 389-404.

The authors theoretically evaluate the relative contribution of various ground elements to the signal at the receiver for a two-coil induction logging system in a homogeneous medium. The analysis accounts for the skin effect. In most cases the radius of investigation is less than twice the transmitter-receiver separation.

- Rubin, L. A., Fowler, J. C., and Marino, G. G., 1978, Multiple borehole radar: EnSCO, Inc. Final Report to National Science Foundation, NSF Grant No. APR76-03300, 101 p.

This report describes the development and initial field evaluation of a short pulse electromagnetic borehole radar system with principal energy of the radar antenna in the 50 MHz to 150 MHz range. The system can acquire data in either the single hole or crosshole mode.

- Ryss, V. S., 1971, Contact method of polarization curves, *in* Borehole Mining Geophysics: G. K. Volosyuk and N. T. Safranov, editors, Leningrad, Nedra.

A method of mineral discrimination using contact polarization curves is described.

- Ryss, V. S., 1973, The search and exploration for ore bodies by the contact method of polarization curves: Nedra, Leningrad.

The author describes studies which attempt to discriminate between common massive sulfide minerals by measuring reaction potentials with respect to a saturated calomel electrode, when an electric current is passed through an ore body and/or country rock. Typical reaction potentials were -0.5 to 1.4 v (cathode processes) and +0.2 to +0.7 (anode processes).

- Ryss, V. S., 1981, The use of the contact polarization curve (CPC) techniques to evaluate and explore ore deposits: *Geoexploration*, **18**, 281-295.

This paper describes the contact polarization curve (CPC) method. An electrode is placed in contact with mineralization intersected by a borehole and electric current of variable intensity is transmitted between the ore body and the surface current ground. Electrochemical reactions are monitored.

- Schlumberger, C., 1920, *Étude sur la Prospection électrique du sous-sol*, 94 p., Paris: Gauthier-Villars.

This paper describes the first use and early development of the mise-a-la-masse method.

- Scott, J. H., Daniels, J. J., Hasbrouck, W. P., and Guu, J. Y., 1975, Hole-to-hole geophysical measurements research for mineral exploration: *Trans. of*

the 16th Annual Logging Symp. of the SPWLA, paper KK.

This paper presents an application of hole-to-hole resistivity, induced polarization, and seismic measurements.

Seigel, H. O., 1952, Ore body size determination in electrical prospecting: *Geophysics*, **17**, 907-914.

The author describes a technique to estimate ore body size when current and potential probes are located along the axis of rotation of an oblate spheroidal ore zone. The probes are located in a boring which penetrates the body.

Seigel, H. O., 1974, The magnetic induced polarization (MIP) method: *Geophysics*, **39**, 321-339.

This paper describes the theory and application of the magnetic induced polarization method of surface mineral exploration.

Sender, F., Thierbach, R., and Weichart, H., 1983, Obtaining enhanced data in HF-pulsed borehole radar by new direction-finding antenna system: abstract, EAEG 45th Annual Meeting, Oslo, 14-17 June; *Tech. Prog. and Abstracts of Papers*, p. 46.

The authors presented a new design for a borehole radar antenna system which uses established radio direction-finding methods modified for use in the borehole environment.

Snyder, D. D., 1976, A method for modeling the resistivity and IP response of two-dimensional bodies: *Geophysics*, **41**, 997-1015.

An integral equation solution is derived for resistivity and induced polarization of two-dimensional bodies using a Fredholm integral equation of the second kind. A solution is obtained in the wavenumber domain, then inverse Fourier transformed to arrive at the electric potential at any point of interest.

Snyder, D. D., and Merkel, R. M., 1973, Analytic models for the interpretation of electrical surveys using buried current electrodes: *Geophysics*, **38**, 513-529.

The IP response and apparent resistivity resulting from a buried current pole in the presence of a stratigraphic target and a three-dimensional target are discussed. Analytic solutions are presented for the potential due to a buried electrode in a three-layered half-space and for a spherical inhomogeneity in a half-space.

Somerstein, S. F., Berg, M., Chang, D., Chung, H., Johnson, H., Richardson, B., Pizzicara, J., and Salisbury, W. W., 1984, Radio frequency geotomography for remotely proving the interiors of operating mini- and commercial-sized oil shale retorts: *Geophysics* (in publ).

The authors describe cross-borehole, radio-frequency geotomographs made across two different sized in-situ oil-shale retorts. Measured



attenuation coefficients at 25 MHz and 1.5 MHz were observed to increase in the retorting and combustion zones.

Spies, B. R., 1981, Electrical geophysics in the USSR: Bureau of Mineral Resources, Australia, Record 1981/66 (unpublished); BMR Microform MF 181.

A review of the KSPK (contact technique of polarization curves) method as used in the USSR is presented.

Spies, B. R., 1983, Recent developments in the use of surface electrical methods for oil and gas exploration in the Soviet Union: *Geophysics*, **48**, 1102-1112.

Electrical geophysical methods as used in the Soviet Union are reviewed. Hole-to-surface and cross-hole techniques are not discussed.

Stefanescu, S. S., 1950, Modeles theoriques de milieux heterogenes pour les methods de prospection electrique a courants stationnaires: *Studii Tehnice si Economice*, ser. D, n. 2, 51-71, Bucurest.

The basic theory of the magnetometric resistivity (MMR) method is presented.

Stefanescu, S. S., 1970, Nouvelles applications de la theorie des milieux alpha harmoniques a la prospection electrique en courant continu: *Geophys. Prosp.*, suppl. **28**, 786-800.

The theory and use of alpha centers in the interpretation of electrical resistivity data are discussed.

Stefanescu, S. S., and Nabighian, M. N., 1962, Uber magnetische storfelder als folge senkrechter schichtungen im gleichstrom: *Rev. Geologie et Geographie, Acad. Repub. Pop. Roumaine*, **6**, 139-155.

The anomalous vertical magnetic field due to the disturbed current flow near a contact is derived.

Stefanescu, S. S., and Stefanescu, D., 1974, Mathematical models of conducting ore bodies for direct current electrical prospecting: *Geophys. Prosp.*, **22**, 246-261.

The calculation of apparent electrical resistivity response for dc electrical prospecting arrays using alpha centers is generalized in this paper.

Tang, Muoi, 1972, Sur le champ magnetique des courants electriques stationnaires dans les milieux heterogenes alpha exponentiels: *Rev. Roumaine de Geologie, Geophysique et Geographie*, ser. Geophysique, **16**, 51-90.

The magnetic field due to an anomalous current flow in a conductivity distribution occupying the half-space  $z > 0$  is determined for a buried alpha center.

Tikhonov, A. N., Dmitriyev, V. I., and Zarkharov, Ye. V., 1977, Solution of electrical prospecting problem for inhomogeneous media: *Izvestiya, Physics of Solid Earth (U.S.S.R.)* 13, 833-839.

The mathematics are developed for calculating the electromagnetic field in a stratified media with an arbitrary number of layers. The authors calculate the integrals from boundary value problem solutions in terms of Green's functions.

Van Nostrand, R. G., 1953, Limitations on resistivity methods as inferred from the buried sphere problem, *Geophysics*, 18, 423-433.

The author derives the expression for the apparent resistivity (Wenner array) of a buried conducting sphere in bipolar coordinates. The detectability of the buried sphere is examined as a function of electrode spacing and depth.

Van Nostrand, R. G., and Cook, K. L., 1966, Interpretation of resistivity data: U.S.G.S. Prof. Paper 499, 310 p.

Theoretical solutions are presented for buried electrodes in a one- or two-layered medium.

Wagg, D. M., and Seigel, H. O., 1963, Induced polarization in drill holes: *Canadian Mining Journal*, 84, 54-59.

The authors describe two basic surface-borehole electrode arrays which are used for drill hole detection logging or for drill hole directional surveying.

Wait, J. R., ed., 1963, Special issue on electromagnetic waves in the earth: *IEEE Trans. on Antennas and Propagation*, AP-11, 206-387.

This special issue contains twenty-five papers concerned with antenna design, dipole arrays, physical properties and electromagnetic wave propagation in the earth's crust.

Wait, J. R., 1982, *Geo-electromagnetism*: Academic Press, New York, 268 p.

This text includes a chapter (5) which discusses vertically oriented electrical dipole sources which relate to borehole geophysical measurements.

Webb, J. H., 1931, Potential due to a buried sphere: *Phys. Rev.*, 37, 292-302.

Laplace's equation is solved for the potential due to a buried conducting sphere and surface electrodes. A numerical approximation to the exact solution is presented.

Webb, J. H., 1931, The potential due to a buried sphere: *Phys. Rev.*, 38, 2056-2067.

A solution is derived for the potential due to a buried spheroid. An image spheroid is placed in the upper half-space to satisfy boundary

conditions on the surface of the half space. The solution is effected in spheroidal harmonics.

Witherly, K. E., 1980, The application of the applied potential and downhole pulse EM techniques to the exploration for massive sulfide deposits in eastern Canada: presented at the 50th Annual Intl. Mtg. of the Soc. Expl. Geophysicists, Houston, Nov. 16-20.

This paper describes a downhole application of a pulse EM (time-domain EM) system. This downhole pulse EM (DHPEM) method uses a transmitter loop laid out on the surface while the drill holes are logged to determine the conductor's position and attitude.

Woods, D. V., 1975, A model study of the Crone borehole pulse electromagnetic (PEM) system: Queen's University, Kingston, Ontario, M.Sc. thesis.

Woods, D. V., and Crone, J. D., 1980, Scale model study of a borehole pulse electromagnetic system: Canadian Min. and Metall. Bull., 73, 96-104.

This paper describes the Crone borehole pulse electromagnetic (PEM) system, field tests, and a scale model study of the system.

Worthington, M. H., Kuckes, A., and Oristaglio, M., 1981, A borehole induction procedure for investigating electrical conductivity structure within the broad vicinity of a hole: Geophysics, 46, 65-67.

The authors describe a two-coil induction logging system in which an alternating magnetic field is established by transmitting current through a horizontal loop of wire symmetrically positioned about the borehole on the surface of the earth.

Yang, F., and Ward, S. H., 1984, Theoretical modeling of thin spheroids and ellipsoids in borehole geophysics: submitted to Geophysics, 20 p. (?)